UNIVERSITY OF SOUTHAMPTON

Modelling the freshwater balance and influence of icebergs in the Amundsen Sea, Antarctica

by

David T. Bett

A thesis submitted in partial fulfillment for the
degree of Doctor of Philosophy

in the
Faculty of Environmental and Life Sciences
School of Ocean and Earth Science

December 2020

UNIVERSITY OF SOUTHAMPTON

ABSTRACT

FACULTY OF ENVIRONMENTAL AND LIFE SCIENCES
SCHOOL OF OCEAN AND EARTH SCIENCE

Doctor of Philosophy

by David T. Bett

The Amundsen Sea has some of the highest thinning rates of ice shelves in Antarctica. This imbalance is caused by changes in ocean melting, induced by warm Circumpolar Deep Water (CDW) intrusions. The resulting changing freshwater balance could affect the on-shelf currents and mixing. However, a clear understanding of the behaviour of fresh water in the region is lacking. This thesis addresses that question. Firstly, an idealised model, with a passive ice shelf freshwater tracer, is used to show that the vertical distribution of ice shelf meltwater changes with CDW layer thickness variation. This model is used to determine the local freshwater feedback effect of ice shelf meltwater on ice shelf melt rates. Secondly, a model of the Amundsen Sea is used, with passive freshwater tracers, to investigate the relative magnitudes and spatial distributions of freshwater components from different sources. In the surface and on a depth-average all freshwater tracer concentrations are of comparable magnitude, though on a depth-average sea ice and ice shelf meltwater are largest. The total freshwater tracer distribution is similar to that of the ice-shelf meltwater tracer field. This implies a potential for ice-shelf meltwater feedbacks, whereby abundant ice-shelf meltwater alters the ocean circulation and stratification, affecting melting. Thirdly, the effect of including grounded icebergs and their freshwater flux are studied in detail. The presence of icebergs increases CDW intrusions that reach the base of ice shelves. This suggests another possible feedback mechanism, whereby more icebergs induce greater ice-shelf melting and hence more icebergs. However, the strength of this potential feedback is dependent on poorly constrained sea-ice model parameters.

Author's note: Some of the results in Chapter 4 and 5 in this thesis are summarised in Bett et al. (2020), which has been accepted by the *Journal of Geophysical Research: Oceans*.

Contents

Declaration **xvii**

Acknowledgements **xix**

Nomenclature **xxi**

1 Introduction **1**
1.1 Sea level rise . . . 1
1.2 Southern Ocean . . . 2
1.3 Amundsen Sea . . . 4
1.4 Inter-annual variability in the Amundsen Sea . . . 6
1.5 Freshwater sources . . . 11
1.5.1 Sea ice . . . 12
1.5.2 Precipitation and evaporation . . . 13
1.5.3 Icebergs . . . 14
1.5.4 Ice shelves . . . 14
1.6 Existing knowledge of freshwater in the Amundsen Sea region . . . 17
1.6.1 Field observations . . . 17
1.6.2 Satellite observations . . . 18
1.6.3 Numerical models . . . 18
1.7 Aim of research . . . 20

2 Model set-up and development **23**
2.1 MITgcm . . . 23
2.1.1 Passive tracers . . . 25
2.1.2 Ice shelf melt . . . 28
2.2 Idealised model . . . 30
2.2.1 Model set-up . . . 30
2.2.2 Freshwater feedback method . . . 31
2.3 Regional Amundsen Sea model . . . 32
2.3.1 Model set-up . . . 32
2.3.2 Precipitation and evaporation . . . 33
2.3.3 Sea ice model . . . 35
2.3.4 Iceberg set-up . . . 35
2.3.5 Convection issues . . . 37

3 Idealised model results **41**
3.1 Model oceanic conditions . . . 41

3.2 Vertical distribution of local ice shelf freshwater 44
3.3 Local ice shelf freshwater feedback 50
3.4 Conclusions 59

4 Freshwater in the Amundsen Sea **61**
4.1 Regional model validation 62
4.2 Freshwater spatial distribution 68
4.2.1 Horizontal tracer spatial distribution 69
4.2.2 Vertical tracer distribution 73
4.3 Freshwater seasonality 75
4.4 Inter-annual variability 79
4.4.1 Inter-annual variability of horizontal spatial distribution 83
4.4.2 Inter-annual variability of vertical distribution 86
4.5 Conclusions 89

5 Effect of Icebergs **93**
5.1 Effect on sea ice and freshwater relations 94
5.2 Effect of icebergs on CDW intrusions and feedbacks 98
5.2.1 Average continental shelf oceanic effects of icebergs 100
5.2.2 Iceberg effect on OHC inter-annual variability in front of ice shelves 104
5.2.3 Influence of parameter choices 108
5.3 Conclusions 114

6 Conclusions **117**
6.1 Idealised vertical distribution of ice shelf freshwater tracer 118
6.2 Local ice shelf freshwater feedbacks 118
6.3 Average freshwater distribution 119
6.4 Freshwater seasonal cycle and inter-annual variability 120
6.5 Impact of icebergs on sea ice and oceanic heat content 121
6.6 Implications and future work 122

Bibliography **125**

List of Figures

1.1 Figure shows the thickness changes of ice shelves over the period 1994-2012, where red circles denote a thinning and blue circles a thickening, with their respective size denoting the magnitude. The rates of thickness change are similarly shown on the ice shelves. The line graph shows the volume change of the West Antarctic Ice Sheet (red), the East Antarctic Ice Sheet (blue) and the total (black) (Paolo et al. 2015). 2

1.2 Schematic of the three-dimensional circulation of the Southern Ocean overlaid on regional bathymetry (Meredith 2016). 3

1.3 The Southern Ocean geography, principal fronts, and oceanographic zones taken from Talley et al. (2011). Subantarctic Front (SAF), Polar Front (PF), southern ACC front (SACCF) and Southern Boundary (SB) , with front locations from Orsi et al. (1995). 4

1.4 Map of Amundsen Sea region showing region bathymetry and ice shelves (Kimura et al. 2017). 5

1.5 Schematic of processes and the resulting oceanic regimes in the a) Weddell Sea and b) Amundsen Sea (Petty et al. 2013). 6

1.6 Observed and simulated ocean conditions in a) 2009 and b) 2012. Section of observed and simulated (under ice shelf) 2009 and 2012 potential temperatures (colour) and salinity (black contours) along the Pine Island Trough and underneath the PIG Ice Shelf (Dutrieux et al. 2014). 7

1.7 Schematic of the processes leading to a period of warming in the Amundsen Sea in the two troughs of Pine Island and Dotson (Dotto et al. 2019). 8

1.8 A) Monthly mean zonal winds at 10 m (black) and its running 12 month preceding integral (red) averaged over the black box in (B). Green shows the monthly sea surface temperature anomaly averaged over the magenta box in (C). B) Annual mean of anomalies in surface wind in surface wind and wind stress curl of 2011 in respect to the 1979-2011 average. C) Annual mean of anomalies in atmospheric geopotential height at 200 hPa (colour) and sea surface wind (contour) in 2011, with respect to 1979-2011 climatology, with white (black) contours denoting negative (positive) (Dutrieux et al. 2014). 9

1.9 The un-grounding process of Pine Island Glacier and the timescale of the process, as determined by sediment cores. Top panel show the overall positions of the ice shelf and the bottom panel is zoomed in on the ridge region for the periods a) pre - 1945 b) 1945 - 1970 c) 1970 - present (Smith et al. 2017). 11

1.10 (a) Spring satellite observations of the AMSR-E sea ice concentrations (2003-2010) (Cavalieri et al. 2014). (b)(c) Satellite image mosaic composed of Copernicus Sentinel-1 SAR (Synthetic Aperture Radar) data. The composite uses imagery acquired between 30th April 2017 and 6th May 2017. Image composite was processed by BAS using Google Earth Engine. The black box in (c) shows the area in (b). Key locations are shown in (a)(c), where DOT = Dotson Ice Shelf, BRI = Bear Ridge grounded Icebergs, PIG = Pine Island Glacier Ice Shelf, PIP = Pine Island Polynya and ASP = Amundsen Sea Polynya. 15

2.1 Idealised domain, showing the triangle like ice shelf and the area in which there is linearly increasing restoring zone (red). Diagram edited, but original from Holland (2017). 30
2.2 Restoring profiles for temperature and salinity for four illustrative cases, which are applied on the northern boundary of the idealised model. 31
2.3 a) Regional model bathymetry. b) Regional continental shelf bathymetry. Derived from the global 1 min Refined Topography data set (RTOPO) (Timmermann et al. 2010). Grey denotes land and ice shelves are excluded. 34
2.4 Model bathymetry over the grounded BRI region. a) Grounded iceberg representation distribution for the reference case and ice shelf representation. b) 50 % permeability case of grounded BRI. 35
2.5 Steady surface iceberg melt freshwater flux distribution applied to the regional model. Shown for over study area only. 36
2.6 A) Hovmöller diagram of potential temperature 1991-2016 averaged over the eastern Amundsen Sea before sea level fall correction is applied. B) Hovmöller diagram over the same area after sea level correction is applied. 38
2.7 Hovmöller diagram of potential temperature 1991-2006, averaged over the eastern Amundsen Sea. A) Iceberg melt with scale factor 1 B) scale factor 2 C) scale factor 5. 39
2.8 Hovmöller diagrams of potential temperature 1991-2006, averaged over the eastern Amundsen Sea for the cases of iceberg flux distribution range set to A) $x = 10$ km C) $x = 100$ km E) $x =$ Infinite, with the corresponding iceberg melt freshwater flux fields shown in B), D) and F) respectively. 40

3.1 Restoring profiles for temperature and salinity for the four key cases, which are applied on the northern boundary of the idealised model. 44
3.2 A cross-section of steady state potential temperature and salinity along the center of the domain in the idealised model, for a illustrative cold (a)(c) and warm case (b)(d). Straight solid horizontal white lines represent the top and bottom of the thermocline and the pycnocline of the restoring applied to the model. 45
3.3 Oceanic flow conditions for illustrative warm case: a) Overturning streamfunction b) The plan view of ice shelf melting and flow in top grid cells under ice shelf. c) The plan view of the barotropic streamfunction, for the same example case, with the ice shelf position marked by black lines. . 46
3.4 Idealised model ice-shelf average melt rates, for a range of CDW + thermocline thicknesses for initial conditions and restoring applied to the northern boundary. All melt rates are when the model has reached a steady state. 47

3.5 A cross-section on the western boundary of ice-shelf meltwater tracer concentration in the idealised model, shown for different cases of CDW thickness. Straight solid horizontal white lines represent the top and bottom of the thermocline and the pycnocline of the restoring applied to the model. The black lines represent salinity contours, with the cyan ones representing the salinity of the top and bottom of the thermocline of the forcing. 48
3.6 Ice shelf meltwater tracers for year a) 2009 and b) 2014 in front of Pine Island Glacier (PIG) in a full regional Amundsen Sea model (Kimura et al. 2017). 49
3.7 Idealised model ice shelf average melt rates, for a range of CDW + thermocline thicknesses for initial conditions and restoring applied to the northern boundary. Melt rates shown are for the reference case (black), the ColdMelt-fixed cases (blue) and the WarmMelt-fixed cases (red). All melt rates are when the model has reached a steady state. 52
3.8 Plan view of the spatial distribution of steady state ice-shelf melt rates for: a) All Winter Water forcing reference case, b) All CDW forcing reference case, c) WW forcing case but with CDW forcing case ice shelf freshwater flux applied (WarmMelt-fixed case), d) All CDW forcing case but with WW forcing ice shelf meltwater flux applied (ColdMelt-fixed case), e) Difference of WarmMelt-fixed case - WW forcing reference case and f) Difference of ColdMelt-fixed case - CDW forcing reference case. 54
3.9 Plan view of the spatial distribution of steady state ice shelf friction velocity u^* for: a) All Winter Water forcing reference case, b) All CDW forcing reference case, c) WW forcing case but with CDW forcing case ice shelf freshwater flux applied (WarmMelt-fixed case), d) All CDW forcing case but with WW forcing ice shelf meltwater flux applied (ColdMelt-fixed), e) Difference of WarmMelt-fixed case - WW forcing reference case and f) Difference of ColdMelt-fixed case - CDW forcing reference case. 56
3.10 Plan view of the spatial distribution of steady state ice shelf temperature forcing for: a) All Winter Water forcing reference case, b) All CDW forcing reference case, c) WW forcing case but with CDW forcing case ice shelf freshwater flux applied (WarmMelt-fixed case), d) All CDW forcing case but with WW forcing ice shelf meltwater flux applied (ColdMelt-fixed case), e) Difference of WarmMelt-fixed case - WW forcing reference case and f) Difference of ColdMelt-fixed case - CDW forcing reference case. 57
3.11 Idealised model ice shelf average melt rates, for the a) realistic range and b) extreme range of CDW + thermocline thicknesses for initial conditions and restoring applied to the northern boundary. Melt rates shown are for the reference case (black), the realistic ColdMelt-fixed cases (green), the ColdMelt-fixed cases (blue), the realistic WarmMelt-fixed cases (yellow) and the WarmMelt-fixed cases (red). All melt rates are when the model has reached a steady state. 58

4.1 Depth maximum climatological subsurface potential temperature (1994-2012, but using only observational available years) from: (a) model and (b) observations (Dutrieux et al. 2014). The black box in (b) shows the area in (c)(e). (c) Spring satellite observations of the AMSR-E sea ice concentrations (2003-2010) (Cavalieri et al. 2014). (e) Model bathymetry with representation of grounded icebergs. (d)(f) Satellite image mosaic composed of Copernicus Sentinel-1 SAR (Synthetic Aperture Radar) data. The composite uses imagery acquired between 30th April 2017 and 6th May 2017. Image composite was processed by BAS using Google Earth Engine. The black box in (f) shows the area in (d). Key locations are shown in (a)(c)(f), where SI = Siple Island, DOT = Dotson Ice Shelf, BRI = Bear Ridge grounded Icebergs, THW = Thwaites Ice Shelf, PIG = Pine Island Glacier Ice Shelf, ABT = Abbot Ice Shelf and ASP=Amundsen Sea Polynya. 63

4.2 Observed (solid red lines) and model output from reference case (solid black line) mean profiles for salinity and potential temperature near PIG and Dotson ice shelves. The shaded areas represent one standard deviation of the inter-annual variability from the mean. CTD profiles taken from Jenkins et al. (2018) for Dotson and Dutrieux et al. (2014) for PIG, taking CTD locations that are either within the red and green boxes in Figure 4.1a or closer to the ice shelves. Model is sampled at the closest grid point to the individual CTD observations and at the same month and year. The number of CTD profiles for each austral summer are indicated for both regions. 64

4.3 Hovmöller diagrams of potential temperature and salinity in front of PIG Ice Shelf (a-b) and Dotson Ice Shelf (c-d). Hovmöller diagrams are averaged over the red and green boxes shown in Figure 4.1a and include 10-year model spin up. A 2-year running average is applied at each depth. Vertical black dashed lines indicate end of model spin up period. 65

4.4 Climatological seasonal cycle of the satellite observations of the AMSR-E sea ice concentrations (a-d) (Cavalieri et al. 2014). Model climatological seasonal cycle of sea ice concentrations (e-h) and the sea ice thickness (i-l). All averaged over the period 2003-2010. 66

4.5 Climatology of freshwater fluxes (1989-2018) for (a) total freshwater, (b) iceberg melt, (c) precipitation - evaporation (PmE), (d) sea ice and (e) ice shelf melt. Black line represents the 1000 m depth contour of the continental shelf break. 69

4.6 Climatology of surface freshwater tracer concentration (1989-2018) for (a) total freshwater, (b) iceberg melt, (c) precipitation - evaporation (PmE), (d) sea ice and (e) ice shelf melt. Black line represents the 1000 m depth contour of the continental shelf break. 71

4.7 Climatology of depth averaged freshwater tracer concentration (1989-2018) for (a) total freshwater, (b) iceberg melt, (c) precipitation - evaporation (PmE), (d) sea ice and (e) ice shelf melt. Black line represents the 1000 m depth contour of the continental shelf break. 72

4.8 Maximum climatological subsurface potential temperature (1994-2012), but using only observational available years for model. 73

4.9 Climatology of freshwater tracer concentration (1989-2018) along south–north cross-section, shown by the red line in Figure 4.8, for (a) total freshwater, (b) iceberg melt, (c) precipitation - evaporation (PmE), (d) sea ice and (e) ice shelf melt. Black contours indicate salinity. 74
4.10 Climatology of freshwater tracer concentration (1989-2018) along west–east cross-section shown by the cyan line in Figure 4.8, for (a) total freshwater, (b) iceberg melt, (c) precipitation - evaporation (PmE), (d) sea ice and (e) ice shelf melt. Black contours indicate salinity. 76
4.11 Eastern Amundsen Sea mean seasonal cycle for (a) freshwater component fluxes and (b) tracer concentration. Fluxes and concentration are averaged over the area and volume of the blue box shown in Figure 4.1a, and ice-shelf meltwater flux is taken to be the combined fluxes from Thwaites and PIG ice shelves. 77
4.12 Average seasonal cycle of the sea ice freshwater fluxes (1989-2018). Black line represents the 1000 m depth contour of the continental shelf break. . 78
4.13 Average seasonal cycle of the surface (10 m) sea ice tracer. Averaged over the period 1989-2018. Black line represents the 1000 m depth contour of the continental shelf break. 78
4.14 Average seasonal cycle of the surface (10 m) salinity. Averaged over the period 1989-2018. Black line represents the 1000 m depth contour of the continental shelf break. 79
4.15 Eastern Amundsen Sea mean seasonal cycle for (a) freshwater component fluxes and (c) tracer concentration, along with inter-annual variability of (b) freshwater component fluxes and (d) tracer concentration. Fluxes and concentration are averaged over the area and volume of the blue box shown in Figure 4.1a, and ice-shelf meltwater flux is taken to be the combined fluxes from Thwaites and PIG ice shelves. Inter-annual variability is calculated as monthly anomalies from the mean seasonal cycle, with a 2-year running mean subsequently applied. Dashed vertical lines show end of model spin up period. 81
4.16 a) Correlation values ($r|r|$) for different month lags between ice shelf freshwater flux and sea ice freshwater flux (red), and between ice shelf freshwater flux and heat flux (blue). b) Maximum climatological subsurface potential temperature (1994-2012), but using only observational available years for model. c) Scatter plot of ice shelf melting anomaly against sea ice freshwater flux anomaly at 10 month lag. d) Maps of correlation $r|r|$ values of meridional wind stress anomalies to a scalar time series of sea ice melting anomalies at zero lag. e) Scatter plot of ice shelf melting anomaly against CDW heat flux at 6 month lag. f) Scatter plot of sea ice freshwater flux anomaly against meridional wind stress anomalies at marked location at 0 month lag. Correlations are calculated after 10 years of spin up and after applying a 2-year running mean. 82
4.17 Warm year averaged surface freshwater tracer concentration (2010) for (a) total freshwater, (b) iceberg melt, (c) precipitation - evaporation (PmE), (d) sea ice and (e) ice shelf melt. Black line represents the 1000 m depth contour of the continental shelf break. 83

4.18 Cold year averaged surface freshwater tracer concentration (2000) for (a) total freshwater, (b) iceberg melt, (c) precipitation - evaporation (PmE), (d) sea ice and (e) ice shelf melt. Black line represents the 1000 m depth contour of the continental shelf break. 84
4.19 Warm year averaged depth averaged freshwater tracer concentration (2010) (a) total freshwater, (b) iceberg melt, (c) precipitation - evaporation (PmE), (d) sea ice and (e) ice shelf melt. Black line represents the 1000 m depth contour of the continental shelf break. 85
4.20 Cold year averaged depth averaged freshwater tracer concentration (2000) (a) total freshwater, (b) iceberg melt, (c) precipitation - evaporation (PmE), (d) sea ice and (e) ice shelf melt. Black line represents the 1000 m depth contour of the continental shelf break. 85
4.21 Hovmöller diagrams of (a) total freshwater, (b) iceberg melt, (c) precipitation - evaporation (PmE), (d) potential temperature, (e) sea ice and (f) ice shelf melt averaged over red box in front of PIG Ice Shelf, shown in Figure 4.1a. Black contours indicate salinity averaged over the same area. Model spin up of 10 years included. A 2-year running mean at each depth is applied to the tracers and the salinity to remove the seasonal cycle. The vertical black dashed lines indicate the end of the spin up period. 87
4.22 Hovmöller diagrams of (a) total freshwater, (b) iceberg melt, (c) precipitation - evaporation (PmE), (d) potential temperature, (e) sea ice and (f) ice shelf melt averaged over green box in front of Dotson Ice Shelf, shown in Figure 4.1a. Black contours indicate salinity averaged over the same area. Model spin up of 10 years included. A 2-year running mean at each depth is applied to the tracers and the salinity to remove the seasonal cycle. The vertical black dashed lines indicate the end of the spin up period. 88

5.1 (a) Climatological austral winter (JAS) sea ice freshwater flux out of the ocean (1989-2018) with grounded BRI, and (c) without BRI. (b) Climatological winter (JAS) sea ice concentration and drift (1989-2018) with grounded BRI and (d) without BRI. Difference in (e) winter (JAS) sea ice freshwater flux out and (f) winter (JAS) sea ice concentration and velocities (with minus without the representation of the grounded Bear Ridge Icebergs). Note uneven colour bar in (e)(f). 96
5.2 (a) Climatological austral winter (JAS) sea ice freshwater flux out of the ocean (1989-2018) with 50 % permeability grounded BRI, and (c) without BRI. (b) Climatological winter (JAS) sea ice concentration and drift (1989-2018) with grounded BRI and (d) without BRI. Difference in (e) winter (JAS) sea ice freshwater flux out and (f) winter (JAS) sea ice concentration and velocities (with minus without the representation of the grounded Bear Ridge Icebergs). Note uneven colour bar in (e)(f). . . 97
5.3 (a) Climatological austral winter (JAS) sea ice freshwater flux out of the ocean (1989-2018) with grounded ISBRI, and (c) without BRI. (b) Climatological winter (JAS) sea ice concentration and drift (1989-2018) with grounded BRI and (d) without BRI. Difference in (e) winter (JAS) sea ice freshwater flux out and (f) winter (JAS) sea ice concentration and velocities (with minus without the representation of the grounded Bear Ridge Icebergs). Note uneven colour bar in (e)(f). 99

5.4 Maps of correlation $r|r|$ values of sea ice freshwater flux anomalies to a scalar time series of PIG and Thwaites melting anomalies at zero lag: (a) with grounded icebergs present and (b) without grounded icebergs present. Correlations are calculated after 10 years of spin up and after applying a 2-year running mean. 100
5.5 Maximum climatological subsurface potential temperature (1994-2012), but using only observational available years for model. 100
5.6 Cross-section of potential temperature along the cyan line in Figure 5.5 for: (a) grounded BRI and iceberg melt, (b) no grounded BRI but with iceberg melt, (c) grounded BRI but without iceberg melt, (d) no grounded BRI and no iceberg melt. Averaged over the period 1989-2018. 101
5.7 Cross-section of meridional velocities along the cyan line in Figure 5.5 for: (a) grounded BRI and iceberg melt, (b) no grounded BRI but with iceberg melt, (c) grounded BRI but without iceberg melt, (d) no grounded BRI and no iceberg melt. Averaged over the period 1989-2018. 102
5.8 Cross-section of salinity along the cyan line in Figure 5.5 for: (a) grounded BRI and iceberg melt, (b) no grounded BRI but with iceberg melt, (c) grounded BRI but without iceberg melt, (d) no grounded BRI and no iceberg melt. Averaged over the period 1989-2018. 103
5.9 Cross-section of potential temperature along the cyan line in Figure 5.5 for: (a) grounded BRI, (b) no grounded BRI, (c) Ice shelf BRI, (d) 50 % permeability. Averaged over the period 1989-2018. 104
5.10 Cross-section of meridional velocities along the cyan line in Figure 5.5 for: (a) grounded BRI, (b) no grounded BRI, (c) Ice shelf BRI, (d) 50 % permeability. Averaged over the period 1989-2018. 105
5.11 Cross-section of salinity along the cyan line in Figure 5.5 for: (a) grounded BRI, (b) no grounded BRI, (c) Ice shelf BRI, (d) 50 % permeability. Averaged over the period 1989-2018. 105
5.12 Hovmöller diagram of potential temperature in front of PIG Ice Shelf for: (a) grounded BRI and iceberg melt, (b) no grounded BRI but with iceberg melt, (c) grounded BRI but without iceberg melt, (d) no grounded BRI and no iceberg melt. (e-h) the same for the area in front of Dotson Ice Shelf. Hovmöller diagrams are averaged over the red and green boxes shown in Figure 5.5 and include 10-year model spin up. A 2-year running average is applied at each depth. 107
5.13 Hovmöller diagram of potential temperature in front of PIG Ice Shelf for: (a) grounded BRI, (b) no grounded BRI, (c) Ice shelf BRI, (d) 50 % permeability. (e-h) the same for the area in front of Dotson Ice Shelf. Hovmöller diagrams are averaged over the red and green boxes shown in Figure 5.5 and include 10-year model spin up. A 2-year running average is applied at each depth. 109
5.14 Potential temperature Hovmöller diagrams averaged over PIG Ice Shelf front with iceberg melt and with and without grounded icebergs for sea ice drag parameters values of 0.002 (a)(d), 0.0025 (b)(e), 0.003 (c)(f) respectively. Hovmöller diagrams are averaged over the red box in Figure 5.5 and include 10-year model spin up. A 2-year running mean is applied at each depth. 111

5.15 Potential temperature Hovmöller diagrams averaged over PIG Ice Shelf front with and without both grounded icebergs and iceberg melt for sea ice drag parameters values of 0.002 (a)(d), 0.0025 (b)(e), 0.003 (c)(f) respectively. Hovmöller diagrams are averaged over the red box in Figure 5.5 and include 10-year model spin up. A 2-year running mean is applied at each depth. 111
5.16 Potential temperature Hovmöller diagrams averaged over Dotson Ice Shelf front with iceberg melt and with and without grounded icebergs for sea ice drag parameters values of 0.002 (a)(d), 0.0025 (b)(e), 0.003 (c)(f) respectively. Hovmöller diagrams are averaged over the green box in Figure 5.5 and include 10-year model spin up. A 2-year running mean is applied at each depth. 113
5.17 Potential temperature Hovmöller diagrams averaged over Dotson Ice Shelf front with and without both grounded icebergs and iceberg melt for sea ice drag parameters values of 0.002 (a)(d), 0.0025 (b)(e), 0.003 (c)(f) respectively. Hovmöller diagrams are averaged over the green box in Figure 5.5 and include 10-year model spin up. A 2-year running mean is applied at each depth. 113

List of Tables

4.1 Comparison of average model ice shelf melt rates (1989-2018) to other modelled melt rates and observed melt rates. The ± represents one standard deviation from the mean. Some ice shelf names have been shortened, where DOT = Dotson, CROS = Crosson, THW = Thwaites, PIG = Pine Island Glacier, COS= Cosgrove, VEN= Venables. a) Modelled melt rate from the reference simulation in this study (1989-2018). b) Modelled melt rates (1991-2014). c) Satellite based estimate of melt rates (1979-2010). Note that melt rate of Crosson is included within the Dotson melt rate. d) Satellite based estimate of melt rates (2003-2008). e) Oceanographic estimate of melt rate, with observations taken in 1994 (47 Gt/yr), 2007 (102 Gt /yr), 2009 (73 Gt/yr), 2010 (69 Gt/yr) and 2012 (34 Gt/yr). Oceanographic estimate of melt rate, with observations taken in 2000 (25 Gt/yr), 2006 (56 Gt/yr), 2007 (44 Gt/yr), 2009 (91.6 Gt/yr), 2011 (54 Gt/yr), 2012 (20 Gt/yr), 2014 (21 Gt/yr) and 2016 (20 Gt/yr). 68

Research Thesis: Declaration of Authorship

Print Name: David T. Bett

Title of thesis: Modelling the freshwater balance and influence of icebergs in the Amundsen Sea, Antarctica

I declare that this thesis and the work presented in it is my own and has been generated by me as the result of my own original research.

I confirm that:

1. This work was done wholly or mainly while in candidature for a research degree at this University;
2. Where any part of this thesis has previously been submitted for a degree or any other qualification at this University or any other institution, this has been clearly stated;
3. Where I have consulted the published work of others, this is always clearly attributed;
4. Where I have quoted from the work of others, the source is always given. With the exception of such quotations, this thesis is entirely my own work;
5. I have acknowledged all main sources of help;
6. Where the thesis is based on work done by myself jointly with others, I have made clear exactly what was done by others and what I have contributed myself;
7. None of this work has been published before submission;

Signature: Date: 08/05/2020

Acknowledgements

I would like to thank and acknowledge the people who have helped me in the journey of producing this thesis.

I would first like to thank and acknowledge my supervisors Paul R. Holland, Alberto C. Naveira Garabato, Pierre Dutrieux and Adrian Jenkins for their support and guidance throughout. I would especially like to thank Paul for his encouragement, support and patience during days of convective models and "yoda speak". I am also thankful for the assistance from my other co-authors Satoshi Kimura and Andrew Fleming for the submission of my first paper. I would also like to acknowledge the Natural Environmental Research Council studentship [grant number NE/L002531/1] that has funded my research.

In addition, I would like to thank the support from Chloé and my house mates Jake, Ryan and Matt, as well as my office mates and the BAS student community as a whole. Lastly I would like to thank my family for their continued support.

Nomenclature

ACC	Antarctic Circumpolar Current
AASW	Antarctic Surface Water
ASP	Amundsen Sea Polynya
CDW	Circumpolar Deep Water
BRI	Bear Ridge Icebergs
HSSW	High Salinity Shelf Water
mCDW	modified Circumpolar Deep Water
MITgcm	Massachusetts Institute of Technology General Circulation Model
OHC	Oceanic Heat Content
PIG	Pine Island Glacier
PmE	Precipitation minus Evaporation
WW	Winter Water

Chapter 1

Introduction

1.1 Sea level rise

The Antarctic Ice Sheet has been persistently losing mass during the satellite era and has enough ice in it to have the potential of increasing sea levels by 58 m if it were to be all melted (Fretwell et al. 2013). It is estimated to have added ∼7.6 mm to sea level rise (1992-2017), with most of the rise coming from ice loss from the West Antarctic Ice Sheet totaling ∼6.5 mm over the same period (Shepherd et al. 2018).

This loss of ice sheet mass must be due to an imbalance between the sources and sinks of mass within it. The Antarctic Ice Sheet gains mass from snow precipitation and marine ice formation, and loses mass from the melting of floating ice shelves, iceberg calving, surface meltwater runoff and surface sublimation. The ice shelves are melted by the ocean and atmosphere, causing the floating ice shelves to thin towards the edge and calve icebergs, and in a steady state situation this loss of mass is replaced by the influx of ice from grounded ice upstream. However, if there is an imbalance of the mass fluxes into and out of the ice shelves this could lead to the ice shelves to thin overall. These ice shelves restrain the grounded glaciers via the internal stresses between the flowing ice and the surrounding stationary ice. Therefore the thinning of the ice shelves reduces this internal stress and can increase the flow rate of the glacier leading to increased ice loss and a further possible mass imbalance. Therefore the state of the ice shelves greatly determines the long term stability of glaciers.

Overall average ice shelf volume change has accelerated from negligible loss of 25 ± 64 km^3/y for 1994-2003 to rapid loss of 310 ± 74 km^3/y for 2003-2012 (Paolo et al. 2015). There is a clear west/east spilt in Figure 1.1, with the West Antarctic Ice Sheet having the vast majority of the thinning, whereas the ice shelves in the east on average have a small amount of thickening. The largest ice shelf thickness losses occur in the Amundsen and Bellingshausen sea regions, with these two regions accounting for just 20 % of the

West Antarctic ice shelf area, but combined providing over 85% of the total ice shelf volume loss from West Antarctica (1994-2012) (Paolo et al. 2015). This is thought to be due to the ocean forcing applied to these ice shelves (Shepherd et al. 2004), as the surface melting on these ice shelves is too low to produce the thinning observed and the coherent glacial change suggests climatic forcing.

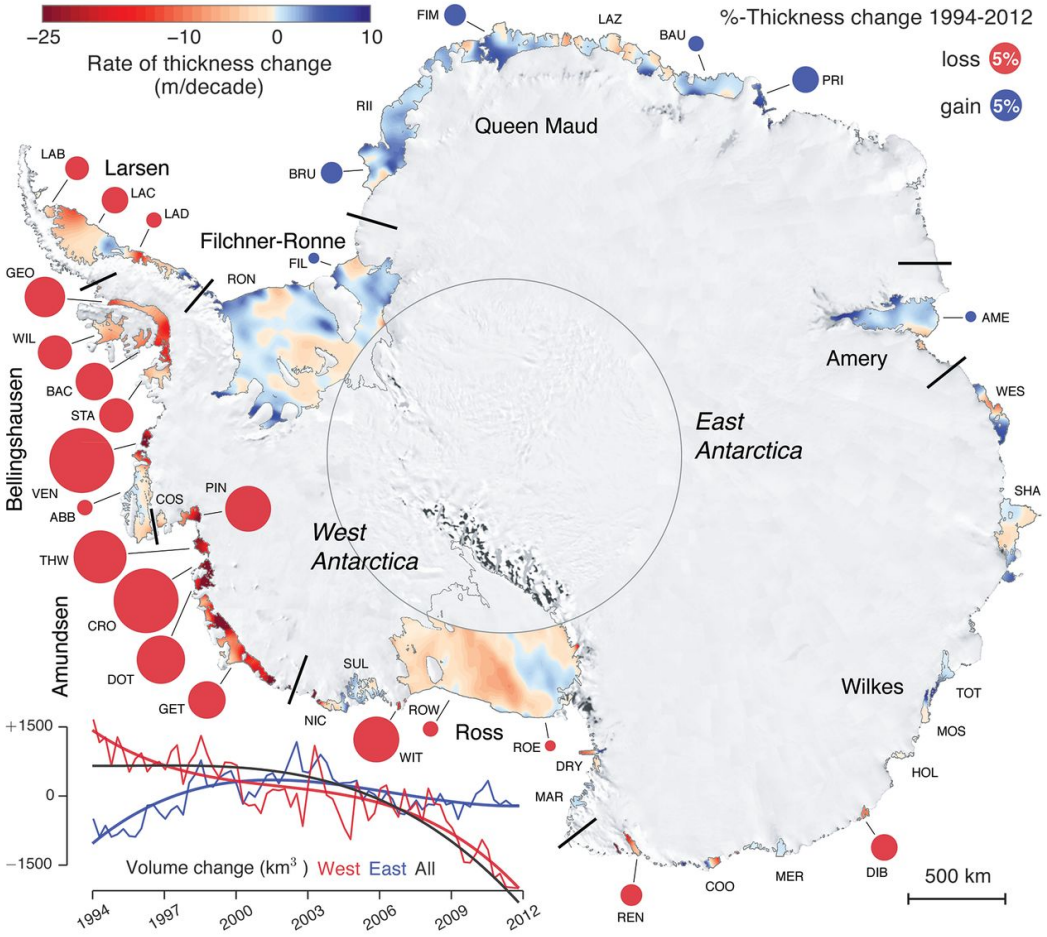

FIGURE 1.1: Figure shows the thickness changes of ice shelves over the period 1994-2012, where red circles denote a thinning and blue circles a thickening, with their respective size denoting the magnitude. The rates of thickness change are similarly shown on the ice shelves. The line graph shows the volume change of the West Antarctic Ice Sheet (red), the East Antarctic Ice Sheet (blue) and the total (black) (Paolo et al. 2015).

1.2 Southern Ocean

In the previous section ice shelf thinning in the Amundsen Sea was linked to ocean forcing. This section therefore explores the Southern Ocean in order to start to understand the ocean conditions around Antarctica. The Southern Ocean connects up the worlds three main basins and so transports, modifies and forms most of the ocean water masses. Therefore, the Southern Ocean is very important to the world's climate system

and its circulation is shown in Figure 1.2. The circulation is complex, with the zonal Antarctic Circumpolar Current (ACC), which interacts with a meridional thermohaline circulation.

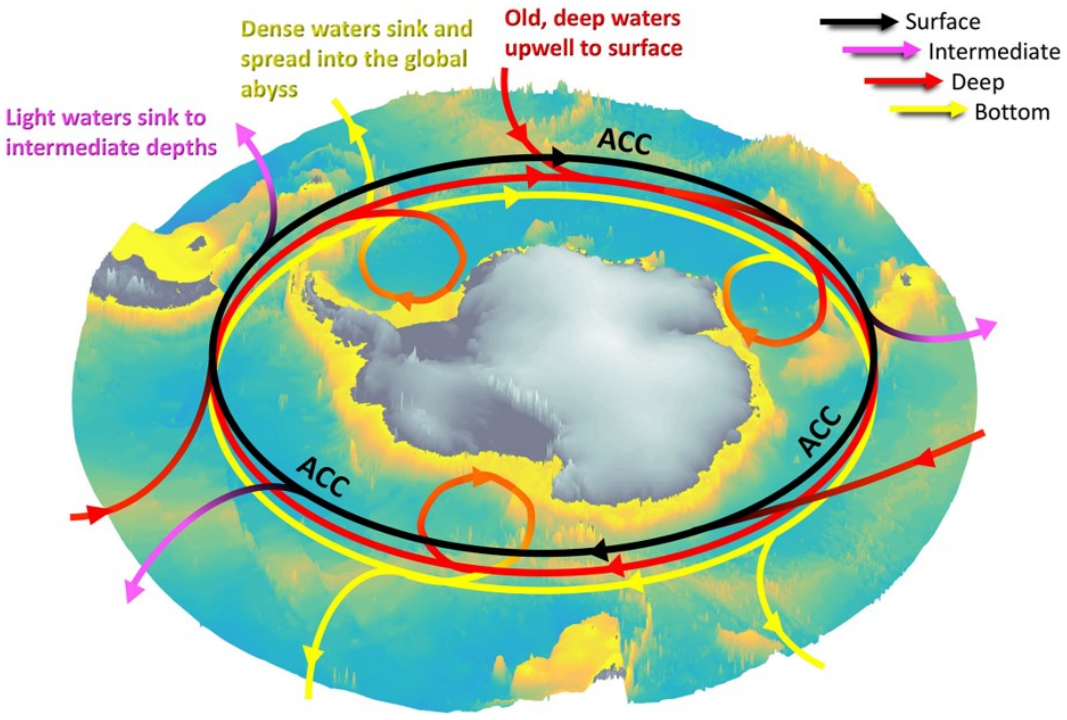

FIGURE 1.2: Schematic of the three-dimensional circulation of the Southern Ocean overlaid on regional bathymetry (Meredith 2016).

The thermohaline circulation is driven by dense water formation over continental shelf areas, due to strong sea ice growth in the Weddell and Ross seas, and along the Wilkes Land coast. The dense water then sinks and descends down the continental slope to the abyssal depths (Carter et al. 2008). This dense cold water migrates northwards into the Atlantic, Indian and Pacific oceans, where the deep water then upwells through the thermocline therefore completing the global circulation.

In contrast the ACC is formed in part by the lack of land blockages to its flow, which results in a largely wind driven eastward current that encircles Antarctica (Talley et al. 2011). It is the world's largest current with transport of about 140×10^6 m^3 of water per second, due to the depth of the current (about 4 km) and width (500–1000 km) (Fyfe & Saenko 2005). The meridionally tilted isopycnals within this current enable the surface waters and deep waters to be connected (Boening et al. 2008). Therefore this enables significant upwelling of deep waters, which are able to rise without changing their density. This also means that the ACC is of great importance for air-sea exchanges, being for example a potential atmospheric carbon sink and with the Southern Ocean air-sea exchanges affecting half the global ocean's properties (Fyfe & Saenko 2005).

The ACC contains four fronts, the Subantarctic Front (SAF), Polar Front (PF), Southern ACC Front (SACCF) and Southern Boundary (SB) (Orsi et al. 1995), with locations

shown in Figure 1.3. Antarctic Surface Water (AASW) extends mostly uniformly from the PF to the continental regions of Antarctica. Below AASW resides the warm and salty Circumpolar Deep Water (CDW) water mass. This is can separated into upper and lower CDW, with the upper CDW being characterised by high nutrients and low oxygen, while lower CDW is characterized by higher salinities. The poleward boundary of the ACC is defined as the southern terminus of upper CDW (Orsi et al. 1995).

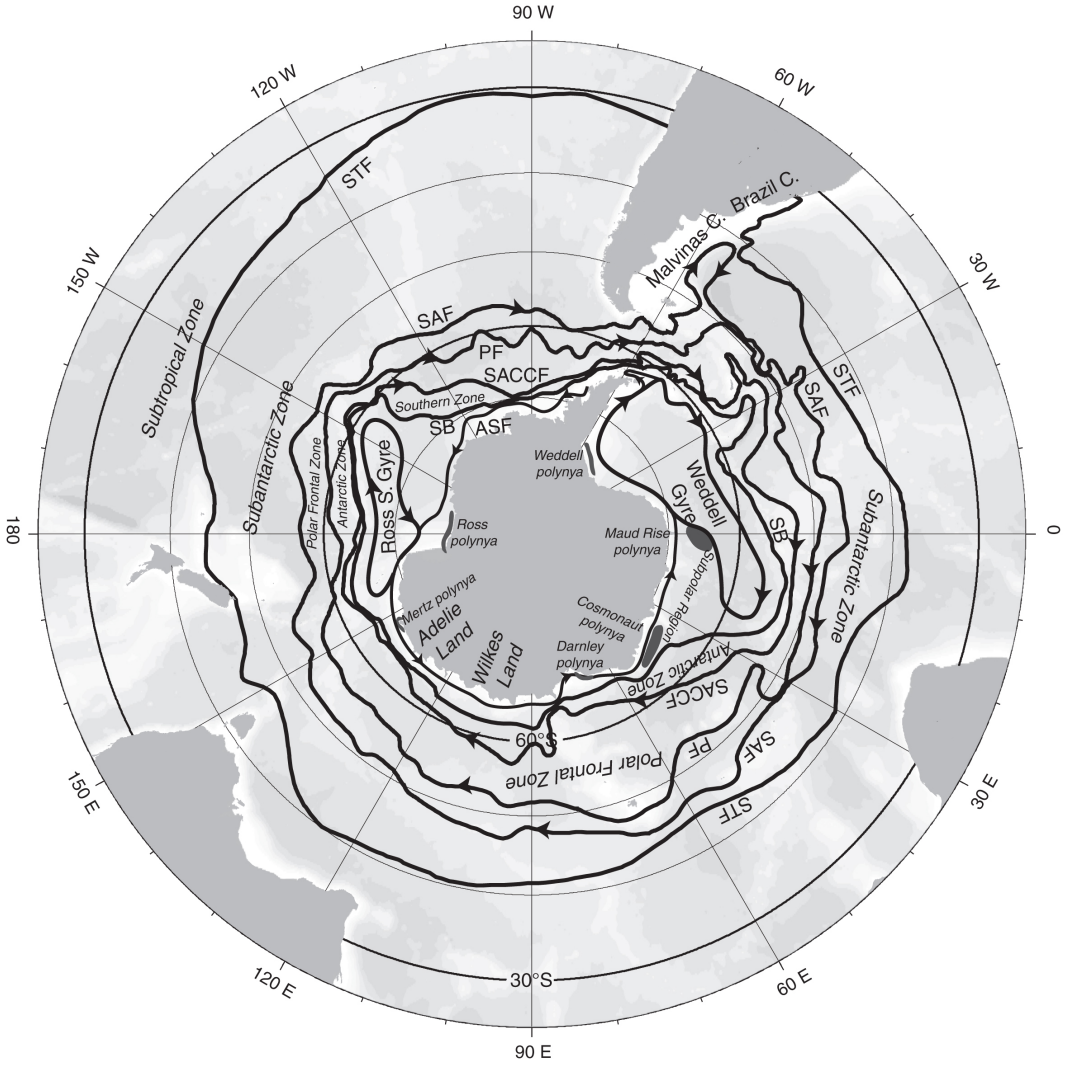

FIGURE 1.3: The Southern Ocean geography, principal fronts, and oceanographic zones taken from Talley et al. (2011). Subantarctic Front (SAF), Polar Front (PF), southern ACC front (SACCF) and Southern Boundary (SB) , with front locations from Orsi et al. (1995).

1.3 Amundsen Sea

The previous section explored the large scale processes and conditions in the Southern Ocean. This section therefore focuses on the oceanic conditions in the Amundsen Sea in order to start to understand the oceanic forcings that are applied to ice shelves

in the region. The Amundsen Sea is located west of the Bellinghausen Sea, between approximately 140°W and 80°W, as shown in Figure 1.4. The continental shelf in the region can extend out close to 70°S. The continental shelf has many troughs in the bathymetry with some of these being 1000 m deep, but on the continental shelf it can also rise up to be only 200 m deep as well (Fretwell et al. 2013).

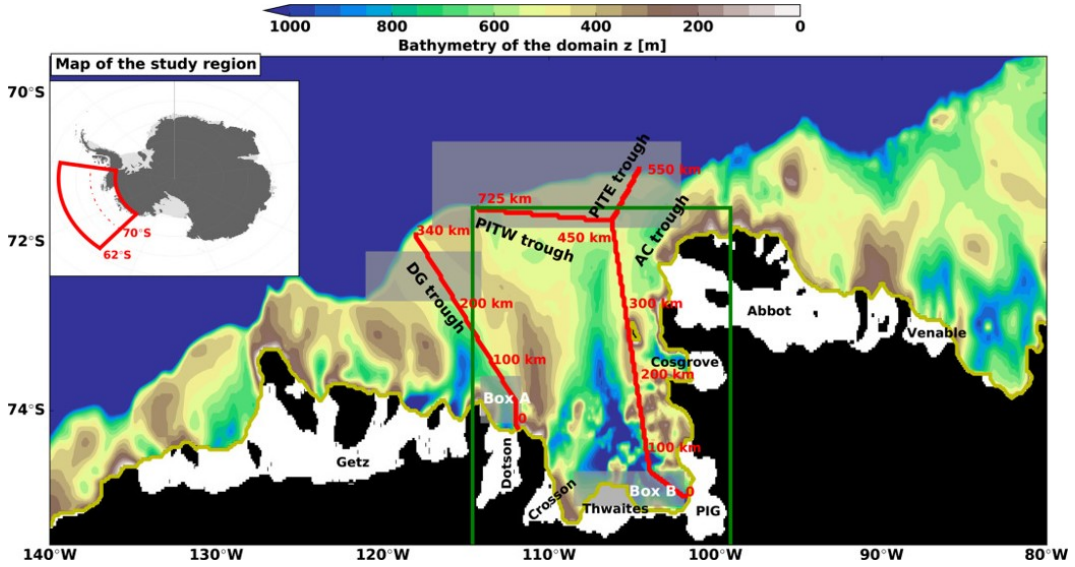

FIGURE 1.4: Map of Amundsen Sea region showing region bathymetry and ice shelves (Kimura et al. 2017).

There are different continental shelf ocean regimes that exist around Antarctica, as shown in Figure 1.5. The top panel shows the continental shelf regime in the Weddell Sea, whereas the bottom shows for the Amundsen Sea's regime. In the Weddell Sea strong sea ice growth forms High Salinity Shelf Water (HSSW), which, as it is denser than CDW, blocks CDW from intruding onto the continental shelf. This leads to a cold regime, where the CDW does not reach the base of the ice shelves and therefore the region has low ice shelf melt rates (Rignot et al. 2013, Depoorter et al. 2013). However, in the Amundsen Sea brine rejection from sea ice growth isn't strong enough for convection to reach the sea bed and create HSSW. Therefore the Amundsen Sea is in a warm regime, where warm CDW reaches the base of ice shelves, leading to high ice shelf melt rates in this region (Rignot et al. 2013, Depoorter et al. 2013). The fundamental difference that is thought to cause the differences in regimes is the difference in atmospheric forcing applied to the two regions (Petty et al. 2013). The differences in the wind forcing drives different rates of sea ice export, leading to different sea ice production rates and mixed layer depths. In addition, it is thought that the differences of the wind forcing over the continental shelf break to be a factor in creating the different regimes, with this forcing in the Amundsen Sea thought to help drive CDW onto the continental shelf.

Therefore in the Amundsen Sea warm and saline modified Circumpolar Deep Water (mCDW) resides below colder and fresher Winter Water (WW). WW is formed by sea ice growth, with the subsequent brine rejection causing convection in the winter, increasing

the mixed layer depth. Then the following summer's sea ice melt leads to the creation of the WW layer in the water column, which is the remains of the previous winter's mixed layer. The poleward boundary of the ACC abuts the continental shelf break in the Amundsen Sea (Orsi et al. 1995). Therefore CDW resides off the continental shelf in the ACC and intrudes onto the shelf via troughs in the bathymetry (Jacobs et al. 1996). These troughs extend to the base of ice shelves in the region, enabling the mCDW to cause high melt rates (Walker et al. 2007) (Figure 1.6a). However, in the case of PIG Ice Shelf, there is a ridge in the bathymetry under the ice shelf which prevents the majority of the mCDW from reaching the grounding line, therefore leading to greatly reduced melting compared to what would have otherwise occurred (Dutrieux et al. 2014).

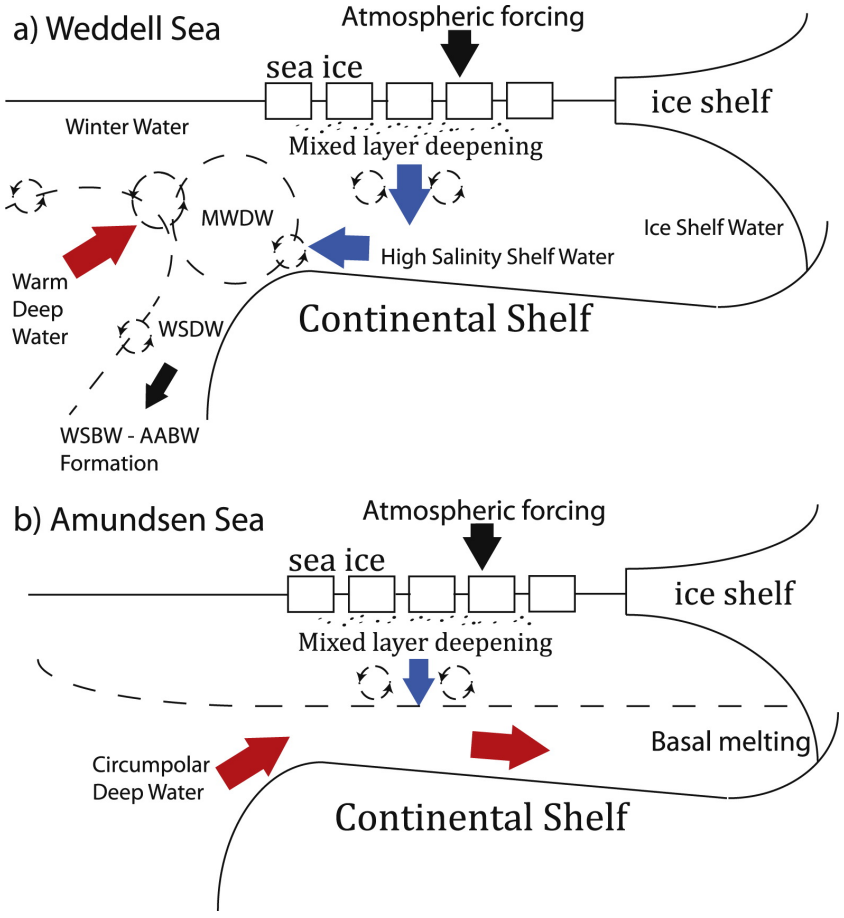

FIGURE 1.5: Schematic of processes and the resulting oceanic regimes in the a) Weddell Sea and b) Amundsen Sea (Petty et al. 2013).

1.4 Inter-annual variability in the Amundsen Sea

The average oceanic conditions in the Amundsen Sea were discussed in the previous section. However, the region experiences a strong inter-annual variability. This section discusses this inter-annual variability and the possible drivers of it.

Observations taken on the continental shelf in the Amundsen Sea show that the mCDW layer exhibits a strong seasonality and inter-annual variability in its thickness and temperature with, for example, a pronounced cooling in 2012 (Dutrieux et al. 2014) (Figure 1.6). In this year the top of the thermocline is about 250 metres deeper compared with that of any year previously measured at that time. This therefore leads to large inter-annual variability in the oceanic heat content (OHC) on the continental shelf in the Amundsen Sea.

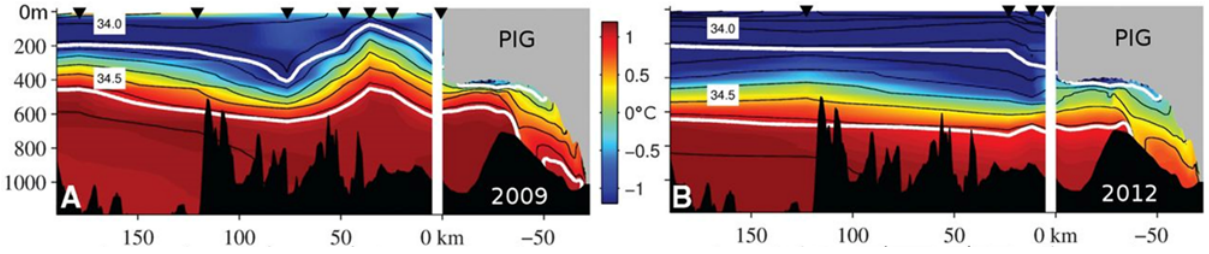

FIGURE 1.6: Observed and simulated ocean conditions in a) 2009 and b) 2012. Section of observed and simulated (under ice shelf) 2009 and 2012 potential temperatures (colour) and salinity (black contours) along the Pine Island Trough and underneath the PIG Ice Shelf (Dutrieux et al. 2014).

This inter-annual variability is hypothesised to be linked to inter-annual variability in the winds over the continental shelf break affecting the ocean surface stresses over trough entrances (Kimura et al. 2017, Thoma et al. 2008, Webber et al. 2019). Westerly wind anomalies result in offshore Ekman transport, sloping the pressure gradient and thus barotropically strengthening an eastward shelf break CDW undercurrent that is present in the region (Assmann et al. 2013). This undercurrent is present, because of sloped isopycnals present off the shelf break at depth. The strengthening of the undercurrent enhances OHC flux onto the continental shelf, via a speeding up of the undercurrent as shown in Figure 1.7. This increase in OHC flux at the shelf break drives changes in the OHC on the continental shelf. However, the enhancing of the heat flux onto the continental shelf is suggested to be via different processes occurring in the different troughs, due to bathymetry and thermocline differences (Dotto et al. 2019). The troughs in the east leading to the PIG Ice Shelf have deeper entrances and shallower thermoclines, enabling CDW to intrude onto the shelf. Therefore, for a warming example, as the undercurrent accelerates this increases CDW volume flux onto the shelf, leading to increases in the thickness of the CDW layer in this trough. However, in the west, at the entrance to the Dotson Trough that leads to Dotson Ice Shelf, the thermocline is deeper and the entrance to the trough is shallower. Therefore an acceleration of the eastward undercurrent subsequently uplifts isopycnals, via Ekman pumping, enabling a warmer type of CDW to enter this trough (Dotto et al. 2019).

The wind anomalies over the continental shelf break have been linked to inter-annual tropical Pacific variability (Dutrieux et al. 2014). This hypothesis has received direct observational support, as the cooling shown in 2012 was preceded by La Niña conditions

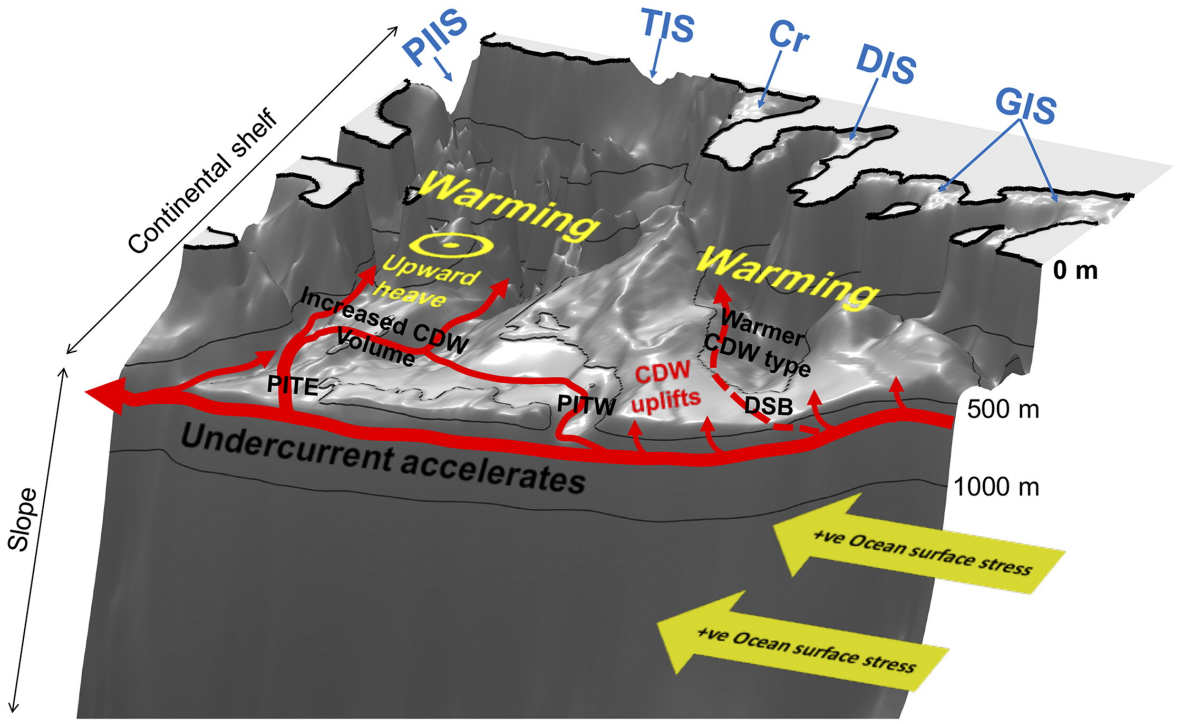

FIGURE 1.7: Schematic of the processes leading to a period of warming in the Amundsen Sea in the two troughs of Pine Island and Dotson (Dotto et al. 2019).

in the central Pacific. La Niña and El Niño affect the surface wind velocities in the central Pacific, which is suggested to affect the atmospheric forcing around the Amundsen Sea and specifically for this hypothesis the atmospheric forcing over the continental shelf break. The hypothesis follows where El Niño favours enhancing melting and La Niña favours decreased melting. This is because in general El Niño is associated with increased westerly wind stress over the continental shelf edge and La Niña is associated with easterly anomalies in the wind stress. Before the 2012 cold ocean anomaly there was unusual atmosphere forcing applied to the Amundsen Sea. In the preceding year, the 12 month integral of zonal wind north of the continental shelf (taken over the black box in Figure 1.8B) became easterly, shown in Figure 1.8A, which is unprecedented within the recorded data sets (Dutrieux et al. 2014). This change is suggested to be caused by a Rossby wave from the central Pacific area shown in Figure 1.8C. However, the specifics of the processes involved within this hypothesis are beyond the scope of this thesis.

Although the role of winds affecting the CDW flux onto the continental shelf appears to be the dominant driver of the inter-annual variability of OHC on the shelf, there is evidence also for the role of sea ice growth in modulating OHC (St-Laurent et al. 2015, Webber et al. 2017). In this hypothesis sea ice growth drives convection, which increases the mixed layer depth. The mixed layer therefore mixes with the deeper CDW, which leads to a cooling and reduction in thickness of the CDW layer, as well as a warming and increase in thickness of the mixed layer. The gain in heat in the mixed layer is consequently vented to the atmosphere. Therefore an inter-annual variability in sea ice

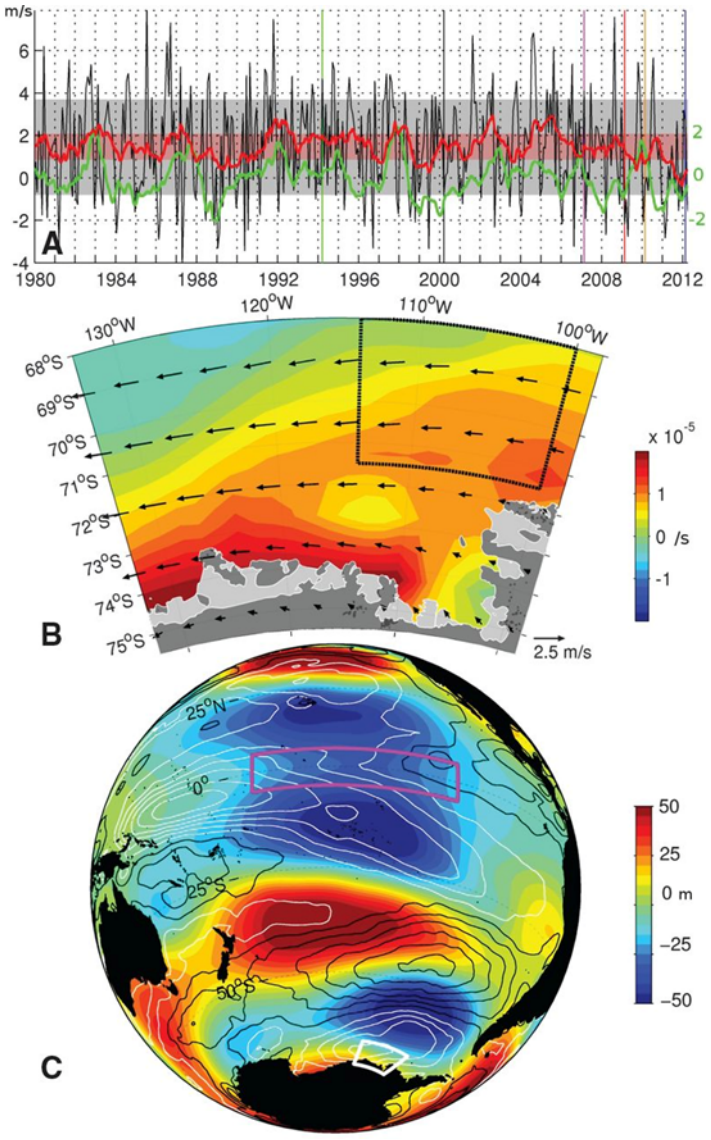

FIGURE 1.8: A) Monthly mean zonal winds at 10 m (black) and its running 12 month preceding integral (red) averaged over the black box in (B). Green shows the monthly sea surface temperature anomaly averaged over the magenta box in (C). B) Annual mean of anomalies in surface wind in surface wind and wind stress curl of 2011 in respect to the 1979-2011 average. C) Annual mean of anomalies in atmospheric geopotential height at 200 hPa (colour) and sea surface wind (contour) in 2011, with respect to 1979-2011 climatology, with white (black) contours denoting negative (positive) (Dutrieux et al. 2014).

growth could, due to this hypothesis, drive inter-annual variability in the OHC on the continental shelf. In addition to the role of salt fluxes some studies have investigated the effects of heat fluxes on the annual cycle and inter-annual variability of OHC. Heat loss is suggested to drive progressive cooling and deepening of the mixed layer, with localised intense heat loss in polynyas causing convective chimneys (Webber et al. 2017). This process therefore could drive inter-annual variability of OHC in front of ice shelves like PIG Ice Shelf. However, several studies disagree on the length period of sea ice production and cooling that could have caused a substantial cold event in late 2012,

with a modelling study suggesting it originated from a short period of intense sea ice production and heat loss (St-Laurent et al. 2015), while an observational data study suggested the heat loss was more prolonged (Webber et al. 2017).

Therefore there are two hypothesises for what causes the observed inter-annual variability in OHC on the continental shelf in the Amundsen Sea. One hypothesis is that large scale atmospheric events affect winds over the continental shelf break, which affect the OHC flux onto the shelf. Another hypothesis is that the inter-annual variability is driven by local processes like sea ice growth modulating OHC on the continental shelf. Therefore the two hypothesises are for whether OHC variability is driven via local processes or far field forcings. In addition to effects of sea ice, other local processes, including the inter-annual variability of the regions other freshwater sources could effect the inter-annual variability of the OHC. Understanding the inter-annual variability of the OHC on the continental shelf is important as it directly drives the inter-annual variability of the ice shelf melting on the continental shelf.

The changes in the ocean forcing applied to the ice shelves in the region not only affect the melt rates of the ice shelves, but over time their structure and position, possibly leading to the glacial retreat. This has been investigated in the Pine Island Glacier case by taking sediment cores at A, B and C, shown in Figure 1.9. It was found that this current phase of retreat of the ice shelf started in the 1940s (Smith et al. 2017), by a climatically induced peak of the ocean forcing in the area, with the previous stable grounding line being on a ridge shown in Figure 1.9a. Comparing these sediment cores revealed that an oceanic connection was created to the inner cavity at 1945 ± 12 years, allowing sediments to enter the inner cavity. This progressed, leading to the ice shelf becoming un-grounded from the ridge in 1970 ± 4 years. Once the ice shelf was un-grounded from the ridge more warm water would be able to reach the ice shelf close to the grounding line, vastly increasing the basal melting that would have occurred. Therefore once this change had occurred glacier retreat would have been set in motion. It is however possible for the West Antarctic Ice Sheet to be stable on longer time scales even with decadally varying oceanic forcing (Snow et al. 2017). However, superimposed on the natural variability of the winds is evidence of an anthropogenic increase of westerly wind anomalies over the continental shelf break, suggesting that warm CDW anomalies may have become more prevalent and could possibly have led to the imbalance of the glaciers in the region (Holland et al. 2019).

In addition, to the direct effect of the changing of OHC on the melting of the ice shelves in the region, other processes also affect the retreat of these glaciers. Most of the West Antarctic Ice Sheet lies below sea level and so it is a marine ice sheet. Therefore many of the glaciers in the Amundsen Sea region are susceptible to marine ice sheet instability. This is whereby oceanic melting and the subsequent retreat of these glaciers cause the glacier to ground in deeper water. This is because the grounding line in this region has a reversed sloped bed, where it becomes deeper inland. Therefore thicker ice is exposed,

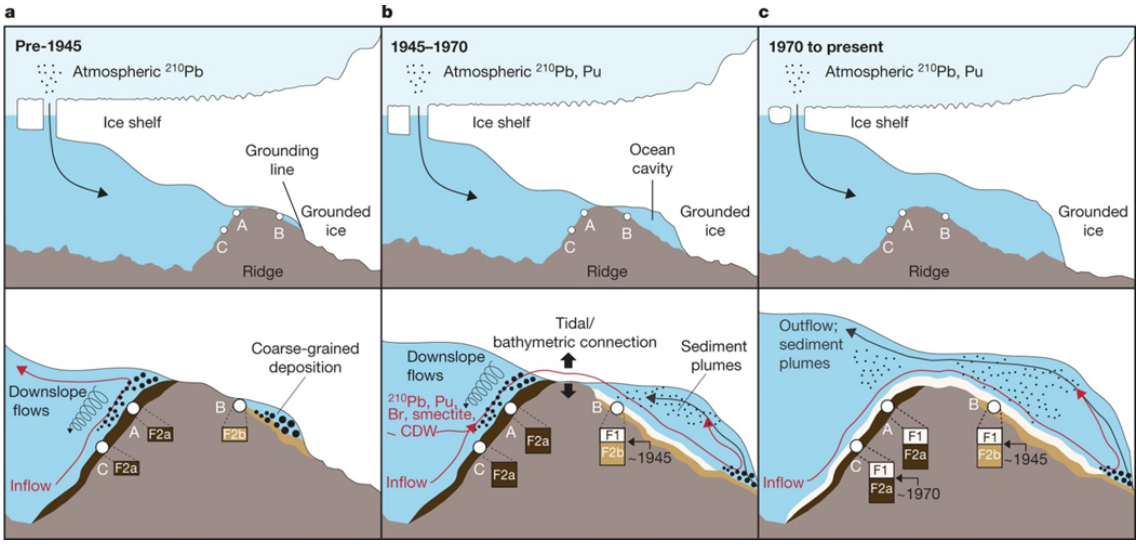

FIGURE 1.9: The un-grounding process of Pine Island Glacier and the timescale of the process, as determined by sediment cores. Top panel show the overall positions of the ice shelf and the bottom panel is zoomed in on the ridge region for the periods a) pre - 1945 b) 1945 - 1970 c) 1970 - present (Smith et al. 2017).

which is a key factor for determining the ice flux across the grounding line (Joughin & Alley 2011). This thicker ice is also exposed to more oceanic forcing, leading to flotation, basal melting and iceberg production causing to a positive feedback loop. This positive feedback could lead to rapid retreat and substantial sea level rise.

1.5 Freshwater sources

So far oceanic conditions have been explored in order to understand the ocean forcings causing ice shelves to thin in the Amundsen Sea region. This ice shelf thinning could change the freshwater balance in the region. This section therefore describes the different sources of freshwater in the Amundsen Sea region and their effects on the ocean.

The different inputs of freshwater change the density of seawater by changing its salinity and temperature. For illustrative purposes and in order to motivate the importance of freshwater in the polar regions, the linear equation of state is stated as

$$\rho \approx \rho_0 + \alpha(T - T_0) + \beta(S - S_0). \tag{1.1}$$

This equation describes the density of seawater ρ for small changes in density, where ρ_0, T_0 and S_0 are reference density, temperature and salinity respectively and T and S are in-situ temperature and salinity. α and β are the thermal expansion and haline contraction coefficients respectively.

In the the polar regions freshwater is more important to ocean dynamics and processes compared to the other regions. This is because density is strongly dictated by salinity

in the polar regions (Gill 1982), as thermal expansion is less at lower temperatures, going down to 0.05 kg m^{-3} K^{-1} in the polar regions, while thermal expansion increases to 0.32 kg m^{-3} K^{-1} in the tropical regions (Roquet et al. 2015). In contrast the haline contraction is relatively constant between different regions and conditions around the world, with it having a value of 0.80 kg m^{-3} $(g/kg)^{-1}$ in the polar regions and a value of 0.74 kg m^{-3} $(g/kg)^{-1}$ in the tropical regions. In addition there are changes to the ranges of temperature and salinity present in the different types of regions, with the polar regions having a smaller thermal range and a higher salinity range compared to the tropical regions, leading to the polar oceans being salt stratified. In particular, in the Amundsen Sea there is an observed vertical salinity range of $\sim$ 0.8 g/kg between the CDW and WW layers on the continental shelf and only a $\sim$ 2 °C vertical range in temperature (Dutrieux et al. 2014), with the warmest water at the bottom of the water column which implies that the water column must be salt stratified.

Some freshwater sources like precipitation, ice shelf meltwater and iceberg melt originate from the atmosphere. Therefore, these sources are referred to as meteoric freshwater.

1.5.1 Sea ice

Sea ice is an important feature of the Amundsen Sea, with persistent sea ice in the region making the region historically and even presently one of the hardest regions to access in Antarctica. Net sea ice salt flux from sea ice growth/melt is the most important factor in determining the evolution of the mixed layer in the Amundsen Sea (Petty et al. 2014), which has implications for biological production and oceanic circulation in the region. Observations in the region and the similar Bellinghausen Sea to the east show an average sea ice concentration of 81 %, with a standard deviation of 28 % and an average thickness of 0.9 m, with a standard deviation of 0.87 m (Worby et al. 2008). In the austral winter in the south of the Amundsen Sea there is an average sea ice growth, with average sea ice transport northward and then sea ice melt in the austral spring (Abernathey et al. 2016), so the region is thought to be a net sea ice export region. Modelling studies suggest that one quarter of sea ice volume is due to snow-ice formation, due to high precipitation in the Amundsen Sea, aiding the formation of thick sea ice in the region, despite the sea ice divergence (Assmann et al. 2005).

The seasonal cycle in the melting and freezing of sea ice creates a seasonal cycle in the upper column of the ocean and therefore the water column stratification. Sea ice melt in the austral spring/summer freshens the surface layer and hence increases stratification in the water column. However, in the winter, sea ice formation and the subsequent brine rejection cause convection, increasing the mixed layer depth and hence reducing the stratification of the water column. The following summer's sea ice melt leads to the creation of the Winter Water (WW) layer in the water column, which is the remains of the previous winter's mixed layer. The mixing that occurs in the winter can lead it to

interact and mix with the CDW at depth. This process entrains warmer water below into the mixed layer, limiting sea ice growth (Martinson 1990).

The covering of sea ice affects the wind forcing on the ocean, acting like a mediator between the atmosphere and the ocean (Kim et al. 2017, Dotto et al. 2019). Wind forcing on sea ice and blockages caused by land, ice shelves or grounded icebergs can create convergence and divergence zones, with divergence zones possibly creating persistent sea ice free areas of ocean, which are known as polynyas. Two such notable polynyas are present in the Amundsen Sea, which are the Amundsen Sea Polynya (ASP) and the Pine Island Polynya (PIP), with locations shown in Figure 1.10, along with other smaller coastal polynyas.

Sea ice variability is mainly wind driven in the West Antarctic regions of Antarctica (Assmann et al. 2005, Holland & Kwok 2012). A large inter-annual variability in sea ice extent is present in the Amundsen Sea with for example large decreases in summer sea ice in the late 1980s and 1990s, which removed much of the multi-year ice present in the region at the time (Jacobs & Comiso 1993). Long term changes of sea ice duration in localized areas of the Amundsen Sea have also been observed over the period 1979 to 2014, with a negative trend in sea ice duration off the continental shelf and in the Amundsen Sea and Pine Island polynyas, with wind changes partially explaining these trends (Stammerjohn et al. 2015).

1.5.2 Precipitation and evaporation

Precipitation in the Amundsen Sea is a source of the meteoric water to the ocean. It enters the ocean either directly or first onto sea ice and the ice sheet, where it then subsequently eventually enters the ocean. The Amundsen Sea is a region of relatively high precipitation (Lenaerts et al. 2012). Therefore precipitation is a potentially important freshwater source for the region, as well as for importance in its role in meteoric ice formation. Precipitation can fall in different forms for example snow and rain, with the former therefore requiring latent heat to melt on contact with the ocean. Due to the high concentration of sea ice in the region precipitation will mostly land on the sea ice, rather than directly into the ocean, and hence be advected by the dynamics of the sea ice. Therefore sea ice dynamics and concentrations in the region may play an important role in the distribution of the effects of precipitation. Evaporation from the ocean would also be affected by the high sea ice concentrations present in region as it forms a barrier between the ocean and the atmosphere.

Remote atmospheric forcings have been found to affect precipitation in the region (Marshall et al. 2017, Bromwich et al. 2000). However, when dominant modes of variability are removed a trend of increased precipitation in the Amundsen region is observed between 1801-2000 based off ice core records (Medley & Thomas 2019).

1.5.3 Icebergs

Icebergs are formed in the Antarctic by calving events at the edges of ice shelves or by the break up of larger icebergs. These icebergs can travel great distances from their sources, usually following oceanic currents (Gladstone et al. 2001), but wind forcing can affect smaller iceberg drift as well (Wagner et al. 2017). Icebergs, as a freshwater source, differ from sources like sea ice melt and precipitation, as icebergs can release cold and fresh meltwater in the surface layers and at depth, which can effect sea ice formation in opposing ways (Jenkins 1999, Merino et al. 2016). In addition, icebergs impact biological production in the Southern Ocean (Biddle et al. 2015) and can influence local ocean circulation around the iceberg (Stern et al. 2015).

With the Amundsen Sea hosting several rapidly melting and thinning ice shelves, it is known for its abundance of icebergs. Icebergs are found to be produced by a stream of small to medium icebergs calving from the region's ice shelves, with inter-annual variability largely caused by the episodic calving of giant icebergs (Mazur et al. 2019). The proportion of ice loss from ice shelves in the Amundsen Sea region due to iceberg calving, rather than basal melting, varies significantly depending on the specific ice shelf. However, on average ice loss due to iceberg calving and basal melting are of comparable magnitudes over the Amundsen Sea region (Rignot et al. 2013, Depoorter et al. 2013). Over the period 2006-2012 the average period of time where icebergs remained in the Amundsen Sea was estimated using satellite data to be 2.5 years (Mazur et al. 2019), with also Amundsen Sea icebergs modelled to stay close to the coast (Merino et al. 2016). Therefore iceberg melt is a potentially significant source of freshwater in the Amundsen Sea.

There is also a semi-permanent feature of grounded icebergs on a seabed feature which shall be referred to as Bear Ridge (Mazur et al. 2019, 2017) and these grounded icebergs will henceforth be referred to as the Bear Ridge icebergs (BRI). The location of the BRI are shown in the satellite images in Figure 1.10b,c. The presence of BRI forms the Amundsen Sea Polynya (ASP) to its west (Figure 1.10a), by blocking the westward movement of sea ice (St-Laurent et al. 2017, 2015). A recent study suggests more icebergs grounded on this topographic feature during the period 2006 to 2012 compared to observations in 1997 (Mazur et al. 2019), possibly due to an increase in iceberg calving from local ice shelves.

1.5.4 Ice shelves

In Amundsen Sea region there are multiple small and medium sized ice shelves (Figure 1.4), which are the (west to east) Getz, Dotson, Crosson, Thwaites, PIG, Cosgrove and Abbot ice shelves. These ice shelves have some of the highest thinning rates in all

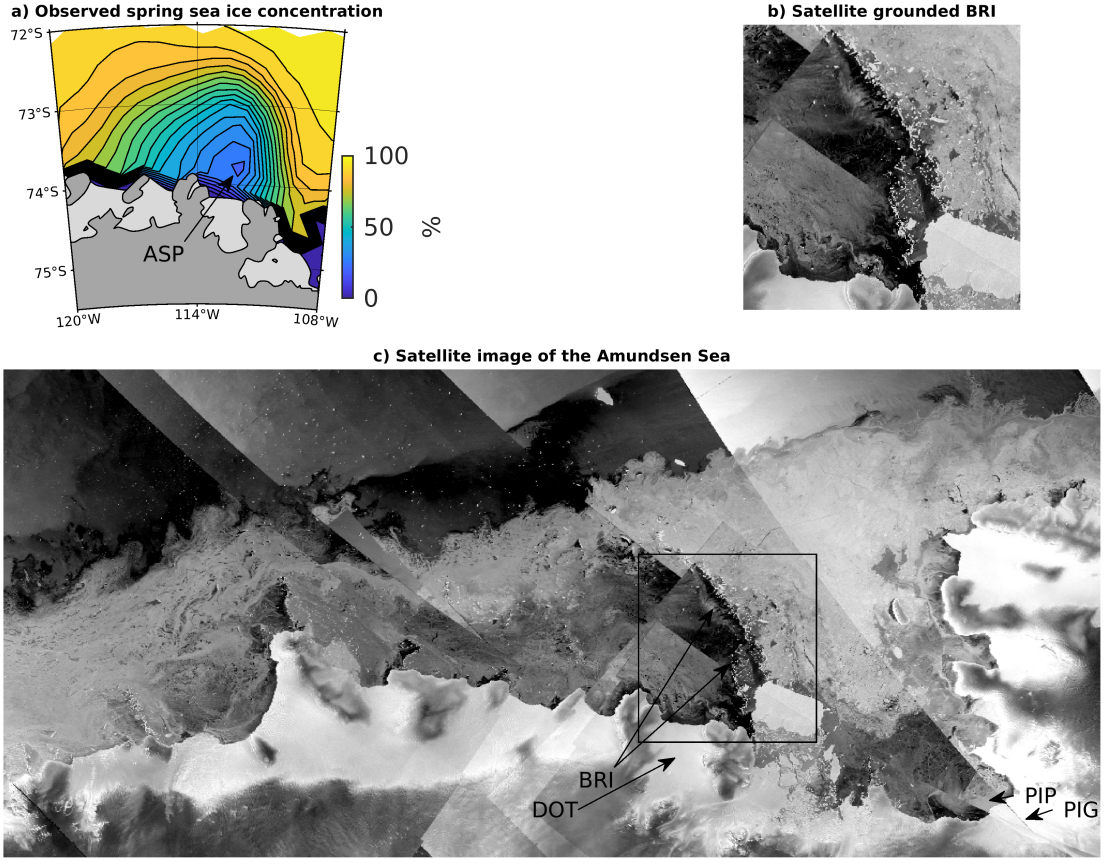

FIGURE 1.10: (a) Spring satellite observations of the AMSR-E sea ice concentrations (2003-2010) (Cavalieri et al. 2014). (b)(c) Satellite image mosaic composed of Copernicus Sentinel-1 SAR (Synthetic Aperture Radar) data. The composite uses imagery acquired between 30th April 2017 and 6th May 2017. Image composite was processed by BAS using Google Earth Engine. The black box in (c) shows the area in (b). Key locations are shown in (a)(c), where DOT = Dotson Ice Shelf, BRI = Bear Ridge grounded Icebergs, PIG = Pine Island Glacier Ice Shelf, PIP = Pine Island Polynya and ASP = Amundsen Sea Polynya.

of Antarctica (Paolo et al. 2015)(Figure 1.1), due to the warm CDW that intrudes to their bases.

As a freshwater source, basal melting from ice shelves is different compared to most other freshwater sources, as it is input at depth. This could alter the stratification of the water column, possibly stabilising the water column where convection would have otherwise happened due to brine rejection from sea ice growth (Hellmer 2004). This change in the stratification can strengthen currents, for example a coastal current exists in the region due to ice shelf meltwater, as shown in observations (Biddle et al. 2017, Nakayama et al. 2013) and modelling studies (Kimura et al. 2017, Jourdain et al. 2017). An increase in the ice shelf freshwater fluxes could impact other circulations in the region as well. There is evidence that increasing ice shelf freshwater could increase overturning circulations, with the increased freshwater output from the ice shelf driving a buoyancy

driven increase to the overturning circulation present (Jourdain et al. 2017). In addition, in front of PIG Ice Shelf there is a cyclonic gyre circulation spanning Pine Island Bay. An increase in ice shelf freshwater from PIG Ice Shelf could impact the strength of the gyre that is present in front of the ice shelf. However, there could be other drivers for this gyre, like wind forcing that could impact or possible drive the gyre strength. Therefore the drivers of inter-annual variability of the strength of the gyre and the overturning circulation are still uncertain and therefore it is uncertain what the full impact of an increased ice shelf freshwater flux would have on these circulations.

The ice shelf melting in the Amundsen Sea was found to have a seasonal cycle in a modelling study (Kimura et al. 2017). The seasonal cycle of the melt rates of the thinner portions of the ice shelves were found to peak in the January and February, which coincides with the timing of peak surface warming by shortwave radiation. However, the overall melting of the different ice shelves were found to have different peak times, with for example PIG and Thwaites peaking in August-October instead. This was because the melting in the deeper parts of the ice shelves was not linked to surface processes. Instead the overall melting was found to correspond to the seasonal cycle of zonal wind stress and wind stress curl over the continental shelf break, thus possibly linked with peak seasonal OHC flux onto the continental shelf (Kimura et al. 2017). However, this is in contrast with some observations of ice shelf melting of PIG Ice Shelf, where a clear seasonal cycle was not observed (Davis et al. 2018). This does have the caveat though that this observation time series was only one year long.

Due to the strong inter-annual oceanic variability in the region as discussed in Section 1.4, the ice shelves could be expected to have a large inter-annual variability in ice shelf melting. The change in ice discharge from ice shelves in the Amundsen Sea will change the poorly known freshwater balance of the region. This increased input of freshwater could affect the on-shelf currents and mixing, due to density being strongly controlled by salinity in the polar regions (Gill 1982). This could have many effects, including regional sea level rise (Rye et al. 2014) and a freshening of the downstream Ross Sea (Jacobs & Giulivi 2010). Another study found that an increase of ice shelf freshwater in the Amundsen sea reduces the sea ice extent in this region, while in other regions the opposite occurs (Merino et al. 2018).

Observed vertical distribution of ice shelf meltwater finds it to be present within the thermocline (Kim et al. 2016, Biddle et al. 2019) It has been suggested that a overturning centrifugal instability, which is triggered as the meltwater leaves the ice shelf cavity, promotes vigorous lateral export and turbulent mixing which settles the ice shelf meltwater at depth (Naveira-Garabato et al. 2017). Observations of ice shelf meltwater are sparse and therefore there is large uncertainty as to the variability of the iceshelf meltwater vertical distribution. However, some studies do show some variability in the magnitude and vertical distribution in meltwater concentration in front of PIG and

Dotson ice shelves by comparing different years of summer observations(Dutrieux et al. 2014, Jenkins et al. 2018).

1.6 Existing knowledge of freshwater in the Amundsen Sea region

So far the oceanic conditions and the different sources of freshwater in the region have been examined. In this section previous work done to investigate the sources and distribution of freshwater as well as their effects in the Amundsen Sea are discussed, along with the various techniques other studies have employed. This section will specifically explore studies and methods using field observations, satellite observations and numerical models.

1.6.1 Field observations

The ratio of stable oxygen isotopes can used as a indicator for the presence of meteoric freshwater in the ocean, with this ratio defined as

$$\delta_{sam} = \frac{R_{sam} - R_{std}}{R_{std}} \times 1000, \tag{1.2}$$

where sam is the sample value and std is the reference value (Rohling 2013). R is the heavy/light ratio (^{18}O/ ^{16}O), with ^{18}O and ^{16}O being the two main oxygen isotopes present in seawater. Their content can be altered by condensation and evaporation. Most evaporation occurs at mid latitudes, with evaporation extracting a higher proportion of the lighter ^{16}O (Epstein & Mayeda 1953) and a higher proportion of the heavier ^{18}O is precipitated out before precipitation occurs in the polar regions (Rohling 2013). Therefore in the polar regions meteoric water, which includes iceberg melt and ice shelf meltwater, is relatively depleted in ^{18}O compared to seawater. At depth δ_{sam} can considered as a conservative tracer and therefore the calculation of δ_{sam} of seawater samples can be used as an indicator of meteoric freshwater in the polar regions, with a lower δ_{sam} indicating the presence of meteoric freshwater (Meredith et al. 2008, Price et al. 2008, Randall-Goodwin et al. 2015). However, this technique cannot distinguish between different meteoric freshwater sources for example precipitation, iceberg melt and ice shelf meltwater. Noble gases can used instead as an unambiguous tracer of glacier meltwater, with the five inert noble gases exhibiting a unique dissolved saturation pattern due to formation and addition of glacial meltwater to seawater (Loose & Jenkins 2014).

While oxygen isotope measures meteoric freshwater content in the ocean and noble gas measurements can determine freshwater content in the ocean, the data is sparse and

only in the summer time. In addition, noble gas measurements are expensive and time consuming. However, a few such studies have been undertaken in the Amundsen Sea. Ice shelf meltwater has been traced in the Amundsen Sea with its highest concentrations close to the coast (Biddle et al. 2017, Nakayama et al. 2013). In addition, one study has examined the meteoric and sea ice freshwater sources in and around the ASP (Randall-Goodwin et al. 2015). Noble gas observations of ice shelf meltwater are very sparse but a few such studies in the Amundsen Sea do exist, which observe the spreading of ice shelf meltwater in the region (Biddle et al. 2019, Kim et al. 2016).

1.6.2 Satellite observations

Satellites have been increasingly used to observe oceanographic, atmospheric and cryospheric features. These enable the gaining of large amounts of data over large areas and are especially useful in gaining data from hard to reach regions like Antarctica.

Satellites have been used to gain information on the various inputs of freshwater into the Amundsen Sea region. Satellites have been used to quantify basal melt rates from surface height changes of ice shelves (Rignot et al. 2013, Depoorter et al. 2013). Sea ice concentrations can also be determined from satellites with various data sets available enabling observations over the full season and over the whole region (e.g. Cavalieri et al., 2014). Iceberg tracking can also be done via satellites, increasing understanding of iceberg pathways, iceberg residence time in the region and on grounded iceberg features like the BRI (Mazur et al. 2019, 2017).

Satellite altimetery data has also been used in order to investigate the effect that excess ice shelf freshwater has had on regional sea level rise (Rye et al. 2014). Only austral summer months were used in the study in order to avoid sea ice, as this interferes with satellite sea level measurements. This study found that sea level rise along the Antarctic coast was 2 $\pm$ 0.8 mm yr^{-1} greater than that of the regional mean for the Southern Ocean south of 50° S (1.2 $\pm$ 1.5 mm yr^{-1} above the global mean sea level rise). Model simulations were used to confirm that this is due to mainly steric (density induced) adjustment, rather than barystatic (mass induced), as the waters around Antarctica have become fresher, especially the surface waters, due to the increased freshwater input from various sources.

1.6.3 Numerical models

In regions that lack widespread observations, like in the Amundsen Sea, models can be a useful tool in order to further understand the region. Here the benefits and limitations of oceanographic models will be discussed, along with details of modelling studies of the Amundsen Sea.

The type of model used depends on hypothesis that is to be tested and the computational resources available. Models can range from simple 1D models depicting one process, to general circulation models and up to Earth systems models. It is possible to couple oceanic models to the atmosphere, sea ice and ice shelves/ice sheet models. However, it is not always beneficial nor possible due to computational restrictions.

The small internal Rossby radius of deformation that occurs in Antarctic regions provides a minimum model resolution requirement. However, due to model resolution being restricted because of restrictions on computational power, it is impossible to resolve all process that occur. Therefore models have to rely on parameterisations to account for the effects of those unresolved processes. For example parameterisations can be employed to take into account vertical mixing and small scale ice shelf melting processes.

Modelling studies have already used to try and improve our knowledge of the distributions of freshwater sources in Antarctic regions. Regan et al. (2018) examined the freshwater balance of the nearby Bellingshausen Sea by adding tracers to track the influence of each source of freshwater in a regional ocean model. There, it was found that sea ice dominates the seasonal freshwater cycle, all freshwater sources make comparable contributions to the annual mean, and sea ice and precipitation dominate the inter-annual variability. Studies of ice shelf freshwater alone have been performed in the Amundsen Sea (Kimura et al. 2017, Nakayama, Timmermann, Rodehacke, Schroeder & Hellmer 2014), with ice shelf meltwater found to have highest concentrations close to the coast, setting up the strong westward geostrophic coastal current. However, no such study has examined the freshwater balance in the Amundsen Sea by tracing all freshwater components.

Several modelling studies have been undertaken to investigate different feedback mechanisms involving ice shelf meltwater in the Amundsen Sea. One possible feedback mechanism is the effect of ice shelf meltwater on oceanic currents. It was found that increased ice shelf meltwater strengthens the circulation and coastal currents, which increases the amount of heat that enters the ice cavity, driving more melting (Jourdain et al. 2017, Donat-Magnin et al. 2017, Kimura et al. 2017). In addition, Webber et al. (2019) shows the importance of the ice shelf meltwater driven overturning circulation on heat transport, suggesting that heat driven melting and melt driven heat transport both occur. However, it is also possible that other feedback mechanisms exist in the Amundsen Sea involving the other freshwater sources.

Some modelling studies have included representations of the grounded BRI in model simulations (St-Laurent et al. 2015, 2017). However, only an initial study into the effects of the grounded BRI on CDW intrusions has been conducted by Nakayama, Timmermann, Schröder & Hellmer (2014), in which static sea ice was used to simulate the grounded BRI. In this study a regional Amundsen Sea model was simulated from 1979-1988 using a reference atmospheric reanalysis and one where the average eastern Amundsen Sea

winter air temperature is $\sim$ 20 ^{o}C colder. This study found that there was a blocking effect of the grounded BRI on sea ice export from Pine Island Polynya and the consequent reduction in sea ice growth in this polynya. However, this study found that BRI had little effect on bottom CDW temperature in front of PIG Ice Shelf under standard atmospheric forcing, but ocean conditions in Pine Island Bay were slightly warmer with the BRI, when the cold-biased forcing was used. This suggests that grounded BRI may act as a buffer to CDW modulation in anomalously cold years in atmospheric forcing.

1.7 Aim of research

It has been shown that freshwater is important in the polar regions, with salinity strongly dictating density. Therefore freshwater can effect the currents and mixing in the region. In addition, it has been shown that ice shelves are thinning in the Amundsen Sea region, due to changes in ocean forcing, which could change the local freshwater balance. However, it has been shown that the freshwater balance in the Amundsen Sea is poorly known. Oxygen isotope and noble gas studies in the region can reveal the distribution of freshwater sources in the region. However, this data is very sparse and only in summer time. In addition, the thinning of the ice shelves could change the iceberg distribution and iceberg melt in the region.

Motivated by these points, this thesis has two main aims, i) to quantify the local freshwater balance and ii) to examine the influence of grounded BRI and iceberg melt. In both of these, to determine possibilities for feedbacks on ice shelf discharge is an overarching aim. This thesis therefore has the aim to understand the physics behind the freshwater balance and processes described in order to gain predictive skill for projections of future sea level rise. Currently icebergs are not represented in large scale climate models and they may be important for the Amundsen Sea region. Therefore examining their influence on the region has the purpose of determining if they are required to be represented in large scale models. This includes determining whether or the not the represented icebergs need to simulated to be able to ground and if their interaction with sea ice should be represented in large scale models as well. The aim of understanding feedbacks in the model and system is to help understand the non linear relationship of ice shelf melting and therefore to help improve parameterisations of ice shelf melting in large scale models and ice sheet models.

Therefore the aim of this thesis is to determine the local freshwater spatial and temporal distribution in the region and to the determine the possibilities of feedbacks in the thinning of the ice shelves in the region. In addition this thesis will extend the initial work done by Nakayama, Timmermann, Schröder & Hellmer (2014) on the effects of grounded BRI by considering the role of grounded BRI over the whole Amundsen

Sea, also considering the effects of iceberg meltwater, and investigating all underlying processes in detail, with focus of investigating possible feedbacks in the system.

Chapter 2 describes the two model set-ups that are used in this study, as well as improvements that have been made to them. One model is an idealised model based on the model used in Holland (2017), but has a passive ice shelf meltwater tracer coded into it for this thesis. In addition, the model is developed to enable a new method to calculate the effect of ice shelf freshwater flux on the ice shelf's melt rates and so to calculate the freshwater feedback effect. The other model is a regional Amundsen Sea model based on the model used in Kimura et al. (2017). A sea level fall is corrected, the model is tuned against observations and an addition of a representation of grounded BRI is added to the regional model for this thesis.

Chapter 3 employs the idealised model with ice shelf meltwater tracer. This model will be used to answer the question of how the vertical distribution of ice shelf meltwater changes with varying CDW thickness. This is because any distributional changes in the meltwater could affect the vertical salinity structure and currents, and a large inter-annual variability in CDW layer thickness is present in the region. In addition, this chapter employs this model to find out the strength of the freshwater feedback effect, which is the effect of the freshwater flux from the ice shelf on the melt rate of the ice shelf.

Chapter 4 employs the high-resolution regional model with passive freshwater tracers. This chapter first validates the model to observations and investigates the relative magnitudes and spatial distributions of the different freshwater components: ice shelf melt, sea ice melt/freeze, parameterized iceberg melt and the combined effect of precipitation and evaporation. This chapter then analyses the different freshwater fluxes' seasonality and inter-annual variability, along with investigating the covariance of inter-annual anomalies of freshwater fluxes. Finally, the chapter investigates the inter-annual variability of freshwater tracer distributions and the local freshwater balance in front of PIG and Dotson ice shelves.

Chapter 5 investigates the effect of grounded icebergs and iceberg melt in the region, using the regional Amundsen Sea model. The chapter first determines the effect of different representations of the grounded BRI on sea ice distributions and freshwater fluxes. Then the chapter investigates the effect of iceberg melt and grounded BRI on average OHC on the continental shelf and on the inter-annual variably of OHC in front of PIG and Dotson ice shelves. The potential for feedbacks in the system is considered, along with the effect of poorly constrained parameters.

Chapter 6 summarises the main conclusions from this thesis and discusses future research that could be undertaken.

Chapter 2

Model set-up and development

This chapter describes the model used in this thesis, its governing equations and the model set-ups used. Two different ocean model set-ups have been used to produce the results shown in this thesis: an idealised model and a full regional Amundsen Sea model. Both models use the Massachusetts Institute of Technology general circulation model (MITgcm). The idealised model will be used to investigate the vertical distribution of ice shelf meltwater, and to investigate the potential effect of local ice shelf freshwater on ice shelf melting. The realistic model will be used to look into the importance of the different sources in the freshwater budget of the region and investigating their distributions, along with the effect of iceberg melt and grounded icebergs in the region.

2.1 MITgcm

The MITgcm is a general circulation model which can be configured to be used for a range of scales and for both oceanic and atmospheric studies. The model can be used with and without the hydrostatic approximation. However, due to computational restrictions the models are simulated in the hydrostatic version, therefore the pressure at any point in the ocean is considered to be due to the weight of the ocean above it. The model was, however, developed to perform efficiently on a wide variety of computational platforms, enabling the intensive model setups planned to be used in this study. In addition, the model includes a packages for the inclusion of ice shelves and sea ice in the model, which are essential for this study. However, a weakness of the MITgcm model is the stepped representation of the ice shelf drafts, due to use of the z coordinate system. In addition, the use of z coordinate system, leads the simulation of the deep ocean to be generally of low resolution, due to the generally lower resolution set at depths due to computational limits. However, other models like the Regional Ocean Modeling System (ROMS) required bathymetry to be smoothed, which could impact results in this region.

Crucially models like ROMS struggle to representing ice shelf fronts, which is essential for the studies in this thesis.

The MITgcm model has several parameterisations which could be improved in the future. For example the model can employ the K-profile parameterization (KPP) scheme (Large et al. 1994), as a vertical mixing parameterisation. However, this vertical mixing parameterisation is unverified, due to lack of observations. In addition, the KPP mixing scheme was designed for open ocean, rather than for sea ice conditions and the Amundsen Sea has usual sea conditions compared to the rest of Antarctica regions. Alternatively, a constant vertical diffusion could be used as a vertical mixing parameterisation. However, this is a very idealised method for representing vertical mixing. Therefore the vertical mixing options are a parameterisation which could be improved in the future, though the options are deemed to be sufficient for use in the studies in this thesis.

The upper surface of the ocean in the models is set to be a linear free surface, where η is the height difference from the top model cell. This is a good approximation when $\eta << H$, where H is a fixed in time bottom depth. After this approximation the equation for the free surface becomes:

$$\partial_t \eta + \nabla_h . (\int_{-H}^{0} \overline{v}_h) dz = K \tag{2.1}$$

$$\partial_t \eta + \nabla_h . (H \overline{v}_h) = K \tag{2.2}$$

where K is an arbitrary volume flux and $\overline{v}_h$ is the depth-mean horizontal velocity (Campin et al. 2004). In both of the set-ups used in this thesis the model is set to use real freshwater fluxes, instead of being set to virtual salt fluxes. Therefore freshwater fluxes in the model affect the sea surface height rather than just the salinity content. The MITgcm code used in the idealised model study is checkpoint c65z, whereas for the regional model it is checkpoint c62r.

MITgcm calculations are based off the Navier Stokes equations with some assumptions applied. MITgcm assumes the flow is incompressible i.e. $D_t \rho << \rho \nabla . \vec{v}$. In addition the model assumes that density variations that occur due to dynamics are small compared to the reference density i.e. $\rho - \rho_0 << \rho_0$, which enables the model to use the Bossinesq approximation meaning that the momentum equations are simplified ($\rho \vec{v} \approx \rho_0 \vec{v}$). Therefore equations (2.3)-(2.8) show respectively the horizontal and vertical momentum equations, equation of continuity, equations for heat and salt and the equation of state (Marshall et al. 1997a,b):

$$D_t \vec{v_h} + (2\vec{\omega} \times \vec{v})_h + \frac{\nabla_h p}{\rho_0} = \vec{F}, \tag{2.3}$$

$$\partial_z p = -\rho g, \tag{2.4}$$

$$\nabla.\vec{v} = 0, \tag{2.5}$$

$$D_t\theta = Q_0, \tag{2.6}$$

$$D_tS = Q_s, \tag{2.7}$$

$$\rho = \rho(S, \theta, p), \tag{2.8}$$

where $\vec{v}$ and $\vec{v_h}$ are the three and horizontal two dimensional velocity vectors respectively, p is pressure, ρ is in-situ density, θ is the potential temperature and S is salinity. ρ_0 is a constant reference density, g is the constant gravitational acceleration. $\vec{F}$, Q_0, Q_s are arbitrary forcing fields. $\vec{\omega} = (0, \Omega\cos\theta, \Omega\sin\theta)$ is the rotation of the Earth, where θ is latitude and Ω is the angular velocity of the Earth.

The set-ups of the model used in this study use the equation of state derived in McDougall et al. (2003) and is of the form:

$$\rho(S, \theta, p) = \frac{P_1(S, \theta, p)}{P_2(S, \theta, p)}, \tag{2.9}$$

where the coefficients for the polynomials are:

$$\begin{aligned} P_1(S,\theta,p) = {} & 9.997 \times 10^2 + 7.352 \times 10^0\theta - 5.459 \times 10^{-2}\theta^2 + 3.984 \times 10^{-4}\theta^3 \\ & + 2.969 \times 10^0 S - 7.233 \times 10^{-3} S\theta + 2.124 \times 10^{-3} S^2 \\ & + 5.188 \times 10^{-6} pS + 1.040 \times 10^{-2} p + 1.040 \times 10^{-7} p\theta^2 \\ & - 3.240 \times 10^{-8} p^2 - 1.239 \times 10^{-11} p^2\theta^2 \end{aligned} \tag{2.10}$$

and

$$\begin{aligned} P_2(S,\theta,p) = {} & 1.000 + 7.286 \times 10^{-3}\theta - 4.608 \times 10^{-5}\theta^2 + 3.684 \times 10^{-7}\theta^3 \\ & + 1.808 \times 10^{-10}\theta^4 + 2.147 \times 10^{-3} S - 9.270 \times 10^{-6} S\theta \\ & + 4.765 \times 10^{-6} S^{3/2} - 1.783 \times 10^{-10} S\theta^3 + 1.634 \times 10^{-9} S^{3/2}\theta^2 \\ & + 5.308 \times 10^{-6} p - 3.032 \times 10^{-16} p^2\theta^3 - 1.279 \times 10^{-17} p^3\theta. \end{aligned} \tag{2.11}$$

2.1.1 Passive tracers

Model diagnostics of identifying individual freshwater fluxes are not sufficient to investigate the local freshwater balance, as this omits oceanic processes of advection and mixing that occur to the freshwater after entering the ocean. However, MITgcm has the passive tracer package, which enables passive tracers, that don't affect the ocean, but are affected by oceanic processes like advection. This package enables the tracking of the total surface freshwater. Under this package when freshwater is added to domain a volumetric flux of tracer occurs.

In order to understand the passive tracer package and demonstrate how the tracer sources will be implemented, a simple case is considered with no diffusion and advection occurring, but with the presence of a surface freshwater flux forcing. Therefore for a surface flux F and water column thickness $H_w = H + \eta$:

$$\frac{\partial H_w}{\partial t} = F \tag{2.12}$$

and for concentration ϕ and source concentration ϕ_s in the absence of any other forcing other than the surface freshwater flux,

$$\frac{\partial H_w \phi}{\partial t} = \phi_s F. \tag{2.13}$$

Then the product rule gives

$$\frac{\partial H_w \phi}{\partial t} = \phi \frac{\partial H_w}{\partial t} + H_w \frac{\partial \phi}{\partial t}. \tag{2.14}$$

Therefore substituting (2.13) and (2.12) into (2.14) gives after rearranging

$$\frac{\partial \phi}{\partial t} = \frac{F(\phi_s - \phi)}{H_w}. \tag{2.15}$$

This package was however modified and developed further by Regan et al. (2018), by linking the passive tracer package to the continuous release of individual freshwater fluxes, allowing the tracking of multiple individual freshwater sources. These improvements include the ability to trace freshwater fluxes which occur at depth as well, therefore enabling ice shelf meltwater to be traced in the model. This tool will be used in order to investigate the freshwater balance in the Amundsen Sea.

The tracing of multiple tracers in the model enables the possibility of different tracers interacting with each other. Therefore now the equations for the example of two surface freshwater fluxes, F_1 and F_2 instead of one effecting the change in the surface height H_w, is

$$\frac{\partial H_w}{\partial t} = F_1 + F_2. \tag{2.16}$$

This now yields two tracer concentrations ϕ_1 and ϕ_2, with source concentration of ϕ_{S1} and ϕ_{S2}. Therefore

$$\frac{\partial H_w \phi_1}{\partial t} = \phi_{s1} F_1. \tag{2.17}$$

Then using the product rule like before yields

$$\phi_1 \frac{\partial H_w}{\partial t} + H_w \frac{\partial \phi_1}{\partial t} = \phi_{s1} F_1, \tag{2.18}$$

and therefore substituting in (2.16) obtains

$$\phi_1 (F_1 + F_2) + H_w \frac{\partial \phi_1}{\partial t} = \phi_{s1} F_1. \tag{2.19}$$

Rearranging and completing the same steps for flux F_2 yields

$$\frac{\partial \phi_1}{\partial t} = \frac{1}{H_w}(F_1 \phi_{s1} - (F_1 + F_2)\phi_1), \tag{2.20}$$

$$\frac{\partial \phi_2}{\partial t} = \frac{1}{H_w}(F_2 \phi_{s2} - (F_1 + F_2)\phi_2). \tag{2.21}$$

This was expanded to n tracers, therefore enabling the tracing of all freshwater sources into the model. Therefore modifying (2.16) yields

$$\frac{\partial H_w}{\partial t} = \sum_{i=1}^{n} F_i. \tag{2.22}$$

Using (2.18), substituting in (2.22) and rearranging yields

$$\frac{\partial \phi_1}{\partial t} = \frac{1}{H_w}(F_1 \phi_{s1} - \phi_1 \sum_{i=1}^{n} F_i). \tag{2.23}$$

Therefore for j= 1,...,n, the general equation is:

$$\frac{\partial \phi_j}{\partial t} = \frac{1}{H_w}(F_j \phi_{sj} - \phi_j \sum_{i=1}^{n} F_i). \tag{2.24}$$

Setting $\phi_{sj} = 1$ to represent freshwater and defining the total freshwater flux to be $F_{tot} = \sum_{i=1}^{n} F_i$ yields the simplified general equation for j= 1,...,n,

$$\frac{\partial \phi_j}{\partial t} = \frac{1}{H_w}(F_j - \phi_j F_{tot}). \tag{2.25}$$

In the full 3D spatial version that is present in the model setups used in this study, the rate of change of tracer concentration in a given grid cell is also dependent on the process of the advection of the tracers. Therefore tracers can be advected from one grid cell to another following the velocities calculated for the ocean dynamics.

The simulations start with zero tracer and then the model is simulated with freshwater tracked from traced freshwater fluxes. The model then reaches a steady state of tracers in the domain, with the time period required for a tracer steady state to be reached being dependent on the model setup and domain. In the idealised setup this time period is found to be ~ 1 year and in the Amundsen Sea regional model set-up for the continental shelf region it is found to be ~ 10 years. This is because no tracers enter the model in the boundary conditions in set-ups used in this thesis and therefore the boundaries are a tracer sink.

The tracing of freshwater components yields negative tracers in the system. These occur when freshwater is removed from the domain i.e. a negative freshwater flux, which can occur due to evaporation and sea ice growth. This represents that the concentration of freshwater has decreased from an arbitrary initial condition. These negative concentrations which correspond to a loss in freshwater were tested by Regan et al. (2018) and were found to be conservative and suitable for study. Therefore as an example, in a self contained box model if both negative and positive freshwater fluxes are applied to it and the net freshwater flux is zero, then the total tracer in the box would be zero with the positive and negative tracers cancelling each other out.

For this thesis the ability to passively trace ice shelf freshwater was coded into the latest version of MITgcm (c65z). This was based on work done previously by Regan et al. (2018) in which an older version of MITgcm was used, however much of layout of MITgcm has changed since then. The tracers were tested to check that they are conserved within the model and that the expected amount of tracer was released.

2.1.2 Ice shelf melt

In both the idealised model set-up and regional model set-up, ice shelves are simulated in the models. MITgcm has a "shelfice" package, which is a thermodynamic model for basal melting underneath ice shelves. This model requires inputs of ice shelf draft topography and a reference pressure load file.

In order for the model to calculate the basal melting q_m (m/s), the model employs a parameterisation by Hellmer & Olbers (1989), which was modified by Jenkins et al. (2001). This parameterisation employs a system of three equations that express the conservation of heat and salt, along with a linear relationship between the temperature at the interface and the salinity. The equation for the conservation of heat and its turbulent transfer across the interface is

$$c_p \rho \gamma_T (T - T_b) + \rho_I c_{pI} \kappa \frac{T_s - T_b}{h} = -L \rho q_m, \tag{2.26}$$

with the first term in the equation representing the turbulent oceanic transfer of heat, while the second term is the transfer of heat from the ice shelf and the third term is the latent heat term. In the equation, $\rho = 999.8$ kg m^{-3}, c_p is the specific heat capacity of water. $L = 334 \times 10^3$ J kg^{-1} is the latent heat of fusion. γ_T is the turbulent exchange coefficient of temperature, $\rho_I = 917$ kg m^{-3}, $c_{pI} = 2000$ J kg^{-1} K^{-1} and $T_s = -20^oC$ are the density, heat capacity and temperature of the ice shelf. $\kappa = 1.54 \times 10^{-6}$ m^2 s^{-1} is heat diffusivity through the ice shelf and h is the ice shelf draft. T_b is the temperature at the interface. The equation for the conservation of salt and its turbulent transfer across the interface is

$$\gamma_S(S - S_b) = -S_b q_m, \tag{2.27}$$

where γ_s is the turbulent salinity exchange coefficient and S_b is the salinity at the interface. The salinity of the ice shelf is set to 0.

The relationship between the freezing point and salinity is weakly non linear, while it is a linear function of pressure (Millero 1978). However, for simplicity this method uses a linear relationship between the temperature at the interface and the salinity to yield

$$T_b = A_0 S_b + B_0 p_b + C_0. \tag{2.28}$$

The linear freezing equation coefficients are set to $A_0 = -0.0575$°C psu^{-1}, $B_0 = -7.61 \times 10^{-}4$°C Pa^{-1} and $C_0 = 0.0901$ °C (Holland & Jenkins 1999). p_b is the pressure at the interface.

In the regional model set-up with MITgcm version c62r the heat and salt turbulent exchange coefficients are set to $\gamma_T = 1 \times 10^{-4}$ m/s and $\gamma_s = (5.05 \times 10^{-3}) \times \gamma_T = 5.05 \times 10^{-7}$ m/s (Holland & Jenkins 1999). These $\gamma_{T,S}$ values have an implicit value of friction velocity (u^*) in them. However, in the idealised model with MITgcm version c65z, γ_s and γ_T have a direct velocity dependency and therefore are no longer constant. In this case this relationship is applied

$$\gamma_{T,S} = u^* \gamma^f_{T,S}, \tag{2.29}$$

where the friction velocity $u^* = \sqrt{c_d u_o^2}$, and where $\gamma^f_T = 0.011$ and $\gamma^f_S = 0.00031$. u_o is the matrix of the magnitudes of the velocities under the ice shelf in the boundary layer.

Therefore a more advanced ice shelf melting parameterisation is used in the idealised model set-up. The melting parameterisation in the regional model set-up is kept to be without velocity dependence, as the ice shelf cavities in the region's ice shelves are poorly known. This therefore means that the ice shelf cavity currents generated in the model may not be realistic and therefore the friction velocities may not be realistic. In addition keeping the melting parameterisation without velocity dependence means that

this study is consistent with the previous study which used the model set-up that the regional model in this thesis is based off (Kimura et al. 2017).

However, the ice shelf melting parameterisations chosen for the studies in this thesis may affect their results. For example the lack of explicit velocity dependence for the ice shelf melting parameterisation in the regional model may prevent some feedback processes from occurring in the system, which may affect the inter-annual variability of the ice shelf melt rates and OHC on the shelf. However, more generally ice shelf melting parameterisations are highly uncertain due to lack of observations and their effectiveness can vary from region to region. More specifically the Amundsen is a region where observations for ice shelf melting parameterisations are lacking. Therefore further studies are required in order to improve ice shelf parameterisations specifically for the Amundsen Sea region.

2.2 Idealised model

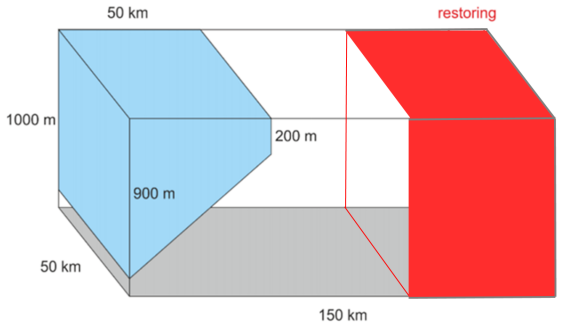

FIGURE 2.1: Idealised domain, showing the triangle like ice shelf and the area in which there is linearly increasing restoring zone (red). Diagram edited, but original from Holland (2017).

2.2.1 Model set-up

The idealised domain model uses the c65z revision of the MIT general circulation model, based on a set-up by (Holland 2017). In the idealised model set-up there is a triangle like ice shelf within a domain of ocean 1 km deep by 150 km by 50 km, with a resolution of 20 m in the vertical by 1 km by 1 km, with this set-up shown in Figure 2.1. The model solves the rotating hydrostatic Boussinesq equations and advection – diffusion equations for temperature and salinity, with a fixed Coriolis parameter for the domain. Restoring boundary conditions are applied to the northern boundary gradually over 50 grid cells, via an increasing linear distribution in restoring strength, with a restoring time scale of 24 hrs. Heat and salt are restored to a pre-set depth dependent distribution and passive tracers are restored to 0. The distributions used in the model are based from observations in Amundsen Sea, where cold fresh Winter Water overlies warm and salty

Circumpolar Deep Water, with example vertical distributions of restoring and initial conditions shown in Figure 2.2 for temperature and salinity. It should be noted that velocities are not imposed at the north boundary and are calculated from the oceanic conditions in the model. Constant uniform vertical diffusivities of 1×10^{-4} m^2/s are applied to salinity, temperature and passive tracer. No surface forcing is applied to this model setup and ice shelf meltwater is added to the model at the calculated freezing temperature.

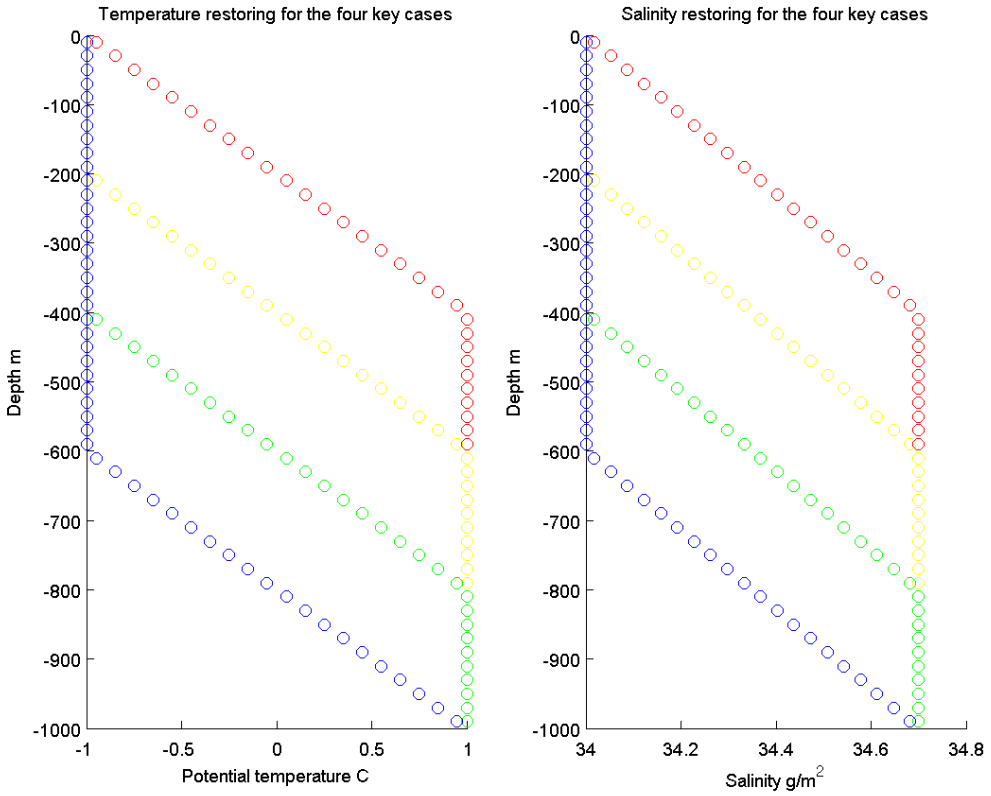

FIGURE 2.2: Restoring profiles for temperature and salinity for four illustrative cases, which are applied on the northern boundary of the idealised model.

2.2.2 Freshwater feedback method

In order to determine the effect of local ice shelf freshwater on ice shelf melt rates a new method is developed and implemented in the idealised model set-up for this thesis. This method will be explained for the illustrative set of reference simulations over a range of thermal drivings, ranging from the case where a cold oceanic forcing is applied, which will be referred to as the 'COLD' simulation, and ranging to the other extreme case with warm oceanic forcing applied, which will be referred as the 'WARM' simulation. These model set-ups are simulated until a steady state develops in both the model set-ups. Then two new sets of simulations are created 'ColdMelt-fixed' and 'WarmMelt-fixed'. These two new sets of simulations are over the same thermal driving range as the default

set of simulations. In the 'ColdMelt-fixed' simulations the ice shelf freshwater flux is fixed to that of the steady ice shelf freshwater flux of the 'COLD' set-up. However, in the 'ColdMelt-fixed' set of simulations the model still calculates and diagnoses the ice shelf melt rate, which would have been outputted as a freshwater flux had it not been fixed. Therefore comparing the steady ice shelf melt rates that are calculated in the reference and 'ColdMelt-fixed' set-ups for the 'WARM' forcing allows for the computation of the freshwater feedback effect for the given forcing range between the 'COLD' and 'WARM' cases. Similarly in the 'WarmMelt-fixed' set of simulations the ice shelf melting is fixed to that of the 'WARM' set-up and a similar freshwater effect can be calculated.

2.3 Regional Amundsen Sea model

2.3.1 Model set-up

Revision c62r of the Massachusetts Institute of Technology general circulation model (MITgcm) is used, coupled to a viscous-plastic sea ice model (Losch et al. 2010), following the configuration used by Kimura et al. (2017). The model employs a curvilinear grid using an Arakawa C-grid finite volume method, with z levels representing the vertical (Marshall et al. 1997a). A longitudinal resolution of 0.1° is used, producing a latitudinal spacing ranging from ∼2.8 km in the southern part of the domain to ∼5.2 km at the northern end of the domain. In the vertical, a z-level coordinate system of 50 levels is used, ranging from 10 m resolution near the top to 200 m near the bottom (reaching 5600 m here). The global 1-minute Refined Topography data set (RTOPO) (Timmermann et al. 2010) is used to create the model seabed and ice-shelf topography, with the whole model domain bathymetry shown in Figure 2.3a and the model bathymetry over the continental shelf in Figure 2.3b. In order to provide a better representation of ice shelf and topography features, partial cells are employed in the model (Adcroft et al. 1997). Monthly mean output is considered throughout in the regional model. The model domain extends from 75.5°S to 62°S and 140°W to 80°W covering the Amundsen Sea embayment, but the analysis in this thesis will concentrate on the region extending from 75.5°S to 71.5°S and 130°W to 95°W.

Freshwater from several different sources (iceberg melt, evaporation, precipitation, sea ice and ice shelf meltwater) are tracked via passive tracers (Regan et al. 2018) and as described in Section 2.1.1. A volumetric source of tracer occurs when freshwater is added, and a volumetric sink occurs when freshwater is removed, for example via evaporation or sea ice growth. Such sinks can create negative tracer concentrations in the domain. Therefore, a freshwater flux into the ocean shall be considered as positive, and a freshwater flux out of the ocean as negative. Only local freshwater sources are traced in the model and therefore freshwater entering the domain via the open boundary conditions are not traced.

Following Kimura et al. (2017), there is no explicit horizontal diffusion of salt, heat or tracers in the model, but the vertical diffusion is parametrized by using the K-profile parameterization (KPP) scheme (Large et al. 1994). Initial conditions were interpolated onto the model grid from the World Ocean Atlas (Locarnini et al. 2013, Zweng et al. 2013). Steady climatological seasonal monthly conditions for ocean velocity, salinity and temperature, taken from Holland et al. (2014), are applied to the eastern, northern and western boundaries. Using climatological seasonal boundary conditions does not capture small remotely-induced variations in CDW temperature (Nakayama et al. 2018), but this temperature variation has a much smaller effect than locally-induced variability of the CDW layer thickness that occurs within the region and is captured by the model. Tides are not accounted for in the model. The model is forced with ERA-Interim reanalysis forcing from 1979-2018 (Dee et al. 2011), but the first 10 years are regarded as model spin up.

For this study, several improvements have been made to the Kimura et al. (2017) model set-up. In order to correct a long-term sea-level fall in the model the open-boundary velocities were edited, and sea ice parameters were tuned to replicate inter-annual variability of the oceanic heat content (OHC) in front of PIG. In particular, the air-ice drag coefficient is set to 0.0025, the demarcation ice thickness is set to 0.5 m, and sea ice advection uses a 3rd-order direct-space-time flux-limited scheme. Ocean parameters were kept the same as those used by Kimura et al. (2017).

2.3.2 Precipitation and evaporation

Precipitation in the model is prescribed by the ERA interim reanalysis that is used to force the the regional model (Dee et al. 2011). Also prescribed by this reanalysis is the atmospheric temperature at 2 m, meridional and zonal wind velocities at 10 m, specific humidity at 2 m and the long and short wave radiation. However, evaporation E is calculated in the model using the formulae in Large et al. (1994). Therefore evaporation is calculated to be:

$$E = -\frac{1}{\rho_f}\tau q^*, \tag{2.30}$$

where ρ_f is the density of freshwater and τ is defined as

$$\tau = \rho_a C_d |W|^2, \tag{2.31}$$

where ρ_a is the mean air density, C_d is the drag coefficient and $|W|$ is the wind velocity magnitude at 10 m.

The turbulent humidity scale (q^*) is calculated using Large & Pond (1982):

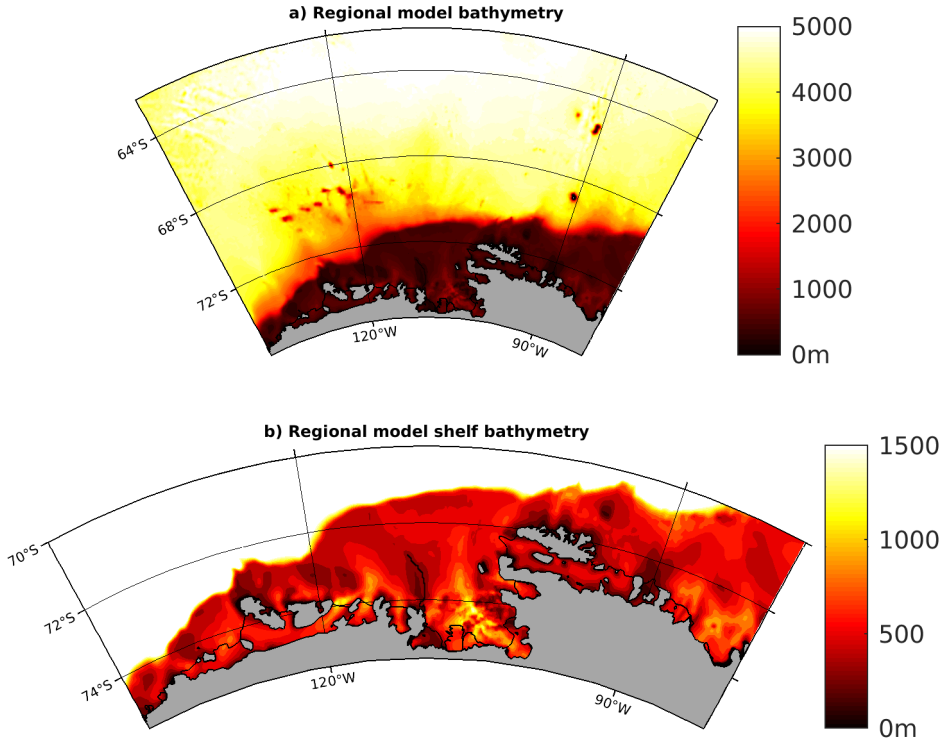

FIGURE 2.3: a) Regional model bathymetry. b) Regional continental shelf bathymetry. Derived from the global 1 min Refined Topography data set (RTOPO) (Timmermann et al. 2010). Grey denotes land and ice shelves are excluded.

$$q^* = -\frac{C_e(q_s - q_a)}{\sqrt{C_d}}, \tag{2.32}$$

where C_e is the Dalton number and, q_s and q_a are the specific humidities at the surface and at 2 m respectively.

It it worth noting that the evaporation calculation in the model interacts with the sea ice model and evaporation over the ocean (E_o) inversely scales with sea ice coverage concentration (A_s) with

$$E_o = (1 - A_s)E. \tag{2.33}$$

In addition evaporation occurs over the sea ice (E_i) with

$$E_i = A_s E, \tag{2.34}$$

though this doesn't affect the tracers in the model.

2.3.3 Sea ice model

The MITgcm sea ice model is based on a variant of the viscous-plastic dynamic-thermodynamic sea-ice model of Zhang & Hibler (1997). The model was rewritten to run off the Arakawa C Grid, which is the same grid that the MITgcm ocean model uses (Losch et al. 2010). The thermodynamic part of the model employs a simple zero-layer model for thermodynamics (Semtner 1976), where upward conductive heat flux is parameterized assuming a zero ice heat capacity and a linear temperature profile. The model allows sea ice motion to be driven by ice-atmosphere, ice-ocean and internal stresses. In the regional model setup no boundary conditions are applied to the sea ice.

2.3.4 Iceberg set-up

Icebergs are represented in the model via iceberg melt and the physical presence of grounded icebergs on Bear Ridge. Grounded Bear Ridge Icebergs (BRI) are built into the model by modifying the seabed, which is raised to the sea surface to create a 'wall' along the 350 m depth contour around the shallow area north of Bear Island (Figure 2.4a). Fast ice surrounding the grounded BRI is not explicitly included in this study, though the sea ice model permits sea ice to build up around the BRI.

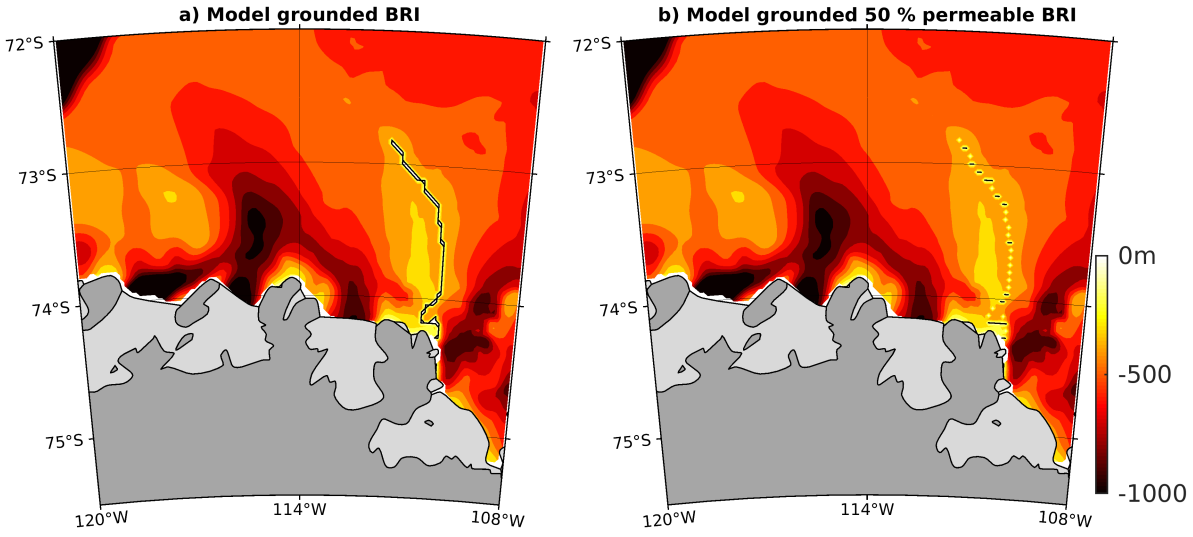

FIGURE 2.4: Model bathymetry over the grounded BRI region. a) Grounded iceberg representation distribution for the reference case and ice shelf representation. b) 50 % permeability case of grounded BRI.

The reference case representation of the grounded BRI in the model (Figure 2.4a) can be compared to satellite images of the grounded BRI shown in Figure 1.10b and in the larger regional satellite image of Figure 1.10c. Comparing these it is observed that the model representation of the grounded BRI matches the distribution of the grounded BRI in the satellite images sufficiently well for this study. However, it is noted that

larger icebergs like the one shown in Figure 1.10(b)(c) can change the distribution of this feature, however it is assumed that these differences are minor for the proposes of this study. One of the reasons it is important for the model to represent the grounded BRI in the model is that, these grounded icebergs form the Amundsen Sea Polynya shown in Figure 1.10a.

In other variations of the model set-up, other grounded BRI representations are used in this thesis. A ice shelf BRI set-up is used where the BRI are represented using a surface 10 m thick ice shelf of the same distribution as shown in Figure 2.4a. In this BRI set-up the ocean is able to be advected under this BRI representation.

A 50 % permeability version is also tested with distribution shown in Figure 2.4b, where every other latitudinal grid row of the distribution in Figure 2.4a is removed to create a permeable wall formed of the bathymetry. Ocean and possibly sea ice can be advected though this representation.

As an initial study of the influence of iceberg freshwater, iceberg melting is crudely represented as a fixed freshwater flux into the ocean surface, in which the effects of latent heat are not accounted for. The total flux into the domain is set to be 198 Gt/yr, which equals the iceberg discharge in the Amundsen Sea (Depoorter et al. 2013, Rignot et al. 2013), as it is assumed that imported and exported icebergs compensate each other. The iceberg freshwater flux is input near the coast, tapering linearly to zero 100 km away, as shown in Figure 2.5. This is because iceberg-modelling studies suggest that Amundsen Sea icebergs stay close to the coast (Merino et al. 2016). The simulation including BRI, iceberg melt and air-sea ice drag coefficient set to 0.0025 will henceforth be referred to as the reference case.

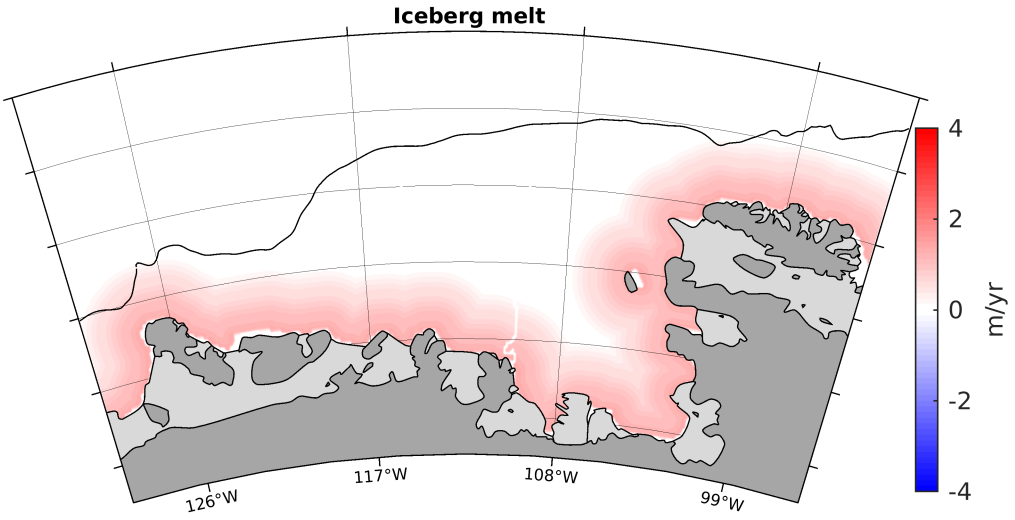

FIGURE 2.5: Steady surface iceberg melt freshwater flux distribution applied to the regional model. Shown for over study area only.

2.3.5 Convection issues

A sea level fall was discovered in the original set-up of the model, this is possible as the regional model setup employs open boundary conditions, which leads to the non conservation of volume in the model domain. Therefore the rate of change of the volume in the domain is dependent on the fluxes applied to the model, including those on the boundary. The the sea level fall was therefore consequently corrected by applying a small convergence to the open boundary conditions in the north, east and west of the domain. However, stopping the sea fall caused convection to occur in the shelf seas regions of the model, making the shelf seas too cold at depth, as shown in Figure 2.6b, whereas before warm CDW was present on the shelf Figure 2.6a. Most notably after the sea level correction was applied there was a strengthening of the previously small and weak convection episode between 1997 and 2002. This causes the whole water column on average to have a potential temperature of -2 °C and the model has not returned to its expected state by 2016. Therefore during this period the region has switched into the mode where dense and cold shelf water is produced, and it is known from observations taken in the Amundsen Sea that this isn't the case for the region (Dutrieux et al. 2014). It is thought that the model was not conserving before the sea level correction and was adding extra freshwater into the model in order to process this sea level fall.

The small convergence that was applied to the model to fix the sea level fall was done by editing the velocity boundary conditions of the east, west and north boundaries. The sensitivity of the velocity boundary conditions adjustments that were applied in order to correct the sea level fall was tested by correcting the sea level fall by only editing the velocities on the northern boundary in another setup. This new setup still caused convection to occur on the continental shelf and therefore yielded the same results as the set-up where the velocities were edited on all boundaries. This suggests a lack of sensitivity for the continental shelf OHC to the location of the velocity adjustments for the sea level correction. In addition, it should be noted that the velocity changes applied to the boundaries are small in comparison to the velocities that are imposed there. Therefore any affect from the edited velocity boundary conditions on the transport of modelled OHC from the boundaries should be expected to be minor compared to pre-existing transport in the model.

The magnitudes of all the freshwater sources into the model have a large uncertainty, which is due to a lack of data to prescribe the freshwater fluxes into the Amundsen Sea region. The iceberg melt field has the largest uncertainty by an order of magnitude, due to the complexity of the production, distribution and dynamics of icebergs. Therefore the sensitivity of this field on the severity of the convection that occurs in the model was tested using a series of shorter model simulations (1991-2006), in which different aspects of this field were varied.

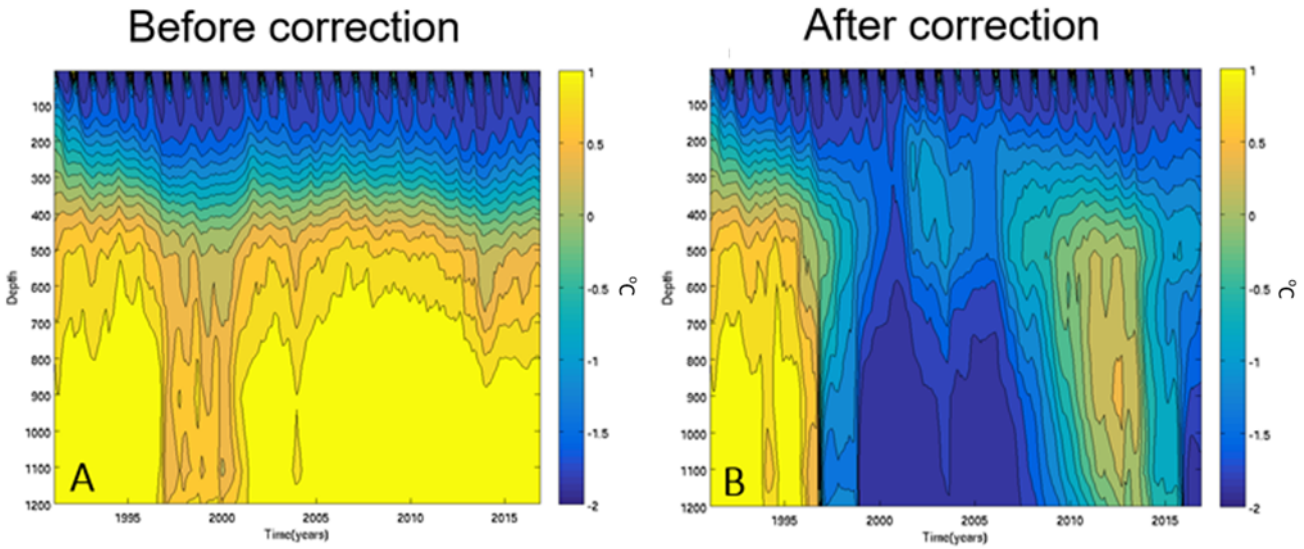

FIGURE 2.6: A) Hovmöller diagram of potential temperature 1991-2016 averaged over the eastern Amundsen Sea before sea level fall correction is applied. B) Hovmöller diagram over the same area after sea level correction is applied.

In the model the iceberg melt is supplied as a constant flux over a fixed distribution in the model, due to a lack of data. In the original set-up of the model by Kimura et al. (2017) the iceberg melt field inputs 150 Gt/yr into the model domain, via a Gaussian distribution with distance from the coast. The effect on the convection of varying the magnitude of this iceberg melt field was investigated using shorter model simulations from 1991 to 2006, comparing the cases where this field has been scaled by a factor of two and five with the original set-up. It was found that increasing the iceberg melt does decrease the convection compared to the orginal set-up (Figure 2.7A). The case where the iceberg is scaled by 2 recovers, albeit slowly, to having warm CDW at depth by the end of the simulation, as shown in Figure 2.7B. The more extreme case, of scaling by 5, leads to convection being stopped completely, which is shown in Figure 2.7C. Though in this case also some of the variability in the model has also been smoothed away. This does however prove that the convection can be eliminated by editing the iceberg melt field magnitude, even if it has to be increased to a possibly unrealistic amount.

The distribution of the fixed iceberg melt flux field is now varied in order to observe its effect on the convection episode. The gridding of the iceberg melt field input file was also set to be finer, where previously it had a 0.75^{o} resolution, it was made to have 0.05^{o} resolution. The total flux into the domain via these test distributions were set to be 282 Gt/yr over the whole domain, taken from the upper 1 standard deviation limit of satellite derived observations in Depoorter et al. (2013).

The distribution is set to be so that the magnitude of iceberg melt flux falls away linearly from land over a distance, x. Iceberg modelling studies suggest that Amundsen icebergs stay close to the coast (Merino et al. 2016). Therefore x was set, while maintaining

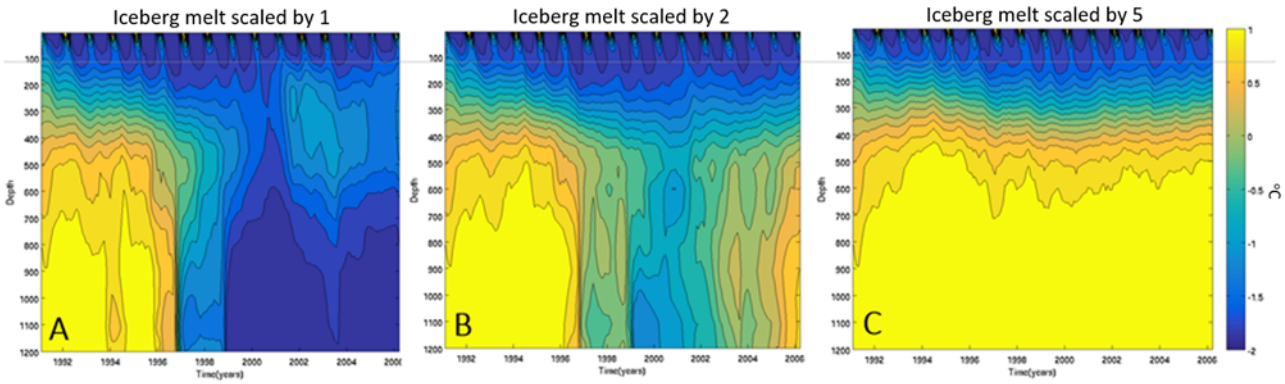

FIGURE 2.7: Hovmöller diagram of potential temperature 1991-2006, averaged over the eastern Amundsen Sea. A) Iceberg melt with scale factor 1 B) scale factor 2 C) scale factor 5.

the total flux, to 10 km and 100 km. It was also set to the extreme case of infinity, so that the flux is applied uniformly over the entire domain. These generated iceberg melt flux fields for $x = 10$ km, $x = 100$ km and $x =$ Infinity are shown in Figure 2.8B,D,F respectively, over just the eastern Amundsen Sea region, though the change affects the distribution across the whole domain.

The distribution of the iceberg melt field does have a strong impact on the magnitude of the convection that occurs in the model. Its appears that convection is reduced the most when the scaling distance is set to 100 km, as shown in Figure 2.8C, with the CDW returning at depth by around 2002. However, this case does have colder water at depth in 2000 than when the scaling 10 km is used, shown in Figure 2.8A. Convection was found to be most severe when the scaling distance was equal to infinity, as shown in Figure 2.8E. The processes that underlie these cases will be investigated further when returned to the model setup used in this thesis.

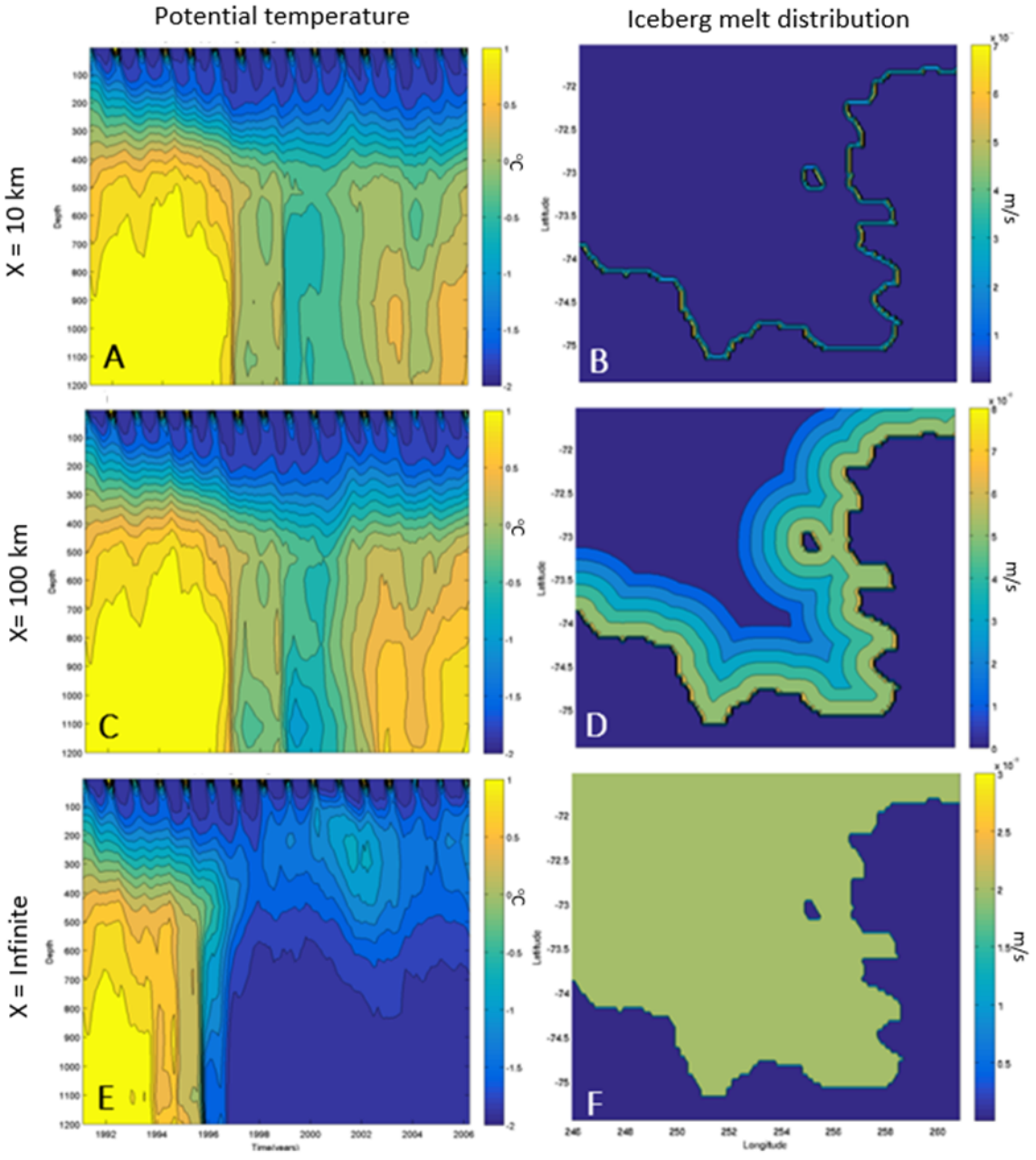

FIGURE 2.8: Hovmöller diagrams of potential temperature 1991-2006, averaged over the eastern Amundsen Sea for the cases of iceberg flux distribution range set to A) x = 10 km C) x = 100 km E) x = Infinite, with the corresponding iceberg melt freshwater flux fields shown in B), D) and F) respectively.

Chapter 3

Idealised model results

In this chapter the vertical distribution of the local ice shelf freshwater is investigated using an idealised model, along with the strength of the local freshwater feedback. The aims of the sections are:

3.1) This section describes the idealised model oceanic conditions, including model currents and boundary conditions.

3.2) In this section the effect of CDW layer thickness variation on the vertical distribution of ice shelf meltwater is investigated using passive freshwater tracers.

3.3) In this section the effect of the local ice shelf cavity freshwater feedback is investigated using the method described in Section 2.2.2.

The idealised model setup, described fully in Section 2.2, employs an idealised domain consisting of a triangle iceshelf in a box ocean domain. Restoring boundary conditions are applied at and linearly away from the northern boundary, restoring to vertical profiles of temperature and salinity and tracers to zero. However, no surface forcing is applied to this model setup and constant uniform vertical diffusivities are applied to the salinity, temperature and tracers. In this setup iceshelf meltwater is traced and ice shelf melting is calculated using heat and salt turbulent exchange coefficients, which have an explicit velocity dependence.

3.1 Model oceanic conditions

In this section the idealised model's steady state conditions are reviewed. The idealised model, with domain shown in Figure 2.1, is used to investigate the vertical distribution of the ice shelf meltwater and freshwater feedback effects, depending on the influx of CDW and hence the thickness of the CDW layer on the continental shelf. The term 'thickness of the CDW + thermocline' will refer to the combined thickness of the CDW layer and

the thermocline, in the initial conditions and boundary conditions. The variation of the amount of CDW entering the continental shelf is represented by four key restoring profiles for salinity and temperature, shown in Figure 3.1, to represent very extreme high and low melting years (red and blue lines) and to represent observed high and low melting years (yellow and green lines). However, a full range of CDW + thermocline thicknesses, from 0 m to 1400 m shall be explored in the melt rate studies, with the thermocline set to be a fixed thickness of 400 m. This range of 0 m is 1400 m is due to the presence of the 400 m thermocline. Therefore, when CDW + thermocline thickness is set to be 0 m the whole water column is filled with WW and when this thickness is set to 1400 m the whole column is filled with CDW, with in both of these cases the thermocline being not present in the domain. Similarly, for example if the CDW + thermocline thickness is set to be 1000 m then the water column is filled with 600 m of CDW layer and the top 400 m is filled with the thermocline, as shown by the red case in Figure 3.1. It is worth noting that while the word 'thermocline' will be used in this study, it is also a halocline and hence a pycnocline. Therefore variation in CDW flux onto the continental shelf between different years are simulated with a variation of the CDW layer thickness in the boundary conditions and initial conditions, rather than a variation in CDW temperature, which was done in other studies (Holland 2017). This is because such CDW temperature changes are tiny compared to the much larger temperature variability caused within the Amundsen Sea by changes in the CDW layer thickness (Dutrieux et al. 2014) and therefore this would be expected it to be the dominant driver of ice-shelf melt rate variation in the region.

It should be noted that a temperature of -1 ^{o}C has been used in this study to represent the WW temperature. This agrees with summer observations in Pine Island Bay (Dutrieux et al. 2014). However, WW forms at the surface freezing point in winter, which is observed further offshore (Biddle et al. 2017, 2019). However, close to the front of ice shelves it is the mixing with the warmer glacial meltwater which increases the WW to the observed -1 ^{o}C. Although melting of the direct iceshelf is included in the model, potential meltwater from ice shelves upstream is not included. In addition, vertical mixing can warm the WW layer and only an idealised representation of vertical mixing is included in the model. In addition this idealised model doesn't include sea ice which would aid vertical mixing. In this study observed oceanic conditions are imposed on the model due to the idealised nature of it and therefore, the choice of the temperature of -1 is deemed to be sufficient for this idealised study. Though it should be noted that the temperature of -1 for WW may be questionable when the CDW layer is non existent in the model. In addition, it should be noted that for simplicity AASW is not included in the initial conditions and boundary conditions in this model set-up.

The model is simulated, in each case, until a steady state develops, yielding different salinity and temperature vertical distributions depending on the forcing applied, as shown in the cross-sections down the middle of the domain in Figure 3.2 for two

illustrative cases. In the steady state that develops, rising buoyant meltwater plumes under the ice shelf are driven left by the Coriolis force, as shown via a plan view of the ice shelf in Figure 3.3b, with the ice shelf's location shown by the black box in Figure 3.3c. This leads to a strong plume developing in the west of the ice shelf (Holland 2017), which shall be denoted as the plume region. These then detach from the ice shelf on the western side, driving an overturning system in the model, as shown by the streamlines in Figure 3.3a. However, the meltwater also drives barotropic circulation in the domain, which is stronger than the overturning, so the circulation in the model is mainly horizontal. The barotropic circulation is shown by the streamlines in Figure 3.3c. It should be noted that as the boundary conditions do not allow for inflow this could affect the the overturning and barotropic circulations present in the model. However, the barotropic circulation in the model is of a comparable magnitude to the gyre in Pine Island Bay in front of PIG Ice Shelf, which was calculated to be ≈ 1.5 Sv from observations (Thurnherr et al. 2014). In addition, the overturning circulation present in the model is comparable to observational estimates of 0.25 Sv of the overturning present in the Pine Island cavity (Jacobs et al. 2011, Thurnherr et al. 2014). However, the idealised model includes no wind forcing in the model and wind forcing may be a driver of gyre. Therefore the model's gyre is only driven by buoyancy forcing and hence any buoyancy driven feedbacks in the model may at the upper bound of their strength. However, despite the limitations of this approach it is deemed to be sufficient for the purposes of this idealised study.

In the ice shelf melting plan view (Figure 3.3c) there are clear "stripe" features across the ice shelf. These could be numerical instabilities in the model. However, this is unlikely as these features have occurred in similar model studies (Holland 2017). They were found to be velocity artifacts caused by the stepped ice shelf base because of the Cartesian coordinate system used, despite partial cells and a boundary layer scheme being used to reduce this problem.

As the thickness of the CDW layer is varied from case to case it is expected to affect the ice-shelf melt rates between cases. Therefore Figure 3.4 shows the average melt rates of the ice shelf while varying the CDW layer thickness of the initial conditions and boundary conditions of the model for the full extreme range. Each of these melt rates are taken after the model has reached a steady state with its particular forcing applied to it. When the CDW + thermocline thickness is 0 m the model has all cold Winter Water as its IC and restoring. Conversely, when CDW + thermocline thickness is 1400 m the model forcing is all warm CDW. As might be expected there are higher melt rates when there is more available heat, so when the thickness of the CDW layer is larger. The shape of the melt rate's relationship to ocean warming is due to the thermal driving, the geometry of the ice shelf and the thermocline. The melt rates in the middle of this extreme range are similar to regional model melt rates for ice shelves like PIG Ice Shelf (Kimura et al. 2017, St-Laurent et al. 2015).

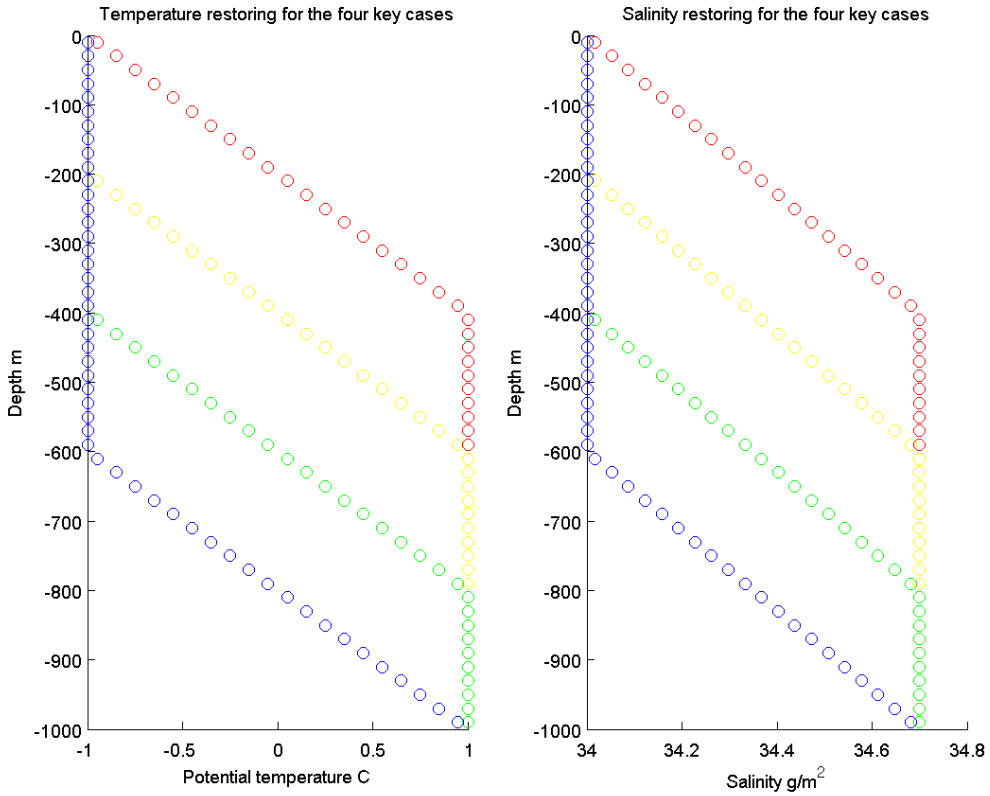

FIGURE 3.1: Restoring profiles for temperature and salinity for the four key cases, which are applied on the northern boundary of the idealised model.

3.2 Vertical distribution of local ice shelf freshwater

In this section the idealised model is utilised to investigate the vertical distribution of ice shelf meltwater in front of ice shelves in the Amundsen Sea and how it varies between years of high and low CDW flux onto the continental shelf. It is found in this experiment that the depth at which the meltwater plumes settle at in the water column varies strongly with the thermocline/pycnocline depth of the restoring profiles and initial conditions applied, which is used to simulate the CDW flux variation. This is shown clearly in Figure 3.5a-d, which shows cross-sections taken on the western side of the domain, for different restoring forcing applied. In these figures the straight solid horizontal white lines in the diagram represents the depth of the top and bottom of the thermocline of the restoring applied to the model. The black lines in the figures represent salinity contours, with the cyan ones representing the salinity of the top and bottom of the thermocline of the forcing. The colour contours show the steady state of concentration of the ice shelf meltwater passive tracer, which is restored to zero at the northern boundary.

In most cases there is both a primary plume and a secondary one, though in some extreme cases these two plumes can merge, for example in Figure 3.5a. The primary plume is

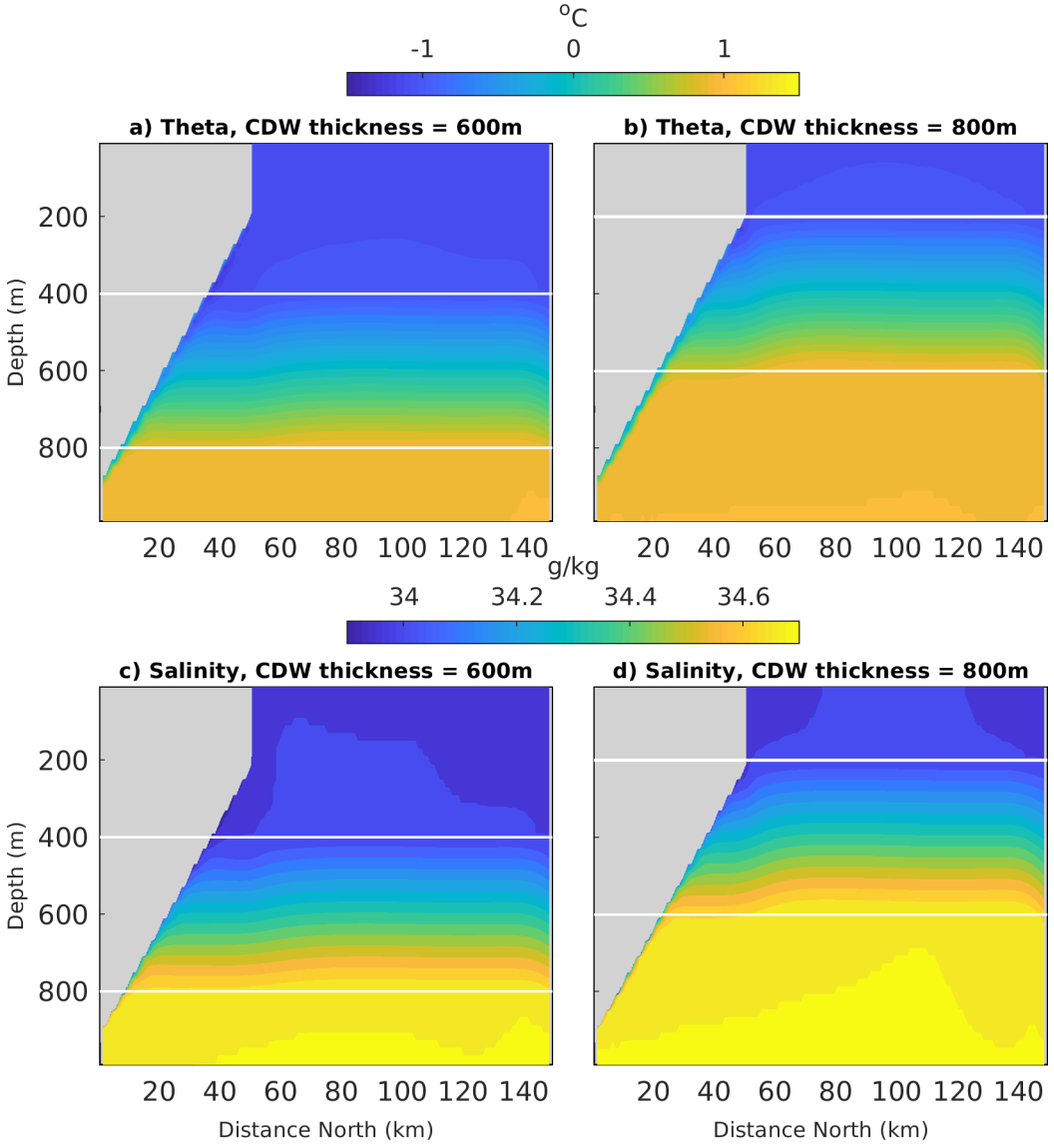

FIGURE 3.2: A cross-section of steady state potential temperature and salinity along the center of the domain in the idealised model, for a illustrative cold (a)(c) and warm case (b)(d). Straight solid horizontal white lines represent the top and bottom of the thermocline and the pycnocline of the restoring applied to the model.

formed due to buoyant meltwater that rises to the surface of the water column. However, not all of the primary plume reaches the surface; a secondary plume is formed by part of the plume peeling off, as it reaches a neutral density in the pycnocline, in which the density of the water changes rapidly with depth. This is due to the plume entraining the denser ambient surrounding water, and therefore increasing its own density, with the outer part of the plume increasing the most, leading to the secondary plume. This secondary plume then proceeds as a gravity current inside the pycnocline.

Within low melting years, when the CDW layer thickness is small, the secondary plume acts as a gravity current along the deep isopycnals. In these cases, only a small proportion of the meltwater rises to the surface in the primary plume, as seen in Figure 3.5c-d.

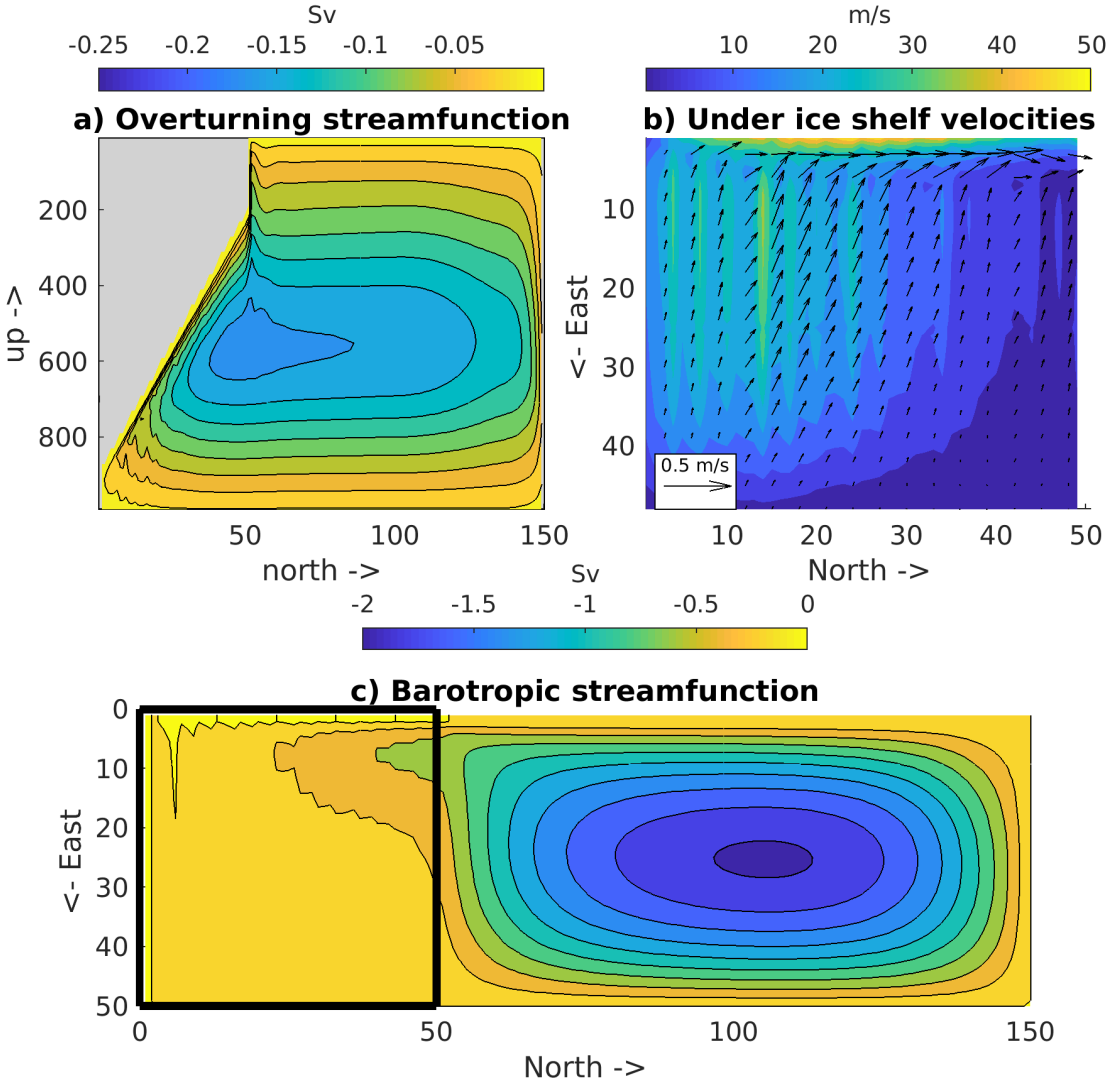

FIGURE 3.3: Oceanic flow conditions for illustrative warm case: a) Overturning streamfunction b) The plan view of ice shelf melting and flow in top grid cells under ice shelf. c) The plan view of the barotropic streamfunction, for the same example case, with the ice shelf position marked by black lines.

This is because of the low melt rates for these CDW layer thicknesses (as shown in Figure 3.4) cause not much of the plume to become fresher than the top of the pycnocline. As the thermocline and the pycnocline of the forcing becomes higher, changing both the temperature and salinity structure, several different effects occur, for example higher melt rates and a faster overturning. These combine to give the result that a higher proportion of the primary plume becomes fresher than the top of the pycnocline, as seen in Figure 3.5b. Also with the pycnocline becoming higher in the water column, this changes the position of the secondary plume. In an extreme case, where the pycnocline is at the top of the water column, the two plumes can merge, as shown in Figure 3.5a. This is all in agreement with and helps explain what was found in Kimura et al. (2017), as shown in Figure 3.6a-b. Figure 3.6 shows ice shelf meltwater cross-sections taken from

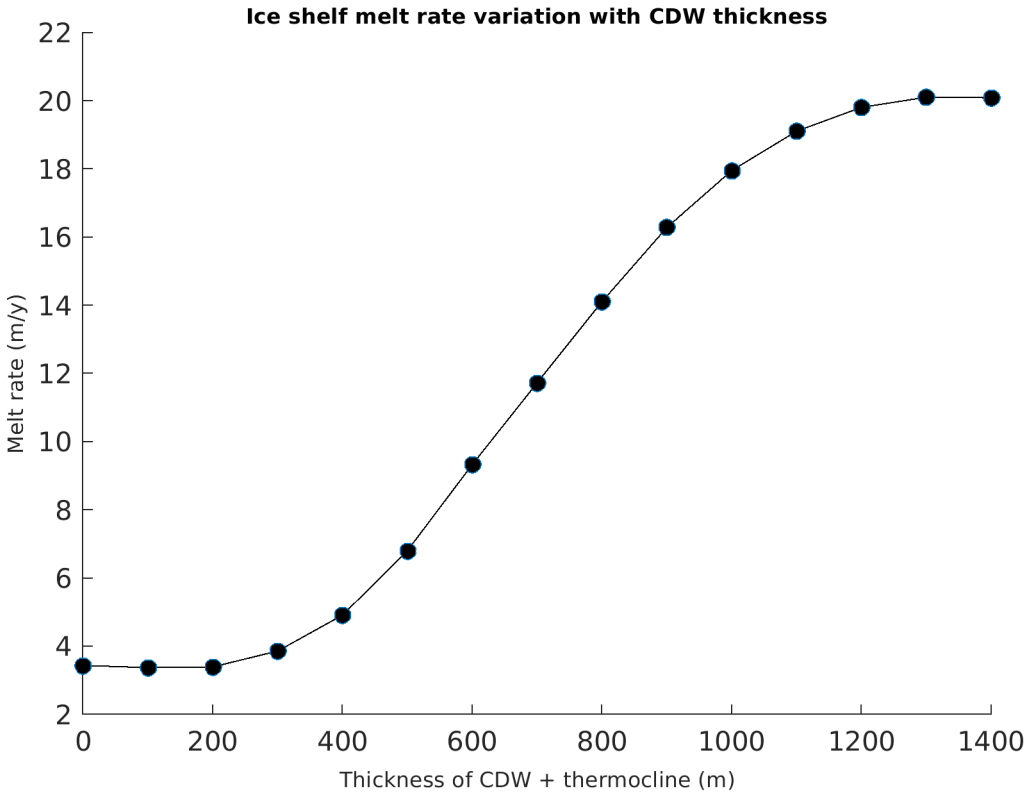

FIGURE 3.4: Idealised model ice-shelf average melt rates, for a range of CDW + thermocline thicknesses for initial conditions and restoring applied to the northern boundary. All melt rates are when the model has reached a steady state.

a regional model in the high melting year of 2009 (Figure 3.6a) and the low melting year of 2014 (Figure 3.6b). The same distributions as what was found in the idealised model are shown, with the ice shelf meltwater intruding along deeper isopycnals in the low melting year and rising to the surface in the high melting year.

Therefore these experiments show that the depths at which ice shelf meltwater settle at in the water column is dependent on the CDW layer thickness. In addition, these experiments show that as the CDW thickness increases, yielding a higher melt rate, a higher proportion of the meltwater is in the primary plume, which reaches the surface layer. Therefore, this may have implications for the vertical stability of the water column. Possibly when the CDW thickness layer is thicker more of the ice shelf meltwater reaches the surface, potential reducing convection from sea ice growth. This potentially aids in the protection of the CDW layer, helping to keep the CDW layer thick. Therefore there is a potential feedback on the CDW layer thickness and this could have implications for modelling CDW thickness inter-annual variability, especially in global models,

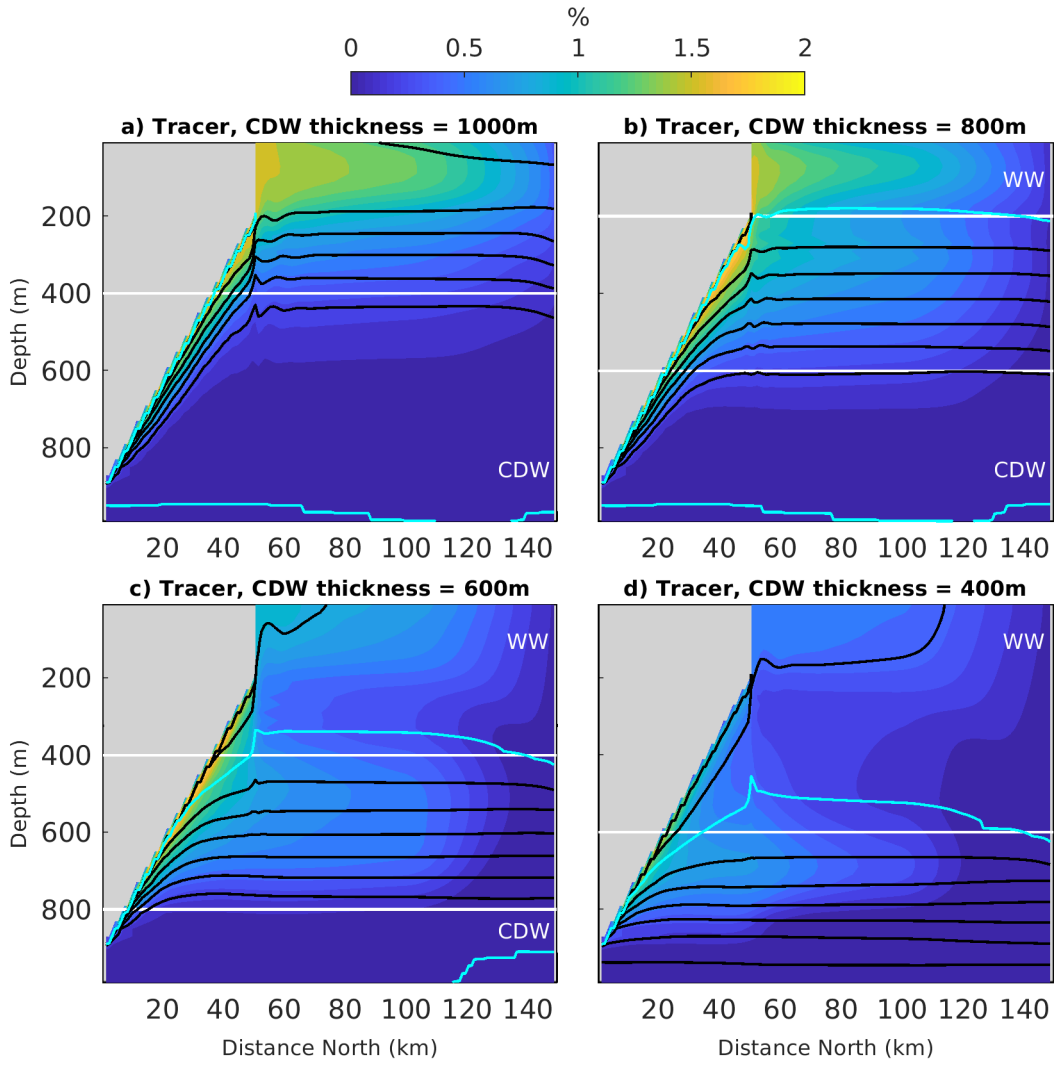

FIGURE 3.5: A cross-section on the western boundary of ice-shelf meltwater tracer concentration in the idealised model, shown for different cases of CDW thickness. Straight solid horizontal white lines represent the top and bottom of the thermocline and the pycnocline of the restoring applied to the model. The black lines represent salinity contours, with the cyan ones representing the salinity of the top and bottom of the thermocline of the forcing.

which would may be unable to resolve this mechanism explicitly. These results will help improve parameterisations for use in large scale models and ice sheet models to improve predictions of ice shelf melting and therefore future sea level rise.

It should be noted that in this model set-up only constant vertical diffusivities are used. Therefore these results on the vertical distribution of ice shelf meltwater would be expected to change with the use of a vertical mixing scheme. The individual distinct plumes observed in most cases may be less clear with such a scheme used, though the processes discussed here would still occur. In addition, the lack of sea ice in the model could effect the top portion of the water column by possibly mixing down meltwater reducing the clear separation of the two plumes observed in this model set-up in some cases. The addition of sea ice would possibly also add an seasonal cycle top portion

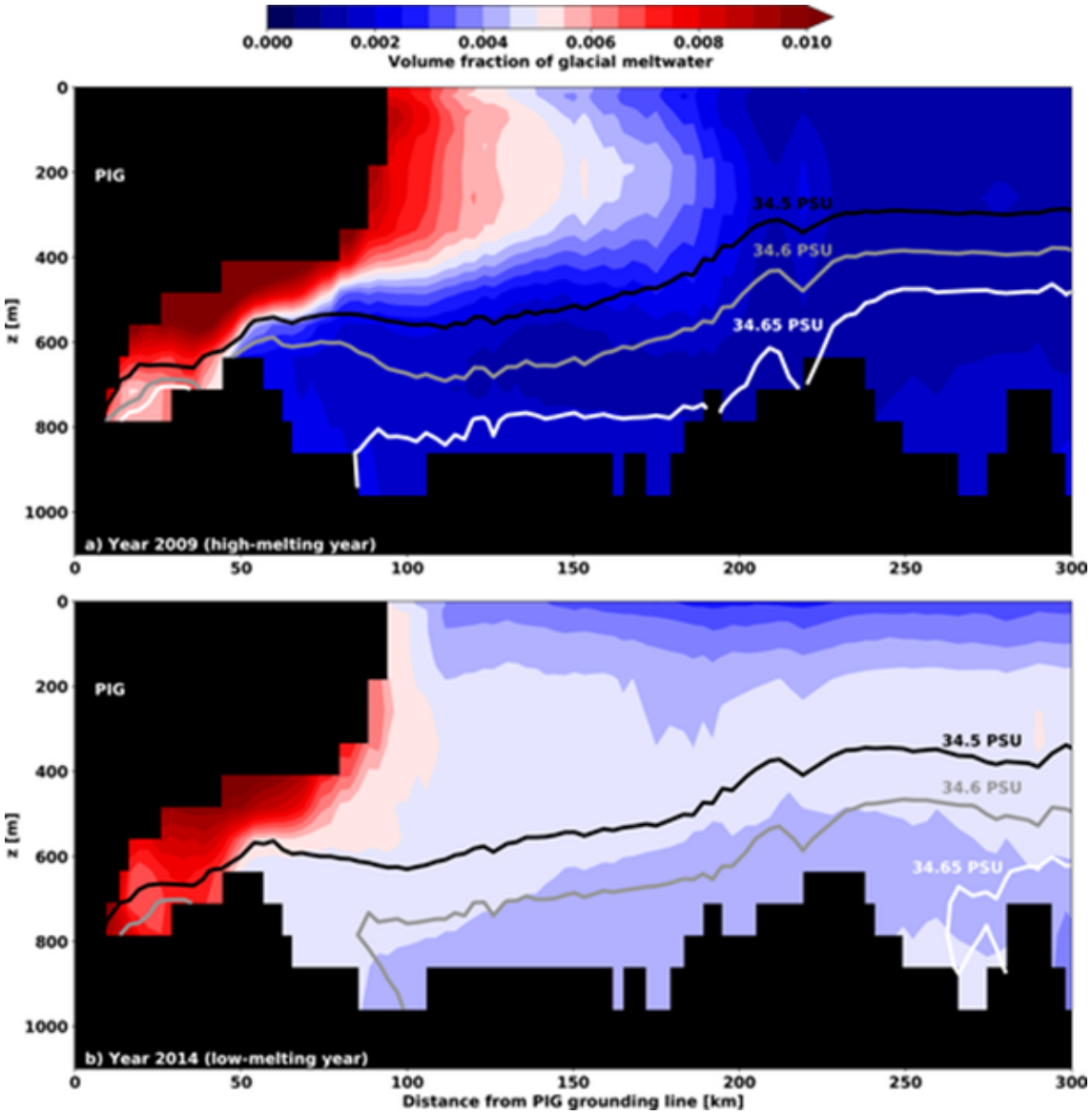

FIGURE 3.6: Ice shelf meltwater tracers for year a) 2009 and b) 2014 in front of Pine Island Glacier (PIG) in a full regional Amundsen Sea model (Kimura et al. 2017).

of the vertical distribution of ice shelf meltwater. However, the results found in this idealised study represent processes that would still occur in a more complex set-up and therefore aid our understanding of the vertical distribution of ice shelf meltwater.

This change in the vertical ice shelf freshwater distribution, depending on high and low melting years, could affect the ocean dynamics of the Amundsen Sea. However, first it needs to be determined whether or not ice shelf meltwater is important in the Amundsen Sea freshwater budget. Therefore a realistic regional Amundsen Sea model, using passive tracers, will be employed later in the thesis to determine this and to further examine the distribution of ice shelf meltwater, along with the other components of the freshwater budget.

3.3 Local ice shelf freshwater feedback

The sensitivity of ice shelf melt rates to heat has two components: the additional heat (the thermal effect), and the additional spin-up of the buoyancy driven circulation due to the additional ice shelf meltwater (freshwater feedback effect). Therefore in this section the local ice shelf cavity feedback effect of ice shelf meltwater on the ice shelf melting is determined, using the idealised model and the feedback method described in Section 2.2.2.

The feedback method described in Section 2.2.2 is used in order to examine the local effect of ice shelf freshwater on the ice shelf melt rates in the idealised model and so determine the local freshwater feedback.

This method will be explained for the illustrative set of reference simulations over a range of thermal drivings, ranging from the case of a cold oceanic forcing applied (thickness of CDW + thermocline = 0 m), which will be referred to as the 'COLD' simulation, and ranging to the other extreme case with warm oceanic forcing applied (thickness of CDW + thermocline = 1400 m), which will be referred as the 'WARM' simulation. These model set-ups are simulated until a steady state develops in both the model set-ups. Then two new sets of simulations are created 'ColdMelt-fixed' and 'WarmMelt-fixed'. These two new sets of simulations are over the same thermal driving range as the default set of simulations. However, in the 'ColdMelt-fixed' simulations the ice shelf freshwater flux is fixed to that of the steady ice shelf freshwater flux of the 'COLD' set-up. However, in the 'ColdMelt-fixed' set of simulations the model still calculates and diagnoses the ice shelf melt rate, which would have been outputted as a freshwater flux had it not been fixed. Therefore comparing the steady ice shelf melt rates that are calculated in the reference and 'ColdMelt-fixed' set-ups for the 'WARM' forcing allows for the computation of the freshwater feedback effect for the given forcing range between the 'COLD' and 'WARM' cases.

In the specific case that will be investigated in the idealised model first, the 'COLD' set-up is set to be that of the all WW forcing case and the 'WARM' set-up to be that of the all CDW forcing case, with the fixed 'COLD' ice shelf freshwater flux applied to all set-ups with forcings in between 'WARM' and 'COLD' set-ups.

The sensitivity of ice shelf melt rates to heat has two components: the additional heat (the thermal effect), and the additional spin-up of the buoyancy driven circulation due to the additional ice shelf meltwater (freshwater feedback effect). Therefore in the ice shelf melting fixed cases, the thermal effect is still present, however the freshwater feedback is denied, because the ice shelf freshwater flux is fixed. These experiments will be used to calculate the strength of the local freshwater feedback effect and the determine processes that cause it. These experiments will also enable the determination of the sign of this feedback effect. The aim of understanding feedbacks in the model is to help

understand the non linear relationship of iceshelf melting and therefore to help improve parameterisations of ice shelf melting in large scale models and ice sheet models.

The black line, in Figure 3.7, is the melt rates curve already shown from the reference simulations. The blue line is where the freshwater outputted from the ice shelf is fixed to be that of the all WW case, so the ColdMelt-fixed cases, but still then diagnosing what the model calculates to be the melt rates when the different forcings are applied to this set-up. The melt rates are reduced when compared to the black line, with an increasing difference. An approximately 40 % reduction is observed in the melt rate change from the full WW case to the full CDW forcing case, when compared to the reference set-up. Thus taking the difference between the ColdMelt-fixed simulation and the reference simulation for the full CDW forcing (thickness of CDW + thermocline = 1400 m) and comparing to reference case melt rate for the full WW case (thickness of CDW + thermocline = 0 m) , the feedback freshwater effect is found to be $\approx$ 6 m/yr from moving between the extreme range of the full WW case to the full CDW case. The remaining change in melt rate from the WW forcing case $\approx$ 11 m/yr, which is the thermal effect from moving between the full WW case to the full CDW case.

In addition this method is also applied with the 'WARM' and 'COLD' set-ups swapped, therefore leading to creation of the 'WarmMelt-fixed' set of simulations. In the 'WarmMelt-fixed' set of simulations the ice shelf freshwater flux is fixed to that of the steady ice shelf freshwater flux from the 'WARM' set-up. This set of simulations again has a range of set-ups with forcings that are between the two 'WARM' and 'COLD' forcings. Again first the 'WARM'/'COLD' set-ups are set to be the set-ups with the all CDW/WW forcings respectively.

The red line in Figure 3.7 shows the WarmMelt-fixed cases, where the ice shelf freshwater flux is fixed to that of the all CDW forcing simulation, while still calculating the ice shelf melt output for different forcings applied to it. Melt rates are reduced when compared to the reference case for the all WW forcing case, with the melt rate for the WarmMelt-fixed case becoming even slightly negative on average. This is because there is still a large cold freshwater flux being applied, even though the forcing temperatures are now cold, enabling freezing to occur. Therefore the WarmMelt-fixed case has the equivalent of an approximately 25 % increase in the melt rate change from the full CDW forcing case to the full WW forced case compared to the reference simulations. Therefore the freshwater effect can be taken to be $\approx$ 4 m/yr while the thermal effect is $\approx$ -20 m/yr moving between the extreme range of the full CDW case and the full WW forcing case.

Therefore the freshwater effect has an opposite sign when moving from warm forcings to cold forcing compared to vice versa. In the ColdMelt-fixed case, fixing the melt rate to a reduced melt rate suppresses the buoyancy driven overturning and thus leads to a reduced sensitivity to warming. However, for the WarmMelt-fixed case, fixing the melt rate to a higher melt rate causes a strong cold freshwater flux, which enhances the

effect of the cooling. This result is perhaps unexpected as it is in contrast with other freshwater feedback studies, which found a positive feedback effect from an increase in meltwater flux (Jourdain et al. 2017, Donat-Magnin et al. 2017, Kimura et al. 2017).

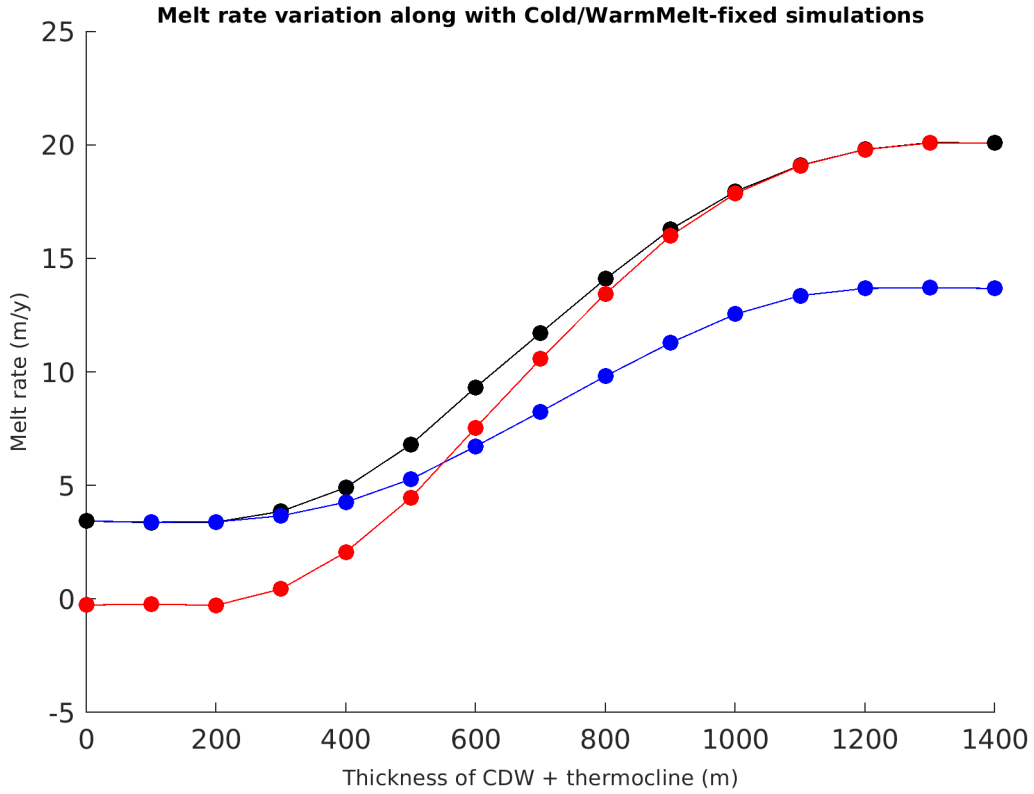

FIGURE 3.7: Idealised model ice shelf average melt rates, for a range of CDW + thermocline thicknesses for initial conditions and restoring applied to the northern boundary. Melt rates shown are for the reference case (black), the ColdMelt-fixed cases (blue) and the WarmMelt-fixed cases (red). All melt rates are when the model has reached a steady state.

The spatial distribution of the ice-shelf melt rates is examined for the full WW and CDW forcing cases and compared to the Warm/ColdMelt-fixed cases respectively for the same forcings (Figure 3.8), in order to understand the differences in the melt rates and the freshwater feedbacks that are occurring. The plan view taken of the ice shelf is the same as is taken in Figure 3.3, with the plume region located on the west side of the ice shelf. The spiked appearance of the melt rate field is most likely due to the stepped slope of the ice shelf in the model set-up as previously discussed in Section 3.1. For the CDW forcing reference case, large melt rates are observed, with the highest in the plume, but with significant melt occurring outside it as well (Figure 3.8b). Comparing the ColdMelt-fixed all CDW forcing case to the reference, a moderate increase in the ice shelf melt rate within the plume is observed, but a slight reduction in melt rates

elsewhere on the ice shelf occurs as well (Figure 3.8f). This leads to the overall lower ice-shelf melt rate of the ColdMelt-fixed case compared to the reference case, shown in Figure 3.7, despite an increase in melt rates within the plume area. The result of reduced overall melt rate of the ice shelf with the reduced freshwater is in line with the results of other such feedback studies (Jourdain et al. 2017, Donat-Magnin et al. 2017, Kimura et al. 2017). However, the increased melt rates inside the plume region is perhaps unexpected and suggests a more complex situation, with possibly multiple feedback processes occurring.

In order to investigate the full reasons for this change in melt rates the ice shelf parameterisation equations are restated:

$$c_p \rho \gamma_T^f u^* (T - T_b) + \rho_I c_{pI} \kappa \frac{T_s - T_b}{h} = -L \rho q_m, \tag{3.1}$$

$$\gamma_S (S - S_b) = -S_b q_m, \tag{3.2}$$

$$T_b = A_0 S_b + B_0 p_b + C_0, \tag{3.3}$$

where they are described fully in Section 2.1.2. The input of oceanic heat term that balances the latent heat term in (3.1) scales with the friction velocity (u^*) and the temperature forcing ($(T-T_b)$ where T_b is the temperature at the interface). Therefore the changes in the forcings applied to the ice shelf between the reference case and the iceshelf meltwater fixed cases are considered, specifically the friction velocity (u^*) (Figure 3.9) and the temperature forcing ($(T - T_b)$ where T_b is the temperature at the interface) (Figure 3.10). A drop in friction velocity over the whole ice shelf is observed in the ColdMelt-fixed case (Figure 3.9f) and while the largest drop in friction velocity is in the plume, elsewhere the friction velocity drops to near zero, leading to minimal heat transfer. This reduction of the friction velocity is because of the prescribed reduction in output of buoyant freshwater, from the ice shelf, which drives the plume and flow under ice shelf. This reduction in friction velocity therefore reduces the exchange of heat between the ocean and the ice, leading to reduced melt rates. However, an increase in melt rates is observed in the plume, which is due to an increase in the temperature forcing applied to the ice shelf especially in the plume region (Figure 3.10f), which is due to decreased output of cold freshwater from the ice shelf. Therefore in the plume region the increase in temperature forcing outweighs the reduced heat transfer, due to decreased ice shelf friction velocities, to lead to an increase in ice-shelf melt rates in this region. In contrast, outside the plume region the friction velocity is decreased down to close to zero, leading to minimal heat transfer occurring, which outweighs the slight increase in temperature forcing, leading to the drop in the ice shelf melt rates in this region and overall.

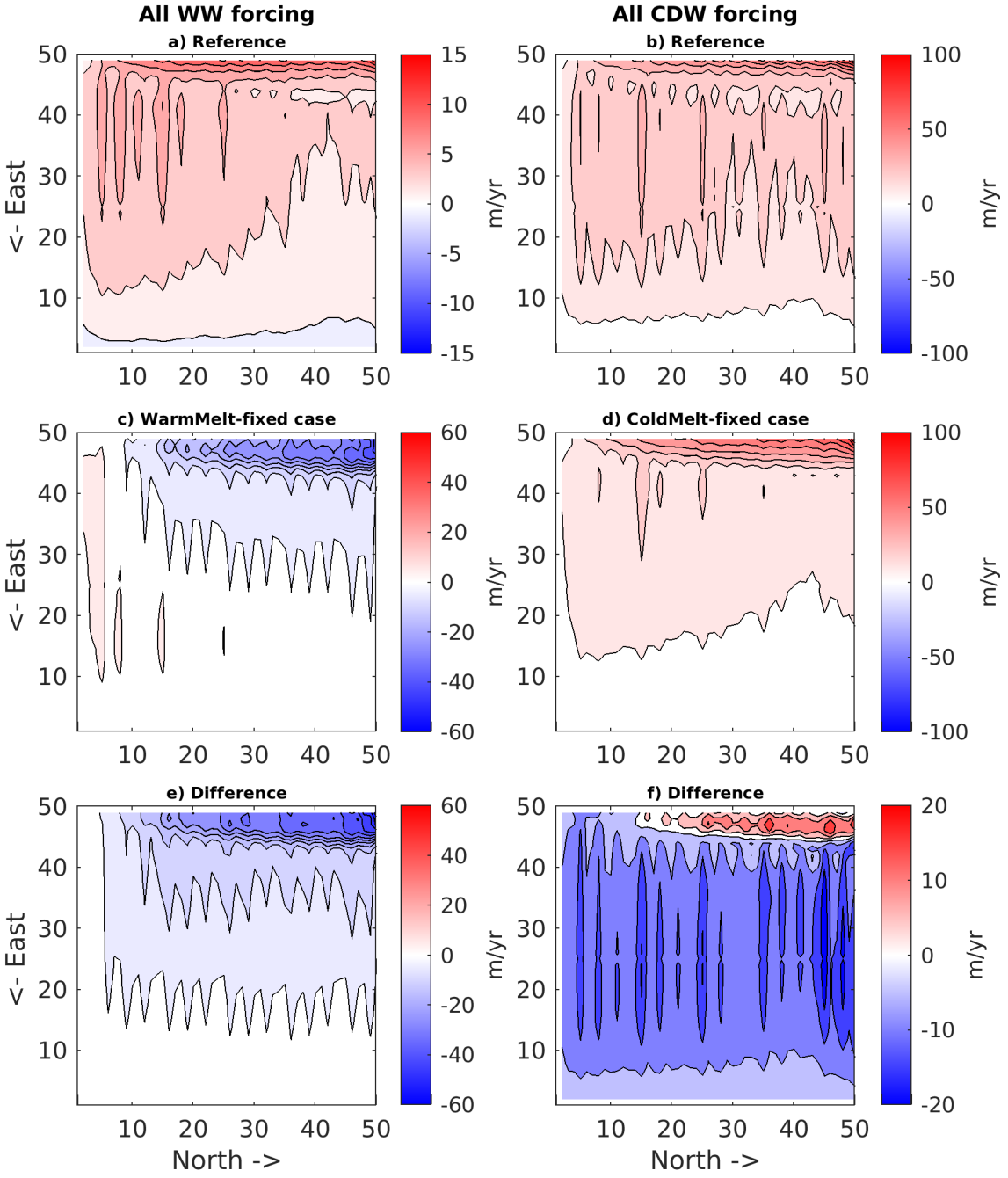

FIGURE 3.8: Plan view of the spatial distribution of steady state ice-shelf melt rates for: a) All Winter Water forcing reference case, b) All CDW forcing reference case, c) WW forcing case but with CDW forcing case ice shelf freshwater flux applied (WarmMelt-fixed case), d) All CDW forcing case but with WW forcing ice shelf meltwater flux applied (ColdMelt-fixed case), e) Difference of WarmMelt-fixed case - WW forcing reference case and f) Difference of ColdMelt-fixed case - CDW forcing reference case.

The spatial distribution of the steady state ice-shelf melt rates for the WarmMelt-fixed case is examined and compared to the reference case for all WW forcing. For the WW forcing reference case, low melt rates are observed but with the highest in the plume region (Figure 3.8a). However, in the WarmMelt-fixed case for the same full WW forcings a strong freezing occurs especially in the plume region, with therefore melt rates becoming negative (Figure 3.8c). This leads to the strong negative melt rate difference in the plume region (Figure 3.8e). This result as mentioned before is perhaps unexpected, as other studies have found a positive feedback effect from an increase in ice meltwater flux (Jourdain et al. 2017, Donat-Magnin et al. 2017, Kimura et al. 2017), but here a drop in ice shelf melting is observed.

Examining the differences in the forcings applied to the ice shelf shows a large increase in the friction velocity in the plume in the WarmMelt-fixed case (Figure 3.9e). However a large drop in the temperature forcing is observed as well (Figure 3.10e), with the temperature forcing for the WarmMelt-fixed case even becoming negative in the plume region, implying freezing can occur (Figure 3.10c). Therefore in the WarmMelt-fixed case for this forcing there is more freshwater being outputted than in the reference case, which increases the velocity of the plume, increasing the exchange of heat between the ice shelf and the ocean. However, in the all WW forcing case there is minimal heat available to melt the ice shelf and increasing the ice shelf meltwater flux increases the amount of cold water at the ice shelf interface, therefore reducing the ice shelf melt rates and making them negative. This therefore confirms that the local cavity freshwater feedback effect is dependent on the available heat within the cavity.

Therefore from an increase in iceshelf meltwater flux a overall negative freshwater feedback is observed in the case. However, the freshwater feedback effect observed is due to the combined effect of a buoyancy driven positive feedback and a temperature driven negative feedback, which leads to the overall reduction in melt rates observed in the model.

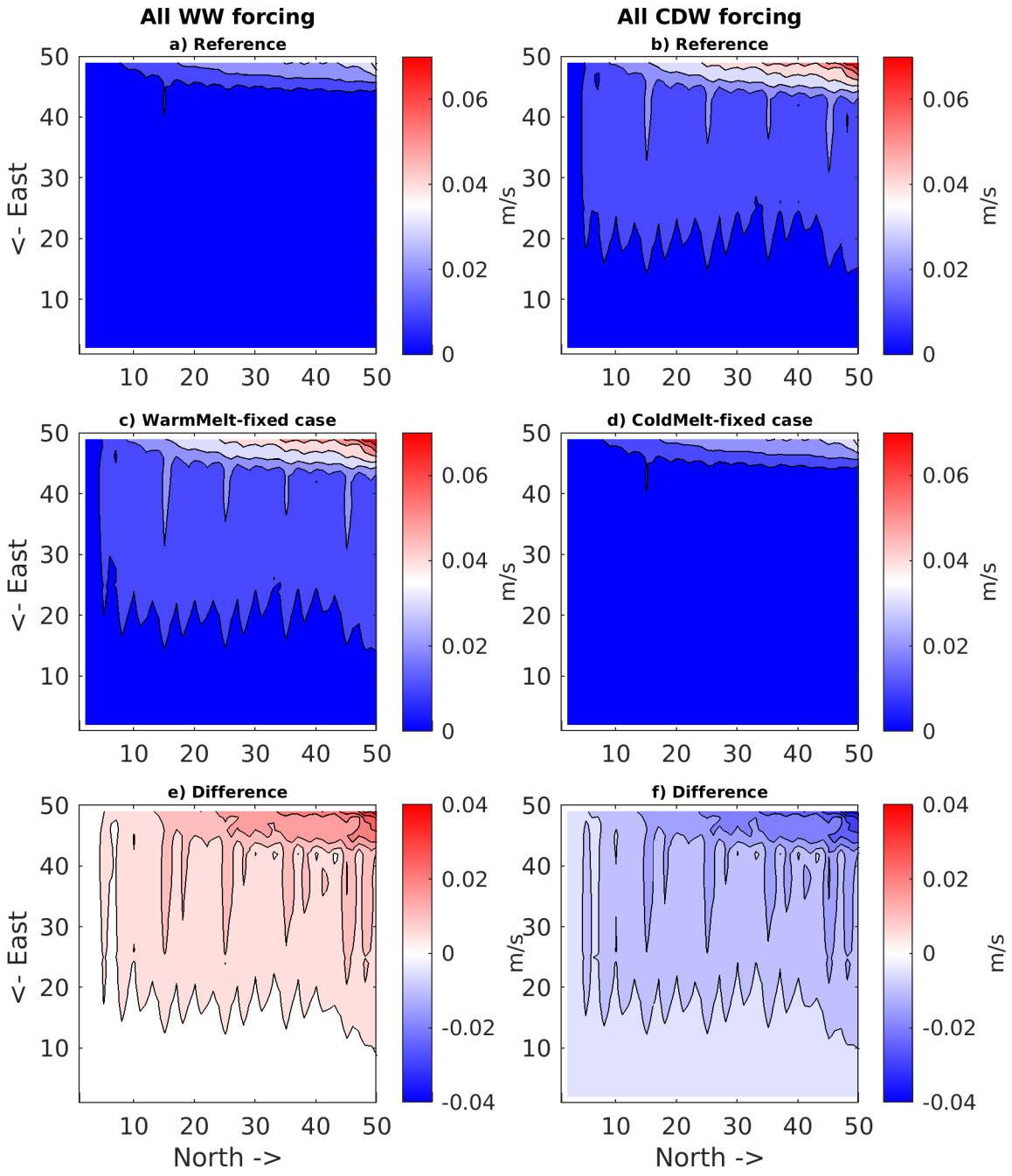

FIGURE 3.9: Plan view of the spatial distribution of steady state ice shelf friction velocity u^* for: a) All Winter Water forcing reference case, b) All CDW forcing reference case, c) WW forcing case but with CDW forcing case ice shelf freshwater flux applied (WarmMelt-fixed case), d) All CDW forcing case but with WW forcing ice shelf meltwater flux applied (ColdMelt-fixed), e) Difference of WarmMelt-fixed case - WW forcing reference case and f) Difference of ColdMelt-fixed case - CDW forcing reference case.

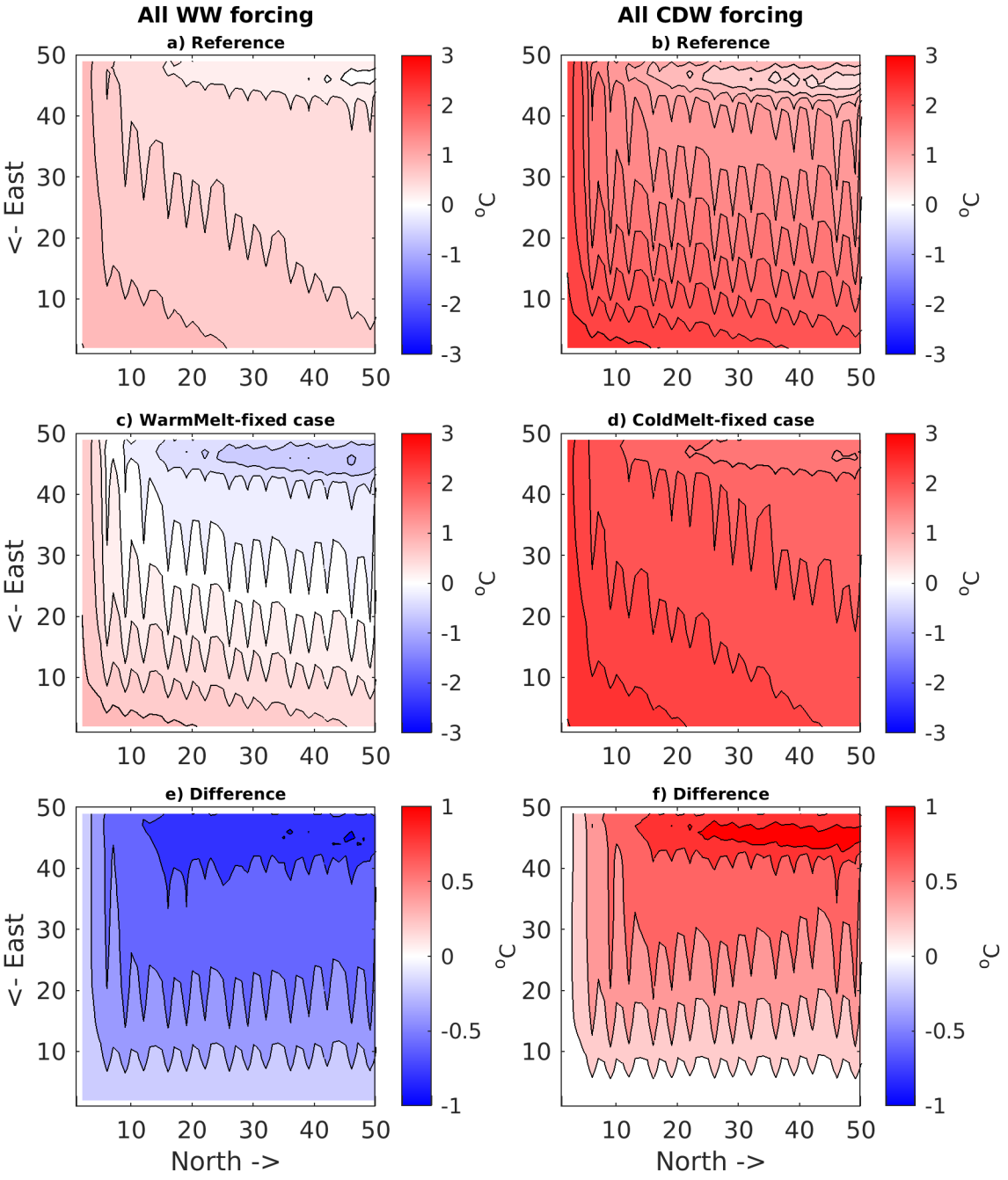

FIGURE 3.10: Plan view of the spatial distribution of steady state ice shelf temperature forcing for: a) All Winter Water forcing reference case, b) All CDW forcing reference case, c) WW forcing case but with CDW forcing case ice shelf freshwater flux applied (WarmMelt-fixed case), d) All CDW forcing case but with WW forcing ice shelf melt-water flux applied (ColdMelt-fixed case), e) Difference of WarmMelt-fixed case - WW forcing reference case and f) Difference of ColdMelt-fixed case - CDW forcing reference case.

However, the strength of the freshwater feedback effect calculated may be dependent on the range of CDW layer thicknesses it is calculated over. So far the freshwater feedback has been calculated over an extreme range of CDW layer thicknesses, as the variability of CDW layer thickness observed in the Amundsen Sea is less than the range proposed in the previous model simulations. This could lead to an over estimate of the local cavity freshwater feedback strength. Therefore the freshwater feedback is now investigated for just the range of CDW + thermocline thickness of 600 m to 800 m, as this better represents the variability in the region. Figure 3.11a displays melt rates over the smaller range of just 600 m to 800 m, where the black line is the reference melt rates and the green line being the cases when the ice shelf freshwater flux is fixed to the 600 m case, which will be referred to as the realistic ColdMelt-fixed cases. The effect is observed to be significantly reduced, with about a 10 % reduction in the melt rates of the 800 m case compared to the reference case. This leads to a thermal forcing effect of ≈ 4 m/yr and a freshwater feedback effect over this range of ≈ 0.75 m/yr, where the freshwater effect is split into as discussed about a buoyancy-driven positive feedback effect and a thermal driven negative effect. Therefore a reduction in the ratio of freshwater feedback effect to thermal effect, compared to what was observed over the larger extreme range studied previously.

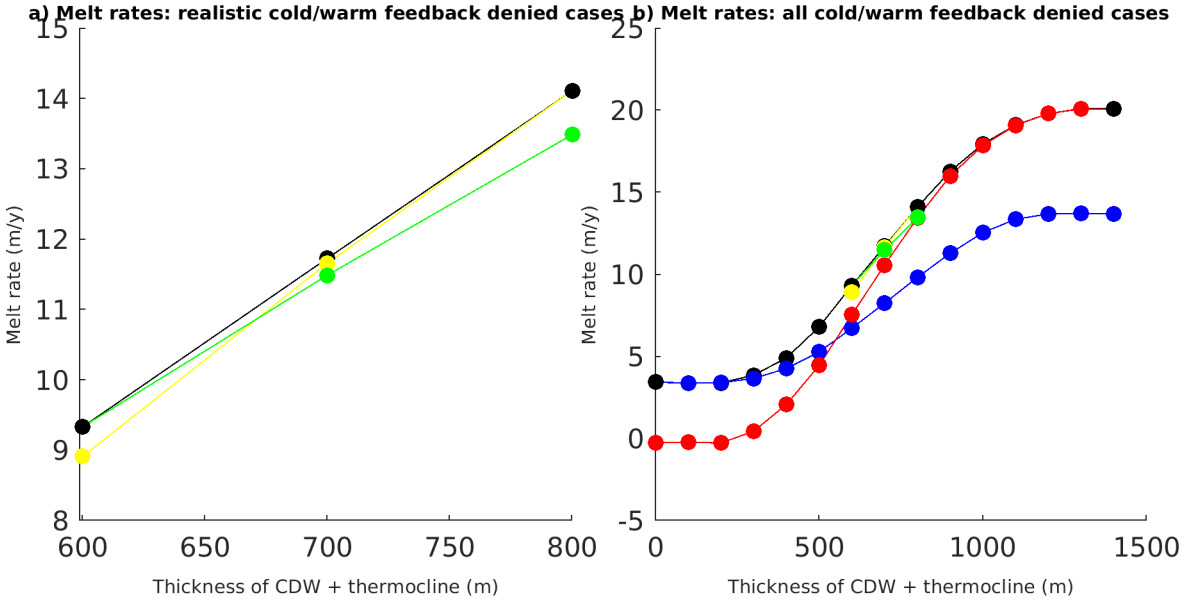

FIGURE 3.11: Idealised model ice shelf average melt rates, for the a) realistic range and b) extreme range of CDW + thermocline thicknesses for initial conditions and restoring applied to the northern boundary. Melt rates shown are for the reference case (black), the realistic ColdMelt-fixed cases (green), the ColdMelt-fixed cases (blue), the realistic WarmMelt-fixed cases (yellow) and the WarmMelt-fixed cases (red). All melt rates are when the model has reached a steady state.

The yellow line in 3.11a shows the calculated melt rates when the freshwater flux is fixed to that of the 800 m CDW plus thermocline thickness case and will be referred to as

the realistic WarmMelt-fixed cases. There is a reduction in melt rates in the realistic WarmMelt-fixed cases compared to the reference case at the 600 m CDW plus thermocline forcing. However, the freshwater effect is significantly reduced when compared to the extreme range simulations, with the freshwater effect being ≈ 0.5 m/yr, which could be split again into buoyancy driven freshwater feedback and a thermal driven freshwater feedback, and the forcing thermal effect being $\approx$ -4.5 m/yr. The reduction in the effect over the realistic range compared to the extreme range can be more easily be observed in 3.11b, when it is compared to the extreme range simulations previous discussed. However, it is worth noting that the signs of the freshwater feedback effects remain the same in the realistic Warm/ColdMelt-fixed cases, as compared to the cases over the extreme range.

3.4 Conclusions

In this chapter an idealised model was utilised in order to examine the vertical distribution of ice shelf meltwater with respect to different CDW forcing and to determine the local cavity freshwater feedback. The key results are listed below in relation to the section's aims:

1. **Investigate the vertical distribution of ice shelf freshwater for varying CDW layer thickness.**

   The depth of ice shelf tracer in the idealised model was found to significantly depend on the CDW thickness of the forcings and initial conditions applied to the model. Though an extreme range of CDW thicknesses were used for this study, even within a more realistic range significant differences do occur. Two plumes are found to form in the model; the primary plume which reaches the surface and a secondary which intrudes into the pycnocline. When the CDW thicknesses is higher more ice shelf meltwater reaches the surface and less intrudes into the pycnocline. However for smaller CDW thickness forcings, comparatively more ice shelf meltwater is found to intrude into the pycnocline than reach the surface. It worth noting that as the CDW thickness changes so does the depth at which the pycnocline is located. These results may be effected by the introduction of vertical mixing schemes, rather than the constant uniform vertical diffusivities used in this study, however the processes discussed here will still occur.

   It should be noted that this idealised model set-up lacks an annual cycle in WW temperature and an annual cycle in near surface vertical stratification. If these were included in the model an annual cycle in the ice shelf meltwater vertical distribution could be observed in the top portion of the water column. This could be especially true if the summer presence of AASW is included in the model. This could impact the vertical distribution of the primary plume with potentially less

reaching the surface in the summer, with potentially part of the plume remaining below the AASW layer. In addition, if a reduction in the strength of the pycnocline occurred in the model more of the plume might be expected to rise above the pycnocline in the primary plume, with less meltwater consequently in the secondary plume. This could have impact on the vertical stratification and potentially lead to a stronger pycnocline again, leading to a potential negative feedback that could be present in the system. However, further research would required to investigate this process.

2. **Investigate the local ice shelf freshwater feedback effect.**

   The effect of the freshwater feedback was determined using a developed freshwater feedback method, as described previously in Section 3.3. The freshwater feedback effect is found to be significant over an extreme range of oceanic forcings, ranging from full CDW forcing to full WW forcing. In addition, the freshwater feedback effect is found to be of different signs compared to the difference in thermal forcings.

   Examining the spatial distribution of the freshwater feedbacks effects over the extreme range showed a strong variation in spatial distribution with the strongest effects on the melt rates occurring in the meltwater plume region on the west side of the ice shelf. A strong reduction in melt rates is observed in the plume region in the WarmMelt-fixed case, when compared to the reference WW forcing case. This is because of a strong reduction in temperature forcing and an increase in the friction velocity, due to the excess cold freshwater flux that is applied. However, the ColdMelt-fixed case observes a moderate increase in melt rates in the plume while elsewhere on the ice shelf a reduction in melt rates occurs when compared to the reference CDW forcing case. This is due to the friction velocity reducing to near zero over the ice shelf, while in the plume region only a small reduction in friction velocity occurs. This coincides with an increase in the temperature forcing in the plume region, due to a decrease of the cold ice shelf freshwater flux, leading to the different changes in melt rates in the different regions of the ice shelf.

   However, the freshwater feedback effect is found to be smaller when examined over a more realistic range of CDW thicknesses compared to the inter-annual variability that is observed in the Amundsen Sea. However, signs of the freshwater feedbacks are the same as in the extreme range cases. In addition in this study only the in cavity local freshwater feedback is investigated. Therefore in the future more far field feedbacks could be investigated using a realistic regional model, and these feedbacks in combination could prove to be more significant.

It should be noted that the results in this chapter are with caveats due to the use of constant vertical diffusivities as a vertical mixing parameterisation. Therefore the use of other parameterisations could effect the results in this idealised study. However, the processes that are discussed in this section would still occur.

Chapter 4

Freshwater in the Amundsen Sea

In Chapter 1 the importance of understanding the Amundsen Sea freshwater balance is shown. Therefore, in this chapter the local freshwater balance in the region is investigated, using the Amundsen Sea regional model and passive freshwater tracers. The aims of the sections in this chapter are:

4.1) The model is validated against available data for the region and the model's performance is assessed.

4.2) The local freshwater average spatial distribution is investigated and compared to available observations.

4.3) The seasonality of the local freshwater balance is investigated using a range of methods and compared to surface oceanic conditions.

4.4) The inter-annual variability of the local freshwater balance is investigated using a range of methods. Relationships between the freshwater sources are discussed.

The regional Amundsen Sea setup, described fully in Section 2.3, has a domain that extends from 75.5°S to 62°S and 140°W to 80°W covering the Amundsen Sea embayment, but the analysis in this section will concentrate on the region extending from 75.5°S to 71.5°S and 130°W to 95°W. This model setup employs open boundary conditions using steady climatological seasonal monthly conditions for ocean velocity, salinity and temperature, taken from Holland et al. (2014). A sea ice model is included in this setup and the model is forced with ERA-Interim reanalysis forcing from 1979-2018 (Dee et al. 2011), but the first 10 years are regarded as model spin up. In this setup ice shelf melting is calculated using using heat and salt turbulent exchange coefficients that have an implicit velocity dependence. There is no explicit horizontal diffusion of salt, heat or tracers in the model, but the vertical diffusion is parametrized by using the K-profile parameterization (KPP) scheme (Large et al. 1994). The air-ice drag coefficient is set to 0.0025, the demarcation ice thickness is set to 0.5 m, and sea ice advection uses a

3rd-order direct-space-time flux-limited scheme. Ocean parameters were kept the same as those used by Kimura et al. (2017).

4.1 Regional model validation

This section aims to validate the model with available data to show how the ocean model, the sea ice model and modelled ice shelf freshwater fluxes compare to available observations. However, wide spread comparison to observations is difficult for remote regions like the Amundsen Sea, where available data is limited temporally and spatially, due to the region's inaccessibility.

In order for the model to accurately simulate the region, one key oceanic feature that needs to be simulated is the intrusions of warm CDW onto the continental shelf. Therefore, as an initial assessment and despite the oceanic conditions in the region having a large inter-annual variability, the climatology of the modified Circumpolar Deep Water's (mCDW) maximum subsurface potential temperature is compared to observations. Note that for this comparison only years where observational data is available are used to create the model climatology. The model broadly recreates the climatology of the mCDW intrusions onto the continental shelf (Figure 4.1a), compared to an observational climatology derived from CTD casts (Figure 4.1b) (Dutrieux et al. 2014). The model recreates the higher mCDW temperatures to the east of the grounded BRI, including the higher temperatures on the eastern side of this region, particularly the region close to the shelf break. However, the model is colder in the Dotson Trough, which is west of the grounded BRI, compared to observations. This could be due to the shallow model bathymetry in this area and at the trough entrance compared to observations, which restricts access of CDW onto the shelf and its intrusion to ice shelves like Dotson Ice Shelf.

In order to assess the performance of the model's inter-annual variability of oceanic conditions in front of ice shelves, the model is compared to summer CTD salinity and potential temperature profiles in front of PIG (Figure 4.2a-b) and Dotson ice shelves (Figure 4.2c-d). This comparison uses observational CTD profiles taken in the red and green boxes (Figure 4.1a), and closer to the ice shelf fronts where present (Dutrieux et al. 2014, Jenkins et al. 2018). For the comparison the model is sampled at the closest model grid point to where the individual observations were taken and at the same month and year as the individual CTD profiles. In both locations, the summer surface salinity is fresher in the model compared to observations. Near PIG Ice Shelf, the model approximately recreates observed mean salinity and temperature profiles, though with a reduced standard deviation (Dutrieux et al. 2014). However, near Dotson Ice Shelf the model approximates the variation observed, but is too cold and unable to simulate the deepest parts of the observational casts, due to a shallow seabed data set.

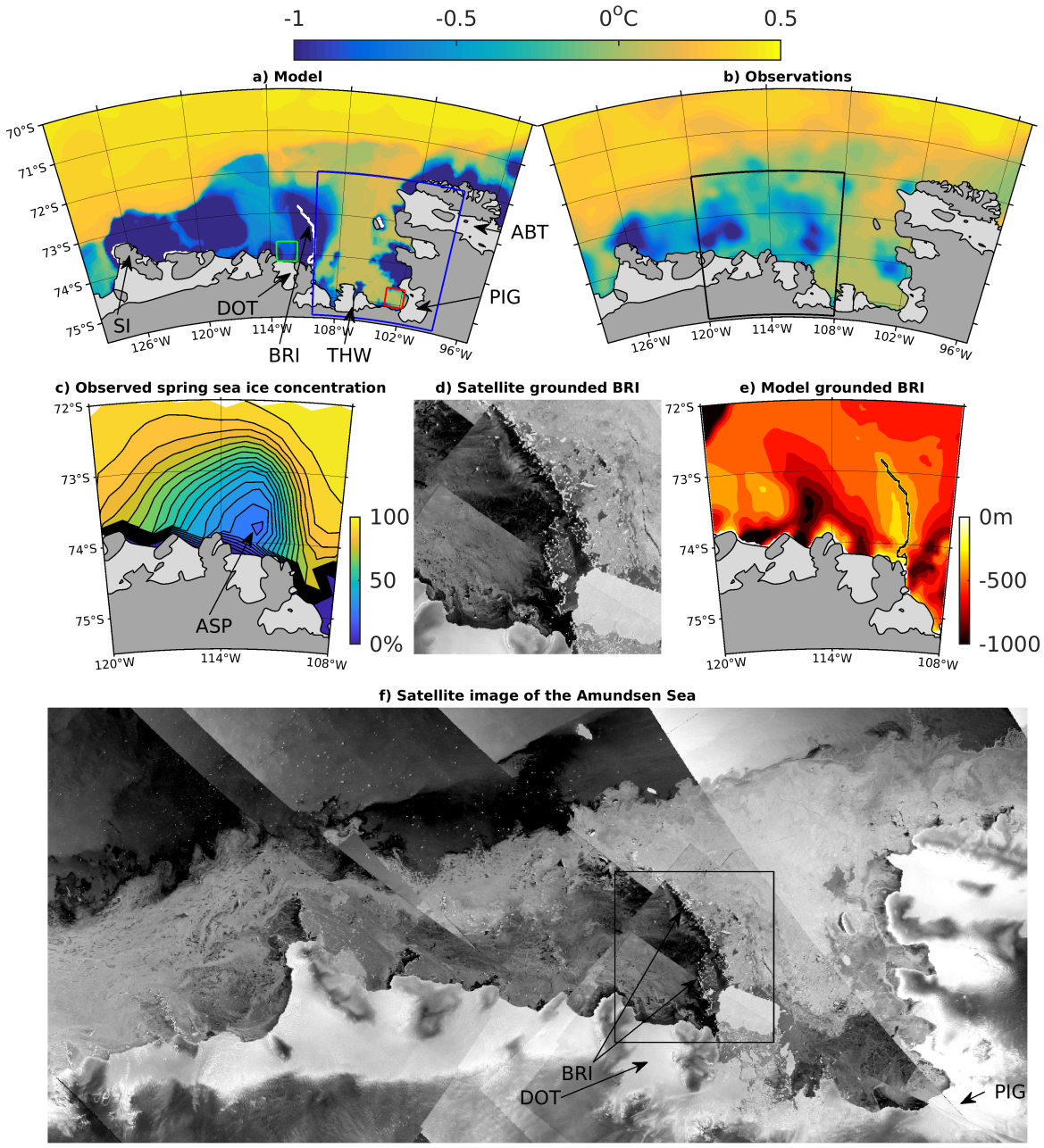

FIGURE 4.1: Depth maximum climatological subsurface potential temperature (1994-2012, but using only observational available years) from: (a) model and (b) observations (Dutrieux et al. 2014). The black box in (b) shows the area in (c)(e). (c) Spring satellite observations of the AMSR-E sea ice concentrations (2003-2010) (Cavalieri et al. 2014). (e) Model bathymetry with representation of grounded icebergs. (d)(f) Satellite image mosaic composed of Copernicus Sentinel-1 SAR (Synthetic Aperture Radar) data. The composite uses imagery acquired between 30th April 2017 and 6th May 2017. Image composite was processed by BAS using Google Earth Engine. The black box in (f) shows the area in (d). Key locations are shown in (a)(c)(f), where SI = Siple Island, DOT = Dotson Ice Shelf, BRI = Bear Ridge grounded Icebergs, THW = Thwaites Ice Shelf, PIG = Pine Island Glacier Ice Shelf, ABT = Abbot Ice Shelf and ASP=Amundsen Sea Polynya.

Comparisons to the detailed vertical structure of the water column are a stringent test for any model, considering the approximations caused by vertical and horizontal grid resolution and uncertain models of ocean mixing and sea ice. The model approximates ocean conditions sufficiently well for the purposes of this study, which is to examine the local freshwater balance of the Amundsen Sea.

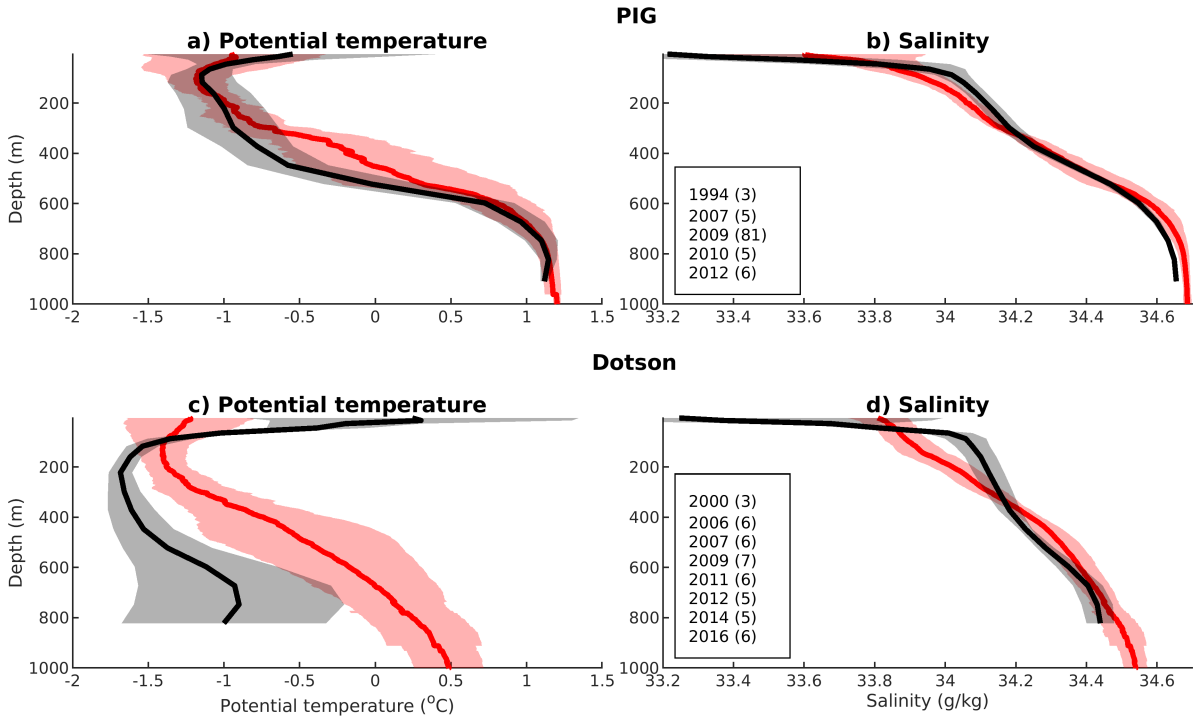

FIGURE 4.2: Observed (solid red lines) and model output from reference case (solid black line) mean profiles for salinity and potential temperature near PIG and Dotson ice shelves. The shaded areas represent one standard deviation of the inter-annual variability from the mean. CTD profiles taken from Jenkins et al. (2018) for Dotson and Dutrieux et al. (2014) for PIG, taking CTD locations that are either within the red and green boxes in Figure 4.1a or closer to the ice shelves. Model is sampled at the closest grid point to the individual CTD observations and at the same month and year. The number of CTD profiles for each austral summer are indicated for both regions.

To better visualize the inter-annual variability of the ocean conditions in front of these ice shelves, Figure 4.3 shows the potential temperature and salinity in front of PIG and Dotson ice shelves, via Hovmöller diagrams averaged over the green and red boxes, in Figure 4.1a. In front of PIG Ice Shelf, similar to observations the model captures the colder conditions in 2000 and warm years of 2007-2010. It also features a cooler period in the mid-2010s, though this cooling is later and less intense than observed (Dutrieux et al. 2014). However, our understanding of the regions inter-annual is with some caveats, as there are large gaps in the oceanographic observations for this region. For example, there are no observations of the cooler year 2000 in front of PIG Ice Shelf. Therefore, it is not possible to compare the intensity of this cooler year in front of PIG Ice Shelf to observations. However, there are observations taken elsewhere in this year which do agree with the general cooler conditions observed in the model in that year. In addition,

there are minimal austral winter observations in the region, with observations primarily being taken in the austral summers months from research cruises to the region. These cruises in addition have only become more frequent after 2006 and many don't venture in front of PIG Ice Shelf. Therefore there is some uncertainty to inter-annual variability in the region. However, with the caveats as discussed above, the model approximately captures the observed inter-annual variability. In front of Dotson Ice Shelf the model captures the large variability observed at the depths simulated in the model, with the model being cold in 2000 and warm approximately from 2006-2011 and cold again 2012-2016 (Jenkins et al. 2018).

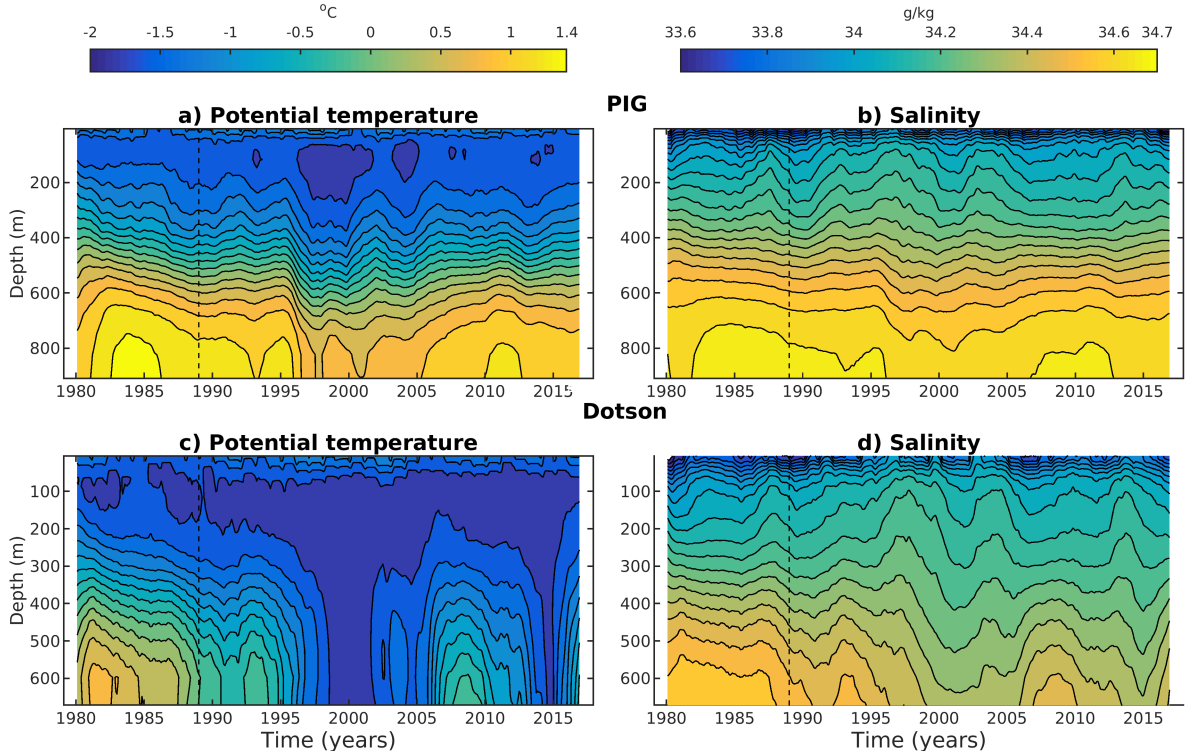

FIGURE 4.3: Hovmöller diagrams of potential temperature and salinity in front of PIG Ice Shelf (a-b) and Dotson Ice Shelf (c-d). Hovmöller diagrams are averaged over the red and green boxes shown in Figure 4.1a and include 10-year model spin up. A 2-year running average is applied at each depth. Vertical black dashed lines indicate end of model spin up period.

Figure 4.4 shows the mean of the seasonal sea ice concentrations from 2003 to 2010 for the model (e-h), so it can be compared to satellite observations taken from AMSR-E satellite (a-d) (Cavalieri et al. 2014). The model replicates the sea-ice concentration observations well in the winter and spring, by recreating the high sea ice concentrations observed, though the ASP polynya is smaller in the model, especially in the spring. However, the model under-predicts sea ice cover in the summer and autumn, though similar distribution patterns of sea ice are still produced in the model for these months. The grounded BRI in the model reproduces the ASP sufficiently well, as well as the higher concentrations of sea ice east of the grounded BRI that are observed in the satellite observations. Though there is an increased seasonal cycle in sea ice concentration the

model, the sea ice model still preforms this difficult task sufficiently well for this study, as key features and distributional patterns are still reproduced.

The seasonal cycle of the sea ice thickness for the model, (Figure 4.4i-l), is within the range of observations for the region (Kurtz & Markus 2012, Worby et al. 2008), though sea ice thickness observations have a large uncertainty. The model shows the thickest sea ice is in the winter and spring and is east of the grounded BRI and along the coast north of Abbot Ice Shelf, peaking at around 2 m in the spring. There is also substantial thickness east of Siple Island.

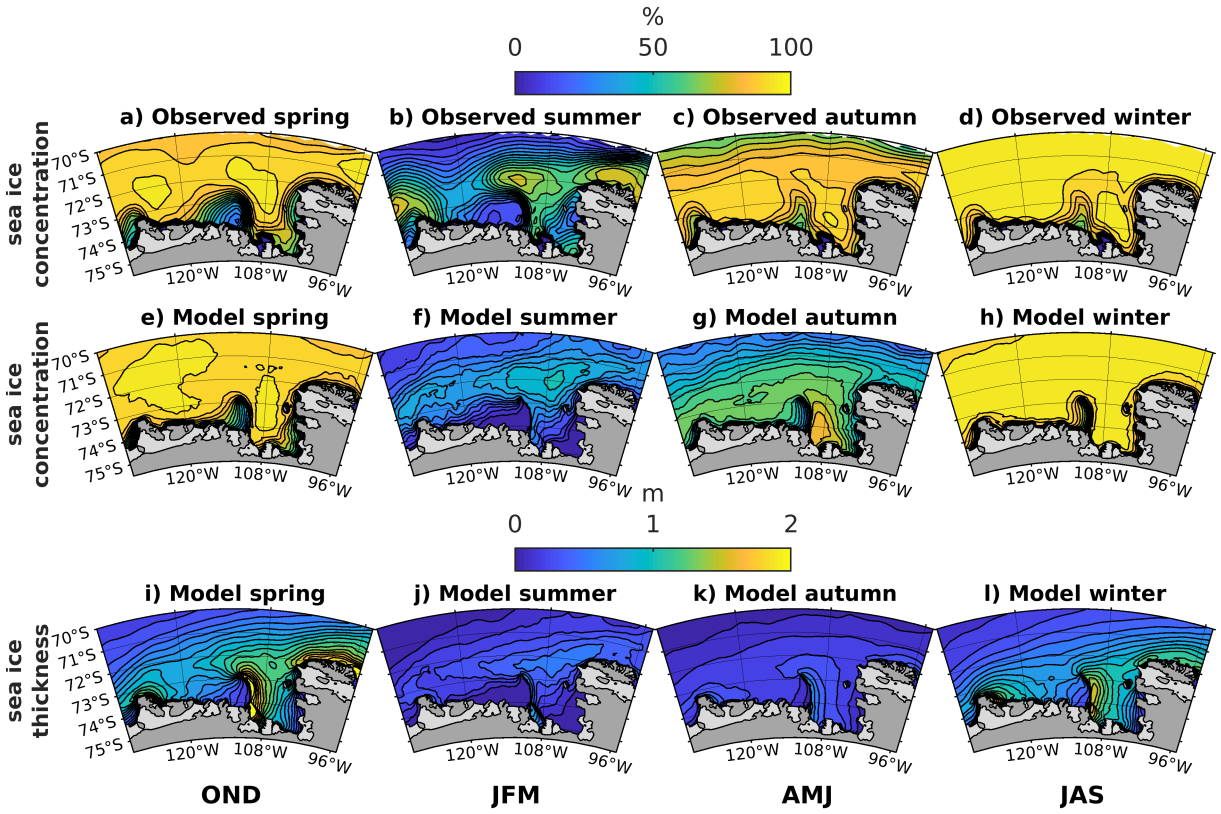

FIGURE 4.4: Climatological seasonal cycle of the satellite observations of the AMSR-E sea ice concentrations (a-d) (Cavalieri et al. 2014). Model climatological seasonal cycle of sea ice concentrations (e-h) and the sea ice thickness (i-l). All averaged over the period 2003-2010.

In order to assess the performance of the modelled ice-shelf melt rates, the average and the variability of ice-shelf melt rates in the model are compared to a recent modelling study and observations. Therefore, Table 4.1 summaries the mean ice-shelf melt rates and standard deviations in the model, as well as in another modelling study and for observations, including those derived from oceanographic observations and from satellite derived glaciological mass budgets. The climatology of the ice shelf melt rates are similar to those simulated and validated extensively in Kimura et al. (2017), with the largest ice-shelf freshwater fluxes originating from PIG and Thwaites ice shelves. Getz Ice Shelf average melt rates in this study are found to be closer to the observed rates, compared to

the modelling study of Kimura et al. (2017), though still with possibly a larger variability than that observed. In this study and in Kimura et al. (2017), low modelled melt rates are observed for Dotson and Crosson ice shelves compared to observations. Low Dotson Ice Shelf melt rates in the model are suggested to be due to the too shallow bathymerty in the model in this region, which restricts warm CDW intrusions reaching the ice shelf. Similarly the low melt rates observed for Crosson Ice Shelf could be due to too shallow bathymetry in front of this ice shelf, because of a lack of data in this particularly inaccessible area, due to high concentrations of icebergs and sea ice. However, the model overall replicates the melt rates of the ice shelves sufficiently well for this study, especially as the ice shelves of PIG, Thwaites, Getz and Abbot are modelled well and these are the ice shelves with the highest observed melt rates. In addition PIG and Thwaites ice shelves are most important to the stability of the West Antarctic Ice Sheet. Therefore the assumption is applied that the low melt rates of Dotson and Crosson ice shelves will not effect the results of this study significantly.

There are a few other reasons to be noted that limit the model's ability to replicate the ice-shelf melt rates that have been observed. The relatively coarse grid of the model compared to the length scales of the ice shelves and the processes that occur in the melting process, means these process are not well resolved in the model. Therefore smaller scale processes like those within the ice shelf boundary layer are reliant on uncertain parametrisations, which are poorly constrained due to lack of observations for ice shelves in the Amundsen Sea. In addition in this study, ice shelf melt rates have no dependence on ocean velocities. However, as more observations are taken in the region in the future more specific parametrisations to the region could improve future model melt rates.

In addition, there is a lack of knowledge of the ice shelf cavities in this remote region. Differences between the model ice shelf draft and bathymetry under ice shelves compared to the actual could be expected to affect ice shelf melt rates (Schodlok et al. 2012). This is because representations of ice shelf cavities are important to the circulations underneath ice shelves and therefore ice shelf melt rates (Holland et al. 2008). An exception is PIG Ice Shelf, which is one of the ice shelves that have had parts of its ice shelf cavity explored using a autonomous submersible, revealing the presence of a ridge in the bathymetry beneath the ice shelf (Jenkins et al. 2010). This blocks part of the warm mCDW from reaching the grounding line of the ice shelf, which strongly affects the melt rate of the ice shelf (De Rydt et al. 2014). Therefore for other ice shelves, for which little is known about their ice shelf cavities, this provides a large problem for recreating observed melt rates. However, as our knowledge of the ice shelf cavities in this region increases, future model melt rates can be improved.

However, the model does have some weaknesses to its simulations of the Amundsen Sea region. The sea ice model is highly unconstrained due to lack of observations, which leads to large uncertainty. This is important issue as sea ice important for the

[Gt/yr]	Getz	DOT	CROS	THW	PIG	COS	Abbot	VEN
Model[a]	158±78	8±3	3±1	65±13	88±16	39±14	54±19	41±11
Kimura et al. (2017)[b]	257±71	13±5	2±1	57±17	78±24	37±16	45±39	35±12
Depoorter et al. (2013)[c]	136±23	78±23		69±18	95±14	11±3	86±22	15± 3
Rignot et al. (2013)[d]	145±14	45±4	39±4	98±7	101±8	9±2	52±19	19±2
Dutrieux et al. (2014)[e]					34-102			
Jenkins et al. (2018)[f]		20-92						

TABLE 4.1: Comparison of average model ice shelf melt rates (1989-2018) to other modelled melt rates and observed melt rates. The ± represents one standard deviation from the mean. Some ice shelf names have been shortened, where DOT = Dotson, CROS = Crosson, THW = Thwaites, PIG = Pine Island Glacier, COS= Cosgrove, VEN= Venables. a) Modelled melt rate from the reference simulation in this study (1989-2018). b) Modelled melt rates (1991-2014). c) Satellite based estimate of melt rates (1979-2010). Note that melt rate of Crosson is included within the Dotson melt rate. d) Satellite based estimate of melt rates (2003-2008). e) Oceanographic estimate of melt rate, with observations taken in 1994 (47 Gt/yr), 2007 (102 Gt /yr), 2009 (73 Gt/yr), 2010 (69 Gt/yr) and 2012 (34 Gt/yr). Oceanographic estimate of melt rate, with observations taken in 2000 (25 Gt/yr), 2006 (56 Gt/yr), 2007 (44 Gt/yr), 2009 (91.6 Gt/yr), 2011 (54 Gt/yr), 2012 (20 Gt/yr), 2014 (21 Gt/yr) and 2016 (20 Gt/yr).

region and will be investigate in this study. However, this is a weakness that effects all models. The model also employs the KPP vertical mixing parameterisation, which is unverified, due to lack of observations and therefore has a large uncertainly. In addition, the model relies on boundary conditions, as the model is a regional model. In these boundary conditions are climatological which could effect the inter-annual variability in the model. However, many of these weaknesses are common to other models and therefore the model is sufficient to examine the freshwater balance in the Amundsen Sea.

4.2 Freshwater spatial distribution

In this section, the average spatial distribution of the local freshwater sources are investigated by examining average freshwater fluxes and tracer fields over the region. Figure 4.5 shows the spatial distribution of the climatological freshwater fluxes (1989-2018), excluding a 10 year model spin up period (1979-1989), for all the different components of the freshwater balance, along with the total freshwater flux. The PmE (precipitation minus evaporation) freshwater contribution is orders of magnitudes less than the other sources, with iceberg melt flux being also smaller, but leading order compared to other sources, with average freshwater fluxes over the continental shelf of 1.3×10^6 m^3/yr and 1.3×10^{11} m^3/yr respectively. Therefore, sea ice and ice shelf sources are the two main climatological contributions to the freshwater budget over the continental shelf in the

Amundsen Sea, with average continental shelf freshwater fluxes of -2.5 $\times$ 10^{11} m^3/yr and 3.4 $\times$ 10^{11} m^3/yr respectively.

The sea ice freshwater flux climatology distribution shows a negative freshwater flux close to the coast and a positive flux in the north. This is due to sea ice growth in the austral winter in the south and average sea ice transport northward and sea ice melt in the austral spring (Abernathey et al. 2016). Therefore, the Amundsen Sea shelf is a net sea-ice export region. There is particularly strong negative freshwater flux on average in the ASP and near PIG Ice Shelf, where there is strong sea ice growth and export/divergence in the austral winter. These results agree with observations in the region finding evidence of average sea ice export in front of PIG Ice Shelf, with reduced or positive melting effect found further north at the shelf break (Biddle et al. 2019). In the total flux, the iceberg melt flux partially mitigates the negative fluxes of the sea ice, but there are still negative fluxes on average in the ASP and near PIG Ice Shelf, which may explain the convection issues in the previous model setup (Section 2.3.5). However, due to oceanic advection and diffusion of freshwater, the effect of freshwater sources cannot be determined by just examining the input fields; instead freshwater tracers need to be considered as well.

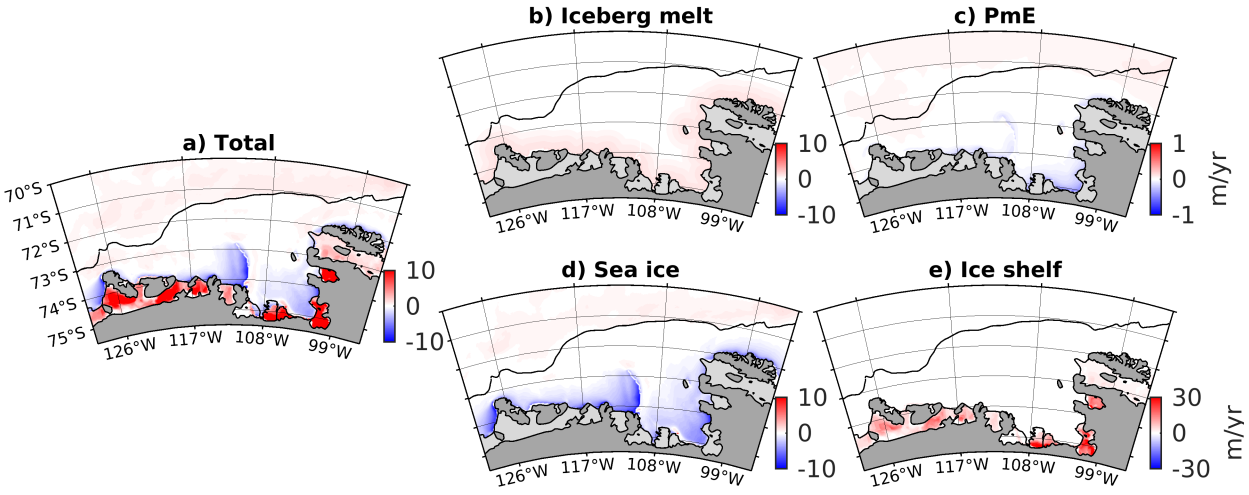

FIGURE 4.5: Climatology of freshwater fluxes (1989-2018) for (a) total freshwater, (b) iceberg melt, (c) precipitation - evaporation (PmE), (d) sea ice and (e) ice shelf melt. Black line represents the 1000 m depth contour of the continental shelf break.

4.2.1 Horizontal tracer spatial distribution

The climatological surface (top 10 m) tracer fields shown in Figure 4.6 reflect the combined processes of the spatial distribution of the flux fields and their redistribution due to oceanic advection and mixing. Off the continental shelf, positive sea ice tracer dominates the climatology of the freshwater balance in the surface. However, on the continental

shelf all sources are of comparable importance to the surface freshwater balance, though with varying spatial distributions for the individual components. This is despite the differences in the fluxes (Figure 4.5), because the larger sources (sea ice and ice shelf) are distributed over depth. Ice shelf freshwater is released at depth, while sea ice growth causes convection, driving its negative tracers deeper.

Ice shelf meltwater has its highest surface concentration within the westward coastal current, which agrees with observations in the region (Biddle et al. 2017, Nakayama et al. 2013) and other modelling studies (Kimura et al. 2017). Its tracer concentration increases towards the west, as it passes an increasing number of traced ice shelves, and spreads further from the coast, though no significant amounts cross the shelf break. It should be noted that a 1 % tracer concentration corresponds to ≈ 10 g/kg, which agrees with observed upper water column ice-shelf meltwater concentration near PIG Ice Shelf (Biddle et al. 2019). However, only local contributions to the freshwater balance are examined, so ice shelf meltwater from the east (Bellingshausen Sea) is not reflected in the tracers (Nakayama, Timmermann, Rodehacke, Schroeder & Hellmer 2014). Sea ice has predominantly negative surface tracer on the shelf, with the notable exception of north west of Abbot Ice Shelf, where inflow from off the shelf brings positive sea ice tracer on average onto the shelf. Iceberg melt and PmE both make an average positive contribution to the surface freshwater balance on the continental shelf.

The climatology of total tracer is positive in the surface for the entire region and has the highest values in the coastal current. This contrasts with the freshwater flux field shown previously (Figure 4.5), which has areas of negative freshwater flux, due mainly to strong negative average sea ice freshwater flux. This negative sea ice contribution in the surface tracer is balanced in part by the advection of ice shelf meltwater. Furthermore negative sea ice freshwater fluxes and evaporation cause convection, mixing negative sources of tracer down out of the surface.

The top 10 m only accounts for a small fraction of the water column, so Figure 4.7 shows the climatology of the depth-average freshwater tracers, calculated by taking the water column integral of tracers and then dividing by the water column height. On the continental shelf, sea ice and ice shelf are the most significant freshwater sources averaged over the water column, though iceberg melt and PmE still make notable positive contributions. Ice shelf freshwater has the largest spatial variation, with the highest concentration near Siple Island, as this area is comparatively shallow and lies downstream of most of the region's ice shelves. Though noble gas observations of ice shelf meltwater are very sparse, the model broadly recreates observed spreading of ice shelf meltwater observed through this technique (Biddle et al. 2019, Kim et al. 2016).

The sea ice tracer is the only source that has a negative average value over the continental shelf, due to average positive sea ice freshwater fluxes occurring off the continental shelf and the long residence time of deep penetrating negative sea ice tracer. The sea

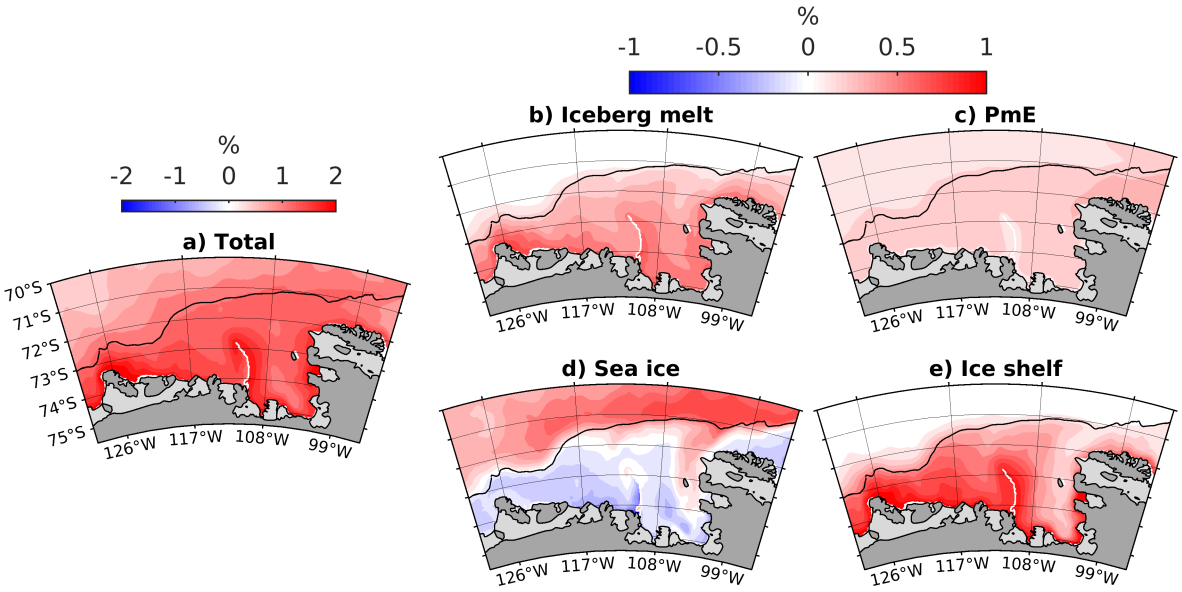

FIGURE 4.6: Climatology of surface freshwater tracer concentration (1989-2018) for (a) total freshwater, (b) iceberg melt, (c) precipitation - evaporation (PmE), (d) sea ice and (e) ice shelf melt. Black line represents the 1000 m depth contour of the continental shelf break.

ice tracer average negative value implies that the region is an average sea ice export region. However, in the model sea ice is not modelling entering the domain from the Bellingshausen Sea, which may mitigate this process leading to possibly more positive average sea ice tracer. There is stronger negative sea ice tracer to the west of the grounded BRI than to the east, in part due to the strong negative sea ice freshwater fluxes in the ASP. This agrees with observations in the region (Biddle et al. 2019, Randall-Goodwin et al. 2015).

Iceberg melt and PmE both have small average positive tracer concentrations, which are spatially uniform in their presence over the continental shelf. The total tracer has a very similar magnitude and distribution to the ice shelf tracer. This implies that on average PmE and iceberg melt cancel out the negative freshwater contribution to the region from sea ice. Within ice shelf cavities a balance between the sea ice negative tracer and the positive ice shelf freshwater tracer occurs, with the cavities being positive on average in the total tracer.

To summarize, sea ice and ice shelf have the largest freshwater fluxes on average in the Amundsen Sea. Despite this, however, all freshwater tracers are of comparable magnitude, both in the surface (10 m) and on a depth-average over the continental shelf. In addition, the distribution of the surface total tracer resembles that of the ice shelf tracer, and the depth-average total tracer field is highly similar to the ice shelf tracer.

Since the total tracer resembles the ice-shelf meltwater tracer, the melting of the ice shelves must play an important role in the circulation and stratification of the Amundsen Sea. This implies there is a strong potential for ice-shelf meltwater feedbacks in the system. For example, an increased presence of meltwater could both accelerate baroclinic currents (Jourdain et al. 2017) and stratify the ocean, potentially enhancing the transport of less-modified CDW towards the ice shelves and causing more melting and hence more meltwater. Further targeted research is required to isolate the precise nature and importance of any such feedbacks. However, it is worth noting that the total tracer resembles the ice-shelf meltwater tracer despite ice shelf and sea ice having almost equally important freshwater fluxes in the region. This is because ice-shelf meltwater distribution is much more strongly spatially varied in the region, with for example strong concentrations in the coastal current. In contrast the sea ice freshwater tracer has weaker spatial variation. In addition, some of the spatial variation that is present in the sea ice tracer is also present in the iceberg freshwater tracer, for example stronger concentrations west of the grounded BRI. Therefore, the sea-ice freshwater tracer is on average counteracted by the equally less spatially varied iceberg meltwater and PmE tracers. This leads to the strong spatial variability remaining in the total tracer causing its resemblance to the ice-shelf freshwater tracer.

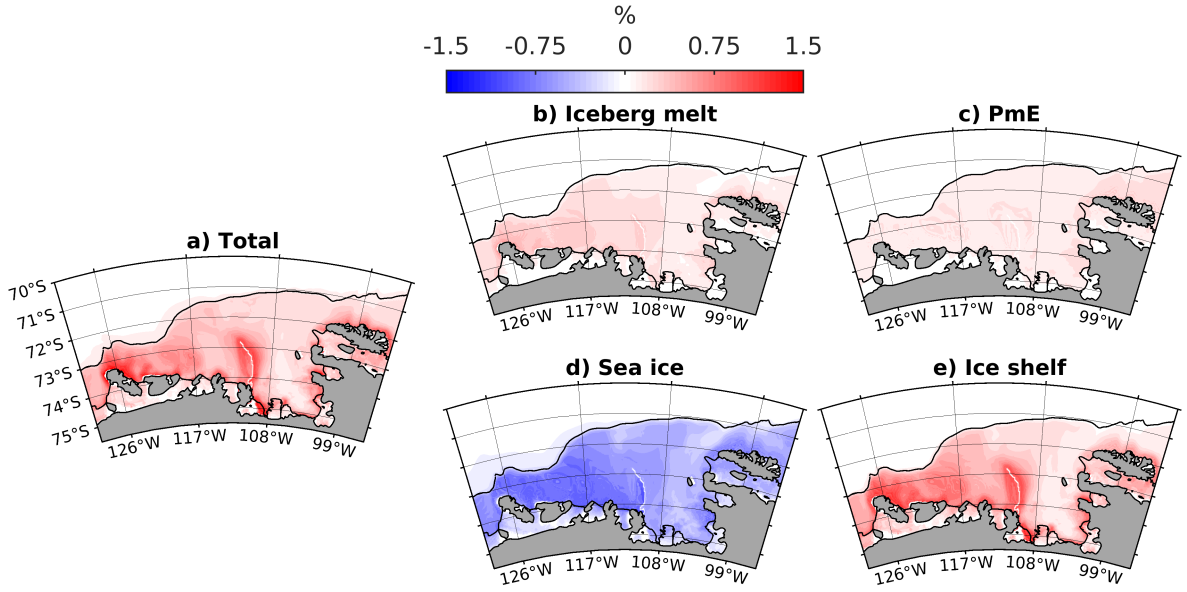

FIGURE 4.7: Climatology of depth averaged freshwater tracer concentration (1989-2018) for (a) total freshwater, (b) iceberg melt, (c) precipitation - evaporation (PmE), (d) sea ice and (e) ice shelf melt. Black line represents the 1000 m depth contour of the continental shelf break.

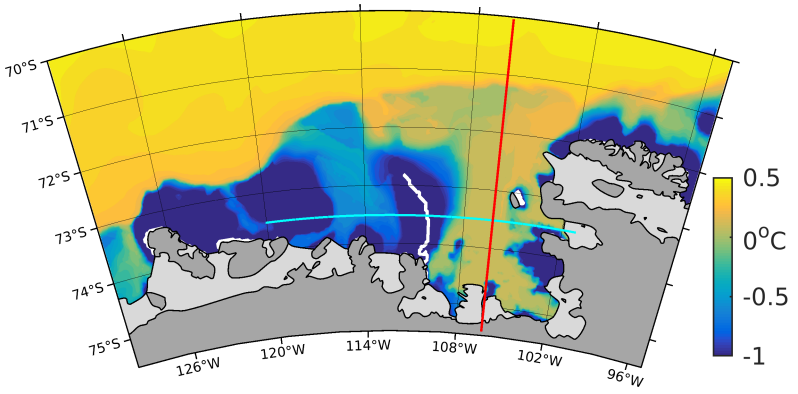

FIGURE 4.8: Maximum climatological subsurface potential temperature (1994-2012), but using only observational available years for model.

4.2.2 Vertical tracer distribution

In order to better examine the vertical distribution and differences in the distribution of freshwater tracers on and off the continental shelf, a south–north cross-section is considered (shown by the red line in Figure 4.8). Note that this cross-section crosses through Thwaites Ice Shelf at its southern end. Average freshwater tracer distributions along this section are shown in Figure 4.9, along with the average potential temperature. Figure 4.9f shows the warm CDW originating off the continental shelf and intruding onto it and towards the ice shelves. A deeper layer of cold WW is present on the continental shelf as well. Figure 4.9 shows that the highest magnitude concentrations of freshwater tracers are located on the continental shelf. However, there is the notable exception of positive PmE and sea ice tracers located off the shelf in the top 100 meters, which is due to these sources both having average positive freshwater fluxes off the continental shelf, while the other sources lack any freshwater fluxes off the continental shelf (Figure 4.5).

The highest concentrations of ice shelf tracer are in the ice shelf meltwater plume under Thwaites Ice Shelf and directly north of the ice shelf in the southern coastal current (Figure 4.9d). Concentrations of ice shelf tracer are present along all the continental shelf part of the cross-section, with the majority of it being in the pycnocline and very little deeper in the mCDW layer. Therefore, this simulation agrees with the idealised model set-up in Section 3.2 about the range of depths that the highest concentrations of ice shelf tracer are located, with the highest concentrations being in the pycnocline and the surface waters. Off the continental shelf there are no concentrations of ice shelf freshwater tracer. A similar distribution is observed for the iceberg meltwater tracer, with its highest concentrations being at the surface and over the pycnocline over the continental shelf, with no significant iceberg tracer present off the continental shelf (Figure 4.9b). However, it is expected that the iceberg meltwater tracer distribution is heavily dependent on the distribution of the iceberg freshwater flux applied in this

study. Sea ice has strong negative tracer on the continental shelf within the pycnocline including in front of and below Thwaites Ice Shelf where the pycnocline becomes deeper (Figure 4.9c).

The total tracer shows consistently high concentrations of positive tracer in the surface layer over the whole cross-section, with slightly higher surface concentrations on the continental shelf (Figure 4.9e). However, there is significantly higher concentrations of positive tracer at depth down to 400 m on the continental shelf compared to off the continental shelf, which follows the lowering of the pycnocline on the continental shelf. Therefore, overall there are strong differences in freshwater tracer concentrations on and off the continental shelf in the Amundsen Sea.

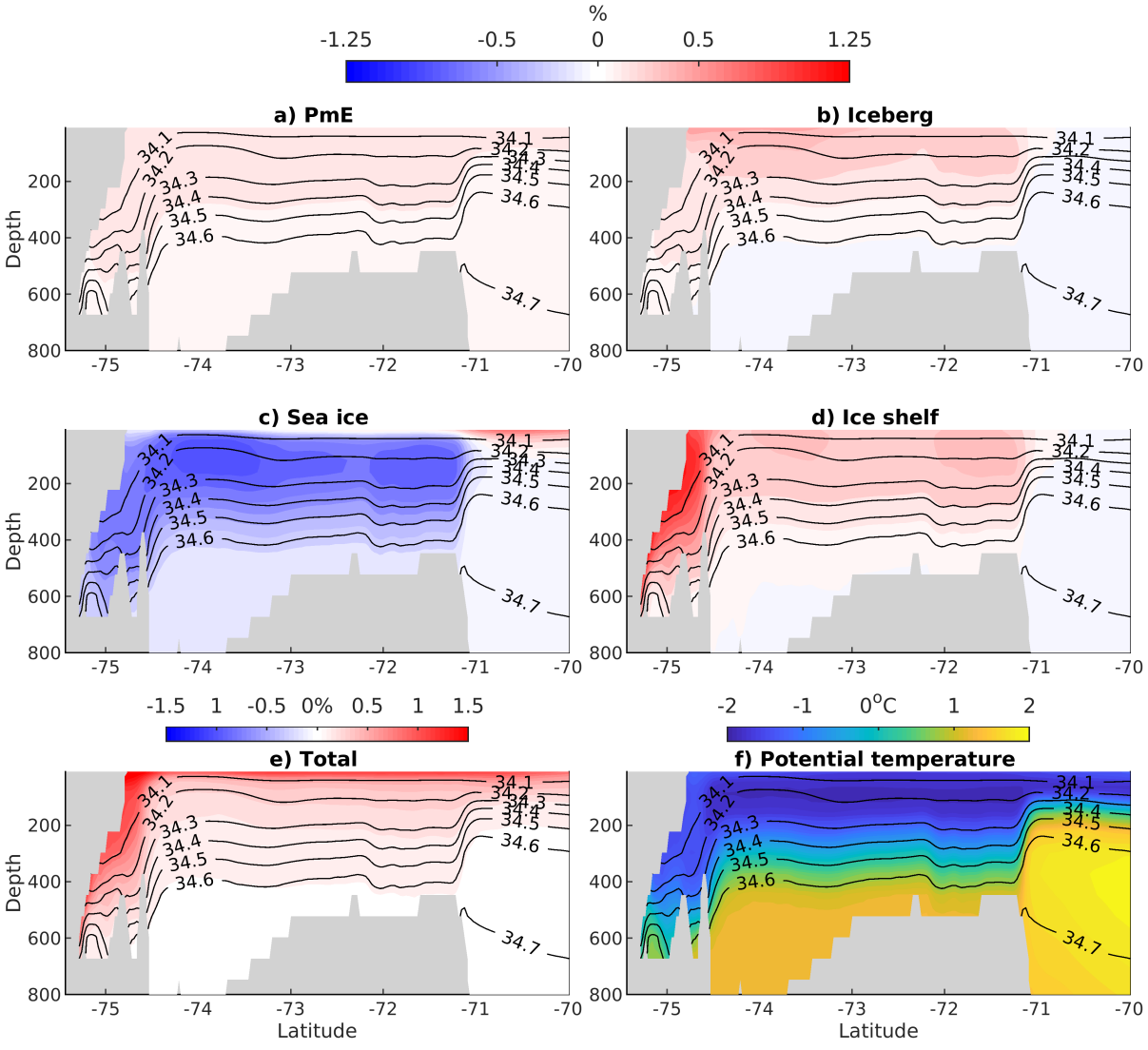

FIGURE 4.9: Climatology of freshwater tracer concentration (1989-2018) along south–north cross-section, shown by the red line in Figure 4.8, for (a) total freshwater, (b) iceberg melt, (c) precipitation - evaporation (PmE), (d) sea ice and (e) ice shelf melt. Black contours indicate salinity.

In order to examine the differences in the distribution of freshwater tracer between the two troughs on either side of the grounded BRI, namely the Dotson Trough to the west and Pine Island Trough to the east, a cross-section shown by the cyan line in Figure 4.8 is examined. The average concentrations of the different freshwater tracers along this west–east cross-section are shown in Figure 4.10, along with the average potential temperature. The eastern trough has a stronger pycnocline and more prevalent mCDW compared to the western trough, where lower mCDW temperatures are observed below a weaker pycnocline. All freshwater tracers appear to have a strong difference in vertical distribution between the two troughs, with tracers west of the grounded BRI in the Dotson Trough observed to be more well mixed though the water column. This could be due to strong sea ice growth in the Amundsen Sea Polynya, which drives convection mixing the tracers deeper into the water column west of the grounded BRI. The reduced stratification and mCDW presence in the Dotson trough aids vertical mixing of the tracers, whereas very low concentrations of freshwater tracer are present in the mCDW layer in the eastern trough.

In the western trough there is more intense negative sea ice tracer, which is also present over the whole water column down to 800 m (Figure 4.10c). Whereas in the eastern trough, negative tracer is reduced and restricted to the pycnocline, with no sea ice tracer in the CDW layer. This suggests a strong difference on the impact of sea ice on either side of the grounded BRI along this cross-section. The second tracer which appears to have the strongest difference between the troughs is the ice shelf tracer. Ice shelf tracer has strong positive tracer only in the coastal currents east of the grounded BRI, which are located at the boundaries of the eastern trough in the cross-section. However, ice shelf tracer is more uniform vertically and horizontally west of the grounded BRI (Figure 4.10d), though with highest concentrations directly west of the grounded BRI, which is in the coastal current.

In the eastern trough the total tracer is restricted to the surface layers and the coastal currents (Figure 4.10e), with very little penetrating deep into pycnocline, where individual tracers must mostly be negating each other. However, west of the grounded BRI, the total tracer highest concentrations are still in the surface layers and coastal currents, but there is also significant concentrations of positive tracer at depth, with no clear boundary between high and low concentrations like what is observed in the eastern trough.

4.3 Freshwater seasonality

The strength of the relative seasonal cycles of the different local fresh water sources could affect the ocean conditions in the Amundsen Sea. Therefore, in this section the

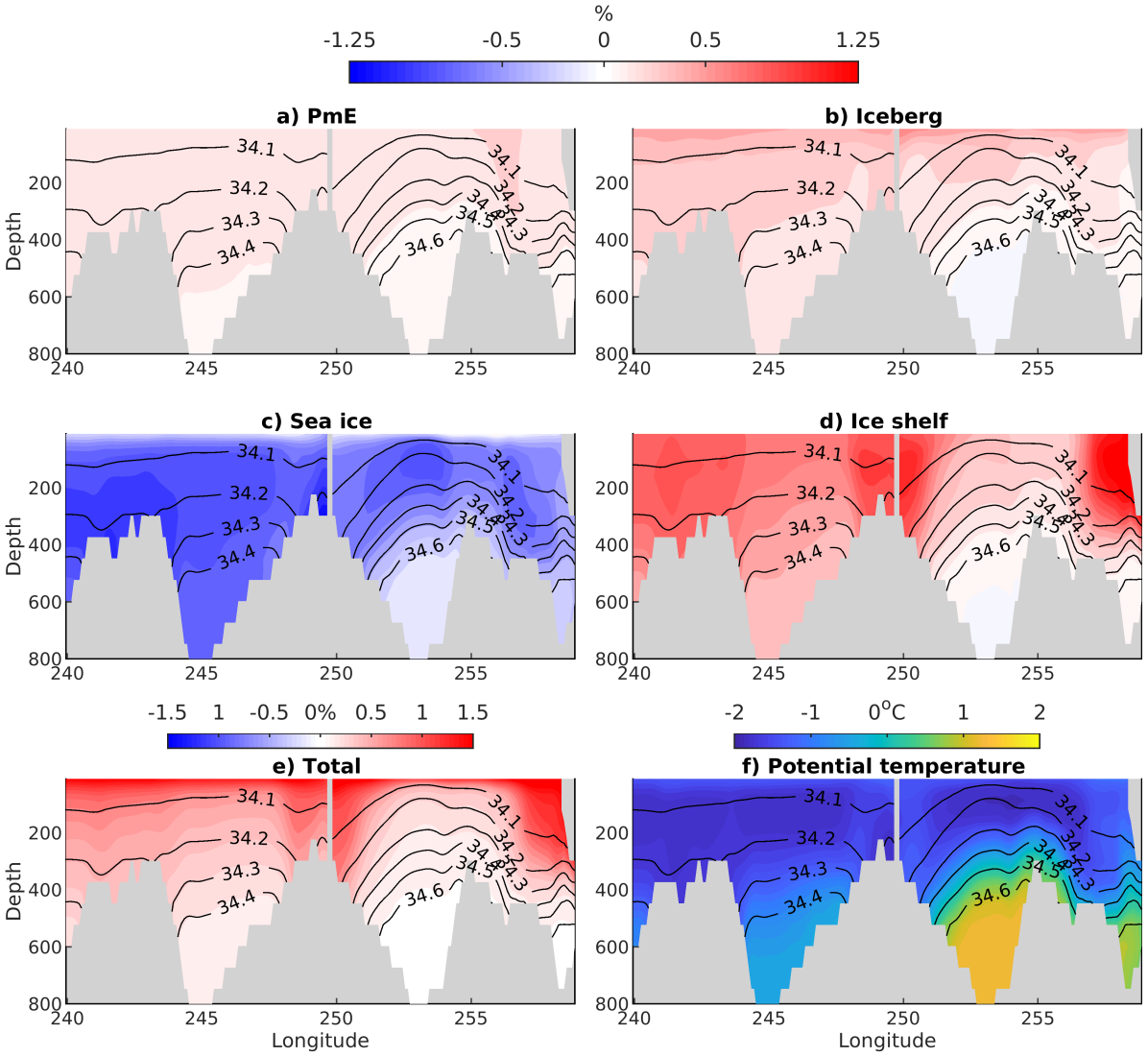

FIGURE 4.10: Climatology of freshwater tracer concentration (1989-2018) along west–east cross-section shown by the cyan line in Figure 4.8, for (a) total freshwater, (b) iceberg melt, (c) precipitation - evaporation (PmE), (d) sea ice and (e) ice shelf melt. Black contours indicate salinity.

freshwater fluxes and tracer seasonal cycles are investigated and dominant terms are compared to oceanic conditions.

The seasonal variability of the eastern Amundsen Sea (the blue box in Figure 4.1) averaged freshwater fluxes and tracer concentration are shown in Figure 4.11. Here, the ice shelf freshwater flux is the combination of PIG and Thwaites ice shelves, as they are most important to the stability of the West Antarctic Ice Sheet. Sea ice has the largest seasonal freshwater flux cycle by an order of magnitude, with the sea ice negative freshwater flux (brine rejection) peaking in April (Figure 4.11a). A small, but not insignificant seasonal cycle is however also present in the ice shelf freshwater fluxes. The sea ice's large seasonal cycle is also apparent in the tracer concentration;

the minimum sea-ice tracer concentration is in November (Figure 4.11b), when sea ice freshwater flux becomes positive. Again a seasonal cycle is also noted in the ice shelf freshwater concentration for area, though this is small compared to the sea ice seasonal cycle.

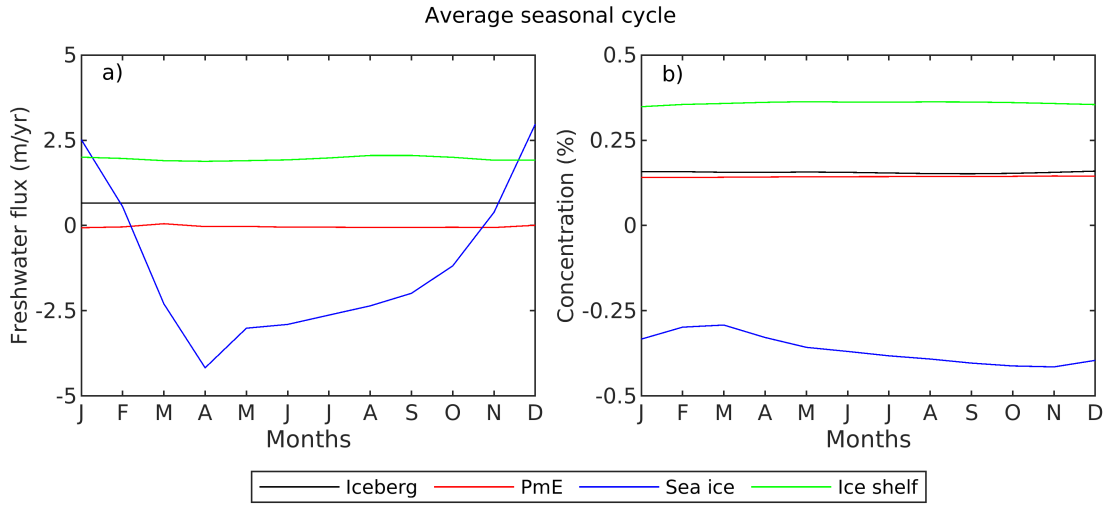

FIGURE 4.11: Eastern Amundsen Sea mean seasonal cycle for (a) freshwater component fluxes and (b) tracer concentration. Fluxes and concentration are averaged over the area and volume of the blue box shown in Figure 4.1a, and ice-shelf meltwater flux is taken to be the combined fluxes from Thwaites and PIG ice shelves.

Therefore, as the sea ice freshwater flux has shown to have the dominant seasonal cycle, the spatial distribution of its freshwater flux seasonal cycle is investigated (Figure 4.12). The peak overall sea ice fluxes happen in the autumn and spring, with negative and positive freshwater fluxes respectively observed over the whole study area. However, in the winter, though less widespread, the negative sea ice freshwater fluxes are more concentrated and stronger in the coastal polynyas and in the ASP. The positive sea ice freshwater fluxes that occur in the spring and summer in the south of the domain are less intense than the sea ice growth in the autumn and winter, which is due to northward sea ice export in the region. This leads the strongest positive sea ice freshwater fluxes to occur in the north around the continental shelf edge.

Figure 4.13 similarly shows the distribution of the average seasonal cycle of surface sea ice tracer, in order for the spatial distribution to be investigated. Peaks in magnitude are observed in the sea ice surface freshwater tracer in the summer and winter, with the summer having a strong positive tracer at the surface, while the winter having a strong negative tracer. The strong surface negative sea ice tracer in winter is notably constrained to be on the continental shelf only. This may be because on the continental shelf is where the negative tracer producing sea ice growth is occurring, whereas off the shelf an average sea ice melt is occurring and shelf break currents limit exchange between the regions. Whereas in the summer the positive ice shelf tracer is more wide spread over the region, with peaks over the continental shelf break and in the eastern Amundsen

Sea. Therefore the contrast between off and on the continental shelf in the summer sea ice surface tracer field is not observed because of the export of solid sea ice over the continental shelf break. This leads to a more uniform sea ice freshwater flux field in the summer off and on the continental shelf, in contrast to the heavy continental shelf dominated negative fluxes in the winter. The autumn and spring seasons show similar distributions of sea ice freshwater tracer, with negative tracer on the shelf and positive tracer past the shelf break, as they transition from the summer and winter distributions.

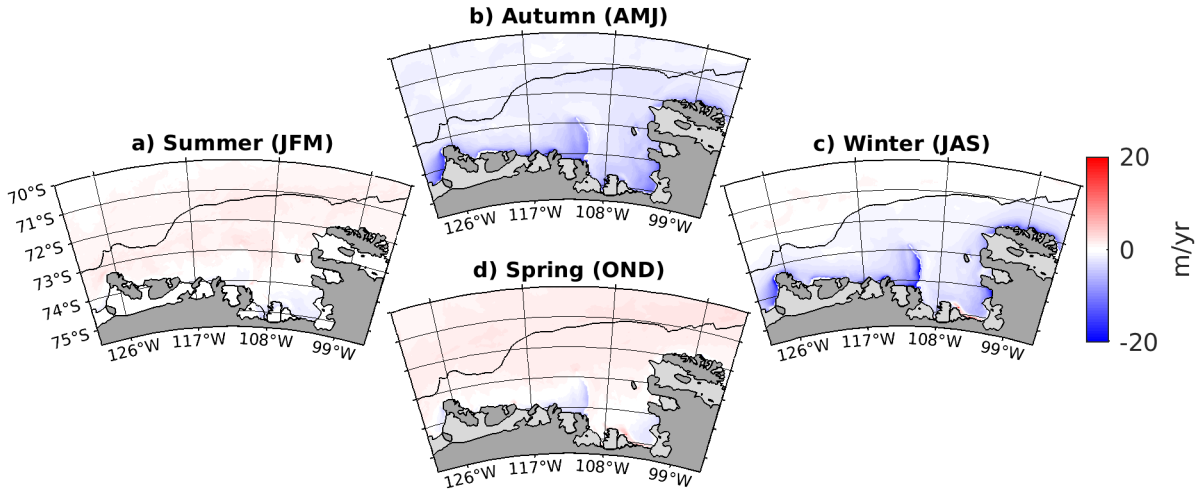

FIGURE 4.12: Average seasonal cycle of the sea ice freshwater fluxes (1989-2018). Black line represents the 1000 m depth contour of the continental shelf break.

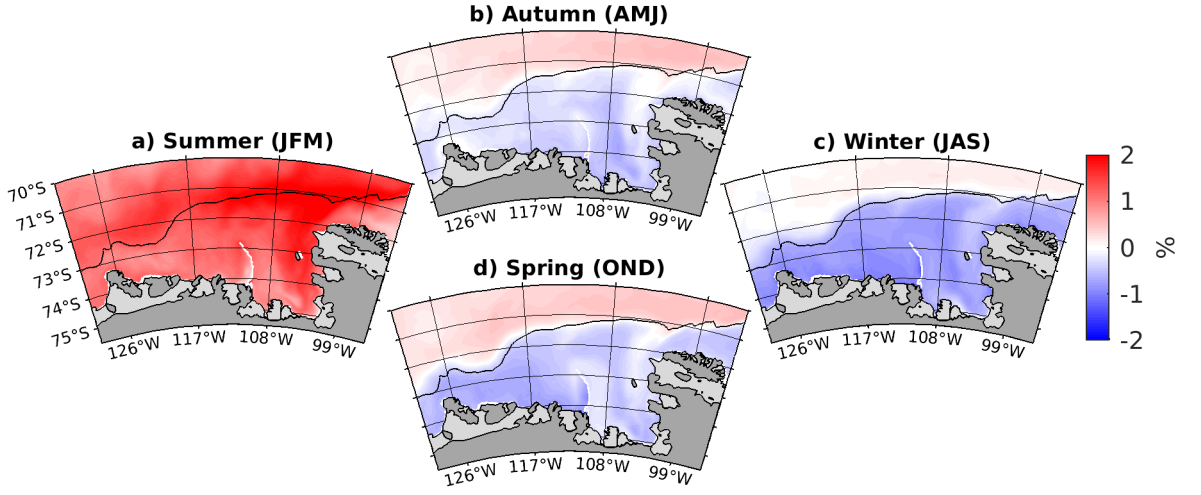

FIGURE 4.13: Average seasonal cycle of the surface (10 m) sea ice tracer. Averaged over the period 1989-2018. Black line represents the 1000 m depth contour of the continental shelf break.

Figure 4.14 shows the average seasonal cycle of the surface salinity, which will be affected by the seasonal cycle of freshwater fluxes. The saltiest surface waters are in the winter,

especially towards the north and in the middle of the eastern Amundsen Sea, whereas the freshest surface waters are in the summer and towards the coast. Autumn and spring have similar salinity distributions, though Autumn is fresher towards the coast in the coastal current.

Therefore, as sea ice dominates the freshwater seasonal cycle, it is possible to compare the seasonal cycle of the surface salinity to the seasonal cycle of the sea ice freshwater fluxes and tracers in the region. The average seasonal cycle of the surface salinity shown in Figure 4.14, correspond overall to the average cycle of surface sea ice tracers with it being saltiest in the winter and freshest in the summer (Figure 4.13). Noticeably, significantly fresher surface waters in the eastern Amundsen Sea correspond to a peak in sea ice freshwater tracer in the summer in this region. A larger seasonal cycle is present in the surface salinity on the continental shelf, which correspond to the larger seasonal cycle in sea ice surface tracer on the shelf compared to off the continental shelf. However, the surface salinity in the winter is fresher on the continental shelf than off, which is contrary to the winter surface sea ice tracer, therefore suggesting that other freshwater sources may negate this effect, so the surface total freshwater tracer would resemble the salinity.

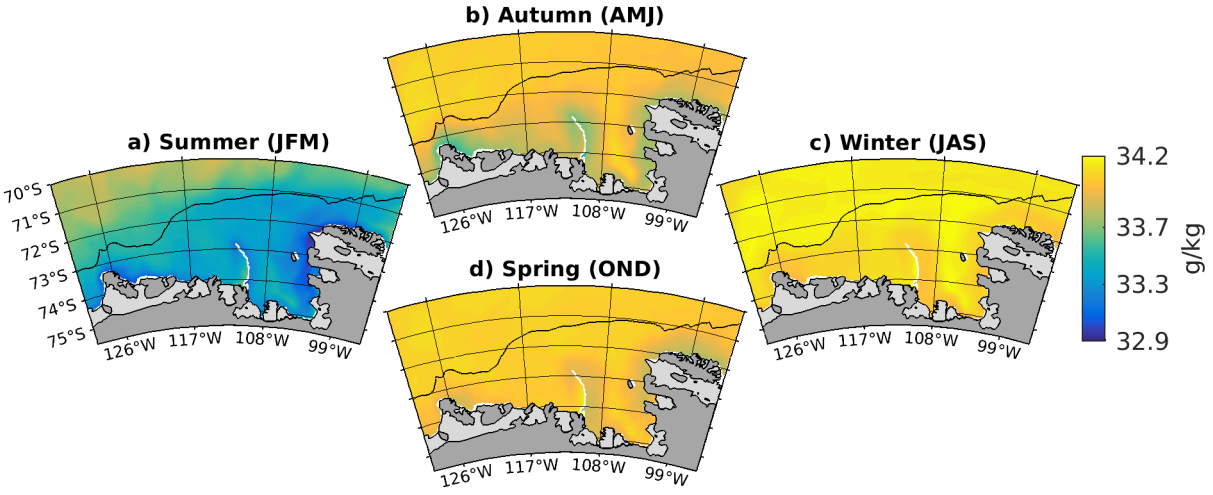

FIGURE 4.14: Average seasonal cycle of the surface (10 m) salinity. Averaged over the period 1989-2018. Black line represents the 1000 m depth contour of the continental shelf break.

4.4 Inter-annual variability

The Amundsen Sea region has a large inter-annual variability in oceanic and atmospheric conditions, which would be expected to effect the inter-annual variability of the freshwater balance in the region. In this section therefore the inter-annual variability of the

local freshwater sources and distribution over the region is examined.

While considering the inter-annual variability in the model it is important is consider the impact of the model's climatological seasonal boundary conditions. One study suggests that the lack of inter-annual variability of the boundary conditions would impact the inter-annual variability of CDW temperature on the continental shelf in the model (Nakayama et al. 2018). However, from observations the CDW layer thickness is the biggest driver of the inter-annual variability of OHC on the continental shelf (Dutrieux et al. 2014) and thus the inter-annual variability of ice shelf melt rates. Several studies have found that wind forcing directly over the continental shelf edge are the main driver of the inter-annual variability of OHC on the continental shelf(Kimura et al. 2017, Thoma et al. 2008, Webber et al. 2019). However, having climatological boundary conditions will affect the inter-annual variability OHC transport from the boundaries. The strength of this effect on the inter-annual variability of OHC in the studied region requires further study. However, any effect should be mitigated by our study region being away from the model boundaries and as shown and discussed previously in section Figure 4.1 the model, with caveats, re-creates the observed inter-annual variability in the study region.

Inter-annual variability of the eastern Amundsen Sea (the blue box in Figure 4.1) averaged freshwater fluxes and tracer concentration, which are anomalies from the mean seasonal cycle, are shown in Figure 4.15b,d, including the 10 year spin up, along with the average seasonal cycle Figure 4.15a,c. Sea ice and ice shelf freshwater fluxes have the largest inter-annual variability, with ice shelf melting attaining a minimum in 1997 (Figure 4.15b). The inter-annual variability of PmE is an order of magnitude less than sea ice and ice shelf freshwater fluxes and iceberg melt freshwater flux has zero inter-annual variability in the model by design.

The inter-annual variability of the average sea-ice tracer concentration is an order of magnitude larger than the other tracers (Figure 4.15d), as negative sea ice tracer is driven deeper in the water column, due to freezing driven convection, and has a longer residence time at depth. The other tracers have similar magnitudes of inter-annual variability over this area, with ice shelf tracer obtaining a minimum, which coincides with the minimum of ice shelf freshwater fluxes, in 1997.

Sea ice and ice shelf freshwater fluxes appear to covary in Figure 4.15b. Therefore examining the correlation between the inter-annual variability of ice shelf and sea ice freshwater fluxes, after the 10 year spin up period, gives a peak $r|r|$ at a lag of ice shelf melting of 10 months, (r is the correlation coefficient), as shown by the red line in Figure 4.16a. At this peak lag of 10 months the $r|r|$ is calculated to be 0.34 (Figure 4.16c). This small but significant correlation could be due to sea ice modulation of CDW affecting the CDW layer's thickness and temperature, and therefore the OHC, which thus affects ice-shelf melt rates (St-Laurent et al. 2015, Webber et al. 2017). However, ice

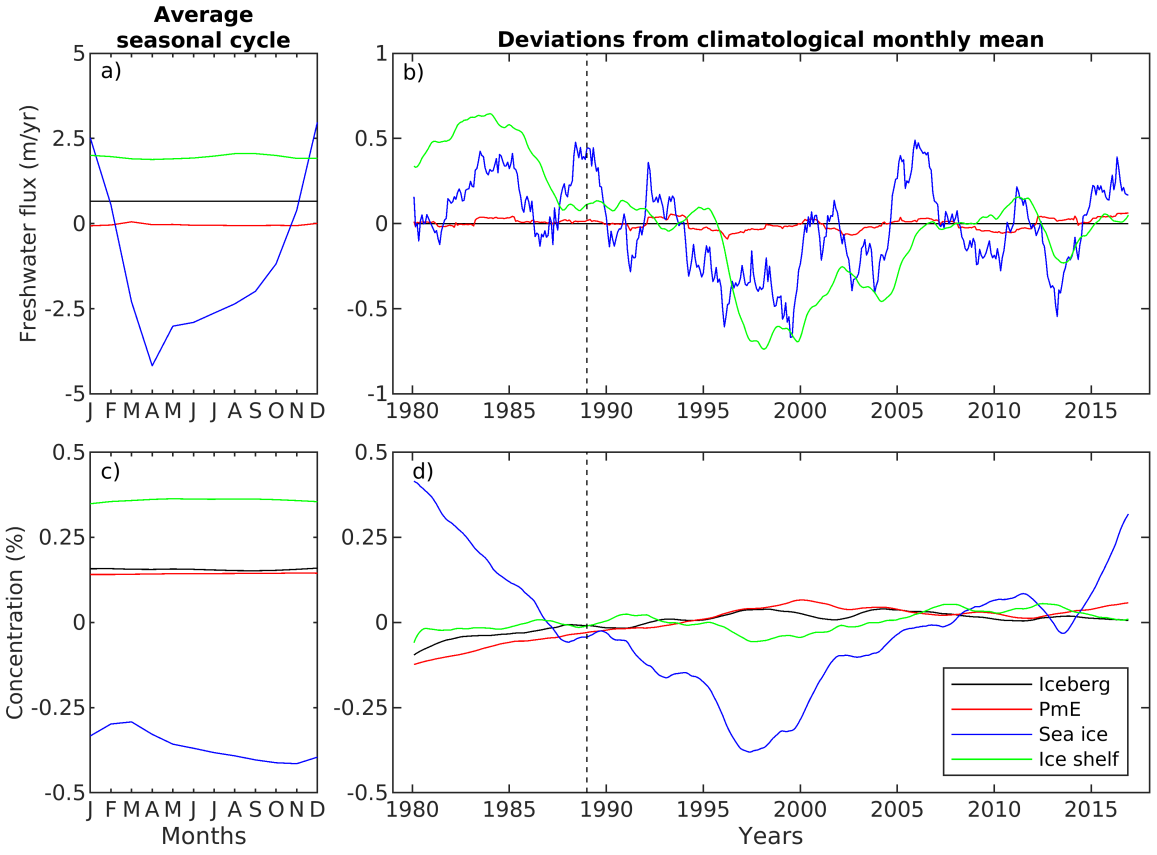

FIGURE 4.15: Eastern Amundsen Sea mean seasonal cycle for (a) freshwater component fluxes and (c) tracer concentration, along with inter-annual variability of (b) freshwater component fluxes and (d) tracer concentration. Fluxes and concentration are averaged over the area and volume of the blue box shown in Figure 4.1a, and ice-shelf meltwater flux is taken to be the combined fluxes from Thwaites and PIG ice shelves. Inter-annual variability is calculated as monthly anomalies from the mean seasonal cycle, with a 2-year running mean subsequently applied. Dashed vertical lines show end of model spin up period.

shelf melting has a strong correlation with the CDW fluxes though the eastern trough at the continental shelf break, where the entrance to the eastern trough is, similarly to other studies like Kimura et al. (2017), taken to be the red line in Figure 4.16b. Therefore calculating the correlation between ice shelf melting and heat flux below the mixed layer through this cross-section gives a peak $r|r|$ of 0.88 at a lag of 6 months, as shown by the blue line in Figure 4.16a and calculated in Figure 4.16e. This is in line with results of Kimura et al. (2017) for melting of PIG Ice Shelf. Thus, the inter-annual variability of the ice shelf freshwater is consistent with the well-established hypothesis of the inter-annual variability of CDW flux onto the continental shelf. However, these results therefore also suggest a role for local processes on the continental shelf. Sea ice freshwater fluxes anticorrelate with the meridional wind stress anomalies over the eastern Amundsen Sea, with a peak $r|r|$ value at zero lag, away from the coast (Figure 4.16d). Figure 4.16f shows $r|r|$ calculated for meridional wind stress near the peak area (shown

by the yellow marker in Figure 4.16d) giving a value of -0.41. This relationship may be due to stronger northward winds opening up coastal polynyas and enhancing the extraction of freshwater by freezing. Therefore, these results suggest that wind anomalies drive both sea ice and ice shelf freshwater flux anomalies, with this common driver possibly leading the two freshwater fluxes to covary.

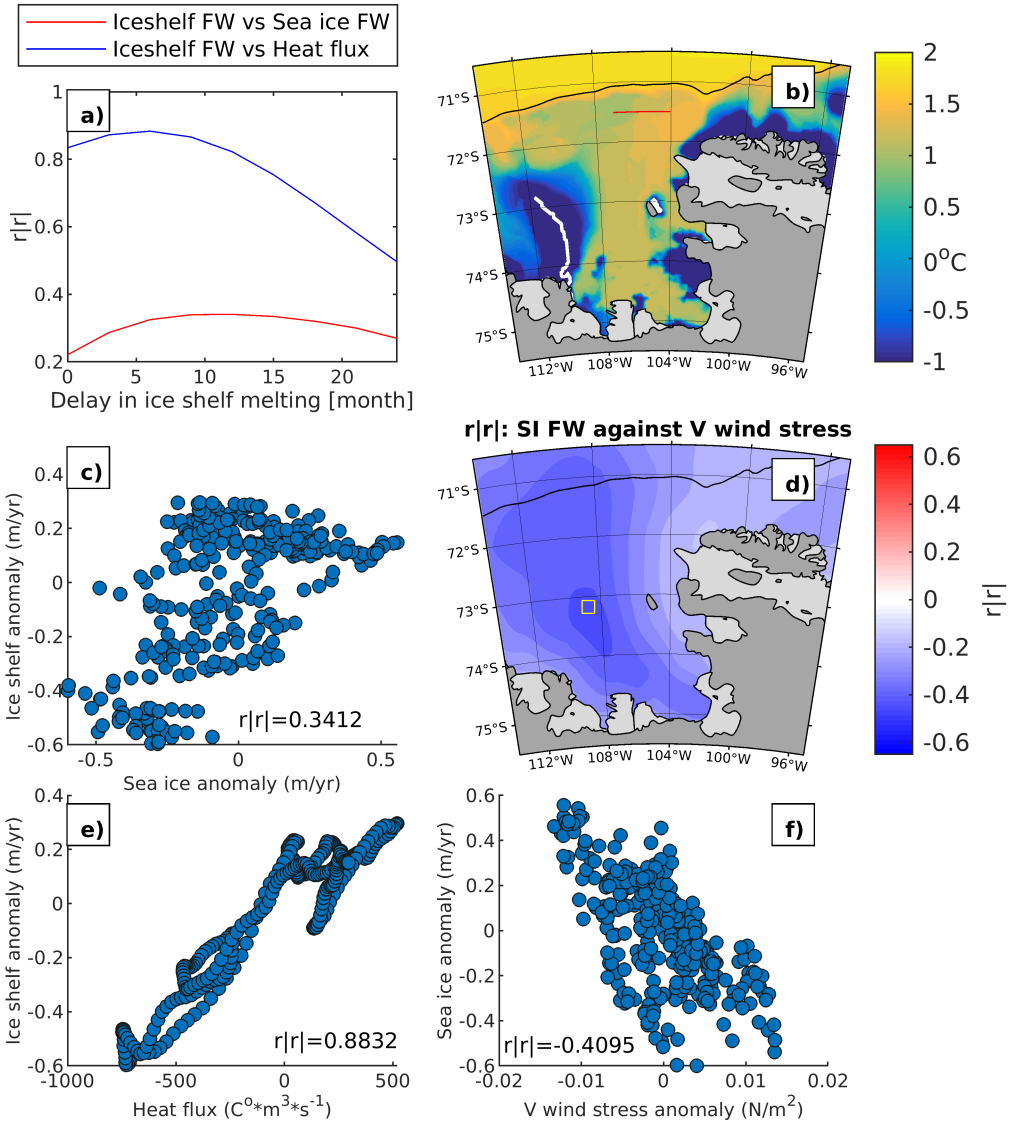

FIGURE 4.16: a) Correlation values ($r|r|$) for different month lags between ice shelf freshwater flux and sea ice freshwater flux (red), and between ice shelf freshwater flux and heat flux (blue). b) Maximum climatological subsurface potential temperature (1994-2012), but using only observational available years for model. c) Scatter plot of ice shelf melting anomaly against sea ice freshwater flux anomaly at 10 month lag. d) Maps of correlation $r|r|$ values of meridional wind stress anomalies to a scalar time series of sea ice melting anomalies at zero lag. e) Scatter plot of ice shelf melting anomaly against CDW heat flux at 6 month lag. f) Scatter plot of sea ice freshwater flux anomaly against meridional wind stress anomalies at marked location at 0 month lag. Correlations are calculated after 10 years of spin up and after applying a 2-year running mean.

4.4.1 Inter-annual variability of horizontal spatial distribution

With the high inter-annual variability of OHC on the continental shelf, it could be expected that during years of high OHC and years of low OHC that the freshwater balance in the region to comparatively change. In order to investigate the inter-annual variability of the different freshwater tracer spatial distributions, the freshwater tracer distributions are examined for 2010, which was a year of high OHC and so a 'warm year', and for 2000, which was a year of low OHC on the continental shelf and so a 'cold year' (Dutrieux et al. 2014). A similar investigation was conducted in Kimura et al. (2017), but only for ice shelf meltwater tracer, whereas here all local sources and the total freshwater tracer are examined.

Figure 4.17 shows the surface tracer distributions averaged over the warm year 2010, while Figure 4.18 shows the same for the cold year 2000. In 2010, compared to 2000, a slight increase in the surface total freshwater tracer to the north and closer to the coast is observed. In addition, as might be expected due to higher OHC that reaches ice shelves in 2010, an increase in ice shelf tracer in the surface is observed compared to in 2000. In 2000 the sea ice tracer has higher magnitudes compared to 2010, with it being more negative on the continental shelf and more positive off the shelf. This suggests increased sea ice export in this cold year compared to 2010, meaning increased sea ice growth in the south and then export and melting in the north past the shelf break. Only minor differences are observed in surface concentrations of iceberg melt and PmE between the two years.

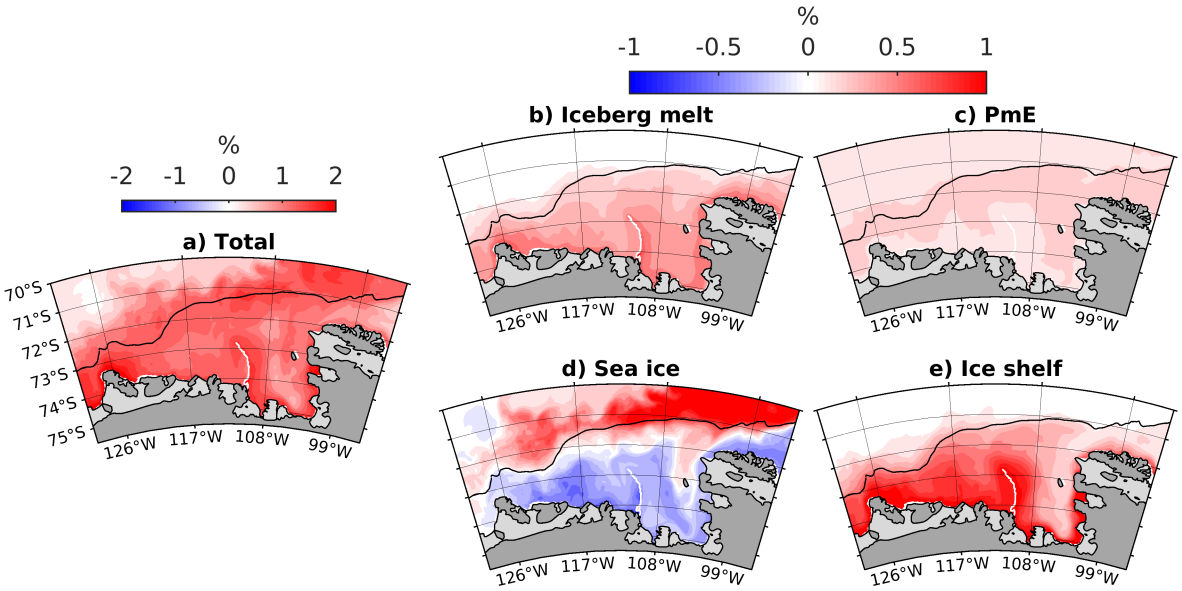

FIGURE 4.17: Warm year averaged surface freshwater tracer concentration (2010) for (a) total freshwater, (b) iceberg melt, (c) precipitation - evaporation (PmE), (d) sea ice and (e) ice shelf melt. Black line represents the 1000 m depth contour of the continental shelf break.

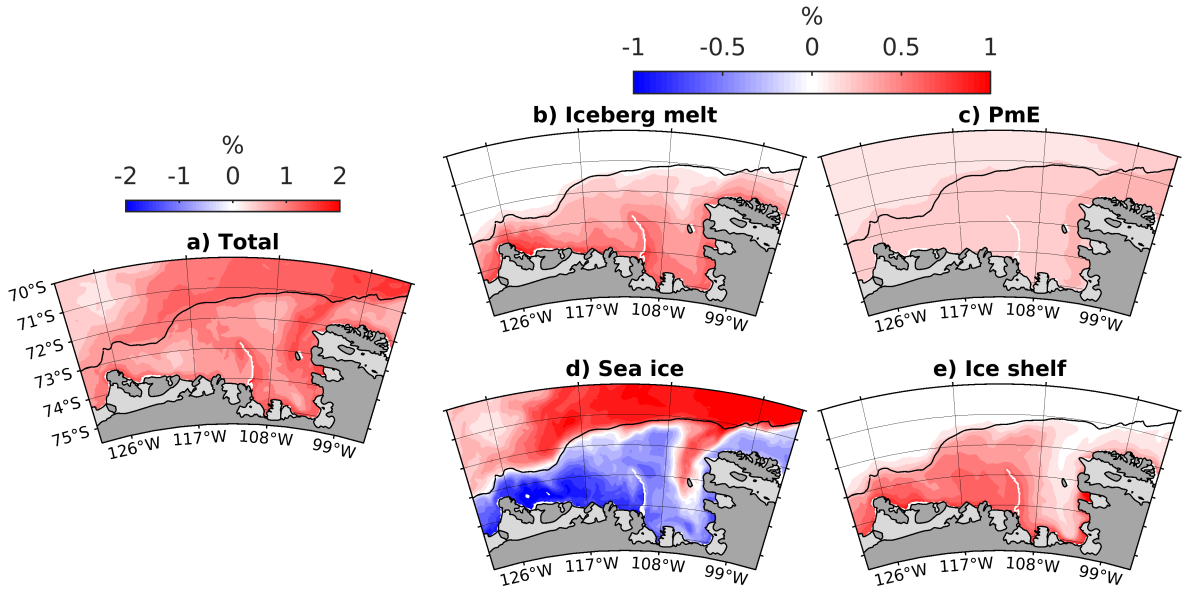

FIGURE 4.18: Cold year averaged surface freshwater tracer concentration (2000) for (a) total freshwater, (b) iceberg melt, (c) precipitation - evaporation (PmE), (d) sea ice and (e) ice shelf melt. Black line represents the 1000 m depth contour of the continental shelf break.

The depth average tracer concentrations of these two years are also compared as well, as shown in Figure 4.19 for the cold year 2010 and Figure 4.20 for the warm year 2000. A substantial increase in average sea ice negative tracer on the continental shelf is observed in 2000 compared to 2010, especially west of the grounded BRI. This corresponds with a small increase in average iceberg melt tracer and positive PmE tracer west of the grounded BRI in 2000. This may be due to increased convection driving these tracers deeper into the water, where they may have a longer residence time. A significant decrease in the average ice shelf tracer concentration close to the coast is observed as well in 2000 compared to 2010, due to the lower ice shelf melt rates. However, average ice shelf tracer away from the coast remains similar suggesting a longer residence time for tracer in these areas.

There are significant differences in the total tracer between the two years. In the year 2000 the total tracer is significantly less positive compared to 2010, with differences occurring in ice shelf cavities as well. The ice shelf cavities become strongly positive in the warm year. In contrast, in the cold year there is a significant reduction in the average magnitude of the positive tracer in the cavities to the east and in the west the cavities concentrations become close to zero, with the sea ice and ice shelf tracers balancing each other out. A total tracer concentration of zero means the local sinks of freshwater equal the local sources, and hence the salinity just reflects what has come through the boundaries. This appears to be due to an increase in the presence of negative sea ice freshwater in the cavities, though a small reduction in average ice shelf tracer does occur as well which compounds the effect. In 2000 the average total tracer distribution is no

longer similar to the distribution of the ice shelf tracer, whereas this similarity holds while examining the warm year 2010. This demonstrates the potential for the ice shelf meltwater feedback previously proposed in Section 4.2, as there is more freshwater in warm years, due to the increased presence of ice shelf meltwater.

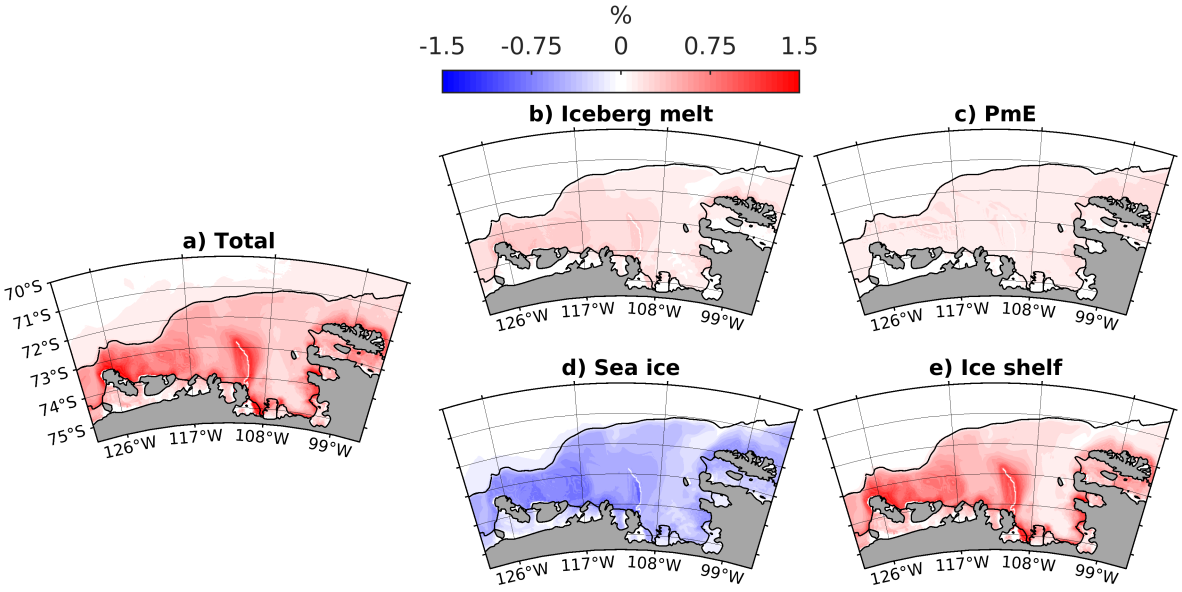

FIGURE 4.19: Warm year averaged depth averaged freshwater tracer concentration (2010) (a) total freshwater, (b) iceberg melt, (c) precipitation - evaporation (PmE), (d) sea ice and (e) ice shelf melt. Black line represents the 1000 m depth contour of the continental shelf break.

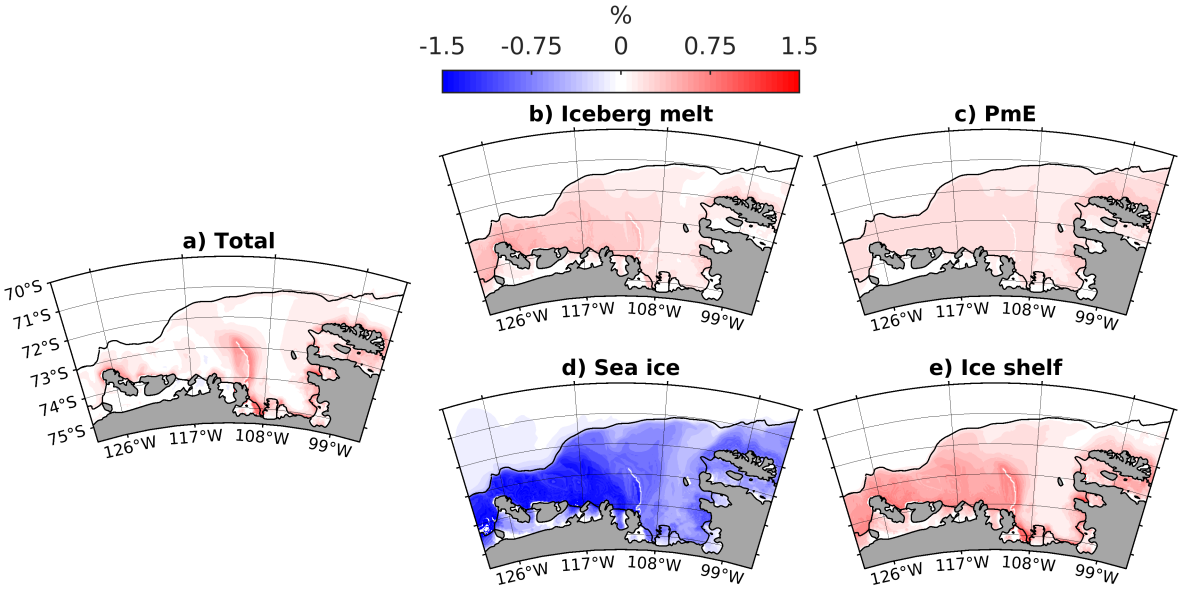

FIGURE 4.20: Cold year averaged depth averaged freshwater tracer concentration (2000) (a) total freshwater, (b) iceberg melt, (c) precipitation - evaporation (PmE), (d) sea ice and (e) ice shelf melt. Black line represents the 1000 m depth contour of the continental shelf break.

4.4.2 Inter-annual variability of vertical distribution

Next considered is the inter-annual variability of the vertical distribution of the total and component freshwater tracers, specifically first focusing on the region in front of PIG Ice Shelf to examine the possible implications for ice shelf melting. Figure 4.21 shows Hovmöller diagrams of the tracers and potential temperature averaged horizontally over the red box in Figure 4.1a. In front of PIG Ice Shelf, sea ice and ice shelf freshwater tracers dominate, though iceberg melt and PmE still make significant positive contributions.

Negative tracer dominates over most of the water column for the sea ice tracer, with strong inter-annual variability in both its vertical extent and intensity. In the period of 1997 to 2000, the sea ice negative tracer extends down the entire water column, as intense sea-ice brine rejection mixes the surface layers down. The sea ice tracer has a small quantity of positive tracer at the surface that displays large inter-annual variability, with e.g. 2017 showing significant sea ice meltwater. The sea ice tracer, therefore, has strong inter-annual variability in its concentration and in its vertical distribution.

Positive ice shelf tracer is mostly concentrated in the top 400 m of the water column, with the highest concentrations occurring during years of high OHC and thus higher salinity at depth. During years of low OHC, ice shelf tracer reduces to a concentration comparable to that of PmE and iceberg melt, while sea ice tracer becomes more negative. Therefore, in years of low OHC, the iceberg melt and PmE components are relatively more important in the freshwater balance and may mitigate freezing driven convection in the front of PIG Ice Shelf. In contrast, during years of high OHC ice shelf meltwater plays a significant role in stabilizing the water column against brine rejection from sea ice growth and the modulation of the OHC.

Iceberg meltwater is concentrated near the top of the water column. However, this is most likely because iceberg meltwater is applied as a surface flux, whereas in reality iceberg melting occurs at depth as well. PmE tracer is more uniform through the water column, though it still exhibits highest concentrations at the surface. Iceberg melt and PmE tracers do exhibit a small inter-annual variability to concentration magnitudes at depth, with their highest concentrations at 400 m coinciding with strong negative sea ice tracer at depth, suggesting this is due to inter-annual variability in sea ice growth and convection. The total freshwater tracer is concentrated in the surface, and its inter-annual variability matches that of the surface salinity. There is a strong inter-annual variability to the total freshwater tracer in the surface layers and at depth. The total tracer even becomes negative at depth below 200 m, between 1997 and 2000, implying that more 'local' freshwater has left these depths than entered them. This is due to the influence of strong sea ice growth not being counteracted by the other freshwater sources at these depths.

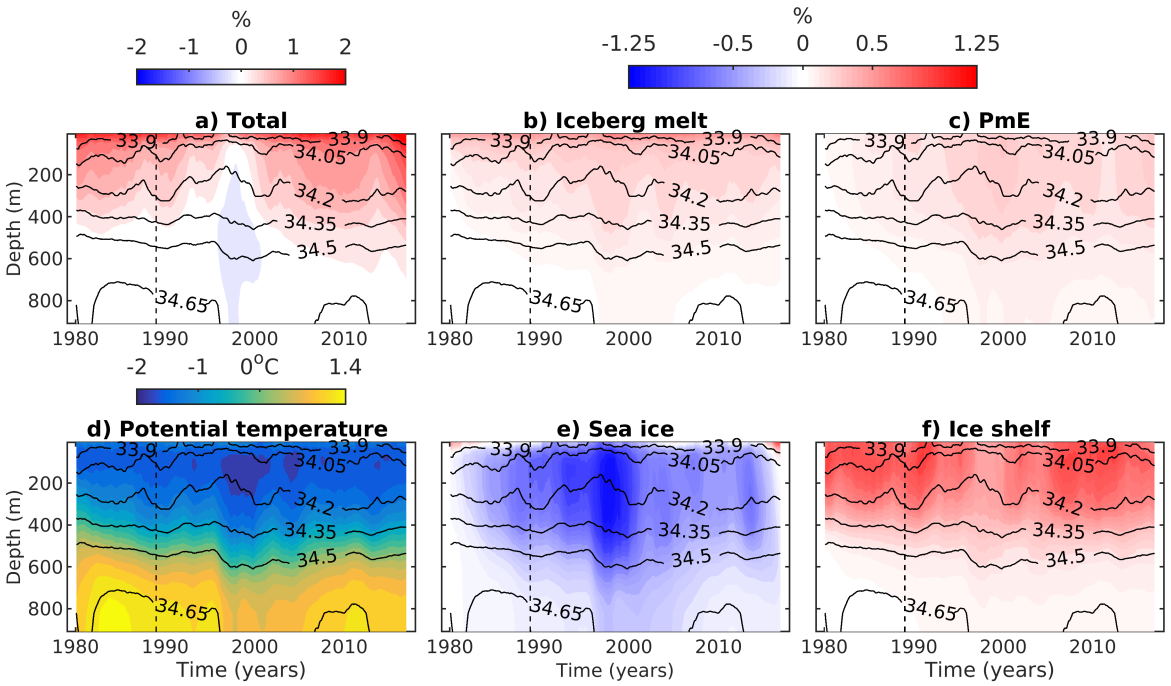

FIGURE 4.21: Hovmöller diagrams of (a) total freshwater, (b) iceberg melt, (c) precipitation - evaporation (PmE), (d) potential temperature, (e) sea ice and (f) ice shelf melt averaged over red box in front of PIG Ice Shelf, shown in Figure 4.1a. Black contours indicate salinity averaged over the same area. Model spin up of 10 years included. A 2-year running mean at each depth is applied to the tracers and the salinity to remove the seasonal cycle. The vertical black dashed lines indicate the end of the spin up period.

The same analysis is conducted in front of Dotson Ice Shelf (Figure 4.22), averaged over the green box in Figure 4.1a, in order to examine the differences that can occur between different ice shelf front regions. These results should be interpreted with the caveat of low Dotson Ice Shelf melt rates in the model compared to observations. Note also the different concentration and depth range used in the plot compared to the previous plots depicting tracers in front of PIG Ice Shelf. Tracer components are observed to be more vertically mixed compared to in front of PIG Ice Shelf, which correspond to a lower vertical stratification present. The sea ice tracer has a higher magnitude in this location compared to in front of PIG Ice Shelf, while there is also a slight increase in the magnitude of the ice shelf tracer. The stronger sea ice tracer is due to the close proximity of the Amundsen Sea Polynya, which causes high sea ice growth and therefore strong freshwater extraction and negative tracer production. The stronger ice shelf tracer in this region is due to its location downstream of high melt ice shelves like PIG and Thwaites. Therefore in front of Dotson Ice Shelf it is a balance mainly between sea ice and ice shelf in the freshwater balance. However, unlike at PIG Ice Shelf most of the ice shelf tracer can be expected to not originate from Dotson Ice Shelf. Therefore the freshwater balance in front of Dotson Ice Shelf is much more dependent on upstream ice shelf fluxes to balance out the strong sea ice fluxes present, which agrees with the hypothesises of a previous study in a different region (Silvano et al. 2018). During the

same period that the total tracer becomes negative in front of PIG Ice Shelf the total tracer in front of Dotson becomes comparatively more negative and for a longer period, which is due to a strong increase in negative sea ice tracer at depth during this period.

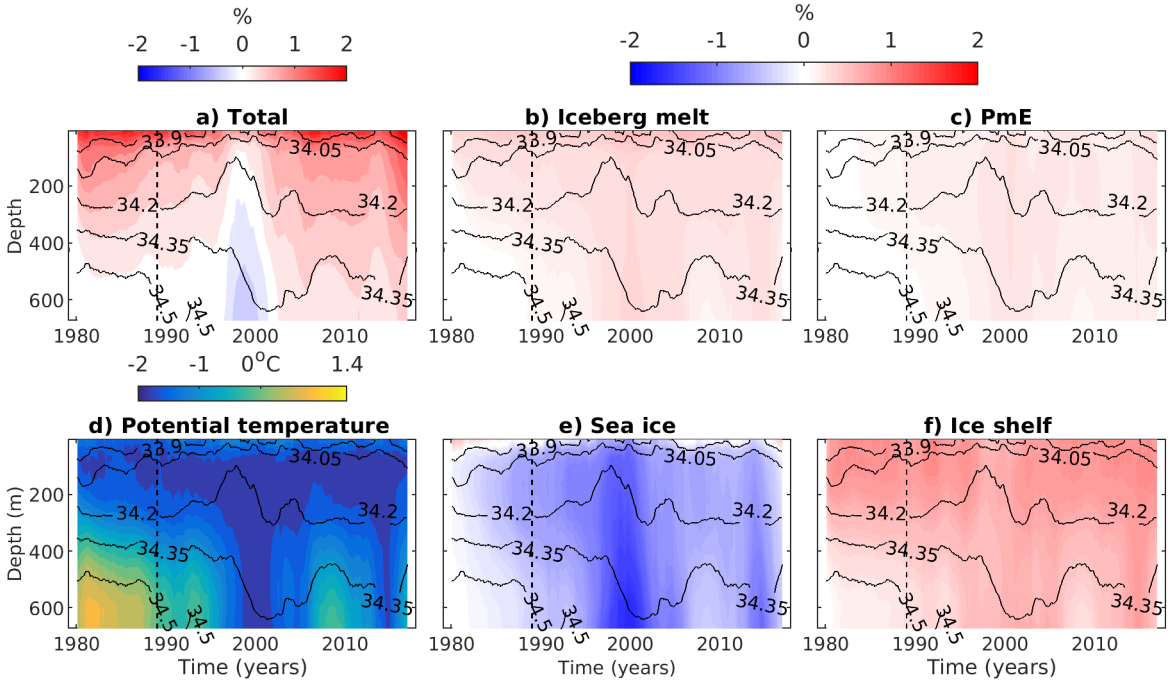

FIGURE 4.22: Hovmöller diagrams of (a) total freshwater, (b) iceberg melt, (c) precipitation - evaporation (PmE), (d) potential temperature, (e) sea ice and (f) ice shelf melt averaged over green box in front of Dotson Ice Shelf, shown in Figure 4.1a. Black contours indicate salinity averaged over the same area. Model spin up of 10 years included. A 2-year running mean at each depth is applied to the tracers and the salinity to remove the seasonal cycle. The vertical black dashed lines indicate the end of the spin up period.

4.5 Conclusions

In this chapter the mean, seasonal and inter-annual variability of the Amundsen Sea's local freshwater balance has been investigated using a regional numerical model with a representation of the grounded Bear Ridge Icebergs (BRI). The key results are listed below in relation to the section's aim:

1. **Validate the regional Amundsen Sea model.**

   The ocean model, sea ice model and modelled ice-shelf freshwater fluxes were found to perform sufficiently well against observations for the purposes of this study.

2. **Investigate local average freshwater spatial distribution.**

   The results show that sea ice and ice shelf freshwater fluxes are climatologically the strongest in the region. In the surface (10 m) and on a depth-average, however, all sources make important contributions to the climatological freshwater tracer balance. The total freshwater tracer in the surface resembles the ice shelf tracer, and the total freshwater tracer field is highly similar to the ice shelf tracer on a depth average as well. This implies that there is the potential for ice-shelf meltwater feedbacks in the Amundsen Sea, since the presence of meltwater affects the ocean currents and stratification that control melting. For example, an increased presence of meltwater could both accelerate baroclinic currents and stratify the ocean, potentially enhancing the transport of less-modified CDW towards the ice shelves.

   Significant differences in freshwater tracer concentrations were found between on and off the continental shelf and between the troughs to the east and west of the grounded BRI. Only two freshwater tracers have notable concentrations off the shelf, namely positive sea ice and positive PmE tracers, as these freshwater sources have fluxes off the shelf. The other tracers are restricted to on the shelf over the examined cross-section. Freshwater tracers are present much deeper in the water column on the shelf, however the total tracer shows high surface concentrations of positive tracer along the whole cross-section. Comparing the two troughs either side of the grounded BRI in the model shows freshwater tracer being mixed further down into the water column west of the grounded BRI, which could be due to the strong sea ice growth in the Amundsen Sea polynya causing convection.

3. **Investigate the seasonality of the freshwater fluxes and concentrations.**

   Sea ice dominates the freshwater seasonal flux cycle and the sea ice tracer seasonal cycle appears to be larger on the continental shelf compared to off the continental shelf. The sea ice seasonal cycle dominates the seasonal cycle of the surface salinity, though it seems other freshwater sources do impact the surface salinity distribution.

4. **Examine the inter-annual variability of freshwater distributions and fluxes, and investigate possible relationships.**

   Both the sea ice and ice shelf freshwater fluxes have the largest inter-annual variability. Sea ice freshwater flux anomalies negatively correlate with meridional wind anomalies and, similarly to other studies, eastern ice shelf freshwater anomalies correlate strongly with CDW flux onto the continental shelf. While there is correlation between sea ice and ice shelf freshwater flux anomalies, these results suggest that wind anomalies drive both sea ice and ice shelf freshwater flux anomalies, with this common driver possibly leading the two fluxes to covary. However, there is also possible evidence that ice shelf melting is effected by local processes like sea ice, which is also effected by the wind. Large inter-annual variability is observed in tracer distributions and magnitudes, leading to a similar inter-annual variability in the ice shelf tracer and the total tracer. This demonstrates the potential for the ice shelf meltwater feedback, as there is more freshwater in warm years, due to the increased presence of ice shelf meltwater.

   Analysis of the freshwater balance in front of the PIG and Dotson ice shelves reveals that there is a large inter-annual variability of the total freshwater tracer, due mainly to the strong inter-annual variability of the sea ice and ice shelf tracers. This implies that other freshwater sources like iceberg melt become relatively more important to the freshwater balance when ice-shelf meltwater flux is low. However, in front of Dotson Ice Shelf, sea ice and ice shelf tracer concentrations are stronger, due to the Amundsen Sea Polynya and the location of Dotson Ice Shelf downstream of high melt ice shelves like PIG Ice Shelf. This leads the freshwater balance of the area in front of Dotson Ice Shelf to be more dependent on other ice shelf melt rates to balance strong sea ice growth.

The analysis of freshwater sources in this section has lead to some important results. In this study, although it was found that ice shelf meltwater correlations strongly with CDW influx at the continental shelf, other more local processes were also found to be important for the local OHC and hence ice shelf melting. In addition ice shelf melt rates were found to anti-correlate with the sea ice freshwater fluxes. This could be due to the direct impact of sea ice growth or due to both sea ice growth and CDW influx at the shelf both correlating to winds over the region. Therefore this implies a complex system, where local and far field forcings may impact ice shelf melting. This has implications for the future of research into ice shelf melting in the region and therefore future predictions of the stability of the West Antarctic ice sheet and hence future sea level rise. In addition, ice shelf and sea ice freshwater sources were found to be the most important freshwater sources in the study, which has implications for future modelling studies. This implies that these two freshwater sources are critical to model effectively in order to model the Amundsen Sea region. In addition, this implies that further observational studies should

be under taken in order to gain further measurements in order to best simulate these two freshwater sources in the Amundsen Sea.

However, there are some caveats to these results, as they could be dependent on the iceberg freshwater flux field used in this study. In this study a fixed surface iceberg melt field is input over a prescribed area, in which the effects of the latent heat are not accounted for. Therefore applying a more sophisticated iceberg model could impact the distribution and variability of the iceberg melt fields compared to this study. In addition no velocity dependence is applied in the calculation of ice shelf melt rates in this study, which could effect the variability of the ice shelf melt rates. However, as the iceshelf cavities are poorly known applying a velocity dependence may not improve the ice shelf freshwater fluxes, as the resulting ice shelf cavity circulations could be unrealistic. Nevertheless, exploring the freshwater balance and tracer distribution has suggested, among other conclusions, that the grounded BRI and iceberg melt could have significant impact on the region. This will now be investigated in Chapter 5.

Chapter 5

Effect of Icebergs

Nakayama, Timmermann, Schröder & Hellmer (2014) found that grounded BRI affected ocean variability in Pine Island Bay. These results are extended in this chapter by considering the role of grounded BRI over the whole Amundsen Sea, also considering the effects of iceberg meltwater, and investigating all underlying processes in detail. The aims of the sections in this chapter are:

5.1) The effects of representations of grounded BRI on winter sea ice concentration and freshwater flux are investigated, along with the effects on correlations between sea ice and ice shelf freshwater fluxes.

5.2) The effects of icebergs on the OHC on the continental shelf and on the OHC variability in front of ice shelves is investigated, along with investigating the effects of a poorly constrained sea ice parameter on the results.

The regional Amundsen Sea setup, described fully in Section 2.3, has a domain that extends from 75.5°S to 62°S and 140°W to 80°W covering the Amundsen Sea embayment, but the analysis in this section will concentrate on the region extending from 75.5°S to 71.5°S and 130°W to 95°W. This model setup employs open boundary conditions using steady climatological seasonal monthly conditions for ocean velocity, salinity and temperature, taken from Holland et al. (2014). A sea ice model is included in this setup and the model is forced with ERA-Interim reanalysis forcing from 1979-2018 (Dee et al. 2011), but the first 10 years are regarded as model spin up. In this setup ice shelf melting is calculated using using heat and salt turbulent exchange coefficients that have an implicit velocity dependence. There is no explicit horizontal diffusion of salt, heat or tracers in the model, but the vertical diffusion is parametrized by using the K-profile parameterization (KPP) scheme (Large et al. 1994). The air-ice drag coefficient is set to 0.0025, the demarcation ice thickness is set to 0.5 m, and sea ice advection uses a 3rd-order direct-space-time flux-limited scheme. Ocean parameters were kept the same as those used by Kimura et al. (2017).

So far, both grounded icebergs on Bear Ridge and imposed iceberg melting have been chosen to be included in the model simulations. These choices have an important effect on the freshwater balance and dynamics in the region. These effects are now shown in four runs: 'Reference', 'no BRI', 'no iceberg melt' and 'no BRI and no iceberg melt'. In addition the effect of using different representations of the grounded BRI is investigated, with an 'ice shelf' BRI and 50 % permeability BRI being tested. The ice shelf BRI has the same BRI distribution as the reference case (Figure 2.4a), but only occupies the top 10m grid cell. The 50 % permeability version has distribution shown in Figure 2.4b.

However, it should be noted that in this chapter only the effect of an idealised steady state representation of iceberg melt and the effect of representations of the grounded BRI are investigated. Therefore, in this chapter other effects of icebergs are unable to investigated for example the effect of individual iceberg presence on ocean currents and the effect of any inter-annual viability of iceberg melt.

5.1 Effect on sea ice and freshwater relations

In this section the effect of grounded BRI on sea ice concentration and sea ice freshwater flux in the Amundsen Sea region is investigated along with discussing the differences in the strengths of the effects when different types of grounded BRI representations are used. In the addition the effect of grounded BRI on sea ice correlations to ice shelf freshwater fluxes is discussed.

The grounded BRI affect the sea ice distribution in the region, and therefore its freshwater fluxes. Figure 5.1a and Figure 5.1b show the average winter sea ice freshwater flux and winter sea-ice concentration and drift, in the eastern Amundsen Sea with the grounded BRI present. The strongest sea ice freshwater fluxes out of the ocean are in the ASP and in coastal polynyas in the east; low sea ice concentration and a high westward drift characterize these regions. Calculating the mean total winter sea ice production in the ASP over the period 2003-2010 (March – October) and over the area shown by the red box in Figure 5.1a, gives a mean and standard deviation of $6.2 \pm 1.9 \times 10^{10}$ m^3, which is comparable to satellite-based estimates of $9 \pm 1.4 \times 10^{10}$ m^3, given the methodological error of 23 % in the latter figure (Nihashi & Ohshima 2015). Figure 5.1c and Figure 5.1d show the same quantities, but with the grounded BRI removed from the model, and Figure 5.1e and Figure 5.1f respectively show the climatological differences (with minus without grounded BRI, and note uneven colour bar).

In Figure 5.1a there is a feature of sea ice melting in the winter on the southern boundary to the east of PIG Ice Shelf. This could be due to the presence of the PIG Ice Shelf meltwater plume warming the surface waters and leading to the observed sea ice melt in the model. Warm meltwater plumes have been found to enhance sea ice melting directly in front of ice shelves creating polynyas (Payne et al. 2007). The extent of the enhanced

melting in the model could be realistic, though it is difficult to determine the extent of effect of ice shelf meltwater plumes on sea ice in observations.

The primary effect of the grounded BRI is to create the ASP, by blocking the westward flow of sea ice. This reduces sea ice concentration to the west of the grounded BRI and significantly increases sea-ice freshwater extraction, via increased sea ice growth. A weaker secondary effect is to increase the concentration of sea ice east of the BRI, by restricting the westward export of sea ice, and so reducing the eastern coastal polynyas. Therefore the grounded BRI affect the winter sea ice freshwater fluxes in front of both Dotson Ice Shelf and the ice shelves to the east, but with opposite effects, which may affect the oceanic conditions in front of these ice shelves.

However, the strength of these effects may be dependent on the representation of grounded BRI used in the simulation. Figure 5.2 shows the effect of 50 % permeability BRI version on winter sea ice concentration and freshwater fluxes. Note different colour bar ranges for the differences. A reduced effect on both sea ice concentration and freshwater fluxes is observed compared to the reference BRI case. East of the grounded BRI a slight increase in sea ice concentration is still observed, with the largest increase west of the Thwaites Ice Shelf, with a small reduction in westward sea ice velocities (Figure 5.2f). This is mirrored in the difference in sea ice freshwater fluxes observed with minimal changes along the eastern coast line, but with larger reductions in sea ice growth on the southern coastline, especially west of Thwaites Ice Shelf (Figure 5.2e). However, while significant reduction in sea ice concentration is observed west of the grounded BRI it is not as strong nor as wide spread as in the reference BRI case (Figure 5.2f), therefore leading to the ASP not being formed in this simulation (Figure 5.2b). This leads to only a small area west of the grounded BRI where sea ice growth is increased rather than the large area in the reference simulation. Calculating the mean total winter sea ice growth over ASP area for over the period 2003-2010 (March – October) and over the area shown by the red box in Figure 5.1a, gives $2.91 \pm 1.36 \times 10^{10}$ m^3, which is a substantial reduction in sea ice growth compared to the reference BRI case. This suggests that a lower permeability of icebergs are required in order for the formation of the ASP and the corresponding strong sea ice growth.

The real-world permeability of the grounded BRI is uncertain and may have different permeabilities depending on what is trying to pass through it. The permeability of the grounded BRI to sea ice can be estimated from satellite images, as shown in Figure 4.1. From satellite images it appears the grounded BRI has very little permeability to sea ice and appears to be a impermeable wall to the sea ice. Therefore, the permeability to sea ice of the grounded BRI in the 50 % permeability set up may be too high compared to recent observations. However, the permeability of the grounded BRI could have been different in the past, where there is evidence that there were fewer icebergs grounded on the ridge (Mazur et al. 2019). In addition, the real-world permeability of the grounded BRI to the ocean is harder to determine. Therefore it is highly uncertain and hence the

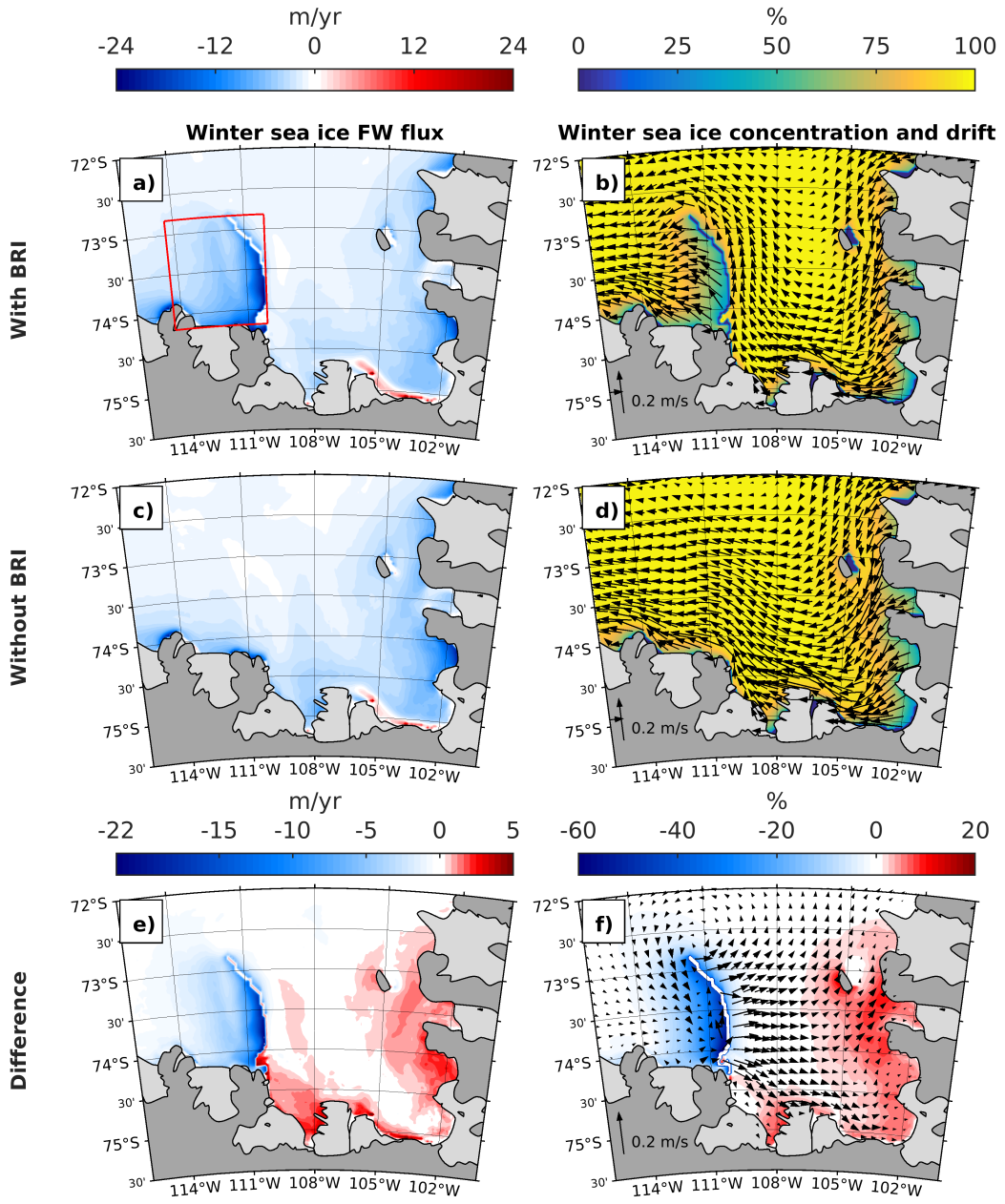

FIGURE 5.1: (a) Climatological austral winter (JAS) sea ice freshwater flux out of the ocean (1989-2018) with grounded BRI, and (c) without BRI. (b) Climatological winter (JAS) sea ice concentration and drift (1989-2018) with grounded BRI and (d) without BRI. Difference in (e) winter (JAS) sea ice freshwater flux out and (f) winter (JAS) sea ice concentration and velocities (with minus without the representation of the grounded Bear Ridge Icebergs). Note uneven colour bar in (e)(f).

permeability of the 50 % permeability set-up may have a realistic permeability to the ocean.

Figure 5.3 shows the effect of the ice shelf version of BRI on winter sea ice concentration and fluxes. As might be expected a similar effect occurs to sea ice concentration and sea ice freshwater fluxes as the reference BRI case, with the creation of the ASP and the

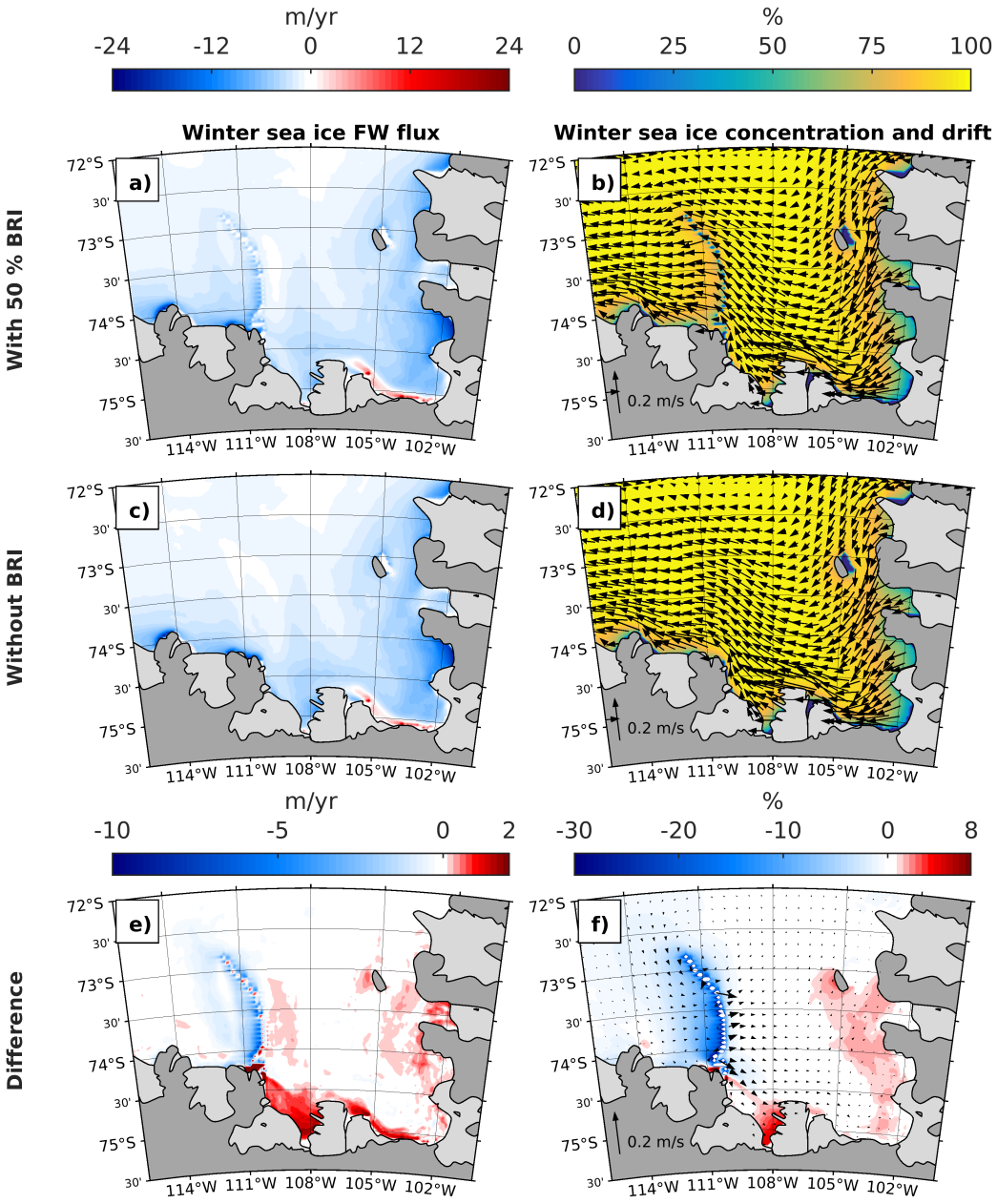

FIGURE 5.2: (a) Climatological austral winter (JAS) sea ice freshwater flux out of the ocean (1989-2018) with 50 % permeability grounded BRI, and (c) without BRI. (b) Climatological winter (JAS) sea ice concentration and drift (1989-2018) with grounded BRI and (d) without BRI. Difference in (e) winter (JAS) sea ice freshwater flux out and (f) winter (JAS) sea ice concentration and velocities (with minus without the representation of the grounded Bear Ridge Icebergs). Note uneven colour bar in (e)(f).

blocking in of sea ice east of the BRI (Figure 5.3f). However, there is a slight reduction in the negative sea ice fluxes in the ASP in the ice shelf BRI case compared to the reference case (Figure 5.3e). The mean total winter ASP production over the period 2003-2010 (March – October) and over the area shown by the red box in Figure 5.1a has reduced to $5.83 \pm 1.75 \times 10^{10}$ m^3 in this case, compared to the reference case. This may be due to ocean salinity and temperature changes at depth in this region affecting sea

ice growth, possibly due to advection of the ocean under this version of the grounded BRI.

Therefore the presence of grounded BRI strongly affects sea ice in the region and the types of representation of grounded BRI vary their effects on sea ice in the region. Therefore the presence of the grounded BRI could effect the relationship between sea ice and ice shelf freshwater fluxes, as discussed in Section 4.4, so this is consequently investigated in Figure 5.4.

Removing the grounded BRI significantly increases the correlation between the inter-annual anomalies of sea ice freshwater flux and anomalies in the combined ice shelf average melt from PIG and Thwaites ice shelves (Figure 5.4b), compared to having grounded BRI present in the model (Figure 5.4a). Positive correlations means that greater winter freezing/ reduced summer melting of sea ice correlates with lower ice shelf melting. The strongest correlations occur in front of the ice shelves in both cases, albeit with different magnitudes, but with high correlations downstream only when the grounded BRI are removed. The area mean correlation over the eastern Amundsen Sea is calculated to have a $r|r|$ of 0.34 at a peak lag of 10 months in Section 4.4, which is in the case with the BRI present. However, if this is calculated again over the same area and for the same delay, for the case with no BRI, an increase in $r|r|$ value occurs, increasing to 0.62.

This represents a fundamental change in the relationship between these two freshwater sources and the cause is uncertain. A potential cause is an increase in the direct effect of sea-ice brine rejection on the modulation of OHC reaching ice shelves and therefore ice-shelf melt rates. Conversely, it could be due to the sea ice being more mobile in the no BRI case, due to the lack of the blocking effect of the BRI. Therefore the wind has more influence on the sea ice movements and growth in the no BRI case. The wind is also one of the mechanisms that is controlling ice shelf melting, via influencing the CDW flux onto the continental shelf, therefore leading to the higher correlation between these two freshwater fluxes in the no BRI case.

5.2 Effect of icebergs on CDW intrusions and feedbacks

The effect of grounded BRI on winter sea ice fluxes could affect the oceanic conditions on the continental shelf and in front of ice shelves. Therefore in this section the effect of grounded BRI and iceberg melt on the OHC on the continental shelf is investigated. In this section the effect on the average CDW layer in the toughs on either side of the grounded BRI is investigated, along with the effects of icebergs on the inter-annual variability of OHC in front of ice shelves in the region. The effect of a poorly constrained sea ice parameter on iceberg effects in front of ice shelves is also investigated. These

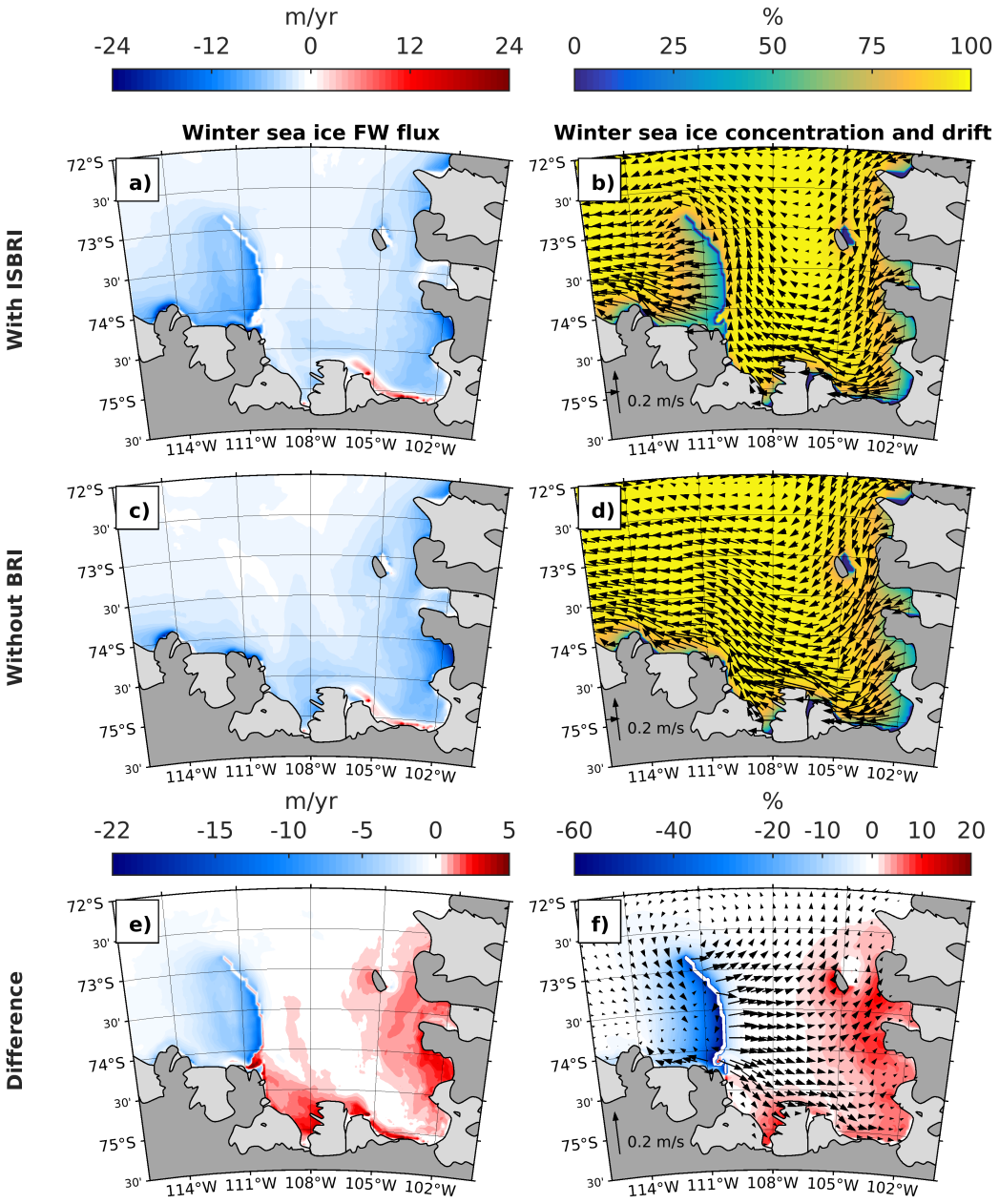

FIGURE 5.3: (a) Climatological austral winter (JAS) sea ice freshwater flux out of the ocean (1989-2018) with grounded ISBRI, and (c) without BRI. (b) Climatological winter (JAS) sea ice concentration and drift (1989-2018) with grounded BRI and (d) without BRI. Difference in (e) winter (JAS) sea ice freshwater flux out and (f) winter (JAS) sea ice concentration and velocities (with minus without the representation of the grounded Bear Ridge Icebergs). Note uneven colour bar in (e)(f).

studies are undertaken with the aim of investigating and identifying possible iceberg feedbacks in the region.

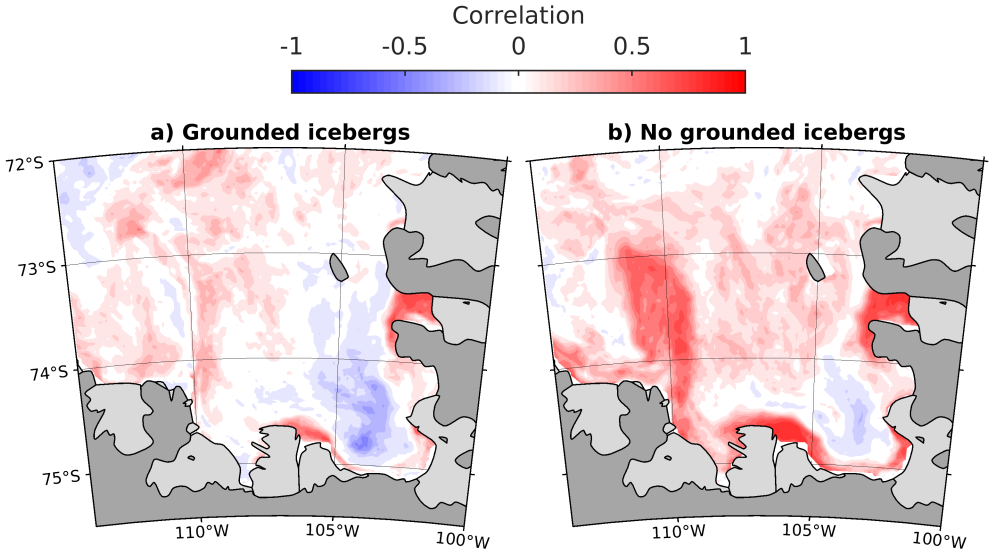

FIGURE 5.4: Maps of correlation $r|r|$ values of sea ice freshwater flux anomalies to a scalar time series of PIG and Thwaites melting anomalies at zero lag: (a) with grounded icebergs present and (b) without grounded icebergs present. Correlations are calculated after 10 years of spin up and after applying a 2-year running mean.

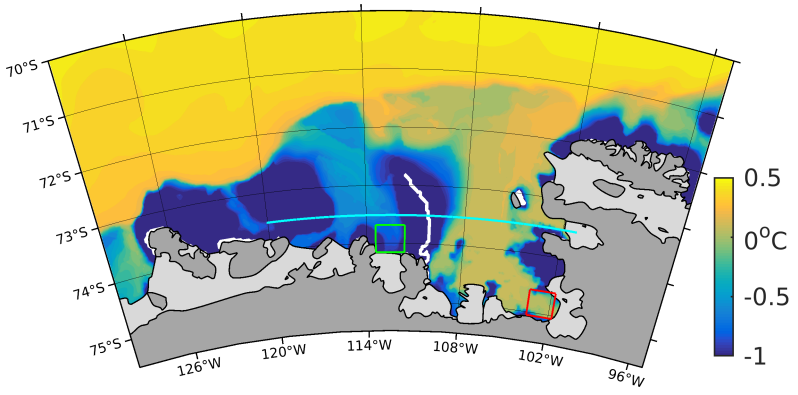

FIGURE 5.5: Maximum climatological subsurface potential temperature (1994-2012), but using only observational available years for model.

5.2.1 Average continental shelf oceanic effects of icebergs

The effect of the different iceberg aspects on the average OHC on the shelf is investigated by examining a cross-section shown by the cyan line in Figure 5.5. This cross-section covers the two troughs on either side of the grounded BRI, namely the Dotson Trough to the west and Pine Island Trough to the east, in order to assess the different effects that icebergs have on each one. In the reference case (Figure 5.6a) the warm CDW is observed, which intrudes along the troughs east of the grounded icebergs, which are denoted with the white vertical break in the cross-section at a longitude of 250°E. West of the grounded icebergs a lower average OHC is observed. When the grounded icebergs are removed cooler temperatures occur close to the coast east of the grounded icebergs,

but the main core of OHC in the eastern trough is relatively unaffected in this simulation by the removal of the BRI. However, west of the grounded icebergs an average increase in OHC is observed (Figure 5.6b), due to the removal of the Amundsen Sea polynya and the corresponding strong sea ice growth. The removal of the iceberg melt however has a stronger effect on the OHC in the troughs with a strong reduction in the average OHC on both sides of the grounded BRI (Figure 5.6c). The removal of the grounded BRI has a stronger effect when no iceberg meltwater is applied, yielding similar effects as to when iceberg melt is applied, but it now affects the OHC in the main trough east of the grounded BRI as well (Figure 5.6d).

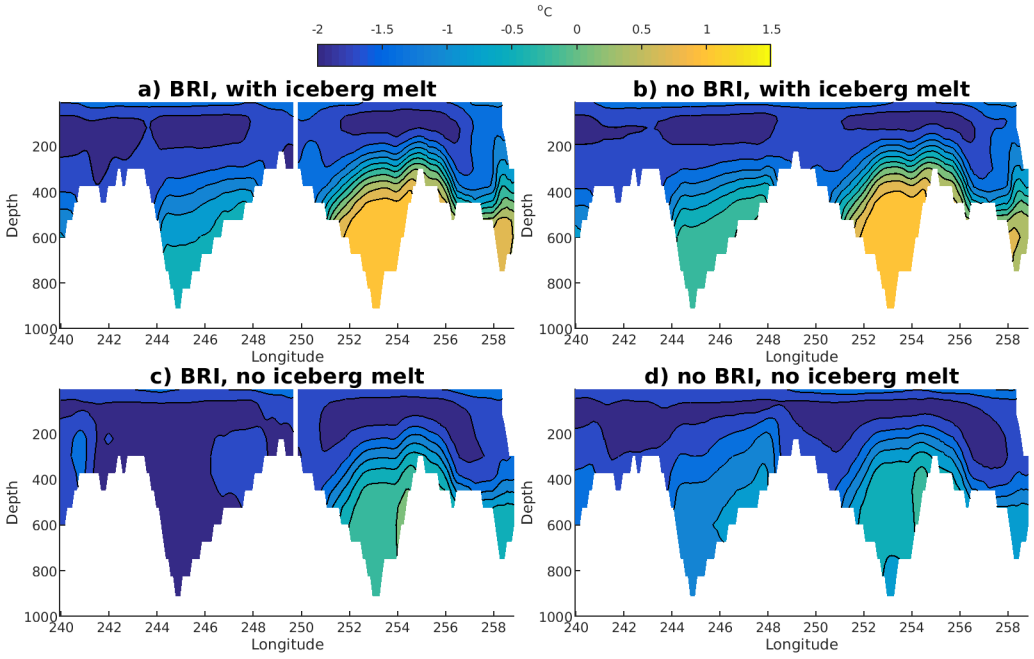

FIGURE 5.6: Cross-section of potential temperature along the cyan line in Figure 5.5 for: (a) grounded BRI and iceberg melt, (b) no grounded BRI but with iceberg melt, (c) grounded BRI but without iceberg melt, (d) no grounded BRI and no iceberg melt. Averaged over the period 1989-2018.

The presence of icebergs in the region may have an effect on the oceanic currents in the region, due to their physical presence and their effect on sea ice freshwater flux, with density being strongly driven by salinity in the polar regions (Gill 1982). Figure 5.7 shows the meridional oceanic velocities along the cross-section with and without the iceberg aspects of grounded BRI and iceberg melt. In the reference case with grounded BRI and iceberg melt a strong circulation is present in the eastern trough due to the presence of coastal currents driven by ice shelf meltwater with a strong southward current west of the ground BRI as well (Figure 5.7a). Both of these currents are driven by the gradients in the corresponding salinity structure shown in Figure 5.8a and the bathymetry structure of the region with the steep slope of Bear Ridge. However, when the grounded icebergs are removed, a small reduction in northward transport directly east of the grounded BRI is observed along with a small reduction in the southward transport west of the grounded

BRI (Figure 5.7b). This is due to higher salinity and a shifted salinity structure over Bear ridge, due to the two troughs now being connected (Figure 5.8b). The presence of the grounded BRI increases the slope in the isopynicals directly east and west of the BRI, due to a freshening of the top 200 m directly either side of the ground icebergs driving a stronger northwards and southwards flow. Removing the iceberg melt causes a strong reduction in the circulations in the region (Figure 5.7c), which is due to a reduction in stratification of the water column (Figure 5.8c), which drives weaker currents in the region. Removing the grounded BRI in the no iceberg melt case further reduces the strength of the currents around Bear Ridge (Figure 5.7d), due to a further reduction in the stratification in this area (Figure 5.8d). Therefore the presence of icebergs in the region can effect the strength of oceanic circulations in the region.

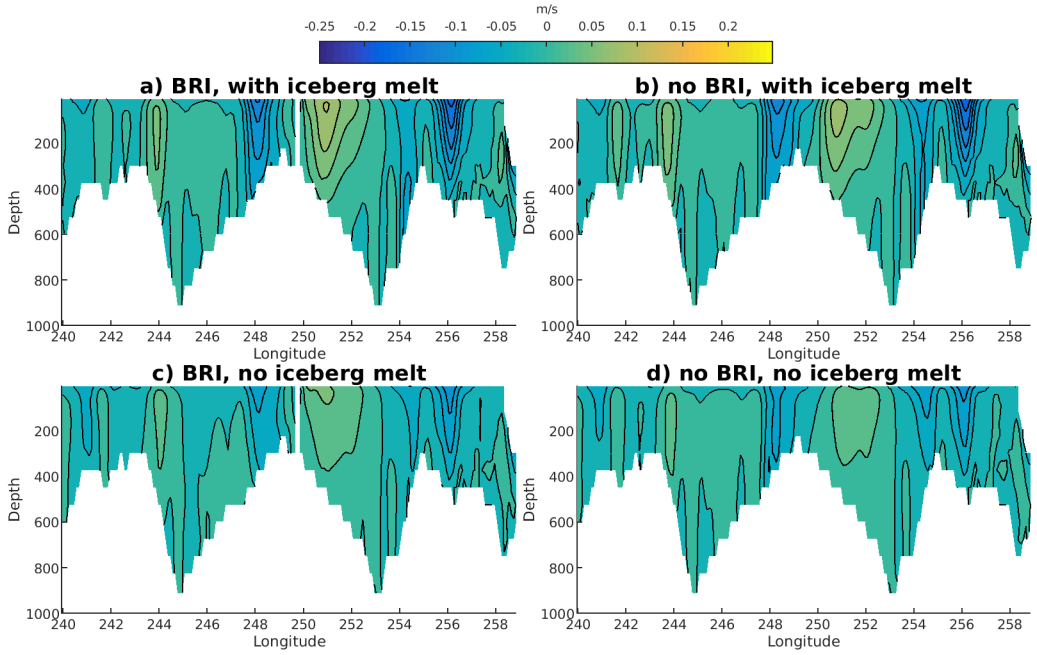

FIGURE 5.7: Cross-section of meridional velocities along the cyan line in Figure 5.5 for: (a) grounded BRI and iceberg melt, (b) no grounded BRI but with iceberg melt, (c) grounded BRI but without iceberg melt, (d) no grounded BRI and no iceberg melt. Averaged over the period 1989-2018.

However, as the strength of the grounded BRI effects on sea ice are dependent on the representation of grounded BRI used and the representations all allow for varying degrees of ocean connectivity through them, the strength of the effects of the grounded BRI on the OHC in these two troughs could be dependent on the representation of the grounded BRI used in the model. Therefore the effect on OHC along the cross-section of using different variants of representing the grounded BRI is investigated in Figure 5.9, where iceberg melt is present in all cases. The different representations are found to have only small differences in OHC in the troughs in the region, with a small increase in CDW temperature in both troughs either side of the BRI in the ice shelf BRI (Figure 5.9c) and 50 % permeability cases (Figure 5.9d). The 50 % permeability case has similar

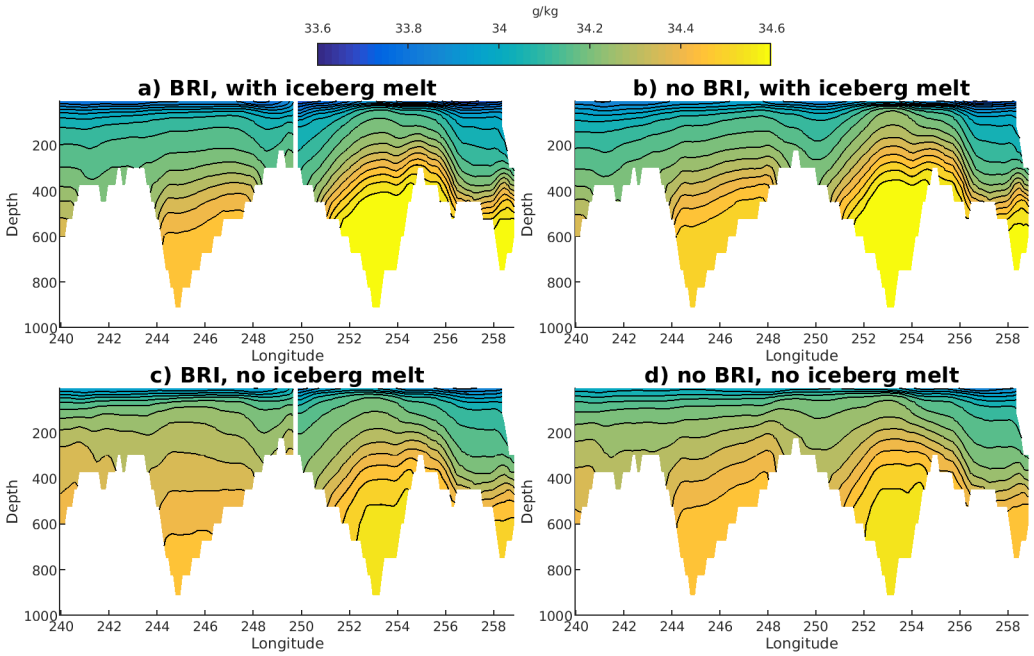

FIGURE 5.8: Cross-section of salinity along the cyan line in Figure 5.5 for: (a) grounded BRI and iceberg melt, (b) no grounded BRI but with iceberg melt, (c) grounded BRI but without iceberg melt, (d) no grounded BRI and no iceberg melt. Averaged over the period 1989-2018.

temperatures in the Dotson Trough to the no BRI case, which is due to the ASP not forming in these two cases.

East of the grounded BRI there are only small changes to the strength of the circulation when the other grounded BRI representations are employed. A slight reduction occurs in northward transport directly east of the grounded BRI in the ice shelf (Figure 5.10c) and 50 % permeability (Figure 5.10d) cases compared to the reference BRI case, which is due to a slight reduction in the slope of the isopynicals, because of the increased connectivity between the two troughs in these cases (Figure 5.11b,d) compared to the reference case. The main southward oceanic transport west of the grounded BRI in the ice shelf case is reduced compared to the reference BRI setup. The southward oceanic transport along the coast east of the grounded BRI in the ice shelf case is very similar to that of the reference BRI setup (Figure 5.10a,c). Therefore as there is only small differences in the northward transport directly east of the grounded BRI in the ice shelf BRI case it implies minimal oceanic advection occurs under the ice shelf BRI. This is due to a potential vorticity constraint, with the current unable to cross contours of water-column thickness, like those over the shallow Bear Ridge, without changing their angular momentum, which must be conserved. West of the grounded BRI there is a splitting of the southward current in the ice shelf BRI case, which is not observed in any other case. This is due to a saltier area that is formed in the ASP west of the grounded BRI, combined with that the two troughs are connected through the BRI in

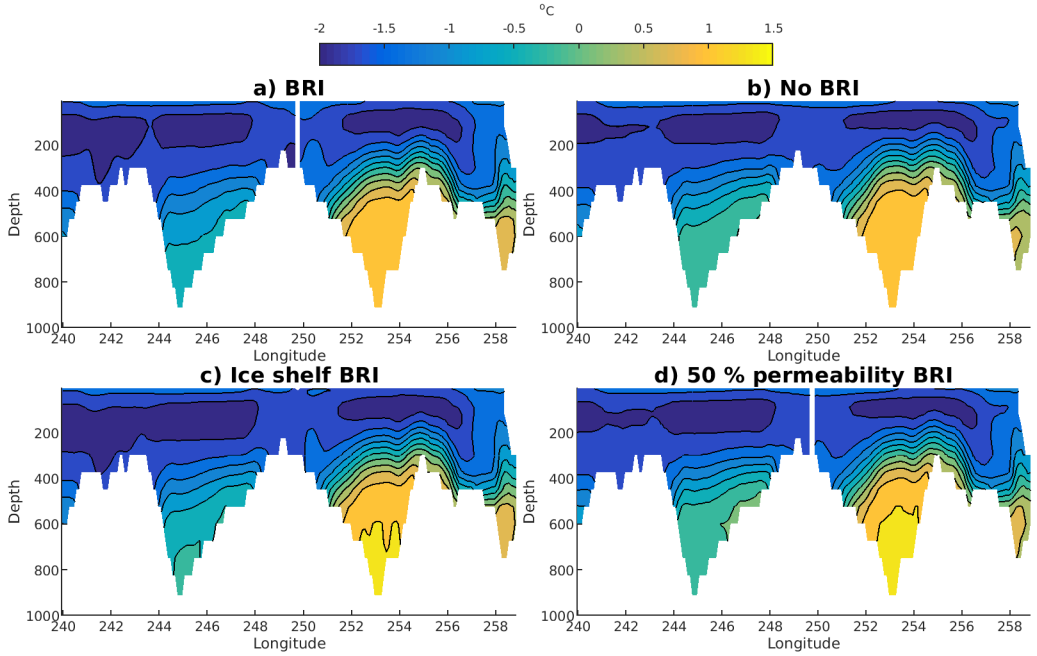

FIGURE 5.9: Cross-section of potential temperature along the cyan line in Figure 5.5 for: (a) grounded BRI, (b) no grounded BRI, (c) Ice shelf BRI, (d) 50 % permeability. Averaged over the period 1989-2018.

this case. The oceanic transport across the section in the 50 % permeability case is very similar to the oceanic transport in the no BRI case, with only a small increase in the southward transport west of the grounded BRI in the 50% permeability case (Figure 5.10b,d). This is because the salinity structure in these cases are very similar, as shown in Figure 5.11b,d.

5.2.2 Iceberg effect on OHC inter-annual variability in front of ice shelves

The effects of icebergs could affect the inter-annual variability of the OHC in front of ice shelves in the region. Therefore the effects of both the grounded BRI and iceberg meltwater on the inter-annual variability of OHC reaching PIG Ice Shelf and Dotson Ice Shelf are now considered, via Hovmöller diagrams of potential temperature (Figure 5.12). In front of PIG Ice Shelf for the reference case (Figure 5.12a), as discussed in Section 4.1, the model approximately follows the observed inter-annual variability of OHC reaching the PIG Ice Shelf. Removing the representation of the grounded BRI slightly lowers the thermocline and increases the depth of the WW (Figure 5.12b). This is due to a small increase in sea-ice brine rejection in front of the ice shelf, as the sea ice is unrestrained by the grounded BRI to the west. Convection increases, especially in the period between 1997 and 2000, thus becoming too cold at depth compared to the 2000 observations in the region (Dutrieux et al. 2014). However, removing iceberg meltwater is more significant,

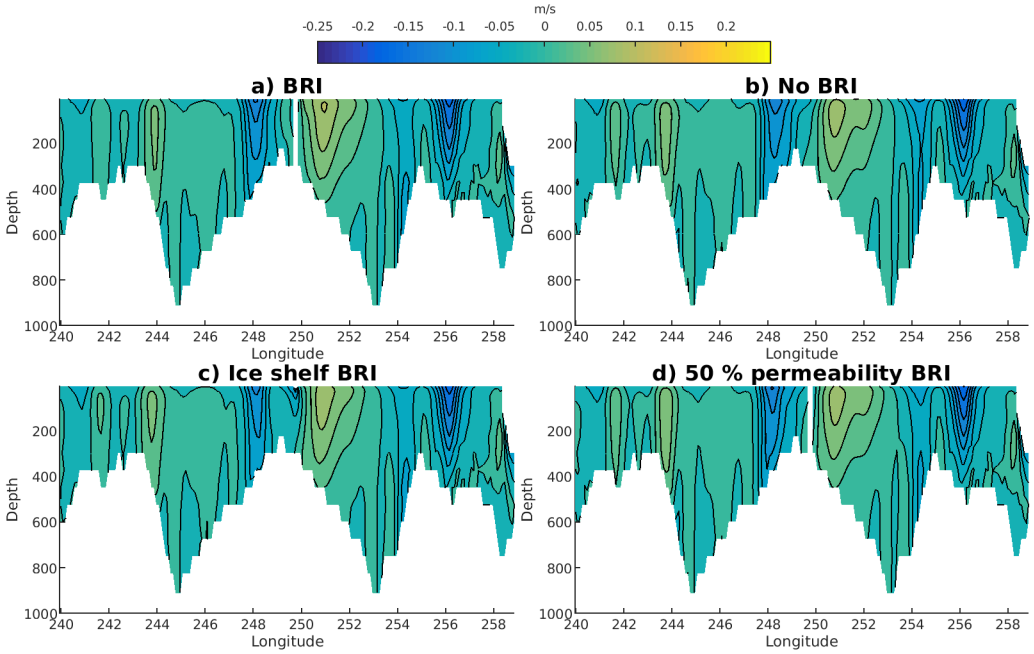

FIGURE 5.10: Cross-section of meridional velocities along the cyan line in Figure 5.5 for: (a) grounded BRI, (b) no grounded BRI, (c) Ice shelf BRI, (d) 50 % permeability. Averaged over the period 1989-2018.

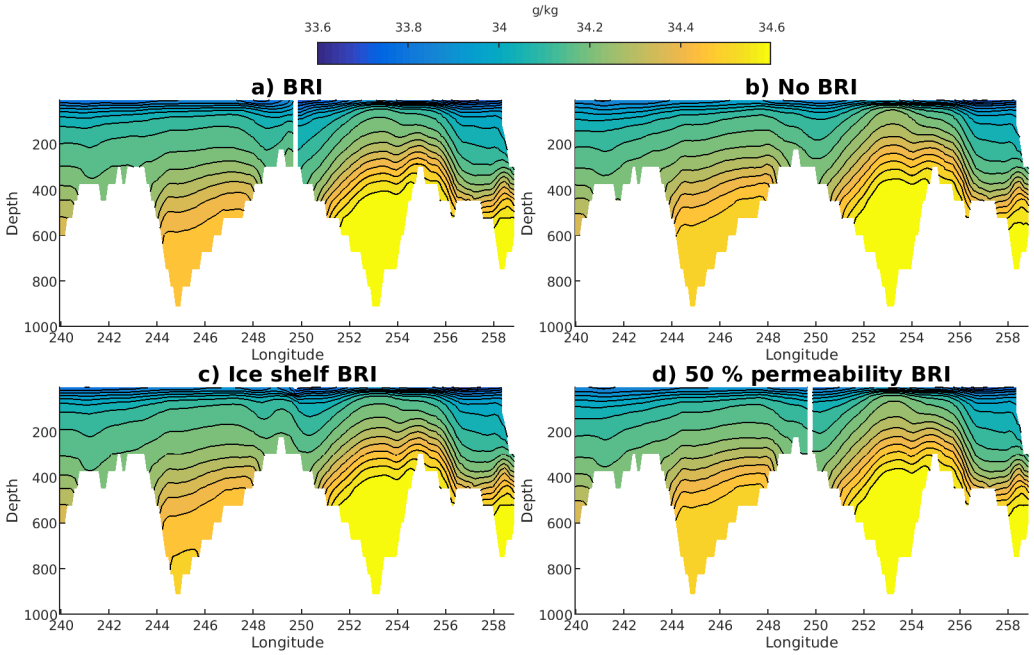

FIGURE 5.11: Cross-section of salinity along the cyan line in Figure 5.5 for: (a) grounded BRI, (b) no grounded BRI, (c) Ice shelf BRI, (d) 50 % permeability. Averaged over the period 1989-2018.

with WW now dominating the whole water column from 1997 and 2007 and a reduction in OHC in other years (Figure 5.12c). The combined effect of having neither the iceberg

meltwater nor the grounded icebergs gives an even greater WW dominance in front of PIG (Figure 5.12d).

In front of Dotson Ice Shelf in the reference case (Figure 5.12e) a large inter-annual variability is observed, which is similar to observations (Jenkins et al. 2018). Without the presence of the grounded BRI (Figure 5.12f), there is a reduction in the inter-annual variability in WW depth, giving this simulation a reduced inter-annual variability compared to observations. This is due to the removal of the ASP, which leads to a strong decrease in sea-ice brine rejection, and thereby modulation of OHC. Removing iceberg melt has a very significant impact (Figure 5.12g), filling the whole water column with all WW after 1990 and stopping the reintroduction of warmer water even in the period of 2005 to 2010, where CDW flux onto the shelf is high in the reference case. These results demonstrate that iceberg melt is required to mitigate the convection caused by the ASP. Perhaps unexpectedly, in the case with neither iceberg aspect (Figure 5.12h), a different inter-annual variability of OHC is observed. This is because the presence of dense shelf water in the eastern Amundsen Sea in this simulation, (Figure 5.12d), redirects modified CDW towards Dotson Ice Shelf. Comparing these results shows that both aspects of icebergs are required in order to simulate the inter-annual variability of OHC observed at Dotson Ice Shelf.

The possible existence of a positive iceberg feedback in the freshwater system is implied by these results, for PIG and similar eastern glaciers in the Amundsen Sea. Both iceberg melt and the presence of grounded BRI enhance modified CDW intrusions that reach the base of the ice shelves, which would enhance ice shelf melting east of the grounded BRI. An increase in basal melting will create an imbalance between the ice mass fluxes into and out of an ice shelf, leading it to thin overall. This will cause the glacier to speed up, as thinning reduces the ice flow-restraining internal stresses within the ice shelf. The increased flow speed of the glacier will therefore lead to an increase in iceberg production, and icebergs calved from glaciers like PIG and eastern Thwaites have a drift path that leads to the Bear Ridge area (Mazur et al. 2019). Therefore, this may increase the number of icebergs grounded on Bear Ridge and increase iceberg melt in the region, and so complete the potential feedback. In addition, as Pine Island Glacier has double it's ice discharge since the 1970s (Rignot et al. 2019) and as Thwaites iceberg tongue has made huge contributions to the BRI in recent decades, this suggests the possibility that this feedback effect has occurred in the last few decades. It is worth noting that this iceberg feedback may help to counteract ocean cold biases on the continental shelf in the Amundsen Sea which is a common problem in oceanographic models of the region (e.g. Naughten et al. (2018)).

In the reference case, the grounded BRI have been represented as a wall in the model, however the different ways to represent the grounded BRI icebergs have the potential to effect the grounded icebergs effect on the amount of OHC that reach the two ice shelves. There is minimal change to the amount of OHC reaching to PIG Ice Shelf by

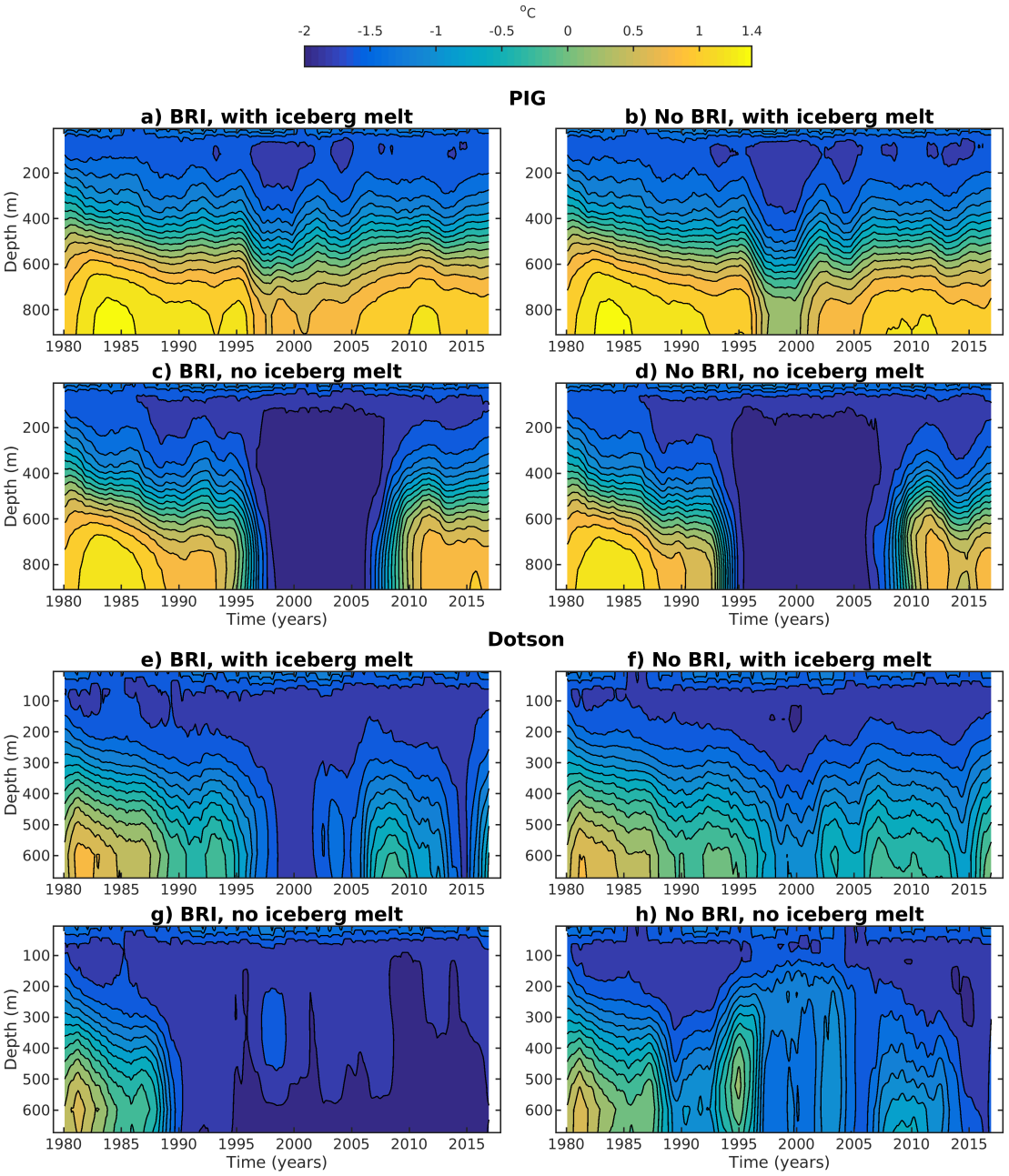

FIGURE 5.12: Hovmöller diagram of potential temperature in front of PIG Ice Shelf for: (a) grounded BRI and iceberg melt, (b) no grounded BRI but with iceberg melt, (c) grounded BRI but without iceberg melt, (d) no grounded BRI and no iceberg melt. (e-h) the same for the area in front of Dotson Ice Shelf. Hovmöller diagrams are averaged over the red and green boxes shown in Figure 5.5 and include 10-year model spin up. A 2-year running average is applied at each depth.

instead using an ice shelf based representation of BRI (Figure 5.13c). However, there is a reduction to the amount of OHC reaching the PIG Ice Shelf if this is changed to the 50 % permeability representation, with this case approximately half way between the full BRI case and the no BRI case, especially in the period 1995 to 2005 (Figure 5.13d). This is due to the decreased effect of this representation of the grounded BRI on sea ice

transport and sea ice growth, therefore enabling more intense convection compared to the reference case.

However, the effect of the different representations of the grounded icebergs is more significant to the OHC that reaches the Dotson Ice Shelf. The ice shelf BRI representation has the effect of a slight increase in OHC in warm years and a slight decrease in temperature in cold years (Figure 5.13g), when compared to the reference case. Therefore this representation increases the inter-annual variability of OHC that reaches the ice shelf, though this effect is minimal. Therefore replacing the BRI representation with the ice shelf version yields a similar OHC inter-annual variability at the PIG and Dotson ice shelves, compared to the reference case set-up.

However, changing to the 50 % permeability BRI representation appears to yield a similar OHC at Dotson Ice Shelf as the no BRI case (Figure 5.13h). Therefore in the 50 % permeability BRI representation case there is a reduced inter-annual variability in WW depth in front of Dotson Ice Shelf compared to observations (Jenkins et al. 2018). This is in contrast with the 50 % permeability representations effect on the OHC in front of PIG Ice Shelf, where an effect that was similar to 50 % of the effect of the reference grounded icebergs occurred. This suggests that the grounded icebergs effects to the west require a lower permeability of grounded icebergs before the effect cuts in, than the effect to the east. This also corresponds with that no ASP formation occurs in the 50 % permeability BRI representation case, as shown in Figure 5.2b. Therefore, reducing the grounded BRI to a 50 % permeability version has a bigger effect on the creation of the ASP to the west, than on the altering of the sea ice to the east.

5.2.3 Influence of parameter choices

The strength of this potential freshwater feedback is dependent on the winds, since sea ice export causes the convection that cools the OHC. In turn, this influence of the winds is dependent on the sea ice-atmosphere drag coefficient, which is a poorly constrained parameter. Some studies into the value of this parameter have been conducted for the Arctic (Petty et al. 2017), but there are few such studies in Antarctica. In this study, a drag coefficient of 0.0025 is used, which was tuned so that ocean conditions in front of PIG Ice Shelf approximately matched observations. To demonstrate the importance of this parameter, further simulations are now considered with different values of the sea-ice drag coefficient, increasing it and decreasing it by 20% from the reference value of 0.0025. These further simulations are used the examine the effect of this parameter on the feedback strength in front of PIG Ice Shelf of just the grounded BRI (Figure 5.14) and the grounded BRI and iceberg melt combined (Figure 5.15). In addition the effect on the OHC in front of Dotson Ice Shelf of just the grounded BRI (Figure 5.16) and the combined effect (Figure 5.17) are examined as well.

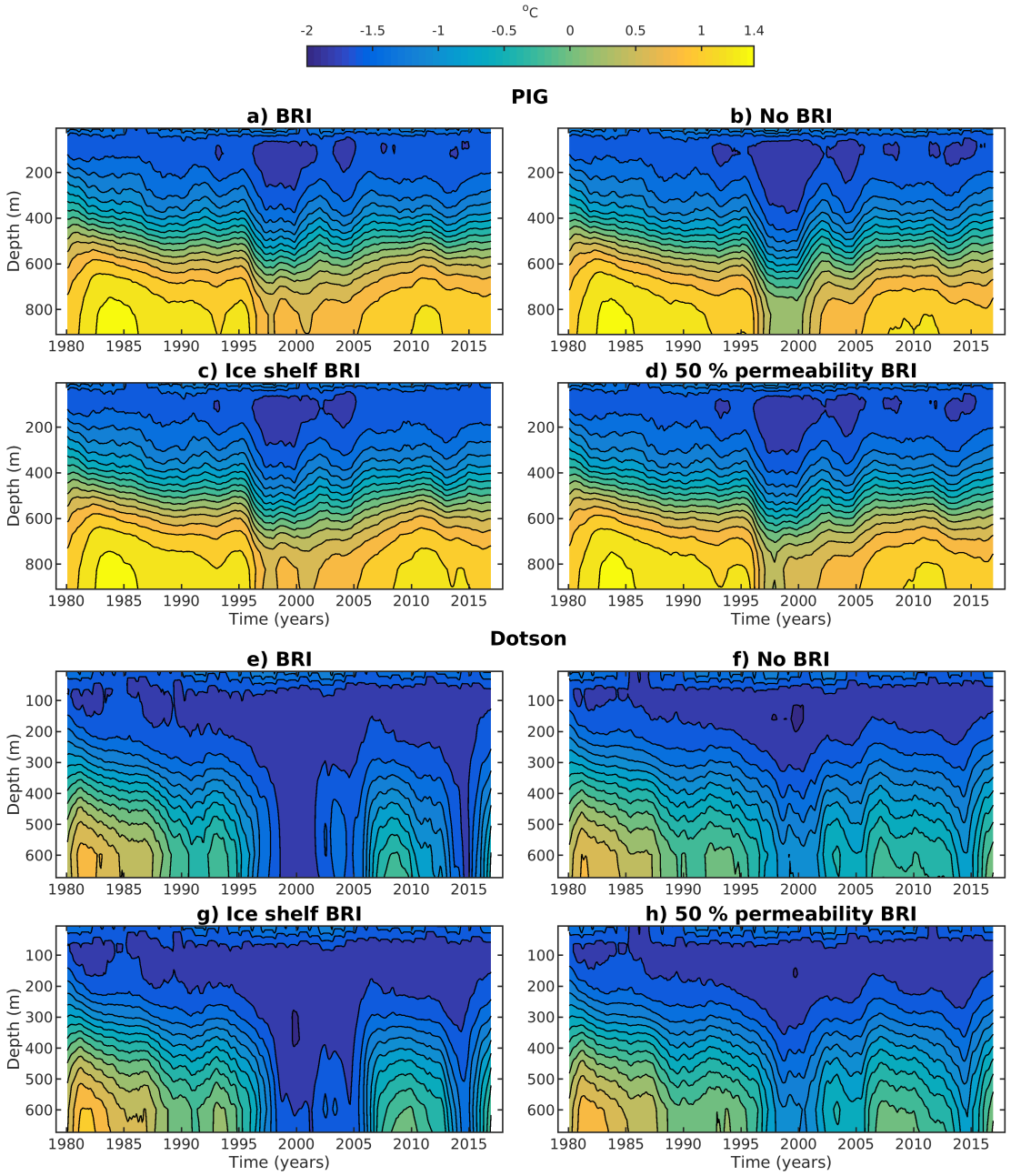

FIGURE 5.13: Hovmöller diagram of potential temperature in front of PIG Ice Shelf for: (a) grounded BRI, (b) no grounded BRI, (c) Ice shelf BRI, (d) 50 % permeability. (e-h) the same for the area in front of Dotson Ice Shelf. Hovmöller diagrams are averaged over the red and green boxes shown in Figure 5.5 and include 10-year model spin up. A 2-year running average is applied at each depth.

However, this will be an idealised study of the effects of this parameter, as the sea ice drag coefficient would be expected to vary spatially in the real world. It would be expected to vary with sea ice concentration and sea ice age, with higher sea concentrations and older sea ice possibly having a higher sea ice drag coefficient. Therefore the model portrays a simplified view of the processes that occur giving all sea ice the same sea ice drag coefficient. However, this will still provide an initial assessment of the effect and

importance of this parameter.

Figure 5.14 shows the inter-annual variability of OHC in front of PIG Ice Shelf for varying sea ice drag coefficients with and without BRI and with iceberg melt. Reducing the sea-ice drag coefficient leads to a decrease in the inter-annual variability of OHC reaching PIG Ice Shelf and a reduction in the WW thickness (Figure 5.14a), due to reduced sea ice export and formation. Conversely, increasing the drag coefficient (Figure 5.14c) increases the inter-annual variability, and significantly so during the 1997-2000 period of low CDW flux onto the shelf, leading to negative potential temperatures during this period in front of PIG Ice Shelf.

Examining the effect of grounded BRI removal reveals that increasing this parameter increases the effect of iceberg blocking on OHC in front PIG Ice Shelf. A more intense convection event now occurs during the period 1997 to 2007, where there is a substantial reduction in OHC reaching PIG Ice Shelf (Figure 5.14f). This is because with increased drag the wind moves sea ice faster, increasing local freshwater extraction via an enlargement of coastal polynyas and more rapid sea ice export from the region. Therefore the blocking effect of the grounded BRI becomes more important to the local freshwater balance. This is also shown in the case when the sea ice drag coefficient is reduced, which leads to minimal difference in OHC inter-annual variability being observed, between the with (Figure 5.14a) and without (Figure 5.14d) BRI simulations.

The effect of varying this parameter on the combined effect of the grounded BRI and iceberg melt is now investigated in Figure 5.15. With a reduction in the sea ice drag parameter, a reduced effect of the icebergs is observed, with the convection event and cold water through the water column present for a shorter period of time (Figure 5.15d) than compared to the reference case (Figure 5.15e). Increasing this parameter leads to an increase in the effect of removing both aspects of the icebergs (Figure 5.15f). Icebergs now mean the difference between the bay being in a warm regime, with modified CDW reaching PIG Ice Shelf and therefore high ice shelf melt, or being in a cold regime with dense shelf water formation and low ice shelf melt. Thus, iceberg melt and the grounded BRI become more important to the freshwater balance to mitigate drag-induced changes and stop a tipping point of dense shelf water being reached, so that warm modified CDW continues to reach eastern ice shelves like PIG.

Therefore the strength of this proposed iceberg feedback on eastern ice shelves like PIG is dependent upon the rate of sea ice export. Note that this parameter sensitivity study can be considered as a crude wind sensitivity study, with an increase in the sea ice drag parameter being comparable to the occurrence of stronger winds over the region. This comparison is imperfect however, as increasing this parameter is analogous to increasing only wind strength, not direction, and only over sea ice. With these caveats this would imply that stronger winds on the region would increase the regions reliance on icebergs in order for the region to remain in a warm regime.

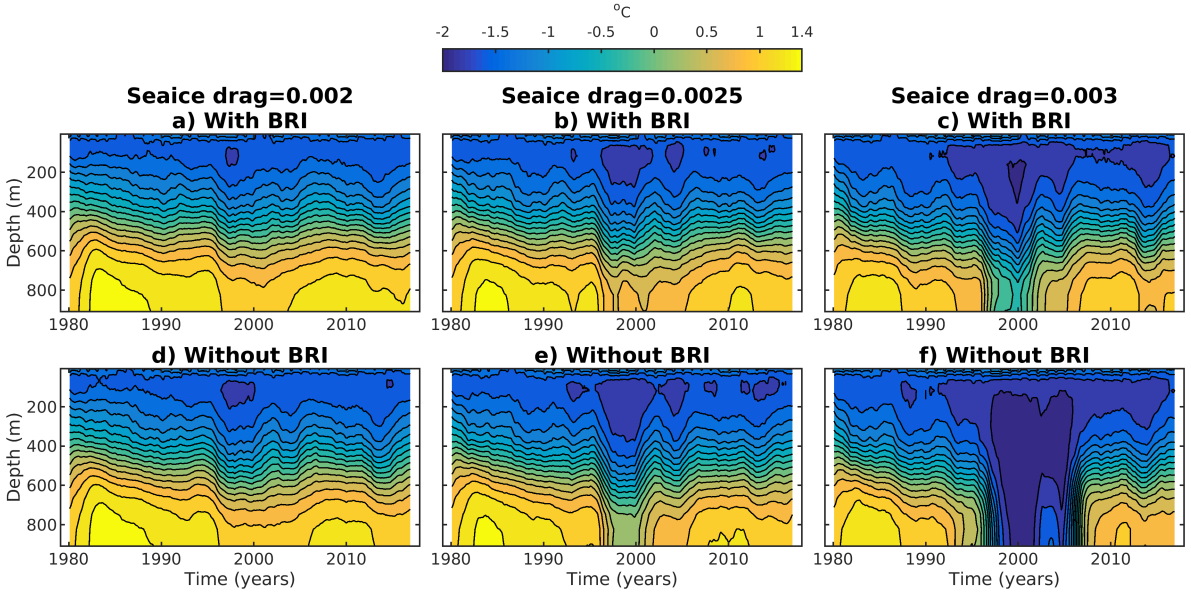

FIGURE 5.14: Potential temperature Hovmöller diagrams averaged over PIG Ice Shelf front with iceberg melt and with and without grounded icebergs for sea ice drag parameters values of 0.002 (a)(d), 0.0025 (b)(e), 0.003 (c)(f) respectively. Hovmöller diagrams are averaged over the red box in Figure 5.5 and include 10-year model spin up. A 2-year running mean is applied at each depth.

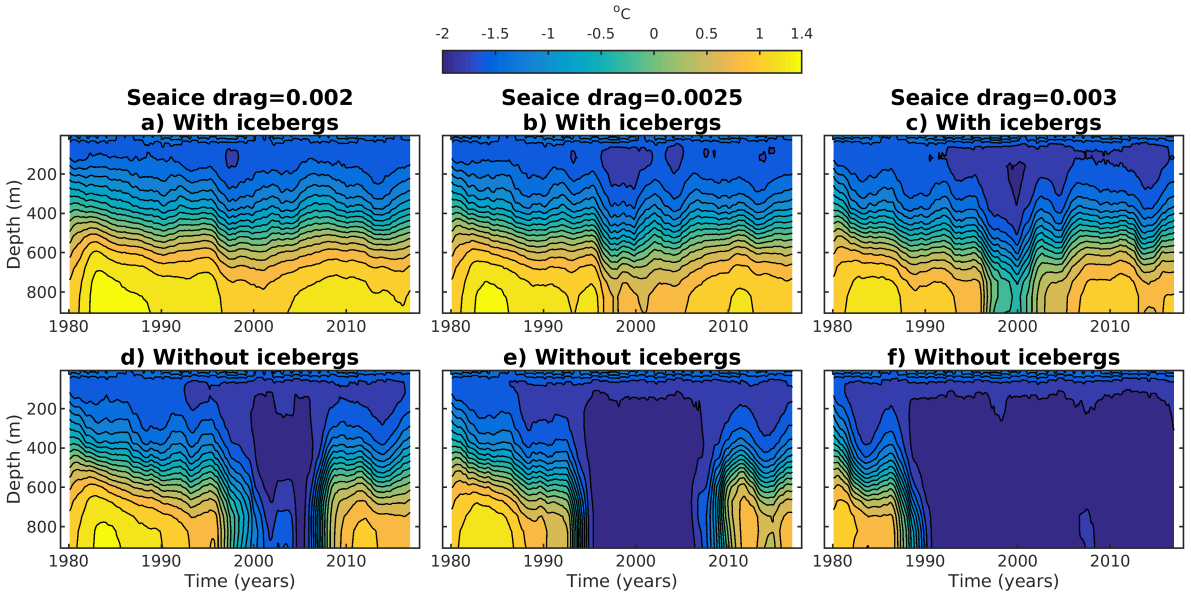

FIGURE 5.15: Potential temperature Hovmöller diagrams averaged over PIG Ice Shelf front with and without both grounded icebergs and iceberg melt for sea ice drag parameters values of 0.002 (a)(d), 0.0025 (b)(e), 0.003 (c)(f) respectively. Hovmöller diagrams are averaged over the red box in Figure 5.5 and include 10-year model spin up. A 2-year running mean is applied at each depth.

The effect of varying the sea ice drag parameter on the grounded BRI's effect on OHC inter-annual variability in front of Dotson Ice Shelf is also investigated in Figure 5.16. It is found that increasing the sea ice drag parameter increases the inter-annual variability

of the OHC and reduces the OHC significantly during the periods of low CDW flux onto the shelf, around 2000 and 2012 (Figure 5.16c). Conversely, by reducing this parameter a reduction in inter-annual variability is observed, along with an increase in OHC when CDW flux onto the shelf is low (Figure 5.16a). The primary driver of this change is the change in winter sea ice growth in the ASP. In the reference case, the mean total winter sea ice growth over the period 2003-2010 (March – October) and over the area shown by the red box in Figure 5.1a, was calculated to have a mean and standard deviation of $6.23 \pm 1.87 \times 10^{10}$ m^3. However, calculating over the same period and area when the parameter has been increased gives an increased winter ASP sea ice growth of $7.20 \pm 2.22 \times 10^{10}$ m^3 and when the parameter is decreased there is a decreased ASP sea ice growth down to $5.27 \pm 1.59 \times 10^{10}$ m^3. Therefore increasing/decreasing the sea ice drag coefficient increases/decreases sea ice export and sea ice growth in the ASP, which affects the OHC in front of Dotson Ice Shelf. Note that the higher ASP sea ice production is still below satellite estimates, though as mentioned previously satellite estimates have a large method uncertainty (Nihashi & Ohshima 2015). When the BRI is removed from the simulation changes in the inter-annual variability of OHC in front of Dotson are still observed with the variation of the sea ice drag parameter (Figure 5.16d-f), but changes are significantly reduced.

The difference in the effect of the combined grounded BRI and iceberg melt, with varying this parameter, on OHC in front of Dotson can also be investigated (Figure 5.17). As the parameter is increased, removing the iceberg aspects has a larger effect on the OHC variability that is observed (Figure 5.17f). When the parameter is decreased a smaller effect of the removal of icebergs occurs (Figure 5.17d), though when they are removed the OHC at depth and its inter-annual variability is still different compared to observations in the region (Jenkins et al. 2018). This is because increasing the parameter, not only increases the grounded BRI's effect on sea ice growth, but it also increases the presence of dense shelf water in the eastern Amundsen Sea, when icebergs are removed (Figure 5.15), which redirects modified CDW towards Dotson Ice Shelf.

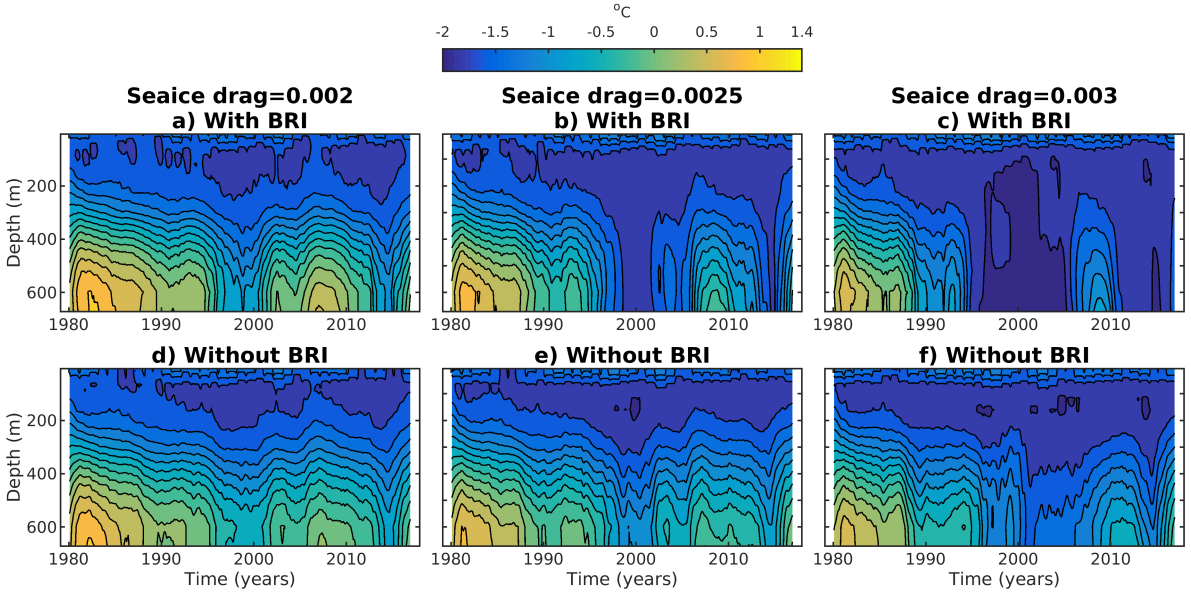

FIGURE 5.16: Potential temperature Hovmöller diagrams averaged over Dotson Ice Shelf front with iceberg melt and with and without grounded icebergs for sea ice drag parameters values of 0.002 (a)(d), 0.0025 (b)(e), 0.003 (c)(f) respectively. Hovmöller diagrams are averaged over the green box in Figure 5.5 and include 10-year model spin up. A 2-year running mean is applied at each depth.

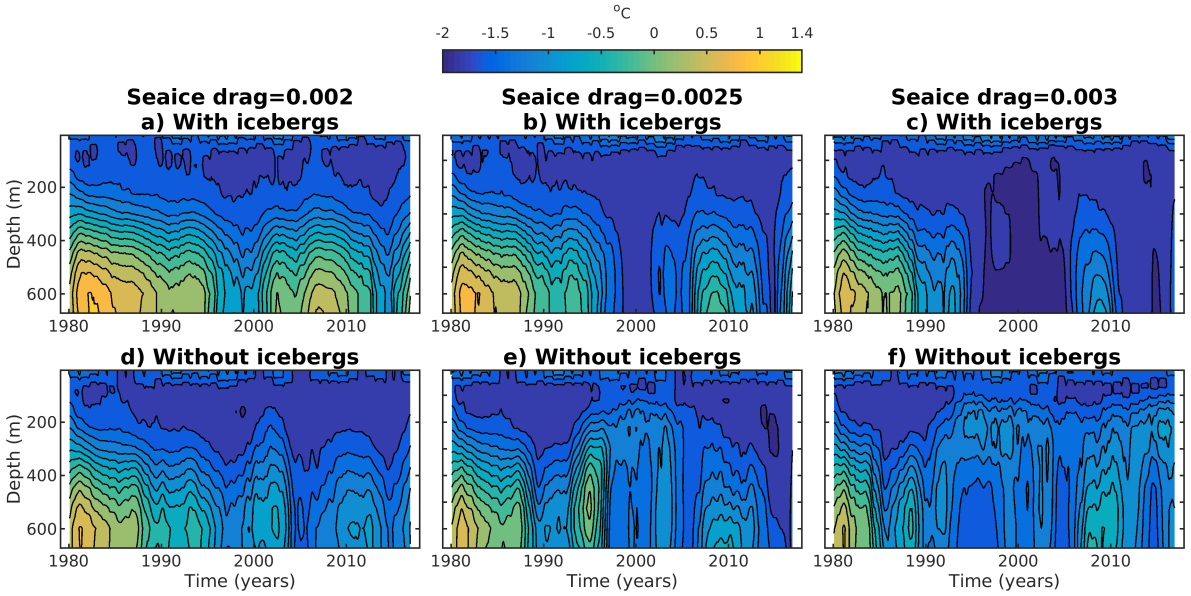

FIGURE 5.17: Potential temperature Hovmöller diagrams averaged over Dotson Ice Shelf front with and without both grounded icebergs and iceberg melt for sea ice drag parameters values of 0.002 (a)(d), 0.0025 (b)(e), 0.003 (c)(f) respectively. Hovmöller diagrams are averaged over the green box in Figure 5.5 and include 10-year model spin up. A 2-year running mean is applied at each depth.

5.3 Conclusions

In this chapter the effect of icebergs in the Amundsen Sea region has been investigated using a regional model, examining the effect of both the grounded Bear Ridge Icebergs (BRI) and iceberg melt.

1. **Investigate the effects of grounded BRI representations on sea ice concentrations and freshwater fluxes and their correlation to other freshwater sources.**

   The grounded BRI affect sea ice distribution and drift. Their presence increases freshwater extraction west of the grounded icebergs due to the formation of the Amundsen Sea Polynya, and decreases it to the east, with the reduction of eastern coastal polynyas due to the grounded icebergs restricting the westward flow of sea ice. Different representations of the grounded BRI can vary these effects however, with these effects being substantially reduced if a 50 % permeable barrier is used instead. The grounded BRI can effect the correlation between the inter-annual anomalies of sea ice and ice shelf freshwater fluxes, with correlations increased in the simulation without the grounded BRI present.

2. **Investigate the effects of icebergs on average OHC on the continental shelf and on the inter-annual variability of OHC reaches ice shelves.**

   Icebergs can affect the average OHC in the two troughs adjacent to them. Grounded icebergs affect and reduce the average heat content mainly in the western trough and at the eastern coast along the cross-section examined. However, iceberg melt has a stronger effect, with its removal reducing the OHC in both troughs and significantly reducing the circulations in both troughs. Differences in average OHC and circulations in the troughs are observed when the ice shelf and 50 % permeability BRI representations are used, with higher OHC in both troughs compared to the reference case.

   The combination of the grounded BRI and iceberg melt influences the inter-annual variability of oceanic heat content reaching the ice shelves, with effects that are different between the two cases on either side of the grounded BRI (e.g. Dotson and PIG). Both iceberg blocking and melting are required to recreate the inter-annual variability of the modified CDW reaching these ice shelves. Employing the 50 % permeability BRI representation suggests an asymmetric relationship to it's effects on either side of the BRI and the permeability of the BRI. This is because this case yields a similar inter-annual variability of OHC in front of Dotson as the no BRI case, but yields a OHC variability in front of PIG which is in-between the reference case and the no BRI case. However, using the ice shelf BRI representation yields similar inter-annual variability in front of the two ice shelves as the reference set-up.

These results suggest a further possible positive feedback mechanism, whereby more icebergs increase modified CDW intrusions that reach the base of eastern ice shelves like PIG, and therefore induce greater ice shelf melting. This causes the ice shelves to thin and thus speed up, hence producing more icebergs. However, the strength of this feedback is dependent on the modelled sea ice growth and export, which depends on the poorly constrained sea ice-atmosphere drag parameter.

In a parameter study, varying the sea ice-atmosphere drag parameter by 20% is found to have a significant control over the strength of this iceberg feedback. In addition varying this parameter strongly effects the strength of winter sea ice growth in the Amundsen Sea Polynya. Therefore poorly constrained parameters relating to the freshwater balance, like those relating to icebergs and sea-ice structure, will impact predictions for melting of the West Antarctic Ice Sheet.

Through these experiments the importance of the representation of icebergs in the region for reproducing the oceanic conditions and variability observed in the region has been determined. It has been shown that both the physical presence of the grounded BRI and iceberg melt are needed in order to reproduce the warm CDW on the continental shelf and its inter-annual variability. This result could through the representation of icebergs could aid larger scale models, which have historically had issues reproducing warm CDW intruding on the continental shelf in this region (e.g. Naughten et al. (2018)). However, the regional model used in this study could be improved by representing the iceberg melt as a freshwater flux which is fluxed over the depth distribution in the top few 100 meters in the ocean, as iceberg melt is released at depth as well as at the surface. Similarly the iceberg melt could also be calculated in the model via tracked iceberg particles in order to try and reproduce the more concentrated iceberg freshwater fluxes present in the real world.

In addition as mentioned these results show the importance of the seaice-drag parameter. However, the the absolute value of this parameter in order to gain optimal results could be dependent on other sea ice parameters for example the sea ice demarcation thickness. The seaice-drag parameter represents a sea ice characteristic that in the real world is dependent on a combination of real world factors. In the real world a spatial variability could be expected to the value of the seaice-drag parameter, due to spatially variable characteristics of sea ice like age, concentration and thickness. This could impact the importance of this parameter in the real world, potentially having a spatial variability to its importance.

Note that the same caveats described in Section 4.5 apply for the results in this chapter as well.

Chapter 6

Conclusions

Chapter 1 motivated the importance of understanding the freshwater balance in the Amundsen Sea. The chapter makes clear that the region has high inter-annual variability in its oceanic conditions and the ice shelves' melt rates in the region. There are still questions on the effects of grounded icebergs in the region and the potential for ice shelf meltwater and icebergs feedbacks are not fully understood. Motivated by this, the aim of this thesis was to: investigate the temporal and spatial variation and average freshwater balance in the region considering each source (iceberg melt, precipitation - evaporation, sea ice growth/melt and ice shelf melt), the potential for feedbacks and the role of icebergs in region. Chapter 2 covered the model employed in this thesis, along with the two setups used and improvements made to them. In Chapter 3 the idealised model's oceanic conditions was described. In Chapter 4 the regional model was validated against available data sets.

This thesis had two main aims, i) to quantify the local freshwater balance and ii) to examine the influence of grounded BRI and iceberg melt. In both of these, to determine possibilities for feedbacks on ice shelf discharge is an overarching aim.

The freshwater balance has been determined by the use of passive freshwater tracers. It was found that ice shelf and sea ice freshwater sources where the most important in the region. In addition, this study found evidence of the potential for a ice shelf freshwater feedback, with the total freshwater tracer having a strong resemblance to the ice shelf freshwater tracer. However, only the local freshwater balance was determined, but this study has improved the understanding of the physical processes in the region and therefore will aid in the predictions of the future sea level rise and a changing local freshwater balance.

For the second aim of this thesis, it was found that iceberg melt and the grounded BRI are important for modelling the OHC inter-annual variability and therefore ice shelf melt rates in the region. Therefore it is concluded that simulating icebergs in large

models is important, as well as including their ability to ground and interact with sea ice. This study also found the present of an iceberg feedback mechanism, which could be important for the region. These results will aid other studies in simulating the Amundsen Sea's continental OHC, where some models have struggled in the past with cold biases. In the idealised domain model studies the vertical distribution of ice shelf meltwater was investigated finding that the ice shelf produces two plumes, which will aid in future ice shelf melting parameterisations. In addition, several feedback mechanisms in the ice shelf melting process were found, which could also help improve parameterisations of ice shelf melting for large scale models and ice sheet models as aimed. The idealised model and regional model's full key findings are summarised below.

6.1 Idealised vertical distribution of ice shelf freshwater tracer

The depth of ice shelf tracer in the idealised model was found to significantly depend on the CDW thickness of the forcings and initial conditions applied to the model. However, an extreme range of CDW thicknesses were used for this study, even within a more realistic range significant differences do occur. Two plumes are found to form in the model; the primary plume which reaches the surface and a secondary which intrudes into the pycnocline. When the CDW thickness is higher more ice shelf meltwater reaches the surface and less intrudes into the pycnocline. However, for smaller CDW thickness forcing comparatively more ice shelf meltwater is found to intrude into the pycnocline than reach the surface. This could have implications for the vertical stability of the water column. If CDW thickness is thicker, more of the ice shelf meltwater reaches the surface, potential reducing convection from sea ice growth and hence potentially aiding in the protection of the CDW layer from convection. This therefore is a potential feedback for the CDW layer thickness. However, these results may be effected by the introduction of vertical mixing schemes, but the processes discussed here will still occur.

6.2 Local ice shelf freshwater feedbacks

The effect of the freshwater feedback was determined using a developed freshwater feedback method, using a reference set of simulations ranging over a range of oceanic thermal forcing from a 'COLD' simulation, to a 'WARM' simulation. This method uses two new sets of simulations, one set where the ice shelf meltwater output is fixed to that of the 'WARM' simulation ('WarmMelt-fixed') and another set where the ice shelf freshwater flux is set to that of the 'COLD' simulation ('ColdMelt-fixed'). Both of these new sets range over the same range of oceanic thermal driving as the reference set and in both sets the ice shelf is allowed to still calculate what it would have otherwise outputted.

These three sets of simulations can be used to calculate the freshwater feedback effect, as described previously in Section 3.3.

The freshwater feedback effect is found to be significant over an extreme range of oceanic forcings, ranging from full CDW forcing to full WW forcing. In addition, the freshwater feedback effect is found to be of different signs compared to the difference in thermal forcings.In the ColdMelt-fixed case, fixing the melt rate to a reduced melt rate suppresses the buoyancy driven overturning and thus leads to a reduced sensitivity to warming. However, for the WarmMelt-fixed case, fixing the melt rate to a higher melt rate causes a strong cold freshwater flux, which enhances the effect of the cooling. This result is perhaps unexpected as it is in contrast with other freshwater feedback studies, which found a positive feedback effect from an increase in meltwater flux (Jourdain et al. 2017, Donat-Magnin et al. 2017, Kimura et al. 2017).

Examining the spatial distribution of the freshwater feedbacks effects showed a strong variation in spatial distribution with the strongest effects on the melt rates occurring in the meltwater plume region on the west side of the ice shelf. The changes in the forcings applied to the ice shelf between the reference case and the iceshelf meltwater fixed cases were considered, specifically the friction velocity and the temperature forcing. The freshwater feedback was found to comprise of a positive buoyancy feedback and a negative thermal feedback. Therefore these two feedback processes combine to give the overall negative freshwater feedback effect observed in the simulations of fixed increased freshwater flux.

However, the freshwater feedback effect is found to be smaller when examined over a more realistic range of CDW thicknesses compared to the inter-annual variability that is observed in the Amundsen Sea. However, signs of the freshwater feedbacks are the same as in the extreme range cases.

6.3 Average freshwater distribution

The results show that sea ice and ice shelf freshwater fluxes are climatologically the strongest in the region. In the surface (10 m) and on a depth-average, however, all sources make important contributions to the climatological freshwater balance. The total freshwater tracer in the surface resembles the ice shelf tracer, and the total freshwater tracer field is highly similar to the ice shelf tracer on a depth average as well. This implies that there is the potential for ice-shelf meltwater feedbacks in the Amundsen Sea, since the presence of meltwater affects the ocean currents and stratification that control melting. For example, an increased presence of meltwater could both accelerate baroclinic currents and stratify the ocean, potentially enhancing the transport of less-modified CDW towards the ice shelves.

Significant differences in freshwater tracer concentrations were found between on and off the continental shelf and between the troughs to east and west of the grounded BRI. Comparing the two troughs either side of the grounded BRI in the model shows freshwater tracer being mixed further down into the water column west of the grounded BRI, which could be due to the strong sea ice growth in the Amundsen Sea polynya causing convection.

6.4 Freshwater seasonal cycle and inter-annual variability

Sea ice dominates the freshwater flux seasonal cycle and the sea ice tracer seasonal cycle appears to be larger on the continental shelf. The sea ice seasonal cycle dominates the seasonal cycle of the surface salinity, though it seems other freshwater sources do impact the surface salinity distribution.

Both the sea ice and ice shelf freshwater fluxes have the largest inter-annual variability. Sea ice freshwater flux anomalies negatively correlate with the meridional wind anomalies and, similarly to other studies, eastern ice shelf freshwater anomalies correlate strongly with CDW flux onto the continental shelf. While there is correlation between sea ice and ice shelf freshwater flux anomalies, these results suggest that wind anomalies drive both sea ice and ice shelf freshwater flux anomalies, with this common driver possibly leading the two freshwater fluxes to covary. Large inter-annual variability is observed in tracer distributions and magnitudes, leading to a similar inter-annual variability in the ice shelf tracer and the total tracer. This demonstrates the potential for the ice shelf meltwater feedback, as there is more freshwater in warm years, due to the increased presence of ice shelf meltwater.

Analysis of the freshwater balance in front of the PIG and Dotson ice shelves reveals that there is a large inter-annual variability of the total freshwater tracer, due mainly to the strong inter-annual variability of the sea ice and ice shelf tracers. This implies that other freshwater sources like iceberg melt become relatively more important to the freshwater balance when ice-shelf meltwater flux is low. However, in front of Dotson Ice Shelf sea ice and ice shelf tracer concentrations are stronger, due to the Amundsen Sea Polynya and the location of Dotson Ice Shelf downstream of high melt ice shelves like PIG Ice Shelf. This leads the freshwater balance of the area in front of Dotson Ice Shelf to be more dependent, than the area in front of PIG Ice Shelf, on other ice shelf melt rates to balance strong sea ice growth.

6.5 Impact of icebergs on sea ice and oceanic heat content

The grounded BRI affect sea ice distribution and drift. Their presence increases freshwater extraction west of the grounded icebergs due to the formation of the Amundsen Sea Polynya, and decreases it to the east, with the reduction of eastern coastal polynyas due to the grounded icebergs restricting the westward flow of sea ice. Different representations of the grounded BRI can vary these effects however, with these effects being substantially reduced if a 50 % permeable barrier is used instead. The grounded BRI can affect the correlation between the inter-annual anomalies of sea ice and ice shelf freshwater fluxes, with correlations increased in the simulation without the grounded BRI present.

Icebergs can affect the average OHC in the two troughs adjacent to them. Grounded icebergs affect and reduce the average heat content mainly in the western trough and at the eastern coast along the cross-section examined. However, iceberg melt has a stronger effect, reducing the OHC in both troughs and significantly reducing the circulations in both troughs. Differences in average OHC and circulations in the troughs are observed when the ice shelf and 50 % permeability BRI representations are used, with higher OHC in both troughs compared to the reference case.

The combination of the grounded BRI and iceberg melt influences the inter-annual variability of oceanic heat content reaching the ice shelves, with effects that are different between the two cases on either side of the grounded BRI (e.g. Dotson and PIG). Both iceberg blocking and melting are required to recreate the inter-annual variability of the modified CDW reaching these ice shelves. Employing the 50 % permeability BRI representation suggests an asymmetric relationship to it's effects on either side of the BRI and the permeability of the BRI. This is because this case yields a similar inter-annual variability of OHC in front of Dotson as the no BRI case, but yields a OHC variability in front of PIG which is in-between the reference case and the no BRI case. However, using the ice shelf BRI representation yields similar inter-annual variability in front of the two ice shelves as the reference set-up.

These results suggest a further possible positive feedback mechanism, whereby more icebergs increase modified CDW intrusions that reach the base of eastern ice shelves like PIG, and therefore induce greater ice shelf melting. This causes the ice shelves to thin and thus speed up, hence producing more icebergs. However, the strength of this feedback is dependent on the modelled sea ice growth and export, which depends on the poorly constrained sea ice-atmosphere drag parameter. In a parameter study, varying the sea ice-atmosphere drag parameter by 20% is found to have a significant control over the strength of this iceberg feedback, with a increase in this parameter causing a increase in the strength of this iceberg feedback effect.

Varying this parameter can be crudely considered as equivalent to varying wind strength, with an increase in the sea ice drag parameter being comparable to the occurrence of stronger winds over the region. This comparison is imperfect however, as increasing this parameter is analogous to increasing only wind strength, not direction, and only over sea ice. With these caveats this would imply that stronger winds on the region would increase the regions reliance on icebergs in order for the region to remain in a warm regime.

In addition, varying this parameter strongly effects the strength of winter sea ice growth in the Amundsen Sea Polynya. Therefore poorly constrained parameters relating to the freshwater balance, like those relating to icebergs and sea-ice structure, will impact predictions for melting of the West Antarctic Ice Sheet.

6.6 Implications and future work

The analysis of freshwater sources in this thesis has led to some important results. Several different freshwater feedback mechanisms have been identified in the system, which will aid our understanding on how the Amundsen Sea region and ice shelf melting with react to future changes. In addition, in this study, although it was found that ice shelf meltwater correlations strongly with CDW influx at the continental shelf, other more local processes were also found to be important for the local OHC and hence ice shelf melting. Icebergs and iceberg melt were found to have an strong impact on the OHC on the continental shelf. In addition, ice shelf melt rates were still found to anti-correlate with the sea ice freshwater fluxes. This could be due to direct impact of sea ice growth, or due to both sea ice growth and CDW influx at the shelf both correlating to winds over the region. Therefore this implies a complex system, where local and far field forcings may impact ice shelf melting. Therefore these experiments have increased our understanding of the drivers in the region. This has implications for the future of research into ice shelf melting in the region and therefore future predictions of the stability of the West Antarctic ice sheet and future sea level rise. In addition, the effects of local and remote forcing on ice shelf melting in this study has shown the possibility of several different feedback systems, through ice shelf melting and icebergs. These show the importance of the decisions of how to represent ice shelf and iceberg melting, along with grounded icebergs in climate models. More specifically these studies have the shown that icebergs should be represented in large scale models, with a representations of iceberg grounded and their interaction with sea ice in other to simulation the Amundsen Sea.

In this study only the in-cavity local freshwater feedback effect is investigated and determined. Therefore in the future more far-field feedbacks could be investigated using a realistic regional model, and these feedbacks in combination could prove to be more

significant. Therefore in the future the freshwater feedback technique could be applied to an regional Amundsen Sea model in order to assess the far field ice shelf freshwater feedback and the possible interactions between the freshwater fluxes between the ice shelves in the region. Therefore in addition to determining the freshwater effect from the region's combined ice shelf flux on individual ice shelves, this method could also be employed to determine the interaction between individual ice shelves. This method could also be combined with tracing of individual ice shelf freshwater fluxes, which could enable the investigation into the individual interactions that occur in between ice shelves in the region. In addition, the in-cavity freshwater feedback is determined in an idealised model setup only and therefore some of the model simplifications could effect the feedbacks strength. For example variation of the Winter Water temperature could effect the strength of feedback investigated. Therefore further analysis into the effect of model setup choices could be investigated to determine the effect of which on the freshwater feedback strength and aid our understanding of important processes that are occurring.

The regional model study is limited by the idealized representations of grounded BRI and iceberg melt. The closely balanced nature of the freshwater components found here emphasizes the need for a more realistic representation of icebergs to be developed for future modelling studies. Moreover, the dependency of the potential iceberg feedback on the poorly constrained sea ice-atmosphere drag coefficient highlights the need for advancing our understanding of sea ice around the Antarctic margins.

In this study the effects of iceberg meltwater and grounded BRI on the OHC on the continental shelf was shown. However, the changes to CDW layer thickness observed on the continental shelf, due to iceberg melt and the grounded BRI, could affect have an impact on the CDW transport onto the shelf. This could happen due to changes in the slope of the sloped isopycnals at the continental shelf, which drive the undercurrent, transporting CDW onto the continental shelf. This is especially likely in the extreme cases, where no CDW is present on the continental shelf. However, a future study is required in order to determine if these changes in OHC on the shelf correspond to any changes in the rate of OHC flux onto the continental shelf.

In this study the decision was made to study only the local component of the freshwater budget in the Amundsen Sea and therefore any sources through the boundaries were not traced. In the future a study could be made using a expanded model domain that includes the Bellinghausen Sea, which would therefore enable the tracing of the Bellinghausen Sea freshwater sources into the Amundsen Sea. This would therefore increase our understanding of a more complete freshwater budget in the Amundsen Sea region and on how Bellinghausen Sea sources of freshwater impact the Amundsen Sea. This has been done before for an ice shelf tracer only study (Nakayama et al. 2017), but a more complete study with all freshwater sources would be beneficial.

Bibliography

Abernathey, R. P., Cerovecki, I., Holland, P. R., Newsom, E., Mazlo, M. & Talley, L. D. (2016), 'Water-mass transformation by sea ice in the upper branch of the Southern Ocean overturning', *Nature Geoscience* **9**(8), 596+.

Adcroft, A., Hill, C. & Marshall, J. (1997), 'Representation of topography by shaved cells in a height coordinate ocean model', *Monthly Weather Review* **125**(9), 2293–2315.

Assmann, K. M., Hellmer, H. H. & Jacobs, S. S. (2005), 'Amundsen Sea ice production and transport', *Journal of Geophysical Research-Oceans* **110**(C12).

Assmann, K. M., Jenkins, A., Shoosmith, D. R., Walker, D. P., Jacobs, S. S. & Nicholls, K. W. (2013), 'Variability of Circumpolar Deep Water transport onto the Amundsen Sea continental shelf through a shelf break trough', *Journal of Geophysical Research-Oceans* **118**(12), 6603–6620.

Bett, D. T., Holland, P. R., Naveira Garabato, A. C., Jenkins, A., Dutrieux, P., Kimura, S. & Fleming, A. (2020), 'The impact of the amundsen sea freshwater balance on ocean melting of the west antarctic ice sheet', *Journal of Geophysical Research: Oceans* **125**(9), e2020JC016305.

Biddle, L. C., Heywood, K. J., Kaiser, J. & Jenkins, A. (2017), 'Glacial Meltwater Identification in the Amundsen Sea', *Journal of Physical Oceanography* **47**(4), 933–954.

Biddle, L. C., Kaiser, J., Heywood, K. J., Thompson, A. F. & Jenkins, A. (2015), 'Ocean glider observations of iceberg-enhanced biological production in the northwestern weddell sea', *Geophysical Research Letters* **42**(2), 459–465.

Biddle, L. C., Loose, B. & Heywood, K. J. (2019), 'Upper Ocean Distribution of Glacial Meltwater in the Amundsen Sea, Antarctica', *Journal of Geophysical Research-Oceans* **124**(10), 6854–6870.

Boening, C. W., Dispert, A., Visbeck, M., Rintoul, S. R. & Schwarzkopf, F. U. (2008), 'The response of the Antarctic Circumpolar Current to recent climate change', *Nature Geoscience* **1**(12), 864–869.

Bromwich, D. H., Rogers, A. N., Kallberg, P., Cullather, R. I., White, J. W. C. & Kreutz, K. J. (2000), 'ECMWF analyses and reanalyses depiction of ENSO signal in antarctic precipitation', *Journal of Climate* **13**(8), 1406–1420.

Campin, J. M., Adcroft, A., Hill, C. & Marshall, J. (2004), 'Conservation of properties in a free-surface model', *Ocean Modelling* **6**(3), 221 – 244.

Carter, L., McCave, I. N. & Williams, M. J. M. (2008), Chapter 4 circulation and water masses of the southern ocean: A review, *in* F. F. & M. S., eds, 'Antarctic Climate Evolution', Vol. 8 of *Developments in Earth and Environmental Sciences*, Elsevier, pp. 85 – 114.

Cavalieri, D., Markus, T. & Comiso, J. (2014), 'Amsr-e/aqua daily l3 12.5 km brightness temperature, sea ice concentration and snow depth polar grids. version 3 for 2006–2011, nasa daac at the natl. snow and ice data cent., boulder, colo.,', pp. 325–336.

Davis, P. E. D., Jenkins, A., Nicholls, K. W., Brennan, P. V., Abrahamsen, E. P., Heywood, K. J., Dutrieux, P., Cho, K.-H. & Kim, T.-W. (2018), 'Variability in basal melting beneath pine island ice shelf on weekly to monthly timescales', *Journal of Geophysical Research: Oceans* **123**(11), 8655–8669.

De Rydt, J., Holland, P. R., Dutrieux, P. & Jenkins, A. (2014), 'Geometric and oceanographic controls on melting beneath pine island glacier', *Journal of Geophysical Research: Oceans* **119**(4), 2420–2438.

Dee, D. P., Uppala, S. M., Simmons, A. J., Berrisford, P., Poli, P., Kobayashi, S., Andrae, U., Balmaseda, M. A., Balsamo, G., Bauer, P., Bechtold, P., Beljaars, A. C. M., van de Berg, L., Bidlot, J., Bormann, N., Delsol, C., Dragani, R., Fuentes, M., Geer, A. J., Haimberger, L., Healy, S. B., Hersbach, H., Holm, E. V., Isaksen, L., Kallberg, P., Koehler, M., Matricardi, M., McNally, A. P., Monge-Sanz, B. M., Morcrette, J. J., Park, B. K., Peubey, C., de Rosnay, P., Tavolato, C., Thepaut, J. N. & Vitart, F. (2011), 'The ERA-Interim reanalysis: configuration and performance of the data assimilation system', *Quarterly Journal of the Royal Meteorological Society* **137**(656, A), 553–597.

Depoorter, M. A., Bamber, J. L., Griggs, J. A., Lenaerts, J. T. M., Ligtenberg, S. R. M., van den Broeke, M. R. & Moholdt, G. (2013), 'Calving fluxes and basal melt rates of Antarctic ice shelves', *Nature* **502**(7469), 89+.

Donat-Magnin, M., Jourdain, N. C., Spence, P., Le Sommer, J., Gallée, H. & Durand, G. (2017), 'Ice-shelf melt response to changing winds and glacier dynamics in the amundsen sea sector, antarctica', *Journal of Geophysical Research: Oceans* **122**(12), 10206–10224.

Dotto, T. S., Garabato, A. C. N., Bacon, S., Holland, P. R., Kimura, S., Firing, Y. L., Tsamados, M., Wahlin, A. K. & Jenkins, A. (2019), 'Wind-Driven Processes Controlling Oceanic Heat Delivery to the Amundsen Sea, Antarctica', *Journal of Physical Oceanography* **49**(11), 2829–2849.

Dutrieux, P., De Rydt, J., Jenkins, A., Holland, P. R., Ha, H. K., Lee, S. H., Steig, E. J., Ding, Q., Abrahamsen, E. P. & Schroeder, M. (2014), 'Strong Sensitivity of Pine Island Ice-Shelf Melting to Climatic Variability', *Science* **343**(6167), 174–178.

Epstein, S. & Mayeda, T. (1953), 'Variation of o18 content of waters from natural sources', *Geochimica et Cosmochimica Acta* **4**(5), 213 – 224.

Fretwell, P., Pritchard, H. D., Vaughan, D. G., Bamber, J. L., Barrand, N. E., Bell, R., Bianchi, C., Bingham, R. G., Blankenship, D. D., Casassa, G., Catania, G., Callens, D., Conway, H., Cook, A. J., Corr, H. F. J., Damaske, D., Damm, V., Ferraccioli, F., Forsberg, R., Fujita, S., Gim, Y., Gogineni, P., Griggs, J. A., Hindmarsh, R. C. A., Holmlund, P., Holt, J. W., Jacobel, R. W., Jenkins, A., Jokat, W., Jordan, T., King, E. C., Kohler, J., Krabill, W., Riger-Kusk, M., Langley, K. A., Leitchenkov, G., Leuschen, C., Luyendyk, B. P., Matsuoka, K., Mouginot, J., Nitsche, F. O., Nogi, Y., Nost, O. A., Popov, S. V., Rignot, E., Rippin, D. M., Rivera, A., Roberts, J., Ross, N., Siegert, M. J., Smith, A. M., Steinhage, D., Studinger, M., Sun, B., Tinto, B. K., Welch, B. C., Wilson, D., Young, D. A., Xiangbin, C. & Zirizzotti, A. (2013), 'Bedmap2: improved ice bed, surface and thickness datasets for Antarctica', *Cryosphere* **7**(1), 375–393.

Fyfe, J. C. & Saenko, O. A. (2005), 'Human-induced change in the Antarctic Circumpolar Current', *Journal of Climate* **18**(15), 3068–3073.

Gill, A. E. (1982), 'Atmosphere-Ocean Dynamics', *Academic Press. 1st edition* **30**.

Gladstone, R. M., Bigg, G. R. & Nicholls, K. W. (2001), 'Iceberg trajectory modeling and meltwater injection in the southern ocean', *Journal of Geophysical Research: Oceans* **106**(C9), 19903–19915.

Hellmer, H. H. (2004), 'Impact of Antarctic ice shelf basal melting on sea ice and deep ocean properties', *Geophysical Research Letters* **31**(10).

Hellmer, H. & Olbers, D. (1989), 'A two-dimensional model for the thermohaline circulation under an ice shelf', *Antarctic Science* **1**, 325–336.

Holland, D. M. & Jenkins, A. (1999), 'Modeling thermodynamic ice–ocean interactions at the base of an ice shelf', *Journal of Physical Oceanography* **29**(8), 1787–1800.

Holland, P. R. (2017), 'The Transient Response of Ice Shelf Melting to Ocean Change', *Journal of Physical Oceanography* **47**(8), 2101–2114.

Holland, P. R., Bracegirdle, T. J., Dutrieux, P., Jenkins, A. & Steig, E. J. (2019), 'West Antarctic ice loss influenced by internal climate variability and anthropogenic forcing', *Nature Geoscience* **12**(9), 718+.

Holland, P. R., Bruneau, N., Enright, C., Losch, M., Kurtz, N. T. & Kwok, R. (2014), 'Modeled Trends in Antarctic Sea Ice Thickness', *Journal of Climate* **27**(10), 3784–3801.

Holland, P. R., Jenkins, A. & Holland, D. M. (2008), 'The response of ice shelf basal melting to variations in ocean temperature', *Journal of Climate* **21**(11), 2558–2572.

Holland, P. R. & Kwok, R. (2012), 'Wind-driven trends in Antarctic sea-ice drift', *Nature Geoscience* **5**(12), 872–875.

Jacobs, S. S. & Comiso, J. C. (1993), 'A recent sea-ice retreat west of the Antarctic Peninsula', *Geophysical Research Letters* **20**(12), 1171–1174.

Jacobs, S. S. & Giulivi, C. F. (2010), 'Large Multidecadal Salinity Trends near the Pacific-Antarctic Continental Margin', *Journal of Climate* **23**(17), 4508–4524.

Jacobs, S. S., Hellmer, H. H. & Jenkins, A. (1996), 'Antarctic ice sheet melting in the Southeast Pacific', *Geophysical Research Letters* **23**(9), 957–960.

Jacobs, S. S., Jenkins, A., Giulivi, C. F. & Dutrieux, P. (2011), 'Stronger ocean circulation and increased melting under pine island glacier ice shelf', *Nature Geoscience* **4**(8), 519–523.

Jenkins, A. (1999), 'The impact of melting ice on ocean waters', *Journal of Physical Oceanography* **29**(9), 2370–2381.

Jenkins, A., Dutrieux, P., Jacobs, S. S., McPhail, S. D., Perrett, J. R., Webb, A. T. & White, D. (2010), 'Observations beneath Pine Island Glacier in West Antarctica and implications for its retreat', *Nature Geoscience* **3**(7), 468–472.

Jenkins, A., Hellmer, H. H. & Holland, D. M. (2001), 'The role of meltwater advection in the formulation of conservative boundary conditions at an ice–ocean interface', *Journal of Physical Oceanography* **31**(1), 285–296.

Jenkins, A., Shoosmith, D., Dutrieux, P., Jacobs, S., Kim, T. W., Lee, S. H., Ha, H. K. & Stammerjohn, S. (2018), 'West Antarctic Ice Sheet retreat in the Amundsen Sea driven by decadal oceanic variability', *Nature Geoscience* **11**(10), 733+.

Joughin, I. & Alley, R. B. (2011), 'Stability of the west antarctic ice sheet in a warming world', *Nature Geoscience* **4**(8), 506–513.

Jourdain, N. C., Mathiot, P., Merino, N., Durand, G., Le Sommer, J., Spence, P., Dutrieux, P. & Madec, G. (2017), 'Ocean circulation and sea-ice thinning induced by melting ice shelves in the amundsen sea', *Journal of Geophysical Research: Oceans* **122**(3), 2550–2573.

Kim, I., Hahm, D., Rhee, T. S., Kim, T. W., Kim, C. S. & Lee, S. (2016), 'The distribution of glacial meltwater in the amundsen sea, antarctica, revealed by dissolved helium and neon', *Journal of Geophysical Research: Oceans* **121**(3), 1654–1666.

Kim, T., Ha, H., Wåhlin, A., Lee, S., Kim, C., Lee, J. & Cho, Y. (2017), 'Is ekman pumping responsible for the seasonal variation of warm circumpolar deep water in the amundsen sea?', *Continental Shelf Research* **132**, 38 – 48.

Kimura, S., Jenkins, A., Regan, H., Holland, P. R., Assmann, K. M., Whitt, D. B., Van Wessem, M., van de Berg, W. J., Reijmer, C. H. & Dutrieux, P. (2017), 'Oceanographic Controls on the Variability of Ice-Shelf Basal Melting and Circulation of Glacial Meltwater in the Amundsen Sea Embayment, Antarctica', *Journal of Geophysical Research-Oceans* **122**(12), 10131–10155.

Kurtz, N. T. & Markus, T. (2012), 'Satellite observations of Antarctic sea ice thickness and volume', *Journal of Geophysical Research-Oceans* **117**.

Large, W. G., Mcwilliams, J. C. & Doney, S. C. (1994), 'Oceanic Vertical Mixing - A Review and a Model with a Nonlocal Boundary-Layer Parameterization', *Reviews of Geophysics* **32**(4), 363–403.

Large, W. G. & Pond, S. (1982), 'Sensible and latent heat flux measurements over the ocean', *Journal of Physical Oceanography* **12**(5), 464–482.

Lenaerts, J. T. M., van den Broeke, M. R., van de Berg, W. J., van Meijgaard, E. & Munneke, P. K. (2012), 'A new, high-resolution surface mass balance map of Antarctica (1979-2010) based on regional atmospheric climate modeling', *Geophysical Research Letters* **39**.

Locarnini, R. A., Mishonov, A. V., Antonov, J. I., Boyer, T. P., Garcia, H. E., Baranova, O. K., Zweng, M. M., Paver, C. R., Reagan, J. R., Johnson, D. R. et al. (2013), 'World ocean atlas 2013. volume 1, temperature'.

Loose, B. & Jenkins, W. J. (2014), 'The five stable noble gases are sensitive unambiguous tracers of glacial meltwater', *Geophysical Research Letters* **41**(8), 2835–2841.

Losch, M., Menemenlis, D., Campin, J. M., Heimbach, P. & Hill, C. (2010), 'On the formulation of sea-ice models. part 1: Effects of different solver implementations and parameterizations', *Ocean Modelling* **33**(1), 129 – 144.

Marshall, G. J., Thompson, D. W. J. & van den Broeke, M. R. (2017), 'The Signature of Southern Hemisphere Atmospheric Circulation Patterns in Antarctic Precipitation', *Geophysical Research Letters* **44**(22), 11580–11589.

Marshall, J., Adcroft, A., Hill, C., Perelman, L. & Heisey, C. (1997a), 'A finite-volume, incompressible Navier Stokes model for studies of the ocean on parallel computers', *Journal of Geophysical Research-Oceans* **102**(C3), 5753–5766.

Marshall, J., Hill, C., Perelman, L. & Adcroft, A. (1997b), 'Hydrostatic, quasi-hydrostatic, and nonhydrostatic ocean modeling', *Journal of Geophysical Research: Oceans* **102**(C3), 5733–5752.

Martinson, D. G. (1990), 'Evolution of the southern ocean winter mixed layer and sea ice: Open ocean deepwater formation and ventilation', *Journal of Geophysical Research: Oceans* **95**(C7), 11641–11654.

Mazur, A. K., Wahlin, A. K. & Kalen, O. (2019), 'The life cycle of small- to medium-sized icebergs in the Amundsen Sea Embayment', *Polar Research* **38**.

Mazur, A. K., Wahlin, A. K. & Krezel, A. (2017), 'An object-based SAR image iceberg detection algorithm applied to the Amundsen Sea', *Remote Sensing of Environment* **189**, 67–83.

McDougall, T. J., Jackett, D. R., Wright, D. G. & Feistel, R. (2003), 'Accurate and computationally efficient algorithms for potential temperature and density of seawater', *Journal of Atmospheric and Oceanic Technology* **20**(5), 730–741.

Medley, B. & Thomas, E. R. (2019), 'Increased snowfall over the Antarctic Ice Sheet mitigated twentieth-century sea-level rise', *Nature Climate Change* **9**(1), 34+.

Meredith, M. P. (2016), 'Understanding the structure of changes in the Southern Ocean eddy field', *Geophysical Research Letters* **43**(11), 5829–5832.

Meredith, M. P., Brandon, M. A., Wallace, M. I., Clarke, A., Leng, M. J., Renfrew, I. A., P.M., N. & King, J. C. (2008), 'Variability in the freshwater balance of northern marguerite bay, antarctic peninsula: Results from δ18o', *Deep Sea Research Part II: Topical Studies in Oceanography* **55**(3), 309 – 322. Dynamics of Plankton, Krill, and Predators in Relation to Environmental Features of the Western Antarctic Peninsula and Related Areas: SO GLOBEC Part II.

Merino, N., Jourdain, N. C., Le Sommer, J., Goosse, H., Mathiot, P. & Durand, G. (2018), 'Impact of increasing antarctic glacial freshwater release on regional sea-ice cover in the southern ocean', *Ocean Modelling* **121**, 76–89.

Merino, N., Le Sommer, J., Durand, G., Jourdain, N. C., Madec, G., Mathiot, P. & Tournadre, J. (2016), 'Antarctic icebergs melt over the Southern Ocean: Climatology and impact on sea ice', *Ocean Modelling* **104**, 99–110.

Millero, F. (1978), 'Freezing point of seawater', *Eighth Report of the Joint Panel on Oceanographic Tables and Standards* **28**, 29–31.

Nakayama, Y., Menemenlis, D., Schodlok, M. & Rignot, E. (2017), 'Amundsen and bellingshausen seas simulation with optimized ocean, sea ice, and thermodynamic ice shelf model parameters', *Journal of Geophysical Research: Oceans* **122**(8), 6180–6195.

Nakayama, Y., Menemenlis, D., Zhang, H., Schodlok, M. & Rignot, E. (2018), 'Origin of circumpolar deep water intruding onto the amundsen and bellingshausen sea continental shelves', *Nature Communications* **9**.

Nakayama, Y., Schroeder, M. & Hellmer, H. H. (2013), 'From circumpolar deep water to the glacial meltwater plume on the eastern Amundsen Shelf', *Deep-Sea Research Part I-Oceanographic Research Papers* **77**, 50–62.

Nakayama, Y., Timmermann, R., Rodehacke, C. B., Schroeder, M. & Hellmer, H. H. (2014), 'Modeling the spreading of glacial meltwater from the Amundsen and Bellingshausen Seas', *Geophysical Research Letters* **41**(22), 7942–7949.

Nakayama, Y., Timmermann, R., Schröder, M. & Hellmer, H. H. (2014), 'On the difficulty of modeling circumpolar deep water intrusions onto the amundsen sea continental shelf', *Ocean Modelling* **84**, 26 – 34.

Naughten, K. A., Meissner, K. J., Galton-Fenzi, B. K., England, M. H., Timmermann, R. & Hellmer, H. H. (2018), 'Future Projections of Antarctic Ice Shelf Melting Based on CMIP5 Scenarios', *Journal of Climate* **31**(13), 5243–5261.

Naveira-Garabato, A. C., Forryan, A., Dutrieux, P., Brannigan, L., Biddle, L. C., Heywood, K. J., Jenkins, A., Firing, Y. L. & Kimura, S. (2017), 'Vigorous lateral export of the meltwater outflow from beneath an antarctic ice shelf', *Nature* **542**(7640), 219–222.

Nihashi, S. & Ohshima, K. I. (2015), 'Circumpolar mapping of antarctic coastal polynyas and landfast sea ice: Relationship and variability', *Journal of Climate* **28**(9), 3650–3670.

Orsi, A. H., Whitworth, T. & Nowlin, W. D. (1995), 'On the meridional extent and fronts of the Antarctic Circumpolar Current', *Deep-Sea Research Part I-Oceanographic Research Papers* **42**(5), 641–673.

Paolo, F. S., Fricker, H. A. & Padman, L. (2015), 'Volume loss from Antarctic ice shelves is accelerating', *Science* **348**(6232), 327–331.

Payne, A. J., Holland, P. R., Shepherd, A. P., Rutt, I. C., Jenkins, A. & Joughin, I. (2007), 'Numerical modeling of ocean-ice interactions under pine island bay's ice shelf', *Journal of Geophysical Research: Oceans* **112**(C10).
URL: *https://agupubs.onlinelibrary.wiley.com/doi/abs/10.1029/2006JC003733*

Petty, A. A., Feltham, D. L. & Holland, P. R. (2013), 'Impact of Atmospheric Forcing on Antarctic Continental Shelf Water Masses', *Journal of Physical Oceanography* **43**(5), 920–940.

Petty, A. A., Holland, P. R. & Feltham, D. L. (2014), 'Sea ice and the ocean mixed layer over the Antarctic shelf seas', *Cryosphere* **8**(2), 761–783.

Petty, A. A., Tsamados, M. C. & Kurtz, N. T. (2017), 'Atmospheric form drag coefficients over Arctic sea ice using remotely sensed ice topography data, spring 2009-2015', *Journal of Geophysical Research-Earth Surface* **122**(8), 1472–1490.

Price, M. R., Heywood, K. J. & Nicholls, K. W. (2008), 'Ice-shelf – ocean interactions at fimbul ice shelf, antarctica from oxygen isotope ratio measurements', *Ocean Science* **4**(1), 89–98.

Randall-Goodwin, E., Meredith, M. P., Jenkins, A., Yager, P. L., Sherrell, R. M., Abrahamsen, E. P., Guerrero, R., Yuan, X., Mortlock, R. A., Gavahan, K., Alderkamp, A. C., Ducklow, H., Robertson, R. & Stammerjohn, S. E. (2015), 'Freshwater distributions and water mass structure in the Amundsen Sea Polynya region, Antarctica', *Elementa-Science of the Anthropocene* **3**.

Regan, H. C., Holland, P. R., Meredith, M. P. & Pike, J. (2018), 'Sources, variability and fate of freshwater in the Bellingshausen Sea, Antarctica', *Deep-Sea Research Part I-Oceanographic Research Papers* **133**, 59–71.

Rignot, E., Jacobs, S., Mouginot, J. & Scheuchl, B. (2013), 'Ice-shelf melting around antarctica', *Science* **341**(6143), 266–270.

Rignot, E., Mouginot, J., Scheuchl, B., van den Broeke, M., van Wessem, M. J. & Morlighem, M. (2019), 'Four decades of antarctic ice sheet mass balance from 1979–2017', *Proceedings of the National Academy of Sciences* **116**(4), 1095–1103.

Rohling, E. J. (2013), 'Oxygen isotope composition of seawater', *The Encyclopedia of Quaternary Science. Amsterdam: Elsevier* **2**, 915–922.

Roquet, F., Madec, G., McDougall, T. J. & Barker, P. M. (2015), 'Accurate polynomial expressions for the density and specific volume of seawater using the TEOS-10 standard', *Ocean Modelling* **90**, 29–43.

Rye, C. D., Garabato, A. C. N., Holland, P. R., Meredith, M. P., Nurser, A. J. G., Hughes, C. W., Coward, A. C. & Webb, D. J. (2014), 'Rapid sea-level rise along the Antarctic margins in response to increased glacial discharge', *Nature Geoscience* **7**(10), 732–735.

Schodlok, M. P., Menemenlis, D., Rignot, E. & Studinger, M. (2012), 'Sensitivity of the ice-shelf/ocean system to the sub-ice-shelf cavity shape measured by nasa icebridge in pine island glacier, west antarctica', *Annals of Glaciology* **53**(60), 156–162.

Semtner, A. J. (1976), 'A model for the thermodynamic growth of sea ice in numerical investigations of climate', *Journal of Physical Oceanography* **6**(3), 379–389.

Shepherd, A., Ivins, E., Rignot, E., Smith, B., van den Broeke, M., Velicogna, I., Whitehouse, P., Briggs, K., Joughin, I., Krinner, G., Nowicki, S., Payne, T., Scambos, T., Schlegel, N., Geruo, A., Agosta, C., Ahlstrom, A., Babonis, G., Barletta, V., Blazquez,

A., Bonin, J., Csatho, B., Cullather, R., Felikson, D., Fettweis, X., Forsberg, R., Gallee, H., Gardner, A., Gilbert, L., Groh, A., Gunter, B., Hanna, E., Harig, C., Helm, V., Horvath, A., Horwath, M., Khan, S., Kjeldsen, K. K., Konrad, H., Langen, P., Lecavalier, B., Loomis, B., Luthcke, S., McMillan, M., Melini, D., Mernild, S., Mohajerani, Y., Moore, P., Mouginot, J., Moyano, G., Muir, A., Nagler, T., Nield, G., Nilsson, J., Noel, B., Otosaka, I., Pattle, M. E., Peltier, R. W., Pie, N., Rietbroek, R., Rott, H., Sandberg-Sorensen, L., Sasgen, I., Save, H., Scheuchl, B., Schrama, E., Schroeder, L., Seo, K., Simonsen, S., Slater, T., Spada, G., Sutterley, T., Talpe, M., Tarasov, L., van de Berg, W. J., van der Wal, W., van Wessem, M., Vishwakarma, B. D., Wiese, D., Wouters, B. & Team, I. (2018), 'Mass balance of the Antarctic Ice Sheet from 1992 to 2017', *Nature* **558**(7709), 219+.

Shepherd, A., Wingham, D. & Rignot, E. (2004), 'Warm ocean is eroding West Antarctic Ice Sheet', *Geophysical Research Letters* **31**(23).

Silvano, A., Rintoul, S. R., Pena-Molino, B., Hobbs, W. R., van Wijk, E., Aoki, S., Tamura, T. & Williams, G. D. (2018), 'Freshening by glacial meltwater enhances melting of ice shelves and reduces formation of Antarctic Bottom Water', *Science Advances* **4**(4).

Smith, J. A., Andersen, T. J., Shortt, M., Gaffney, A. M., Truffer, M., Stanton, T. P., Bindschadler, R., Dutrieux, P., Jenkins, A., Hillenbrand, C. D., Ehrmann, W., Corr, H. F. J., Farley, N., Crowhurst, S. & Vaughan, D. G. (2017), 'Sub-ice-shelf sediments record history of twentieth-century retreat of Pine Island Glacier (vol 541, pg 77, 2017)', *Nature* **549**(7671), 292.

Snow, K., Goldberg, D. N., Holland, P. R., Jordan, J. R., Arthern, R. J. & Jenkins, A. (2017), 'The Response of Ice Sheets to Climate Variability', *Geophysical Research Letters* **44**(23), 11878–11885.

St-Laurent, P., Klinck, J. M. & Dinniman, M. S. (2015), 'Impact of local winter cooling on the melt of Pine Island Glacier, Antarctica', *Journal of Geophysical Research-Oceans* **120**(10), 6718–6732.

St-Laurent, P., Yager, P. L., Sherrell, R. M., Stammerjohn, S. E. & Dinniman, M. S. (2017), 'Pathways and supply of dissolved iron in the Amundsen Sea (Antarctica)', *Journal of Geophysical Research-Oceans* **122**(9), 7135–7162.

Stammerjohn, S. E., Maksym, T., Massom, R. A., Lowry, K. E., Arrigo, K. R., Yuan, X., Raphael, M., Randall-Goodwin, E., Sherrell, R. M. & Yager, P. L. (2015), 'Seasonal sea ice changes in the Amundsen Sea, Antarctica, over the period of 1979-2014', *Elementa-Science of the Anthropocene* **3**.

Stern, A. A., Johnson, E., Holland, D. M., Wagner, T. J. W., Wadhams, P., Bates, R., Abrahamsen, E. P., Nicholls, K. W., Crawford, A., Gagnon, J. & Tremblay, J. E.

(2015), 'Wind-driven upwelling around grounded tabular icebergs', *Journal of Geophysical Research: Oceans* **120**(8), 5820–5835.

Talley, L. D., Pickard, G. L., Emery, W. J. & Swift, J. H. (2011), 'Chapter 13 - southern ocean', *Descriptive Physical Oceanography (Sixth Edition). Academic Press, Boston* pp. 437–471.

Thoma, M., Jenkins, A., Holland, D. & Jacobs, S. (2008), 'Modelling Circumpolar Deep Water intrusions on the Amundsen Sea continental shelf, Antarctica', *Geophysical Research Letters* **35**(18).

Thurnherr, A. M., Jacobs, S. S., Dutrieux, P. & Giulivi, C. F. (2014), 'Export and circulation of ice cavity water in pine island bay, west antarctica', *Journal of Geophysical Research: Oceans* **119**(3), 1754–1764.

Timmermann, R., Brocq, A., Martin, T., Domack, E., Dutrieux, P., Galton-Fenzi, B., Hellmer, H. H., Humbert, A., Jansen, D., Jenkins, A., Lambrecht, A., Makinson, K., Niederjasper, F., Nitsche, F., Nost, O., Smedsrud, L. & Smith, W. (2010), 'A consistent data set of antarctic ice sheet topography, cavity geometry, and global bathymetry', *Earth System Science Data* **2**, 261–273.

Wagner, T. J. W., Dell, R. W. & Eisenman, I. (2017), 'An analytical model of iceberg drift', *Journal of Physical Oceanography* **47**(7), 1605–1616.

Walker, D. P., Brandon, M. A., Jenkins, A., Allen, J. T., Dowdeswell, J. A. & Evans, J. (2007), 'Oceanic heat transport onto the Amundsen Sea shelf through a submarine glacial trough', *Geophysical Research Letters* **34**(2).

Webber, B. G. M., Heywood, K. J., Stevens, D. P. & Assmann, K. M. (2019), 'The impact of overturning and horizontal circulation in pine island trough on ice shelf melt in the eastern amundsen sea', *Journal of Physical Oceanography* **49**(1), 63–83.

Webber, B. G. M., Heywood, K. J., Stevens, D. P., Dutrieux, P., Abrahamsen, E. P., Jenkins, A., Jacobs, S. S., Ha, H. K., Lee, S. H. & Kim, T. W. (2017), 'Mechanisms driving variability in the ocean forcing of Pine Island Glacier', *Nature Communications* **8**.

Worby, A. P., Geiger, C. A., Paget, M. J., Van Woert, M. L., Ackley, S. F. & DeLiberty, T. L. (2008), 'Thickness distribution of Antarctic sea ice', *Journal of Geophysical Research-Oceans* **113**(C5).

Zhang, J. & Hibler, W. D. (1997), 'On an efficient numerical method for modeling sea ice dynamics', *Journal of Geophysical Research: Oceans* **102**(C4), 8691–8702.

Zweng, M. M., Reagan, J. R., Antonov, J. I., Locarnini, R. A., Mishonov, A. V., Boyer, T. P., Garcia, H. E., Baranova, O. K., Johnson, D. R., Seidov, D. et al. (2013), 'World ocean atlas 2013. volume 2, salinity'.